

VOLUME 76

JANUARY 6, 1972

NUMBER 1

JPCA X

THE JOURNAL OF

PHYSICAL

CHEMISTRY

PUBLISHED BIWEEKLY BY THE AMERICAN CHEMICAL SOCIETY

THE JOURNAL OF PHYSICAL CHEMISTRY

BRYCE CRAWFORD, Jr., *Editor*

STEPHEN PRAGER, *Associate Editor*

ROBERT W. CARR, Jr., FREDERIC A. VAN-CATLEDGE, *Assistant Editors*

EDITORIAL BOARD: A. O. ALLEN (1970-1974), J. R. BOLTON (1971-1975),
F. S. DAINTON (1972-1976), M. FIXMAN (1970-1974),
H. S. FRANK (1970-1974), R. R. HENTZ (1972-1976), J. R. HUIZENGA (1969-1973),
W. J. KAUZMANN (1969-1973), R. L. KAY (1972-1976), W. R. KRIGBAUM (1969-1973),
R. A. MARCUS (1968-1972), W. J. MOORE (1969-1973), J. A. POPLE (1971-1975),
B. S. RABINOVITCH (1971-1975), H. REISS (1970-1974), S. A. RICE (1969-1975),
F. S. ROWLAND (1968-1972), R. L. SCOTT (1968-1972),
R. SEIFERT (1968-1972), W. A. ZISMAN (1972-1976)

CHARLES R. BERTSCH, *Manager, Editorial Production*

AMERICAN CHEMICAL SOCIETY, 1155 Sixteenth St., N.W., Washington, D. C. 20036

FREDERICK T. WALL, *Executive Director*

Books and Journals Division

JOHN K. CRUM, *Director (Acting)*

JOSEPH H. KUNEY, *Head, Business Operations Department*

RUTH REYNARD, *Assistant to the Director*

©Copyright, 1972, by the American Chemical Society. Published biweekly by the American Chemical Society at 20th and Northampton Sts., Easton, Pa. 18042. Second-class postage paid at Washington, D. C., and at additional mailing offices.

All manuscripts should be sent to *The Journal of Physical Chemistry*, Department of Chemistry, University of Minnesota, Minneapolis, Minn. 55455.

Additions and Corrections are published once yearly in the final issue. See Volume 75, Number 26 for the proper form.

Extensive or unusual alterations in an article after it has been set in type are made at the author's expense, and it is understood that by requesting such alterations the author agrees to defray the cost thereof.

The American Chemical Society and the Editor of *The Journal of Physical Chemistry* assume no responsibility for the statements and opinions advanced by contributors.

Correspondence regarding accepted copy, proofs, and reprints should be directed to Editorial Production Office, American Chemical Society, 20th and Northampton Sts., Easton, Pa. 18042. Manager: CHARLES R. BERTSCH. Assistant Editor: EDWARD A. BORGER. Editorial Assistant: WILLIAM T. BOYD.

Advertising Office: Century Communications Corporation, 142 East Avenue, Norwalk, Conn. 06851.

Business and Subscription Information

Remittances and orders for subscriptions and for single copies,

notices of changes of address and new professional connections, and claims for missing numbers should be sent to the Subscription Service Department, American Chemical Society, 1155 Sixteenth St., N.W., Washington, D. C. 20036. Allow 4 weeks for changes of address. Please include an old address label with the notification.

Claims for missing numbers will not be allowed (1) if received more than sixty days from date of issue, (2) if loss was due to failure of notice of change of address to be received before the date specified in the preceding paragraph, or (3) if the reason for the claim is "missing from files."

Subscription rates (1972): members of the American Chemical Society, \$20.00 for 1 year; to nonmembers, \$60.00 for 1 year. Those interested in becoming members should write to the Admissions Department, American Chemical Society, 1155 Sixteenth St., N.W., Washington, D. C. 20036. Postage to Canada and countries in the Pan-American Union, \$5.00; all other countries, \$6.00. Single copies for current year: \$3.00. Rates for back issues from Volume 56 to date are available from the Special Issues Sales Department, 1155 Sixteenth St., N.W., Washington, D. C. 20036.

This publication and the other ACS periodical publications are now available on microfilm. For information write to: MICROFILM, Special Issues Sales Department, 1155 Sixteenth St., N.W., Washington, D. C. 20036.

THE JOURNAL OF
PHYSICAL
CHEMISTRY

Volume 76

JANUARY—APRIL 1972

PAGES 1—1388

BRYCE CRAWFORD, JR., *Editor*

STEPHEN PRAGER, *Associate Editor*

ROBERT W. CARR, JR., FREDERIC A. VAN-CATLEDGE, *Assistant Editors*

EDITORIAL BOARD

A. O. ALLEN
J. R. BOLTON
F. S. DAINTON
M. FIXMAN
H. S. FRANK
R. R. HENTZ
J. R. HUIZENGA

W. J. KAUZMANN
R. L. KAY
W. R. KRIGBAUM
R. A. MARCUS
W. J. MOORE
J. A. POPLÉ
B. S. RABINOVITCH

H. REISS
S. A. RICE
F. S. ROWLAND
R. L. SCOTT
R. SEIFERT
W. A. ZISMAN

CHARLES R. BERTSCH, *Manager, Editorial Production*

AMERICAN CHEMICAL SOCIETY

FREDERICK T. WALL, *Executive Director*

BOOKS AND JOURNALS DIVISION

JOSEPH H. KUNEY

Head, Business Operations Department

JOHN K. CRUM
Director

RUTH REYNARD
Assistant to the Director

THE JOURNAL OF
PHYSICAL CHEMISTRY

Volume 76, Number 1 January 6, 1972

JPCHAX 76(1) 1-142 (1972)

Rate Constants for Quenching of $N_2(A^3\Sigma_u^+)$ in Active Nitrogen . . .	J. A. Meyer, D. W. Setser, and W. G. Clark	1
Methylene Produced by Vacuum-Ultraviolet Photolysis. IV. Energy Distribution for the Reaction $C_3H_4 + h\nu$ (123.6 nm) = $CH_2 + C_2H_6$	R. D. Koob	9
Photochemical Addition of Benzene to Bicyclo[2.2.1]hept-2-ene (Norbornene)	R. Srinivasan	15
Solute Radical Cation Yields in the Pulse Radiolysis of Solutions of Aromatic Amines in Chlorinated Hydrocarbons	H. D. Burrows, D. Greatorex, and T. J. Kemp	20
Ion Yields and Ion Neutralization Processes in Pulse-Irradiated Acetone	Shamim A. Chaudhri and K.-D. Asmus	26
Laser-Induced Gas Breakdown: Spectroscopic and Chemical Studies	Ph. de Montgolfier, P. Dumont, Y. Mille, and J. Villiermaux	31
Studies of Surface Reactions of Nitric Oxide by Isotope Labeling. IV. The Reaction between Nitric Oxide and Ammonia over Copper Surfaces at 150–200°	K. Otto and M. Shelef	37
A Kinetic Study of <i>n</i> -Butene Isomerization over Supported Aluminum and Magnesium Sulfates	Makoto Misono and Yukio Yoneda	44
Electron Spin Resonance Spectroscopy of the Bisdithiooxalatonitrosyl Iron Anion	W. V. Sweeney and R. E. Coffman	49
Nuclear Magnetic Resonance Studies of Quadrupolar and Dipolar Relaxation Effects. Complexes of Lithium Halides with Pyridine in Aqueous Solution	David W. Larsen	53
Bisdifluoraminoalkanes: the Mass Spectral Decomposition of Isomeric Propanes	Martin Hertzberg, George White, R. S. Olfky, and F. E. Saalfeld	60
Restricted Rotation about the Exocyclic Carbon–Nitrogen Bond in Cytosine Derivatives	Regitze R. Shoup, H. Todd Miles, and Edwin D. Becker	64
An Evaluation of the Nuclear Magnetic Resonance Total Line Shape Analysis of Uncoupled, Exchanging Two-Site Systems	Regitze R. Shoup, Edwin D. Becker, and Mildred L. McNeel	71
Raman Spectra of Tetrafluoroberylate Ion in Molten Sodium Fluoride and Lithium Fluoride to 686°	Arvin S. Quist, John B. Bates, and George E. Boyd	78
Near-Infrared Spectral Studies on the Effects of Perchlorate and Tetrafluoroborate Ions on Water Structure	S. Subramanian and Harvey F. Fisher	84
The Ion-Product Constant of Water to 350°	James R. Fisher and H. L. Barnes	90
A Thermodynamic Study of Solutions with Liquid Crystal Solvents by Gas–Liquid Partition Chromatography	David G. Willey and Glenn H. Brown	99
Thermochemistry of the Diels–Alder Reaction. II. Heat of Addition of Several Dienes to Tetracyanoethylene	F. E. Rogers	106
A Study of the Nature of Active Sites on Zeolites by the Measurement of Heat of Immersion. II. Effects of Silica/Alumina Ratio to Electrostatic-Field Strength of Calcium-Exchanged Zeolites	Kazuo Tsutsumi and Hiroshi Takahashi	110
Studies of Transition Phenomena of Some Organic Solids by Electrical Conductivity Measurement at Low Temperature	Hajime Kadoi, Yoneho Tabata, and Keichi Oshima	115
Reactions of Coordination Compounds in the Solid State. The Racemization of (+)-[Co(en) ₃]X ₃ · <i>n</i> H ₂ O	Charles Kutal and John C. Bailar, Jr.	119
The Intrinsic Viscosities of Bovine Serum Albumin in <i>n</i> -Propyl Alcohol–Water Mixtures	S. F. Sun	128

NOTES

Proton Magnetic Resonance in Concentrated Aqueous Solutions of Tetraalkylammonium Bromides and Inorganic Halides at 25 and 65°	Antonio LoSurdo and Henry E. Wirth 130
Irradiated Single Crystal Clathrate of Dianin's Compound and 1,2-Dibromo-1,1-difluoroethane: Electron Spin Resonance Observation of the Br ₂ ⁻ Radical	Lowell D. Kispert and Jane Pearson 133
Free-Radical Intermediates in the Reaction of the Hydroxyl Radical with Dialkyl Sulfoxides	Hitoshi Taniguchi, Hideo Takagi, and Hiroyuki Hatano 135
Ethylene as an Actinometer in the Wavelength Region 147-185 Nanometers	L. C. Glasgow and P. Potzinger 138

COMMUNICATIONS TO THE EDITOR

Electron Spin Resonance Detection of Sn ³⁺ and Pb ³⁺ Complexes in γ -Irradiated Stannous, Plumbous, and Plumbic Salts	R. J. Booth, H. C. Starkie, and M. C. R. Symons 141
--	--

AUTHOR INDEX

Asmus, K.-D., 26	Dumont, P., 31	Kutal, C., 119	Potzinger, P., 138	Symons, M. C. R., 141
Bailar, J. C., Jr., 119	Fisher, H. F., 84	Larsen, D. W., 53	Quist, A. S., 78	Tabata, Y., 115
Barnes, H. L., 90	Fisher, J. R., 90	LoSurdo, A., 130	Rogers, F. E., 106	Takagi, H., 135
Bates, J. B., 78	Glasgow, L. C., 138	McNeel, M. L., 71	Saalfeld, F. E., 60	Takahashi, H., 110
Becker, E. D., 64, 71	Greatorex, D., 20	Meyer, J. A., 1	Setser, D. W., 1	Taniguchi, H., 135
Booth, R. J., 141	Hatano, H., 135	Miles, H. T., 64	Shelef, M., 37	Tsutsumi, K., 110
Boyd, G. E., 78	Hertzberg, M., 60	Mille, Y., 31	Shoup, R. R., 64, 71	
Brown, G. H., 99	Kadoi, H., 115	Misono, M., 44	Srinivasan, R., 15	Villiermaux, J., 31
Burrows, H. D., 20	Kemp, T. J., 20	Olfky, R. S., 60	Starkie, H. C., 141	White, G., 60
Chaudhri, S. A., 26	Kispert, L. D., 133	Oshima, K., 115	Subramanian, S., 84	Willey, D. G., 99
Clark, W. G., 1	Koob, R. D., 9	Otto, K., 37	Sun, S. F., 128	Wirth, H. E., 130
Coffman, R. E., 49		Pearson, J., 133	Sweeney, W. V., 49	Yoneda, Y., 44
de Montgolfier, P., 31				

In papers with more than one author the name of the author to whom inquiries about the paper should be addressed is marked with an asterisk in the by-line.

Rate Constants for Quenching of $N_2(A^3\Sigma_u^+)$ in Active Nitrogen

by J. A. Meyer, D. W. Setser, and W. G. Clark

Chemistry Department, Kansas State University, Manhattan, Kansas 66502 (Received June 3, 1971)

Publication costs assisted by the Petroleum Research Fund

Mercury 2537 Å emission was used to monitor the concentration of $N_2(A^3\Sigma_u^+)$ in active nitrogen at room temperature. Analysis of the quenching of the mercury emission upon the addition of reagent gases permitted the measurement of rate constants for removal of $N_2(A^3\Sigma_u^+)$ by the reagent gas relative to the rate constant for removal by nitrogen atoms. Since the nitrogen atom removal rate constant previously has been measured, the method gives absolute values for the rate constants. Eleven gases were investigated, and the magnitude of the rate constants ranged from 1.4×10^{14} cm³ mol⁻¹ sec⁻¹ for NH₃ to $<10^{10}$ cm³ mol⁻¹ sec⁻¹ for CH₄, CO₂, and H₂. These rate constants are compared with other measurements from the literature and the role of $N_2(A)$ in active nitrogen is briefly discussed.

Introduction

The role of $N_2(A^3\Sigma_u^+)$ in the reactivity of active nitrogen has been the subject of many investigations.¹⁻⁶ Direct observation of this first excited molecular state of N_2 in active nitrogen at low pressure has recently been achieved,⁷ but direct observation has not yet been used to study its chemistry. The successful use of mercury 2537 Å emission as a probe to monitor relative concentration of $N_2(A^3\Sigma_u^+)$ in active nitrogen was demonstrated recently in this laboratory¹ after other investigators²⁻⁵ had suggested the possibility. The technique is useful because mercury does not react with nitrogen atoms and the 2537 Å emission is not excited by other atomic and molecular states in active nitrogen.¹ Extremely small amounts ($<10^9$ atoms cm⁻³) of Hg can be used, and the nitrogen atom recombination processes are not affected to any significant extent by the addition of mercury. Furthermore, the small mercury concentration does not remove significant amounts of $N_2(A^3\Sigma_u^+)$. The 2537 Å mercury emission has been employed as supporting evidence for the presence of $N_2(A^3\Sigma_u^+)$ in other than active nitrogen reaction systems.⁸ However, some care must be exercised because other metastable states, for example CO($a^3\Pi$), also can excite the Hg(3F_1) state.^{8c,9}

In this paper the quenching of the mercury emission in active nitrogen by various added reagents, which do not directly react with nitrogen atoms, was studied. Since the dominant removal process of $N_2(A)$ in active nitrogen is $N + N_2(A)$, the quenching rate for added gases can be measured relative to that for nitrogen atoms. Since the nitrogen atom quenching rate con-

- (1) D. H. Stedman, J. A. Meyer, and D. W. Setser, *J. Chem. Phys.*, **48**, 4320 (1968).
- (2) W. R. Brennen and G. E. Kistiakowsky, *ibid.*, **44**, 2695 (1966).
- (3) I. M. Campbell and B. A. Thrush, *Proc. Roy. Soc., Ser. A*, **296**, 201 (1967).
- (4) B. A. Thrush, *J. Chem. Phys.*, **47**, 3691 (1967).
- (5) K. H. Becker and K. D. Bayes, *J. Phys. Chem.*, **71**, 371 (1967).
- (6) A. N. Wright and C. A. Winkler, "Active Nitrogen," Academic Press, New York, N. Y., 1963.
- (7) W. R. Brennen, R. V. Gritowski, and E. C. Shane, private communication (1971).
- (8) (a) A. Granzow, M. Z. Hoffman, N. N. Lichtin, and S. K. Wason, *J. Phys. Chem.*, **72**, 1402 (1968); (b) R. A. Young and G. A. St. John, *J. Chem. Phys.*, **48**, 395, 898, 2572 (1968); (c) C. H. Dugan, *Can. J. Chem.*, **47**, 2314 (1969); (d) J. A. Meyer and D. W. Setser, *J. Phys. Chem.*, **74**, 3452 (1970).
- (9) G. W. Taylor and D. W. Setser, *Chem. Phys. Lett.*, **8**, 51 (1971). The ratio of the NO γ - and β -band emissions excited by CO($a^3\Pi$) reported in this paper was in error because the residual nitrogen in the argon carrier resulted in conversion of some of the CO(a) to $N_2(A)$. The correct ratio of the γ - to β -band intensities is 1.0:1.3 from CO($a^3\Pi$) + NO(X).

stant has been measured,^{8b,10} absolute values for the quenching rate constants of the gases studied in this paper can be derived. Measurement of the absolute intensity of the mercury (2537 Å) emission permitted an order of magnitude estimate of the concentration of $N_2(A^3\Sigma_u^+)$ in active nitrogen.

Experimental Section

A conventional discharge-flow apparatus was used. The main tube was made from 26 mm i.d. Pyrex; the inlet jets were made from 8 mm o.d. tubing and were tapered to a 1 mm i.d. orifice. The jets were 20 cm apart and jet 6 (the mercury addition jet) was 10 cm upstream from a quartz window which was attached to the tube by epoxy cement. The inlet jets, numbered 5-1 in order of proximity to the microwave discharge, served for nitric oxide titrations and for addition of reagents. The surface of the flow tube was treated with phosphoric acid to minimize the surface combination of nitrogen atoms. The pressure could be measured at any of the jets using a silicone oil manometer. The pumping system, which gave a flow velocity of 10^3 cm/sec, consisted of a 500-l. min^{-1} pump, a 15-l. ballast volume, a large trap, and a 22-mm throttling stopcock.

Carrier gas flows were measured with a Cole-Parmer Gilmont ball-type compact flowmeter. Reagent gas flows were measured with calibrated capillary flowmeters filled with DC-704 silicone fluid and metered into the flow tube with Edwards High-Vacuum precision needle valves. Reagent gases were obtained from Matheson Co. with purities ranging from 98 to 99.9%. Each was vacuum distilled before storage in reservoir vessels. The nitric oxide was purified by repeated distillation from a liquid oxygen cooled trap to a liquid nitrogen cooled trap until the solid nitric oxide was colorless.

The discharge was excited with a Raytheon Model PGM-10 microwave power generator of 85-W maximum CW output at 2450 MHz. The power was coupled into the system with an Evenson-type cavity (Ophos Instruments) placed on a 14 mm o.d. Pyrex tube provided with forced air cooling. The discharge region was located 30 cm upstream of jet 1 and was isolated from the observation region by a Wood's horn light trap. A loose glass wool plug was placed inside the flow tube approximately 15 cm downstream of the discharge region; such a plug is claimed to remove vibrationally excited ground electronic state N_2 formed in the discharge without greatly diminishing the number of nitrogen atoms.¹¹

The mercury 2537 Å emission was observed through the quartz window with a Jarrell-Ash Czerny-Turner monochromator of 0.75-m focal length equipped with an E.M.I. 9558Q photomultiplier tube and a P.A.R. phase lock amplification system. Care must be taken

to resolve the 2537 Å mercury emission from the strong nitric oxide β - and γ -band emission that occurs with some quenching gases. We found that a scanning monochromator was essential for this purpose. The Lewis-Rayleigh afterglow was observed through appropriate filters with a 1P28 photomultiplier tube which was placed in a housing that fitted snugly over the flow tube. This allowed easy reproducibility of the geometry as the housing was moved along the flow tube for intensity measurements at different points.

The monochromator and E.M.I. 9558Q photomultiplier tube were calibrated for relative response using a calibrated tungsten filament lamp produced by Electro Optics Associates. The absolute emission intensities were measured by comparison to the air afterglow ($O + NO$) emission¹² in the same apparatus.

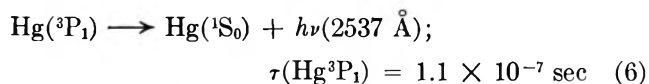
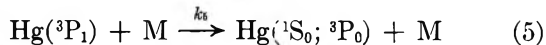
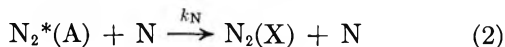
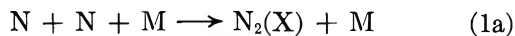
Results

Measurement of Quenching Rate Constants. A flow of active nitrogen was produced by passing approximately $400 \mu\text{mol sec}^{-1}$ of molecular nitrogen through the microwave discharge. The concentration of nitrogen atoms was varied by altering the discharge power. Absolute nitrogen atom concentrations were determined by the nitric oxide titration technique; relative nitrogen atom concentrations were found more simply by measurement of the Lewis-Rayleigh afterglow intensity,³ which is independent of pressure in the range 2-10 Torr. Mercury vapor was added to the flow of active nitrogen by metering a flow of argon or nitrogen which had been saturated with mercury vapor at room temperature. The intensity of the resulting 2537 Å mercury emission, $Hg(^3P_1-^1S_0)$, measured perpendicular to the main gas flow through a quartz window located 10 cm downstream of the mercury addition inlet. The Hg-emission intensity was independent of contact time as was shown by adding a constant flow of mercury vapor at various upstream jets and observing that the mercury-emission intensity remained constant. This experiment showed that the species responsible for excitation was being continuously generated in the active nitrogen and, even if the specie was produced directly by the discharge, the concentration was replenished by downstream processes. The kinetic dependence of the mercury emission intensity, $I_{Hg}(2537 \text{ Å})$, in active nitrogen has been shown to be first order in $[N]$, $[Hg]$, and $[M]$ in the pressure range 2.5-10 Torr.¹ The following reaction sequence provided¹ the simplest explanation of the observations

(10) J. A. Meyer, D. W. Setser, and D. H. Stedman, *J. Phys. Chem.*, **74**, 2238 (1970).

(11) (a) J. E. Morgan and H. I. Schiff, *Can. J. Chem.*, **41**, 903 (1963); (b) P. N. Clough and B. A. Thrush, *Proc. Roy. Soc., Ser. A*, **309**, 419 (1969).

(12) A. Fontijn, C. B. Meyer, and H. I. Schiff, *J. Chem. Phys.*, **40**, 64 (1964).



Undoubtedly there are steps in active nitrogen that lead to $N_2(A)$ which are more complicated than those indicated above. However, we only require that the *main* process forming $N_2(A)$ be second order in (N) and first order in pressure. Other excited states of molecular and atomic nitrogen³ are present in active nitrogen; however, as far as is known,¹⁴ none of these give 2537 Å mercury emission. Since $k_5[N_2] < \tau^{-1}(\text{Hg}, ^3P_1)$ for the pressure range of this study,¹⁵ steady-state analysis for $N_2(A)$ and $\text{Hg}(^3P_1)$ gives the following result

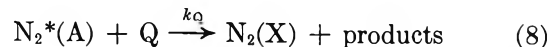
$$I_{\text{Hg}}(2537 \text{ \AA}) = \frac{k_{1b}k_{\text{Hg}}[N]^2[\text{Hg}][M]}{k_N[N] + k_w + k_{\text{Hg}}[\text{Hg}]} \quad (7)$$

This equation reduces to the observed¹ first-order dependence on $[N]$, $[\text{Hg}]$, and $[M]$ if $k_w + k_{\text{Hg}}[\text{Hg}] < k_N[N]$.

In the Appendix experiments using a clean $N_2(A)$ flow source with added Hg are described which give $k_{\text{Hg}} = 4.6 \times 10^{13} \text{ cm}^3 \text{ mol}^{-1} \text{ sec}^{-1}$. The first-order constants for removal of $N_2(A)$ by the surface of an untreated quartz flow tube were measured in this apparatus at various pressures,¹⁶ and $k_w = 120 \text{ sec}^{-1}$ at 4 Torr. The value¹⁰ of k_N is $3 \times 10^{13} \text{ cm}^3 \text{ mol}^{-1} \text{ sec}^{-1}$ at room temperature. For our experiments $[N]$ was always $> 1 \times 10^{-10} \text{ mol cm}^{-3}$. Hence, if the rate of removal of $N_2(A)$ by the wall is the same for untreated quartz (which was nearly the same as that for diffusion to the wall) and phosphoric acid poisoned Pyrex, this process will be, at least, twenty five times less important than reaction 2 for removal of N atoms. For the active nitrogen experiments described here $[\text{Hg}] \leq 2 \times 10^{-13} \text{ mol/cm}^3$; therefore, $k_{\text{Hg}}[\text{Hg}] \simeq 10 \text{ sec}^{-1}$ and this term is negligible relative to either k_w or $k_N[N]$. However, caution should be exercised to keep pressure and $[N]$ high to ensure that $k_N[N] > k_w + k_{\text{Hg}}[\text{Hg}]$.

The addition of NH_3 , N_2O , SO_2 , O_2 , CH_3OH , and CO upstream (20 cm) of the jet through which mercury was added caused strong quenching of the $\text{Hg}(2537 \text{ \AA})$ emission without a noticeable change in $[N]$. These compounds do not react with nitrogen atoms (or the rate is too slow to be detectable under our experimental conditions), but all have been suggested⁶ to react with

$N_2(A^3\Sigma_u^+)$. The relatively short radiative lifetime of $\text{Hg}(^3P_1)$ and the low concentrations of added reagents preclude the direct quenching¹⁵ of $\text{Hg}(^3P_1)$. The addition of a quenching gas was treated as another step for removal of $N_2(A^3\Sigma_u^+)$ and eq 8 must be added to the sequence of chemical reactions.



Including this step in the steady state gives the following expression

$$I_{\text{Hg}}(2537 \text{ \AA}) = \frac{k_{1b}k_{\text{Hg}}[N]^2[M][\text{Hg}]}{k_N[N] + k_Q[Q] + k_w + k_{\text{Hg}}[\text{Hg}]} \quad (9)$$

The intensity of mercury 2537 Å emission in the absence of quenching gas, Q, is denoted by $I_{\text{Hg}}^\circ(2537 \text{ \AA})$, and the intensity in the presence of Q is denoted $I_{\text{Hg}}(2537 \text{ \AA})$. Under conditions such that $k_w + k_{\text{Hg}}[\text{Hg}]$ is not important, the ratio of (7) to (9) is

$$\frac{I_{\text{Hg}}^\circ}{I_{\text{Hg}}} = 1 + \frac{k_Q[Q]}{k_N[N]} \quad (10)$$

Experiments were done at several different nitrogen atom concentrations and plots of $I_{\text{Hg}}^\circ/I_{\text{Hg}}$ against $[Q]$ were linear for each $[N]$ as shown in Figures 1-3. The

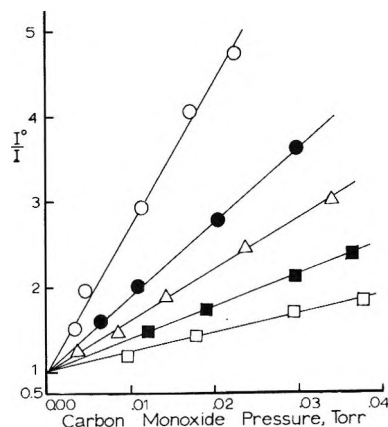


Figure 1. Quenching of mercury emission intensity by carbon monoxide for different nitrogen atom concentrations and a total pressure of 2.6 Torr; $[N]$ in units of 10^{-3} Torr: \circ , 2.6; \bullet , 5.1; \triangle , 6.8; \blacksquare , 12.2, and \square , 18.9.

(13) (a) I. M. Campbell and B. A. Thrush, *Trans. Faraday Soc.*, **65**, 32 (1969); (b) M. F. Golde and B. A. Thrush, *Chem. Phys. Lett.*, **8**, 375 (1971).

(14) It should be emphasized that we only require that the major portion of the 2537 Å emission arise from (4). Other states, for example $N_2(B)$, may excite $\text{Hg}(^3P_1)$, but as far as is currently known such states are in low concentrations. Weak emissions from higher mercury states excited by active nitrogen were reported by ref 2; however, these emissions were quenched more slowly than the 2537 Å emission with added ammonia.²

(15) R. J. Cvetanović, *Progr. React. Kinet.*, **2**, 39 (1964); the quenching collision diameter for $\text{Hg}(^3P_1)$ by N_2 is 0.2 Å.

(16) (a) J. A. Meyer, D. H. Kosterboer, and D. W. Setser, *J. Chem. Phys.*, **55**, 2084 (1971); (b) G. W. Taylor, W. G. Clark, and D. W. Setser, unpublished data. Direct monitoring of $[N_2(A)]$ by observing the Vegard-Kaplan emission along the flow tube has now been achieved.

Table I: Quenching Rate Constants for $N_2(A^3\Sigma_u^+)$, $10^{13} \text{ cm}^3 \text{ mol}^{-1} \text{ sec}^{-1}$

Q	Meyer, Setser, and Klosterboer ^f	This work ^a	Young, Black, and Slinger ^d	Callear and Wood ^e
NH ₃	9.8	10 (18) ^b	11	≤1.2
SO ₂	2.9	2.5		
C ₂ N ₂	3.4	4.1	3.4	
CH ₃ CN		1.2		
CH ₃ OH ^g		3.6 ^g		
CO				
ν = 1	1.3	{ 1.3 (1.4) ^b }	(0.15)	1.4
ν = 0	...			0.09
N ₂ O	0.86	1.2 (1.4) ^b	0.39	0.36
O ₂ ^f	0.39 ^f	0.46	0.23	0.22
H ₂	<10 ⁻³	<10 ⁻³ (no quenching)	<0.4 × 10 ⁻³	~0.18 × 10 ⁻³
CO ₂	<10 ⁻³	<10 ⁻³ (no quenching)	<1.7 × 10 ⁻³	≤0.08 × 10 ⁻³
CH ₄	<10 ⁻³	<10 ⁻³ (no quenching)	<0.4 × 10 ⁻³	≤0.1 × 10 ⁻³
NO		(6.7) ^c	(4.2) ^d	4.8

^a These values (except for NO) were measured relative to quenching of $N_2(A^3\Sigma_u^+)$ by nitrogen atoms, which has a rate constant^{8b,10} of $3 \times 10^{13} \text{ cm}^3 \text{ mol}^{-1} \text{ sec}^{-1}$. ^b These were obtained from completely separate measurements using a different flow tube and different reagent mixtures. ^c See Appendix for explanation of this measurement, which is based upon radiative lifetime of 2.1 sec and is the rate constant for excitation to the $NO(A^2\Sigma^+)$ state. ^d Rate constants in this series (R. A. Young, *et al.*, *J. Chem. Phys.*, **50**, 303 (1969)) were measured relative to the rate constant quoted for nitric oxide. A somewhat larger value may be more appropriate, see Appendix. ^e These rate constants (A. B. Callear and P. M. Wood, *Trans. Faraday Soc.*, **67**, 272 (1971)) were measured by observing the decay of $N_2(A^3\Sigma_u^+)$ for various concentrations of quenching gas. ^f These values are from ref 16a; more recent measurements,^{16b} that are thought to be superior, give a quenching rate constant for $N_2(A, \nu = 0)$ by O₂ of $2 \times 10^{12} \text{ cm}^3 \text{ mol}^{-1} \text{ sec}^{-1}$ in better agreement with A. B. Callear and P. M. Wood, *Trans. Faraday Soc.*, **67**, 272 (1971), and R. A. Young, *et al.*, *J. Chem. Phys.*, **50**, 303 (1969). ^g More recent measurements^{16b} give a quenching rate constant for CH₃OH that is about a factor of 10 lower than the value reported in this table. We suspect that the CH₃OH sample used for the experiments with active nitrogen contained impurities.

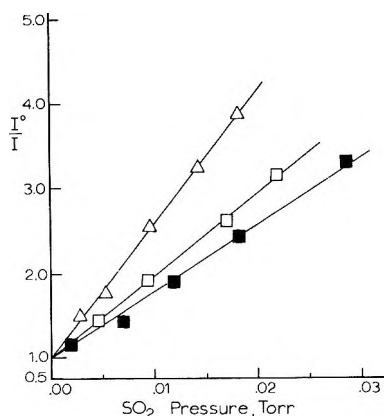


Figure 2. Quenching of mercury emission intensity by sulfur dioxide for different nitrogen atom concentrations and a total pressure of 3.0 Torr; [N] in units of 10^{-3} Torr: Δ , 8.0; \square , 15.2; and \blacksquare , 20.4.

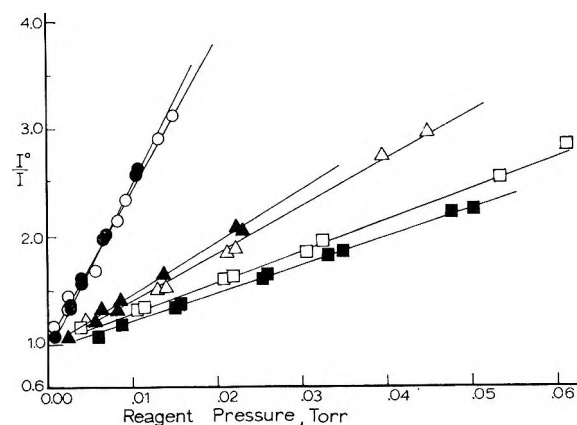


Figure 3. Quenching of mercury emission by ammonia (solid points) and nitrous oxide (open points) for different nitrogen atom concentrations at a total pressure of 3.2 Torr; [N] in units of 10^{-3} Torr: \bullet , 3.6; \blacktriangle , 10.0; \blacksquare , 22.2; Δ , 3.3; \triangle , 11.4; \square , 18.4. The pressure scale should be reduced by a factor of 10 for the ammonia data.

lines in Figures 1-3 intercept the ordinate at $I_{Hg}^{\circ}/I_{Hg} = 1$ and the slopes are $k_Q/k_N[N]$. Plots of the slopes of these lines against $[N]^{-1}$ resulted in straight line through the origin as shown in Figure 4. Slopes of lines from plots such as shown in Figure 4 give k_Q/k_N . A value^{8b,10} of $k_N = 3.0 \times 10^{13} \text{ cm}^3 \text{ mol}^{-1} \text{ sec}^{-1}$ was used to obtain the quenching rate constants tabulated in Table I. Rate constants were obtained from plots of I°/I vs. $[O_2]$ for total pressures from 2 to 10 Torr and constant [N]; these rate constants were found to be independent of pressure. Least-squares fitting of the

lines of Figure 4 indicate a standard error of $\pm 30\%$; however, systematic errors probably are greater than random ones.

For some reagents, experimental problems were encountered. Except for carbon monoxide and carbon dioxide, it was necessary to use the monochromator to scan the Hg 2537 Å line for all reagents containing oxygen. If this was not done, the close lying γ - and β -nitric oxide emission bands interfered with the mer-

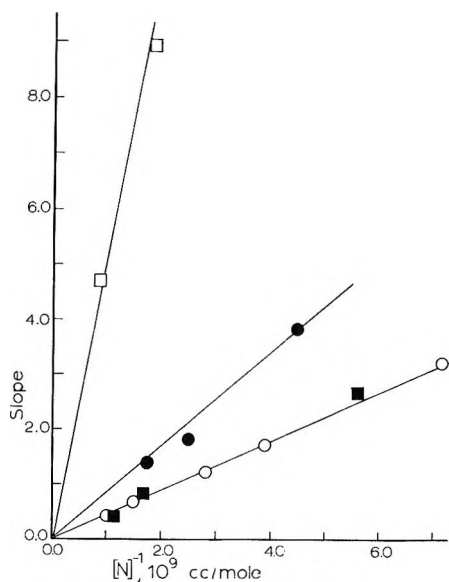


Figure 4. Plots of the slopes, in units of $10^9 \text{ cm}^3 \text{ mol}^{-1}$, of the lines from Figures 1, 2, and 3 vs. $[N]^{-1}$: \square , NH_3 ; \blacksquare , N_2O ; \bullet , SO_2 ; \circ , CO . The data for NH_3 and N_2O correspond to the second entry in Table I; the third point for NH_3 , corresponding to the lowest $[N]$ of Figure 3, is off the graph but still falls on the line.

cury emission. The quenching rate constant for cyanogen was measured, although a slow but perceptible reaction between C_2N_2 and active nitrogen¹⁷ was manifested by a dull red emission which extended the length of the flow tube. Fortunately only very small additions of C_2N_2 were necessary to produce the desired quenching of the Hg (2537 Å) emission, and these small $[\text{C}_2\text{N}_2]$ did not change $[N]$. The addition of larger amounts of C_2N_2 caused complete quenching of the yellow Lewis-Rayleigh afterglow. Plots of $I_{\text{Hg}}^\circ / I_{\text{Hg}}$ vs. $[\text{C}_2\text{N}_2]$ at various $[N]$ were linear and plots of the slopes of these lines against $[N]^{-1}$ were also linear. A value of $k_Q = 4.1 \times 10^{13} \text{ cm}^3 \text{ mol}^{-1} \text{ sec}^{-1}$ was calculated from the plot and represents, at least, an upper limit to the rate constant for C_2N_2 . Problems similar to those just described were encountered with experiments using CH_3CN as the reagent.

An attempt was made to measure the quenching rate constant for oxygen atoms with $\text{N}_2(\text{A})$; however, the high intensity β - and γ -band emission produced by $(\text{O} + \text{N} + \text{M} \rightarrow \text{NO}^* + \text{M})$ were within the spectral bandpass at 2537 Å and made the intensity measurements uncertain. This rate constant subsequently was measured by a different technique¹⁰ and found to be $1.3 \times 10^{13} \text{ cm}^3 \text{ mol}^{-1} \text{ sec}^{-1}$.

Problems were encountered which prevented the study of quenching of $\text{N}_2(\text{A})$ by HCl . The addition of small amounts of HCl to the active nitrogen gave a sharp increase (a factor of 4) in I_{Hg} and, hence, a decrease in $I_{\text{Hg}}^\circ / I_{\text{Hg}}$. At higher HCl concentrations a broad minimum in $I_{\text{Hg}}^\circ / I_{\text{Hg}}$ was reached and the Stern-Volmer plot did not rise to unity until $[\text{HCl}] \approx 5 \times$

$10^{-9} \text{ mol cm}^{-3}$. Examination of the nitrogen first positive emission downstream from the HCl inlet showed a large decrease in the Lewis-Rayleigh intensity for even small $[\text{HCl}]$. These observations imply a substantial increase in the $\text{N}_2(\text{A})$ concentration by a HCl -catalyzed nitrogen atom recombination.⁶ At sufficiently high concentrations of HCl this catalytic effect presumably is overcome by quenching of $\text{N}_2(\text{A})$ by HCl . A further observation was the appearance of a blue glow on the walls of the flow tube which were in contact with organic substances such as epoxy cement, stopcock grease, or pump oil. This indicates that HCl had a strong effect on the wall conditions in the flow tube.

Addition of large amounts of CO_2 , H_2 , and CH_4 as quenching gases produced no detectable diminution of I_{Hg} , and an upper limit of $1 \times 10^{10} \text{ cm}^3 \text{ mol}^{-1} \text{ sec}^{-1}$ was estimated for the rate constants of these compounds.

Attempts were made to cool the reaction tube in order to measure the temperature dependence of the rate constants of Table I relative to k_N . The experiments proved unsatisfactory because the vapor pressure of Hg was too low to obtain a sufficiently intense 2537 Å emission signal. Attempts to increase the signal by using an interference filter rather than a monochromator were unsatisfactory because of interference from NO emission bands.

Concentration of $\text{N}_2\text{A}(^3\Sigma_u^+)$ in Active Nitrogen. Since negligible quenching of $\text{Hg}(^3\text{P}_1)$ occurs under our experimental conditions, the absolute emission intensity from mercury is given by

$$I_{\text{Hg}}^\circ = k_{\text{Hg}}[\text{Hg}][\text{N}_2(\text{A}^3\Sigma_u^+)] \quad (11)$$

If k_{Hg} and $[\text{Hg}]$ are known, the steady-state $\text{N}_2(\text{A})$ concentration can be found from the absolute value of I_{Hg}° . Values for k_{Hg} are discussed in the Appendix; we will use the result from our laboratory, $4.6 \times 10^{13} \text{ cm}^3 \text{ mol}^{-1} \text{ sec}^{-1}$, which is probably a lower limit.

Experiments were done to show that plots of mercury emission intensity vs. added mercury were strictly linear for constant $[N]$ and constant pressure. The conversion of the mercury emission signal into an absolute photon emission rate was done by using the air afterglow calibration and the measured spectral response of the monochromator and photomultiplier tube. The slopes from the plots of I_{Hg}° vs. $[\text{Hg}]$ were used to obtain $[\text{N}_2(\text{A})]$. A typical set of data are $I_{\text{Hg}}^\circ = 4.0 \times 10^9 \text{ photons cm}^{-3} \text{ sec}^{-1}$ for $[\text{Hg}] = 1.3 \times 10^{10} \text{ atoms cm}^{-3}$, $[N] = 3.6 \times 10^{14} \text{ atoms cm}^{-3}$, and total pressure = 2.3 Torr. These data give $[\text{N}_2(\text{A})] = 4 \times 10^9 \text{ molecules cm}^{-3}$. The uncertainties in the absolute emission measurement and the value used for k_{Hg} probably introduce an uncertainty of a factor of

(17) (a) K. D. Bayes, *Can. J. Chem.*, **39**, 1071 (1961); (b) D. W. Setser and B. A. Thrush, *Proc. Roy. Soc., Ser. A*, **288**, 256 (1965); (c) D. R. Safrany and W. Jaster, *J. Phys. Chem.*, **72**, 3305 (1968).

2-4 in the measurement of $[N_2(A)]$. We previously showed that $[N_2(A)]$ depended directly upon $[N]$ and total pressure so this concentration can be scaled to the pressure and $[N]$ desired. According to our other studies^{10,16} in which Vegard-Kaplan $N_2(A^3\Sigma_u^+ - X^1\Sigma_g^+)$ emission was monitored directly, a $N_2(A)$ concentration of $\sim 5 \times 10^9$ molecules cm^{-3} should be just barely detectable. However, Vegard-Kaplan bands could not be detected even with a 30-cm path length active nitrogen. One problem is the nitric oxide β - and γ -band emission (arising from oxygen impurities) which tend to obscure the very weak Vegard-Kaplan bands. Nevertheless, the failure to observe this emission strongly suggest that $\sim 5 \times 10^9$ molecules cm^{-3} is an upper limit for $[N_2(A)]$.

Discussion

Quenching Rate Constants for $N_2(A^3\Sigma_u^+)$. The rate constants obtained in this work are compared to results of other studies in Table I. The $N_2(A)$ vibrational populations may differ for various modes of formation. If the quenching rate constants depend upon the vibrational level of $N_2(A)$, then a real difference could exist between rate constant measurements using different sources of $N_2(A)$. According to the results of Brennen and coworkers,⁷ the $N_2(A)$ in active nitrogen occupies, at least, vibrational levels 0-4. The other set¹⁶ of measurements from this laboratory were done with the metastable argon plus nitrogen discharge flow apparatus, the rate constants were measured by observing the removal of $[N_2(A)]$ in vibrational levels 0 and 1 at a fixed point as a function of added quenching gas. Callear and Wood¹⁸ used flash photosensitization of N_2 to generate $N_2(A)$ in $\nu = 0$ and 1 levels and monitored the decay in the presence of quenching gases by observing the fluorescence of $\text{Hg}(^3P_1)$ or NO γ -band emission. Young, Black, and Slanger¹⁹ generated $N_2(A)$ with an unknown vibrational distribution by photolysis of N_2O at 1470 Å and followed $[N_2(A)]$ from the NO γ -band emission intensity. Their rate constants were measured relative to the quenching rate constant for NO . The general agreement between the various studies confirms that the rate constants derived from our measurements in active nitrogen are indeed for $N_2(A)$.

Although the results show considerable scatter and special problems exist for some of the reagents, the rate constants measured in active nitrogen may have a tendency to be larger than those measured by other techniques. If this indeed proves to be true, the effect may be associated with the $N_2(A)$ vibrational distribution or with the value chosen for the reference rate constant, k_N .

The reaction between $N_2(A)$ and $\text{CO}(X)$ is known to yield $\text{CO}(a^3\Pi)$ and $N_2(X)$ ²⁰ with $\text{CO}(a)$ being formed mainly in the $\nu = 0$ level. The quenching reaction between $\text{CO}(a, \nu = 0)$ and $N_2(X)$ has a rate constant²¹

of 6×10^{12} $\text{cm}^3 \text{mol}^{-1} \text{sec}^{-1}$ and at least an appreciable fraction^{16b} of the quenching events give $N_2(A)$, which by energy balance must be in the $\nu = 0$ level. Thus any measurement of the quenching of $N_2(A^3\Sigma_u^+)$ by CO in an excess of nitrogen must take into account the reverse reaction. An additional complication is that $\text{CO}(a^3\Pi)$ reacts with nitric oxide to give γ -band emission and with Hg to give 2537 Å emission.⁹ For $N_2(A, \nu = 1)$ a rate constant near 1.4×10^{13} $\text{cm}^3 \text{mol}^{-1} \text{sec}^{-1}$ appears to be favored. The low value of the rate constant for CO found by Young, *et al.*,¹⁹ may be explained by the reaction of $\text{CO}(a^3\Pi)$ with $\text{NO}(X)$ which also gives NO γ -band excitation.⁹ In the active nitrogen experiments the removal of $\text{CO}(a^3\Pi)$ by N atoms may have prevented the reverse reaction with $N_2(X)$ from causing complications. Although the reaction rate ($k = 7 \times 10^{13}$ $\text{cm}^3 \text{mol}^{-1} \text{sec}^{-1}$) between $\text{CO}(a)$ and $\text{CO}(X)$ ²¹ is an order of magnitude faster than for $\text{CO}(a) + N_2(X)$, the former should not be a significant $\text{CO}(a)$ removal process in our active nitrogen experiments. We recently have completed independent experiments,^{16b} using the metastable argon atom flow source of $N_2(A)$, for measuring the relative rates of reaction of the $\nu = 0$ and 1 vibrational levels. Under experimental conditions such that the reverse reaction between $N_2(X)$ and $\text{CO}(a)$ was blocked, the quenching of $N_2(A, \nu = 1)$ by $\text{CO}(X)$ was five times faster than for $N_2(A, \nu = 0)$. Our results thus support the trend discovered by Callear and Wood;¹⁸ however, the rate ratios are different. We suggest that the reverse reaction between $N_2(X)$ and $\text{CO}(a)$ yielding $N_2(A, \nu = 0)$ may have influenced their measurements thus yielding too slow a quenching rate constant for the $\nu = 0$ level.

The agreement for the ammonia quenching rate constant is very favorable for all studies except that of Callear and Wood. Since a good correlation was not found between relaxation time and $[\text{NH}_3]$, complications such as flash photosensitization of the ammonia may have affected their measurements. The fast reaction between $N_2(A)$ and NH_3 is consistent with long standing observations of the very efficient quenching of particular emissions, usually attributed to some energy transfer reaction of $N_2(A)$, upon the addition of NH_3 ^{2,3,6} to active nitrogen. The quenching reaction with methane is very slow, so the interaction with NH_3 must be with the nonbonded electron pair rather than with the σ -bonded electrons. Although a triplet state for NH_3 has not yet been observed spectroscopically or by electron scattering,²² the very efficient quenching

(18) A. B. Callear and P. M. Wood, *Trans. Faraday Soc.*, **67**, 272 (1971).

(19) R. A. Young, G. Black, and T. G. Slanger, *J. Chem. Phys.*, **50**, 303 (1969).

(20) D. H. Stedman, J. A. Meyer, and D. W. Setser, *J. Amer. Chem. Soc.*, **90**, 6856 (1968).

(21) (a) G. W. Taylor and D. W. Setser, *ibid.*, **93**, 4930 (1971); (b) T. G. Slanger and G. Black, *J. Chem. Phys.*, **55**, 2164 (1971).

(22) E. N. Lassettre, A. Skerbele, M. A. Dillon, and K. J. Ross, *ibid.*, **48**, 5066 (1968).

by NH_3 implies that a triplet level must exist. The triplet corresponding to the $NH_3(\bar{A} A_2'')$ state²³ should lie well below the energy of $N_2(A)$ and is the probable primary product.

Interaction of $N_2(A)$ with C_2N_2 gives the $C_2N_2(3\Sigma_u^+ - 1\Sigma_g^+)$ emission spectrum.²⁰ In addition weak $CN(B^2\Sigma^+ - X^2\Sigma^+)$ emission was observed which implies that some dissociation of C_2N_2 occurs in the primary step followed by secondary excitation of $CN(X^1\Sigma^+)$ by $N_2(A)$. Supporting evidence is provided by other CN compounds which show the same CN emission spectrum when mixed with a flow of $N_2(A)$ molecules.^{16b} Presumably $N_2(A) + CH_3CN$ also leads to excitation of a triplet state which gives some dissociation. In active nitrogen secondary reactions between the radical fragments (CH_3 , CN , or radicals resulting from addition of these to CH_3CN) and N atoms would be rapid and explain the removal of N atoms with higher flows of substrate.

In contrast to water^{16b,24} ($k = 3.3 \pm 1.8 \times 10^{10} \text{ cm}^3 \text{ mol}^{-1} \text{ sec}^{-1}$)²⁴ methanol quenches $N_2(A)$ with a sizable rate constant, but see footnote *g* of Table I. Water has triplet states below 6 eV; however, the vertical excitation energy is in considerable excess of the minimum energy separation of the ground and triplet states.^{25c} This coupled with the fact that $N_2(A)$ vertical transition release only ~ 4.5 eV may explain the slow quenching rate for H_2O . The excited singlet states for CH_3OH lie below the corresponding states for H_2O , and the situation is probably similar for the triplet states. This energy lowering apparently increases the probability of quenching during an encounter between $N_2(A)$ and CH_3OH . The triplet states are likely to dissociate to OH and CH_3 , and in active nitrogen a rapid reaction between N atoms and these radicals would be expected. Campbell and Thrush²⁶ previously interpreted the reaction of active nitrogen with H_2O according to the mechanism just mentioned for CH_3OH . In view of the slow rate of reaction between $N_2(A, \nu = 0, 1)$ and H_2O , the excited state that initiated the reaction may have been some other N_2 electronic state or possibly higher vibrational levels of $N_2(A)$.

The rate constants for O_2 and N_2O measured in active nitrogen appear to be somewhat high. Other than possible complications associated with the presence of oxygen atoms formed as products we have no explanation for this. Campbell and Thrush²⁶ studied the recombination of nitrogen atoms in the presence of 10–50% added H_2O , N_2O , and CO_2 . They concluded that the observed decomposition of these molecules was due in large part to the $N_2(A)$ molecules formed in the three-body recombination of nitrogen atoms. In view of the wide differences in quenching rate constants for these molecules this conclusion may need revising.

Role of $N_2(A^3\Sigma_u^+)$ in Active Nitrogen. The mecha-

nism for recombination of nitrogen atoms in active nitrogen continues to be the subject of much study and discussion.^{3,26–30} Now that the rate constant for quenching of $N_2(A, \nu' = 0, 1)$ by nitrogen atoms is known,^{8b,10} the steady-state concentration of $N_2(A)$ can be estimated from models of the recombination mechanisms and compared to the estimate made from the absolute Hg-emission data. Under conditions such that reaction with the wall is negligible, the steady-state concentration of $[N_2(A)]$ is given from (1) and (2) by $[N_2(A)] = k_{1b}[N][M]/k_N$. The maximum value of k_{1b} is the total third-order recombination rate constant, which at 298°K is^{3,30} $1.38 \times 10^{15} \text{ cm}^6 \text{ mol}^{-2} \text{ sec}^{-1}$. Using $k_N = 3 \times 10^{13} \text{ mol}^{-1} \text{ cm}^3 \text{ sec}^{-1}$ gives $[N_2(A)] = 46[N][M] \text{ cm}^3 \text{ mol}^{-1}$. For the nitrogen atom concentrations and pressures quoted in the measurement of I_{Hg}^0 , this expression gives $[N_2(A)] = 2 \times 10^9 \text{ molecules cm}^{-3}$. Our experimental estimate was $4 \times 10^9 \text{ molecules cm}^{-3}$. The experimental number easily could be in error by a factor of 2. In fact, Callear and Wood's¹⁸ value for k_{Hg} ($1.7 \times 10^4 \text{ cm}^3 \text{ mol}^{-1} \text{ sec}^{-1}$) would lower the experimental estimate of $[N_2(A)]$ by a factor of 4. The important conclusion is that a very large fraction of the nitrogen atoms which recombine yield the $N_2(A^3\Sigma_u^+)$ state; *i.e.*, k_{1b} contributes very significantly to the total recombination rate constant. This conclusion was reached earlier by Campbell and Thrush³ and is not surprising since, in addition to direct combination, $N_2(B)$ molecules decay by radiation and by collision to $N_2(A)$. Noxon³¹ observed Vegard–Kaplan emission at high pressure in an ozonizer-type discharge. Although nitrogen atoms were present, a large fraction of the $N_2(A)$ may have originated from the ozonizer discharge^{8b} and comparison with the above calculations is not possible. Brennen and coworkers⁷ have recently observed Vegard–Kaplan emission at low pressures in active nitrogen and the preliminary estimate of the concentration is $\sim 10^9 \text{ molecules cm}^{-3}$.

In the absence of added reagents the above expression should provide a good estimate of the steady-state ratio of $[N_2(A)]/[N]$, which is 7.4×10^{-6} at 3 Torr of nitrogen. Since the overall atom recombination rate is similar with an argon carrier and since argon does not

(23) G. Herzberg, "Molecular Spectra and Molecular Structure. III," Van Nostrand, New York, N. Y., 1966.

(24) A. B. Callear and P. M. Wood, *Trans. Faraday Soc.*, **67**, 98 (1971).

(25) (a) R. F. Bader and R. A. Gangi, *J. Amer. Chem. Soc.*, **93**, 1831 (1971); (b) S. Trajmar, W. Williams, and A. Kuppermann, *J. Chem. Phys.*, **54**, 2274 (1971); (c) C. R. Clayton, G. A. Segal, and H. S. Taylor, *ibid.*, **54**, 5799 (1971).

(26) I. M. Campbell and E. A. Thrush, *Trans. Faraday Soc.*, **64**, 1275 (1968).

(27) S. Benson, *J. Chem. Phys.*, **48**, 1765 (1968).

(28) R. L. Brown, *ibid.*, **52**, 4604 (1970).

(29) N. Jonathan and R. Petty, *ibid.*, **50**, 3804 (1969).

(30) W. Brennen and E. C. Shane, *J. Phys. Chem.*, **75**, 1552 (1971).

(31) J. A. Noxon, *J. Chem. Phys.*, **36**, 927 (1962).

quench $N_2(A)$, a similar ratio may hold for an argon carrier. Since the rate of reaction of ground-state nitrogen atoms with many compounds is quite slow while that for $N_2(A)$ is often very fast, the primary interaction in active nitrogen often is with the $N_2(A)$ molecule. The products from this first reaction then may react with N atoms to give products which in turn continue the reaction by interacting with more N atoms or with the reagent. In this context the slow reaction of active nitrogen with saturated hydrocarbons is consistent with the slow reaction between $N_2(A)$ and these molecules and the endothermic primary abstraction reaction with N atoms. The remarkable change in reactivity of halogenated methanes in active nitrogen can be explained by their large quenching rate constants^{16b} for $N_2(A)$, which presumably is accompanied by dissociation to radicals which subsequently react with nitrogen atoms.

The mechanism for the formation of $N_2(B^3\Pi_g)$, which gives rise to the characteristic first positive emission in active nitrogen, is still the subject of controversy.²⁶⁻³⁰ The precursor states are thought to be either $N_2(^5\Sigma_g^+)$ or $N_2(A^3\Sigma_u^+, \text{high } \nu')$. The latter seems to be favored by some^{3, 28, 29} recent investigators; however, a quantitative model has not been developed. In order to fit experimental data it is necessary for the precursor state to be formed by a process that is second order in [N] and to be transferred to $N_2(B)$ by a process that is first order in pressure. Our observations that $[N_2(A)] \propto [N][M]$ does not invalidate $N_2(A)$ in high vibrational levels as a possible precursor since our measurements mainly apply to the lower vibrational levels.⁷ However, it does seem unlikely that higher vibrational levels of $N_2(A)$ will react with N atoms more slowly than with the lower levels. In fact, Brown²⁸ has found a dependence of the vibrational distribution in $N_2(B^3\Pi_g)$ upon [N], and he suggested that the reaction of N with $N_2(A, \text{high } \nu')$ might have to be considered. In a nitrogen carrier the collisional transfer rate, $N_2(A, \text{high } \nu') + N_2 \rightarrow N_2(B) + N_2$, may be faster than quenching by interaction with nitrogen atoms. However, in an argon carrier the reaction of N atoms with $N_2(A, \text{high } \nu')$ should be of some importance. Brennen and Shane³⁰ have provided an excellent summary, and we agree that the rate constants for electronic, vibrational, and rotational relaxation for several molecular nitrogen states will be necessary before details of a model for N atom combination can be evaluated. Since the predissociation of $N_2(B, \nu' = 12)$ by $N_2(^5\Sigma_g^+)$ does exist, and since the inner turning points of $N_2(A)$ and $N_2(B)$ are close together, both precursors may be important. The possible importance of other electronic states^{13, 32} of N_2 in active nitrogen should not be overlooked.³⁰

Acknowledgment. We wish to thank Professor W. R. Brennen for communicating his observations of the Vegard-Kaplan emission in active nitrogen to us and

for his generosity in permitting us to quote those observations. Acknowledgment is made to the donors of the Petroleum Research Fund, administered by the American Chemical Society, and to the National Air Pollution Control Administration, Consumer Protection and Environmental Health Service, Public Health Service for support of this work. W. G. Clark also thanks the Phillips Petroleum Co. for a fellowship.

Appendix

The rate constant for production of $Hg(^3P_1)$ from $N_2(A) + Hg(^1S_0)$ was measured using the discharge flow source of $N_2(A)$ described in ref 16. The method involved the simultaneous measurement of the Vegard-Kaplan and $Hg(^3P_1)$ emission intensities by viewing down a 10-cm path with a monochromator. The mercury was metered by using a saturated flow of argon; the concentration was always kept sufficiently small so that no reduction of $I(VK)$ could be detected. It was shown that the $Hg(^3P_1)$ emission was first order in [Hg] and $[N_2(A)]$. Since deexcitation of $Hg(^3P_1)$ is almost solely by radiation, $I(Hg) = k_{Hg}[N_2(A)][Hg]$ and since the Vegard-Kaplan emission intensity is given by $\tau^{-1}[N_2(A)]$; the ratio of the expressions gives

$$k_{Hg} = \frac{I(Hg)}{I(VK)} \frac{1}{\tau} \frac{1}{[Hg]} \quad (12)$$

The Vegard-Kaplan emission is a band system and the mercury emission is an atomic line, so it was necessary to take into account the spectral band pass of the monochromator. Since it also was desirable to estimate the concentration of $N_2(A)$, the air afterglow was employed to obtain absolute photon emission intensities, although the absolute values are not necessary to obtain the rate constant from eq 12. For a typical experiment at a total pressure of 2.6 Torr, $[Hg] = 5.8 \times 10^{-15} \text{ mol cm}^{-3}$, $I(Hg) = 3.7 \times 10^9 \text{ photons cm}^{-3} \text{ sec}^{-1}$, $I(VK) = 6.7 \times 10^9 \text{ photons cm}^{-3} \text{ sec}^{-1}$. If the most recently measured value³³ of τ (2.1 sec) is used, $k_{Hg(^3P_1)} = 4.6 \times 10^{13} \text{ cm}^3 \text{ mol}^{-1} \text{ sec}^{-1}$.

Callear and Wood¹⁸ have measured the total quenching rate constant for mercury, *i.e.*, formation of $Hg(^3P_{0,1,2})$, and found $17.4 \times 10^{13} \text{ cm}^3 \text{ mol}^{-1} \text{ sec}^{-1}$. Young and St. John^{8b} previously measured the total quenching rate and found $8.4 \times 10^{12} \text{ cm}^3 \text{ mol}^{-1} \text{ sec}^{-1}$. For both of these techniques first-order decay times were measured as a function of [Hg]. Young and St. John's data are not self-consistent. They^{8b} attempted to measure the rate constant for just $Hg(^3P_1)$ excitation under steady-state experimental conditions. Treatment of the data required the radiative lifetime of $N_2(A)$. Use of the currently accepted value³³ gives a rate constant which is about a factor of 2 below our value, but is higher than their value for the total quenching

(32) A. Fontijn and R. Ellison, *J. Chem. Phys.*, **54**, 3649 (1971).

(33) (a) D. E. Shemansky and H. P. Carleton, *ibid.*, **51**, 682 (1969);

(b) D. E. Shemansky, *ibid.*, **51**, 689 (1969).

rate constant. Most of the $\text{Hg}(^3\text{P}_2)$, if formed, is converted to the $(^3\text{P}_1)$ state by collisions¹⁸ with nitrogen. Callear and Wood¹⁸ estimated that the ratio of formation rates of $\text{Hg}(^3\text{P}_{1,2})$ and $^3\text{P}_0$ was 4:1. The evidence, thus, is for a total quenching rate constant $\geq 6 \times 10^{13} \text{ cm}^3 \text{ mol}^{-1} \text{ sec}^{-1}$. The largest potential source for error in our experiments is the $[\text{Hg}]$.

The rate of reaction of $\text{N}_2(\text{A}^3\Sigma_u^+)$ with NO was measured in the manner just described for Hg. The major reaction channel^{18,34} is formation of $\text{NO}(\text{A}^2\Sigma^+)$, which has a lifetime of $2.2 \times 10^{-7} \text{ sec}$ and is not quenched under our experimental conditions. In this case both emissions are band systems and the relative band areas, corrected for monochromator-detector sensitivity, are satisfactory for eq 12. Concentrations of NO were used such that no detectable removal of $\text{N}_2(\text{A}^3\Sigma_u^+)$ was observed. The value measured from eq 12 was $6.7 \times$

$10^{13} \text{ cm}^3 \text{ mol}^{-1} \text{ sec}^{-1}$ for a 2.1-sec radiative lifetime for $\text{N}_2(\text{A}^3\Sigma_u^+)$. Two other studies have reported total quenching rate constants for NO, ours is just for formation of $\text{NO}(\text{A}^2\Sigma^+)$, and the values of Table I are basically in satisfactory agreement. It is known³⁴ that a very small amount of $\text{NO}(\text{B})$ is formed by the reaction, but it is too small to affect our rate constant measurement. The $\text{NO}(\text{a}^4\text{II})$ state, if formed at all, makes a negligible contribution.¹⁸ Young and St. John^{8b} also reported a rate constant for formation of just $\text{NO}(\text{A})$ as well as the total quenching rate constant of Table I. If the new value for the lifetime of $\text{N}_2(\text{A})$ is used, their data, which were based upon relative emission intensities, give a rate constant for $\text{NO}(\text{A})$ formation of $1 \times 10^{14} \text{ cm}^3 \text{ mol}^{-1} \text{ sec}^{-1}$.

(34) D. H. Stedman and D. W. Setser, *Chem. Phys. Lett.*, **2**, 542 (1968).

Methylene Produced by Vacuum-Ultraviolet Photolysis. IV. Energy

Distribution for the Reaction $\text{C}_3\text{H}_8 + h\nu (123.6 \text{ nm}) = \text{CH}_2 + \text{C}_2\text{H}_6$

by R. D. Koob

Department of Chemistry, North Dakota State University, Fargo, North Dakota 58102 (Received June 9, 1971)

Publication costs assisted by the National Science Foundation

A study of the pressure dependence of ethane and the methylene insertion products formed in the photolysis of propane at 123.6 nm is reported. The cofragments formed in the primary photoreaction (1) $\text{C}_3\text{H}_8 + h\nu (123.6 \text{ nm}) \rightarrow \text{C}_2\text{H}_6 + \text{CH}_2$ ($\Delta H = 98 \text{ kcal/mol}$) must carry away 133 kcal of excess energy. The energy of each of these fragments has been estimated by observing rates of their subsequent reactions. As measured relative to an external standard, the yield of ethane does not change in the pressure range 2–760 Torr. Failure to observe any decomposition at pressures as low as 2 Torr suggests that ethane carries less than 70 kcal on the average. Isobutane formed by insertion of singlet methylene into propane decomposes with the rate constant (high pressure limit) $k_d = 1.3 \pm 0.1 \times 10^8 \text{ sec}^{-1}$. Based on a RRKM calculation, this rate corresponds to an average of 31 kcal being supplied to the insertion reaction by the methylene. The energy limits placed on the cofragments of reaction 1, $E^*(\text{C}_2\text{H}_6) < 70 \text{ kcal}$ and $E^*(\text{CH}_2) > 31 \text{ kcal}$ are not consistent with the excess energy associated with reaction 1 being statistically partitioned. Either a $\text{CH}_2(^1\text{A}_1)$ in a higher vibrational state or the production of the electronically excited $\text{CH}_2(^1\text{B}_1)$ would account for this discrepancy. Circumstantial evidence favors the latter, though any choice with the available data is speculative.

Introduction

Despite the simplicity of the molecule, the photolysis of propane has been demonstrated to give a complex product mixture. Not only does one find products rationalized on the basis of elimination of free radicals and small molecules from propane, but also a number of products which would appear to arise from secondary decomposition of the fragments produced in the primary photochemical process.

To trace successfully the course of events commencing with the absorption of a photon and terminating with a collection of thermalized products, it is necessary to have some knowledge of the nature of the excited state(s) involved in the process. Propane is known to have a strong absorption spectrum in the vacuum ultraviolet.¹ The order of magnitude of the

(1) H. Okabe and D. A. Eecker, *J. Chem. Phys.*, **39**, 2549 (1963).

extinction coefficients involved are characteristic of "allowed" transitions, and the propane excited state has been suggested to be of a σ, σ^* type.² Such a characterization is of little use in describing the structure and properties of the excited state, and there has been little agreement as to what structural changes actually occur.³ The relatively little structure found in the absorption spectrum suggests an excited state of short lifetime. That the excited state is negligibly depopulated by fluorescence has been shown by Hirayama and Lipsky.⁴ Presumably, a short lifetime is the result of a rapidly dissociating excited state. It is interesting, in this regard, that a most important feature of propane photolysis is molecular elimination rather than simple bond cleavage. These very fast molecular rearrangements are, to say the least, unusual when compared with the bulk of known chemical reactions, and the excited state producing them is worthy of more study than it has presently received. Because insufficient information about the structure of this excited state is available from direct spectral studies, we have chosen to examine in some detail the fragments it produces. In this paper we report studies of the way in which energy is distributed among two products, methylene and ethane, of a primary photolytic reaction of propane.

Experimental Section

Materials. Phillips research grade propane was used. After purification by gas chromatography using a silica gel column, impurity levels were below 5 ppm. The purified propane was dried over Drierite and vacuum distilled to a storage bulb. The oxygen was Linde CP and the helium was Air Reduction Co. medical grade. Both were used without further purification.

Lamps and Cells. A krypton resonance lamp, similar to those described by Ausloos and Lias,⁵ was used for the photolysis. The lamp was filled on a mercury-free vacuum line capable of achieving pressures less than 1×10^{-6} Torr (Veeco discharge gauge). The lamp was gettered with a titanium gettering assembly. The chromatic purity was greater than 98% in the region between 105 and 165 nm (McPherson 0.3-m vacuum monochromator). MgF_2 windows were used for the lamp. The light intensity, calculated from the yield of acetylene from the photolysis of ethylene,⁶ was $1.9 \pm 0.1 \times 10^{14}$ quanta/sec.

A "T" shaped lamp with windows at each end of the crossbar was used to study the photolysis. Each window looked into individual sample cells. Each cell had a 2.5 cm i.d. with a path length of 2.5 cm. The ratio of light intensities entering each of the two cells was constant over the course of the investigation. Thus, one cell with constant sample conditions was used as an external standard to which runs made in the other cell could be compared.

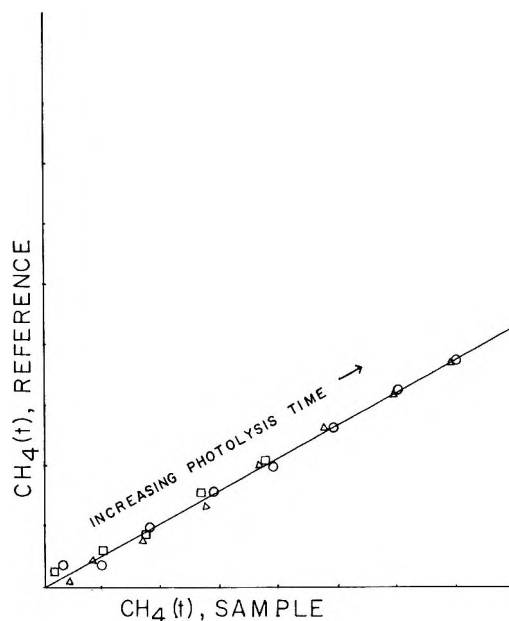


Figure 1. The yields of methane, arbitrary units, from the sample and reference cells of the apparatus described in the Experimental Section. The slope of this plot is the ratio of light intensity entering each of the two cells and is equal to 0.55 ± 0.03 . The absolute value of methane yield increases with photolysis time, but the ratio remains the same. Similarly the ratio of yields is pressure independent. \square , 20 Torr; \blacktriangle , 100 Torr; \circ , 300 Torr.

The yield of methane from the photolysis of oxygen-scavenged propane at a pressure of 20 Torr was used as the external standard. Figure 1 demonstrates the reliability of the technique under a variety of experimental conditions.

All photolyses were conducted with 5% oxygen added to scavenge free radicals and triplet methylene. No products which could be ascribed to these species were found. In all experiments, photolysis was carried to less than 0.1% conversion of parent into product. All analyses were done by gas chromatography (FID) on a 25 ft, 0.25 in. o.d., 35% (w/w) squalane column maintained at room temperature.

Results

The pressure dependence of the relative amounts of ethane, isobutane, and *n*-butane is given in Table I. The yields are relative to the external standard. Each value in Table I is an average of three or more separate experiments. An important feature is the lack of any pressure effect on the yield of ethane. Within ex-

(2) J. Calvert and J. Pitts, Jr., "Photochemistry," Wiley, New York, N. Y., 1966, p 493.

(3) (a) E. N. Lassettre, A. Skerbele, and M. A. Dillon, *J. Chem. Phys.*, **49**, 2382 (1968); (b) J. W. Raymonda and W. T. Simpson, *ibid.*, **47**, 430 (1967).

(4) F. Hirayama and S. Lipsky, *ibid.*, **51**, 3616 (1969).

(5) P. Ausloos and S. G. Lias, *Radiat. Res. Rev.*, **1**, 75 (1968).

(6) S. G. Lias, G. J. Collin, R. E. Rebert, and P. Ausloos, *J. Chem. Phys.*, **52**, 1841 (1970).

perimental error, the ratio of ethane to external standard is constant over the pressure range 2 to 760 Torr. In contrast, the yields of isobutane and *n*-butane increase quite strongly with increasing pressure.

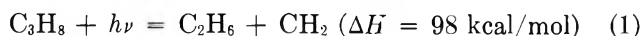
Table I: Variation of Relative Product Yields with Total Pressure^a

Pressure, Torr	[C ₂ H ₆]	[<i>i</i> -C ₄ H ₁₀]	[<i>n</i> -C ₄ H ₁₀]
2	2.26	Nd ^c	Nd
10	2.16	0.206	0.645
20	2.30	0.299	0.827
20 ^b	2.29	0.274	0.715
50	2.25	0.331	0.860
100	2.26	0.364	0.904
380	2.28	0.403	0.966
760	2.25	0.382	0.970
	Av	2.24 ± 0.04	

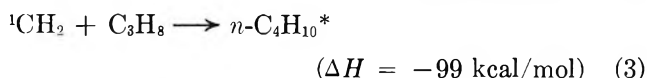
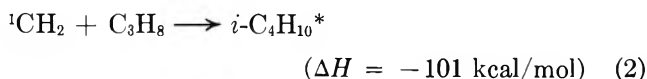
^a Photolysis of propane at 123.6 nm. ^b 1 atm of He added. ^c Nd, not determined.

Discussion

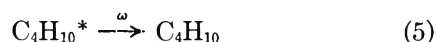
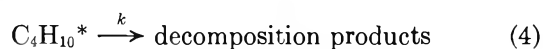
Methylene is produced in the primary photochemical process



The only ethanes obtained in a mixture of C₃D₆ + C₃H₈ + NO photolyzed at 147.0 and 123.6 nm are C₂D₆ + C₂H₆.⁷ This is interpreted as indicating that reaction 1 is the only source of ethane in the photolysis of scavenged propane. The mass balance of eq 1 has been discussed extensively in a previous paper.⁸ Even if all methylenes produced in reaction 1 are singlet, collisional conversion into triplet methylene is competitive with insertion and a number of the methylenes will not be observed as insertion product. However, as triplet methylene will be removed by the oxygen,⁹ one need consider only the reactions of singlet methylene. The insertion reactions of singlet methylene are given by reactions 2 and 3. An asterisk denotes vibrational excitation.



The butanes formed in reactions 2 and 3 can undergo unimolecular decomposition *via* reaction 4 or collisional stabilization *via* reaction 5



Assuming steady-state conditions, it is easily shown

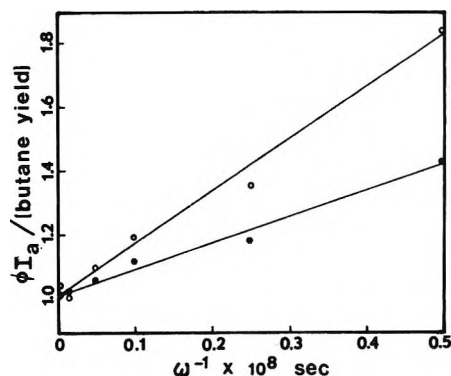


Figure 2. ϕI_a /[butane yield] vs. ω^{-1} : O, isobutane; ●, *n*-butane; and ω , collision frequency. The collision frequency of C₄H₁₀^{*}, ω , has been calculated with the following collision diameters: *i*-C₄H₁₀, 5.82 Å; *n*-C₄H₁₀, 5.87 Å; and C₃H₈, 5.24 Å.

that the yield of a butane will follow the kinetic rate equation, $d[\text{C}_4\text{H}_{10}]/dt = \phi I_a \omega / (\omega + k_4)$. ϕ is the apparent quantum yield, I_a is absorbed light intensity, calculated from the yield of standards, and ω is the rate of collisional deactivation of C₄H₁₀^{*}, assuming unit efficiency and the collisional cross sections given in Figure 2. This may be rearranged to give

$$\phi I_a / \text{yield} = 1 + k_4 / \omega \quad (6)$$

A plot of $\phi I_a / \text{yield}$ vs. ω^{-1} would be expected to be linear with a slope equal to the observed unimolecular rate constant. Figure 2 is a plot of $\phi I_a / [i\text{-C}_4\text{H}_{10}]$ and $\phi I_a / [n\text{-C}_4\text{H}_{10}]$ vs. ω^{-1} . A least-squares treatment of the data gives a unimolecular rate constant of $1.3 \pm 0.1 \times 10^8 \text{ sec}^{-1}$ for isobutane and $6.6 \pm 0.4 \times 10^7 \text{ sec}^{-1}$ for *n*-butane.

In general, at low pressures deviations from linearity for plots of data according to eq 6 may be found. This deviation is predicted by RRKM theory and may reflect either the distribution of energies in the dissociating molecules or inefficiency in energy removal from a reactive molecule by a colliding partner.¹⁰ At higher pressures, the apparent rate constant (experimental value k_4) is equal to the mean of microscopic rate constants for the reaction.¹⁰ It is this mean which is of interest to us in this case. If the low pressure point, 10 Torr, of Figure 2 is not included, a least-squares treatment of the remaining data points gives values for k_4 which fall within the error range quoted above for the slope determined using all of the points. The significance of the lowest pressure point, then, is that it indicates that deviations from linearity are not important yet at 10 Torr. It is, however, the higher

(7) P. Ausloos, S. G. Lias, and I. B. Sandoval, *Discuss. Faraday Soc.*, **36**, 66 (1963).

(8) A. K. Dhingra and R. D. Koob, *J. Phys. Chem.*, **74**, 4490 (1970).

(9) R. L. Russell and F. S. Fowland, *J. Amer. Chem. Soc.*, **90**, 1671 (1968).

(10) B. S. Rabinovitch and D. W. Setser, *Advan. Photochem.*, **3**, 1 (1964).

pressure points which determine the value of the apparent rate constants used in the following discussion.

The total amount of energy to be distributed among the degrees of freedom of the products of reaction 1 is the sum of the absorbed light energy and the thermal energy of the propane less the endothermicity of reaction 1. The heats of formation of propane and ethane have been established at -24.82 and -20.24 kcal/mol, respectively, at 298°K .¹¹ The heat of formation of methylene has been estimated to be 93.7 kcal/mol at 298°K .¹² Therefore, reaction 1 is approximately 98 kcal/mol endothermic at 298°K . The resonance line of krypton at 123.6 nm corresponds to 231 kcal/einstein. Thus, there is approximately 133 kcal/mol to be distributed among the degrees of freedom of the ethane and the methylene. This excess energy may be carried away as electronic, vibrational, rotational, or translational excitation, or various combinations of these. Precisely what combinations of the various types of energy will appear depends on the potential surface upon which reaction 1 occurs. Of course, the shape of this surface is not known, so no *a priori* predictions can be made as to the energy content of the fragments produced in reaction 1. It is our intent to examine a number of models for energy partitioning and note those which are and are not consistent with the experimental observations.

As a first model, we examine the behavior predicted if all energy in excess of the 98 kcal required for the dissociation of propane into ethane and methylene is statistically partitioned over *nonelectronic* degrees of freedom of the dissociation products. The examination must be carried out in two parts since there are two products. Ethane is considered first.

If we treat the energy level spacings of the product molecules as overtones and combinations of the ground-state species, the fraction of ethane molecules having an energy E out of a total available energy E_T may be estimated by

$$f(E) = \frac{D_E(E)D_R(E_T - E)}{\sum D_E(E_i)D_R(E_T - E_i)} \quad (7)$$

where $D_E(E)$ and $D_R(E_T - E)$ are the energy densities of the ethane and "remainder" species, respectively, and the methylene vibrational frequencies and the external degrees of freedom are identified with the "remainder."¹³ E_T is the total amount of excess energy in reaction 1. The energy distribution is shown by the broken curve in Figure 3. If $E_T = 133$ kcal/mol, the average energy in vibrational modes of ethane is 86.6 kcal/mol according to this distribution.

The activation energy required for the decomposition of ethane is 85 kcal.¹⁴ The statistical considerations above predict an *average* energy of ethane greater than the E_{act} . If there were statistical distribution of all available energy in excess of the endothermicity of reaction 1, ethane would show a yield decrease with

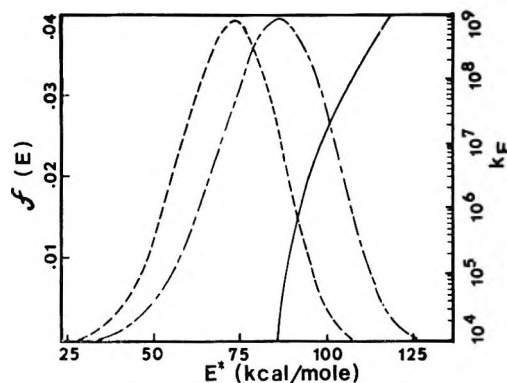


Figure 3. Energy distribution, $f(E)$, assuming a statistical model: ---, $E_T = 133$ kcal/mol; - - -, $E_T = 113$ kcal/mol. Variation of k_E , —, with E^* for the semirigid ethane activated complex.

pressure decrease in the range studied. It has already been noted that the ethane yield is pressure independent in this range. Clearly the assumption of statistical distribution of all energy in excess of the enthalpy change of reaction 1 is not a good one. Distribution functions other than the one used here may be chosen; however, the end result will be qualitatively similar for any reasonable function. Similar treatment for methylene predicts that it would carry approximately 16 kcal as vibrational energy if statistical partitioning occurred under similar assumptions.

An estimate of the energy actually carried by the methylene may be made using the formalisms of the RRKM theory of unimolecular reactions. The general methods of application of the RRKM formulations have been discussed in a review by Rabinovitch and Setser.¹⁰ We calculate microscopic unimolecular rate constants, k_E using these methods and using the approximation of Whitten and Rabinovitch¹⁵ for determining the necessary densities and sum of energy eigenstates of the molecules and the activated complex. The vibrational frequency assignments for the molecule and the activated complex are those of Johnson, Hase, and Simons for isobutane¹⁶ and Rabinovitch and Setser¹⁰ for *n*-butane. The critical energy for the dissociation of both butanes was assumed to be 81 kcal/mol. A plot of k_E vs. E^* for the isobutane and *n*-butane activated complex models is given in Figure

(11) F. D. Rossini, "Selected Values of Physical and Thermodynamic Properties of Hydrocarbons and Related Compounds," Carnegie Press, Pittsburgh, Pa., 1953.

(12) D. D. Wagman, W. H. Evans, V. B. Parker, I. Halow, S. M. Bailey, and R. H. Schumm, *Nat. Bur. Stand. (U. S.), Circ.*, 270 (1968).

(13) R. J. Campbell and E. W. Schlag, *J. Amer. Chem. Soc.*, 89, 5103 (1967).

(14) R. A. Marcus, *J. Chem. Phys.*, 20, 364 (1952).

(15) G. Z. Whitten and B. S. Rabinovitch, *ibid.*, 38, 2466 (1963); 41, 1883 (1964).

(16) R. L. Johnson, W. L. Hase, and J. W. Simons, *ibid.*, 52, 3911 (1970).

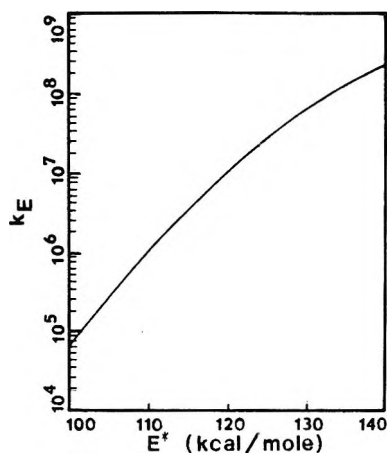


Figure 4. Plot of calculated values of k_E vs. E^* , the excitation energy of the butane molecule. Curves for isobutane and *n*-butane are superimposable.

4. Within the accuracy required by this treatment, the two curves are superimposable.

The observed rate constant, k_a , is related to the microscopic rate constant k_E by the expression¹⁰

$$k_a = \omega \frac{\sum_E \frac{k_E f(E)}{k_E + \omega}}{\sum_E \frac{\omega f(E)}{k_E + \omega}}$$

where $f(E)$ is the energy distribution function of the reacting species. Rabinovitch and Setser have shown that this expression reduces to eq 8 for high pressures of an efficient deactivator

$$k_{a\infty} = \langle k_E \rangle \quad (8)$$

That is, the apparent rate constant, $k_{a\infty}$, is equal to the average of the microscopic rate constant, k_E . When the observed dissociation constants (average microscopic rate constants) are placed on the calculated curve for k_E , they correspond to total energies of 136 and 132 kcal/mol for isobutane and *n*-butane, respectively.

The methylene insertions, reactions 2 and 3, into propane are 101 and 99 kcal/mol exothermic, respectively. The butane formed will carry this energy plus whatever energy is brought into the reaction complex by the reactants. Only thermal energy will be contributed by the propane (~ 3 kcal), and any significant energy in excess of the exothermicity of the reaction must be ascribed to the methylene. The role of translational energy of the methylene has been discussed previously.⁸ The pertinent conclusion is that the methylene produced in reaction 1 undergoes translational equilibration prior to insertion. Thus, the rate of unimolecular dissociation of the butane will depend on the internal energy of the methylene. Subtracting the exothermicity of the insertion reaction, this corresponds to an average of approximately 31

kcal/mol being supplied by the methylene. This is considerably greater than the 16 kcal predicted by a simple statistical model.

The yield of ethane will also follow the rate expression given in eq 6. Using the distribution function calculated for ethane from eq 7 and assuming a "loose" complex for the dissociating ethane (C_2 complex 3 in ref 10), one calculates that at 2 Torr $k_a = 1.9 \times 10^7$ sec⁻¹. Such an apparent rate constant would require that greater than 40% of the ethane from reaction 1 would dissociate at a pressure of 2 Torr. That is clearly inconsistent with our experimental determination that no dissociation occurs. A calculated apparent rate constant consistent with the experimental results ($\leq 2 \times 10^6$ sec⁻¹) may be obtained by shifting the distribution function such that the average energy of ethane is approximately 70 kcal/mol. This new k_a predicts 10% dissociation of ethane at 2 Torr and corresponds to the upper limit of our confidence in the experimental results.

The calculated apparent rate constants are sensitive to the choice of models for the determination of $k_E(E)$ as well as $f(E)$. However, it does appear that ethane carries less energy than would be predicted by the statistical distribution of the excess energy of reaction 1, assuming the excess energy corresponds to the difference between the energy of the incident photon and the endothermicity of the reaction.

While estimates of the average energies of ethane and methylene both are based on a RRKM model and are subject to the limitations of the assumptions of that model, the observed reaction rates, or lack of reaction, are independent observations and calculations of the energy of each fragment are independent.

The assignment of ≤ 70 kcal/mol to vibrational modes of ethane, 31 kcal/mol of internal energy to methylene, and the remainder to external degrees of freedom is consistent with our experimental observations. This assignment is clearly not consistent with a statistical model for partitioning the energy excess. Thus, other possible models must be examined.

A second possible model for the energy partitioning in reaction 1 is making an assumption that the potential energy surface for the dissociation from excited propane requires that excess vibrational energy be deposited in $CH_2(^1A_1)$. An average population peaking near the third lowest state for a symmetric stretch would provide enough energy in the methylene to account for our observations if the fundamental frequency for a symmetric stretch in CH_2 is about 3000 cm⁻¹. One may argue that the rather widely separated vibrational states for a small species such as methylene would not allow rapid relaxation of vibrational energies to the ground state. There is precedent for such a model where a particular fragment is distorted in its bound form from the equilibrium geometry of its unbound form.¹⁷ Since the geometry of excited propane is not

presently known, one can make no statement as to the necessity of geometric relaxation of the expelled methylene fragment.

As a third model, assume that the methylene is formed in the 1B_1 state. A state which is approximately 20 kcal/mol¹⁸ above the lowest singlet state, 1A_1 . E_T , the maximum available energy to the ethane eq 7, is then reduced to $231 - 98 - 20 = 113$ kcal/mol instead of the original estimate of 133 kcal/mol. The statistical distribution with a maximum E of 113 kcal/mol is shown as a dashed line in Figure 3. The average energy of the ethane now would be 73 kcal/mol and k_a (calcd) would be only slightly greater than 2×10^6 sec⁻¹. This agrees very well with the upper limits imposed upon the energy of the ethane. Further, the methylene would have an average vibrational energy of 13 kcal/mol. Thus, the methylene would bring to the insertion reaction 13 kcal of vibrational energy plus 20 kcal of electronic energy for a total of 33 kcal of internal energy. A similar line of reasoning applied to the methylene produced in the photolysis of cyclopropane¹⁹ leads to a predicted internal energy content of 29 kcal/mol in excellent agreement with the value of 31 kcal/mol calculated from the observed dissociation rates of insertion products.

In addition to the similarity of the energy carried by methylenes from both propane and cyclopropane, it is of interest to note that Lindholm, in a recent calculation of the properties of the excited states of methylene, predicts that in all possible cases for which excited methane dissociates to methylene and hydro-

gen, the resultant methylene will be produced in an upper singlet state.²⁰ While these calculations have not been formally extended to propane, the implication of the findings of Lindholm for the data reported here are clear.

Thus, while our data do not distinguish between mechanisms for the deposition of excess energy in the methylene fragment produced by the photolysis of propane, circumstantial evidence available at this time suggests that electronically excited methylene may be produced. Regardless of the mechanism, it is quite clear that, for the primary photolytic decomposition of propane to produce ethane and methylene, energy in excess of the endothermicity of the reaction is not statistically distributed between the fragments. Since other photoinduced reactions may occur by a mechanism similar to the reaction discussed here, it would not be wise to *a priori* assume statistical partitioning in any of the primary chemical steps found for the photolysis of propane.

Acknowledgment. The authors acknowledge with pleasure the support of the National Science Foundation during the course of the research reported here.

(17) F. H. Dorer, E. Brown, J. Do, and R. Kees, *J. Phys. Chem.*, **75**, 1640 (1971); F. H. Dorer, *ibid.*, **73**, 3109 (1969).

(18) G. Herzberg, "Electronic Spectra of Polyatomic Molecules," Van Nostrand, Princeton, N. J., 1967, p 583.

(19) A. K. Dhingra, J. H. Vorachek, and R. D. Koob, *Chem. Phys. Lett.*, **9**, 17 (1971).

(20) E. Lindholm, *Ark. Fysik*, **37**, 37 (1968).

Photochemical Addition of Benzene to Bicyclo[2.2.1]hept-2-ene (Norbornene)

by R. Srinivasan

IBM Thomas J. Watson Research Center, Yorktown Heights, New York 10598 (Received June 14, 1971)

Publication costs assisted by International Business Machines Corporation

Solutions of norbornene in benzene, on irradiation at 253.7 nm, yielded the two dimers of norbornene reported previously⁶ as well as two 1,3 adducts of benzene to the olefin. These adducts were the only significant products when the reaction was carried out at high (~90%) concentrations of norbornene. The quantum yield for the addition (to give either adduct) increased with increasing concentration, the values being 0.27 and 0.05 in 8 M solution. The ratio of the adducts seemed invariant with experimental conditions. The adducts are believed to be isomeric pentacyclo[8.2.1.0^{2,9}.0^{3,5}.0^{4,8}]tridec-6-enes. The minor adduct, since it is quantitatively transformed to the major adduct on heating to 280°, probably is the more strained 2,9-endo (with respect to the benzene), exo (with respect to the norbornene) isomer while the major adduct is the 2,9-exo, endo compound. Quantum yield data for the dimerization reaction were also obtained. The implication of the addition to the kinetics and stereochemistry of the sensitized dimerization is discussed.

Introduction

The first report by Wilzbach and Kaplan^{1a} on the photochemical 1,3 addition of benzene to olefins has been followed by a number of others¹⁻⁵ which have demonstrated the generality of this reaction with respect to a variety of linear and cyclic olefins. In some systems, 1,2^{1c} and 1,4 additions^{1c,5} have also been observed. From theoretical considerations^{2b,d} and some quantitative studies,^{1b,c,4,5} it has been concluded that all of these additions probably originate from the singlet (¹B_{2u}) state of benzene. Detailed quantitative studies have so far been reported only on the benzene-2-butene⁴ and the benzene-cyclobutene⁵ systems.

In this study the photochemical 1,3 addition of benzene to norbornene was investigated. Apart from the general need to obtain quantitative data on the addition reactions in a variety of systems, there are two features of interest in the use of norbornene as the olefin. Earlier work⁶ has shown that norbornene can be photodimerized to give two products by the use of benzene as a sensitizer.⁷ This process is believed to involve the triplet of the olefin that is formed by the transfer of energy from triplet benzene. Quantitative studies on the formation of the dimers and adducts would obviously provide a means to examine the competition between the reactions from the excited singlet and triplet states of benzene assuming that the photoaddition proceeded from the upper singlet as was found to be the case in other work.^{1b,4,5}

A second aspect is the stereochemistry of the adduct(s). To date, the only system in which the stereochemistry of the 1,3 addition has been established from chemical evidence is the benzene-cyclobutene

system. For the products from the *cis*-2-butene-benzene system, the stereochemistry that was assigned (endo for the major product) on the basis of the nmr spectrum^{1a} was disputed.⁴ It was felt that the use of the bulky norbornene ring system as the olefin may give a strong, directive effect to the addition. Further, the establishment of the stereochemistry of the addition in this instance was expected to throw more light on the mechanism of the sensitized dimerization.

Experimental Section

Materials. Norbornene of over 99% purity was obtained from the Chemical Samples Co., Columbus, Ohio. The traces of impurities that it was found to contain were stable to photolysis. The material was used without further purification. Research grade benzene was used as obtained.

The apparatus that was used has been described.⁵

(1) (a) K. E. Wilzbach and L. Kaplan, *J. Amer. Chem. Soc.*, **88**, 2066 (1966); (b) K. E. Wilzbach, A. L. Harkness, and L. Kaplan, *ibid.*, **90**, 1116 (1968); (c) K. E. Wilzbach and L. Kaplan, *ibid.*, **93**, 2073 (1971). The author wishes to thank Drs. Wilzbach and Kaplan for sending him a preprint of this communication.

(2) (a) D. Bryce-Smith, A. Gilbert, and B. H. Orger, *Chem. Commun.*, 512 (1966); (b) D. Bryce-Smith and H. C. Longuet-Higgins, *ibid.*, 593 (1966); (c) D. Bryce-Smith, *Pure Appl. Chem.*, **16**, 47 (1968); (d) D. Bryce-Smith, *Chem. Commun.*, 806 (1969).

(3) (a) K. Koltzenburg and K. Kraft, *Tetrahedron Lett.*, 389 (1966); (b) K. Kraft, Doctoral Dissertation, University of Bonn, 1968.

(4) A. Morikawa, S. Brownstein, and R. J. Cvetanović, *J. Amer. Chem. Soc.*, **92**, 1471 (1970).

(5) R. Srinivasan, *IBM J. Res. Develop.*, **15**, 34 (1971).

(6) (a) D. R. Arnold, D. J. Trecker, and E. B. Whipple, *J. Amer. Chem. Soc.*, **87**, 2596 (1965); (b) D. R. Arnold and V. Y. Abraitys, *Mol. Photochem.*, **2**, 27 (1970).

(7) This study^{6b} mentions that adducts are formed between the sensitizer and the olefin, but there was no information about their identity.

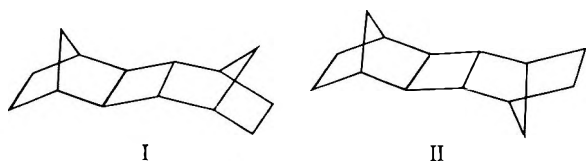
The procedure was similar to the one used earlier⁵ except that the relatively low volatility of the olefin made it unnecessary to use an internal reference for quantitative analysis by vapor phase chromatography. All of the quantitative data (except where noted) were obtained on samples which were degassed at a pressure of 0.1 μ and sealed.

Pure samples of the two adducts were prepared by the irradiation at 253.7 nm of a 10% solution of benzene in norbornene. When nearly all of the benzene had been photolyzed, the solution was distilled first at 1 atm to remove the unreacted norbornene, and then at 1 Torr to give a mixture (60% yield based on norbornene) of adducts of 90% purity. The principal impurity was the endo-trans-exo dimer of norbornene. Further purification and separation of the pure adducts was achieved by gas chromatography.

Anal. Calcd for $C_{13}H_{16}$: C, 90.61; H, 9.36. Found: adduct 1: C, 90.43; H, 9.48; adduct 2: C, 90.35; H, 9.66.

Results

Irradiation of solutions of norbornene in benzene at 253.7 nm gave the two dimers of norbornene (I

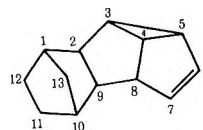


and II) reported previously⁶ as well as two other compounds which analyzed for 1:1 adducts of benzene to norbornene.⁸ Their mass spectra also corresponded to the molecular formula $C_{13}H_{16}$. Both had ultraviolet absorption maxima at 220–221 nm ($\epsilon_{\max}^{\text{EtOH}} \sim 2600$). The infrared spectra, in both instances, exhibited absorptions at 3050 and 1600 cm^{-1} , which could be attributed to a double bond in a cyclopentane ring. Their nmr spectra showed two olefinic protons centered at 5.4 and 5.7 δ , respectively, in the two compounds. Further evidence for the presence of one double bond in each of these compounds was obtained by hydrogenation (separately) at 400 Torr with hydrogen in the presence of Adam's catalyst when each gave a product with the molecular formula $C_{13}H_{18}$. The latter showed no evidence of unsaturation in their spectra.

These data indicate that both photoadducts are pentacyclic in nature and contain one double bond each. The presence of the ultraviolet maxima is difficult to explain except on the basis of a vinylcyclopropane chromophore. Wilzbach and Kaplan have shown^{1a} that this ultraviolet absorption is characteristic of the 1,3 photoadducts of benzene to many olefins. Additional evidence for the presence of a cyclopropane ring was obtained when continued catalytic hydrogenation of the $C_{13}H_{16}$ product mentioned above

at 400 Torr resulted in the smooth uptake of a second mole of hydrogen to give a $C_{13}H_{20}$ compound.

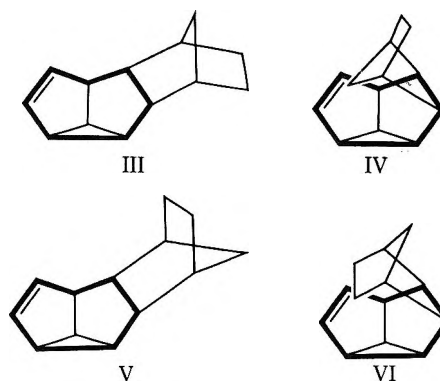
The olefins to which benzene is known to undergo photoaddition include propylene,^{1a} 2-butenes,^{1a,4} tetramethylethylene,^{1a} cyclobutene,⁵ cyclopentene,^{1a} cycloheptene,⁹ and cyclooctene.^{2c} In all of these cases, the mode of addition is predominantly (>90%) 1,3 only. It seems reasonable to expect that benzene would add similarly to norbornene, and the products would be pentacyclo[8.2.1.0^{2,9}.0^{3,5}.0^{4,8}]tridec-6-enes. The nmr



spectra of the adducts lent further support for this formulation. Both adducts gave rise to very similar nmr spectra which consisted of two olefinic protons and complex absorptions from 3.1 to 0.9 δ (major adduct) and 2.8 to 0.9 δ (minor adduct). From the nmr spectrum of the photoadducts of perdeuteriobenzene to norbornene, it was possible to identify the chemical shifts of the protons which were originally attached to the benzene ring. These were as follows: major adduct: δ 5.35 (2H, broad singlet); 2.85 (1H, doublet); 2.32 (1H, quartet); ca. 1.4 (2H, obscured by norbornane protons); minor adduct: δ 5.65 (1H, doublet of doublets); 5.45 (1H, doublet of doublets); 3.16 (1H, triplet); 2.75 (1H, triplet); 1.2 (2H, obscured by norbornane protons).

The distribution and chemical shifts displayed by the protons in both spectra are strikingly similar to the nmr spectra of the other known^{1a,4,5} 1,3 adducts of benzene to olefins. Some attempts were made to study the coupling patterns among the protons by selective decoupling. These were necessarily incomplete because of the masking effect of the protons attached to the norbornane skeleton but the coupling constants correlated well with earlier data.^{1a}

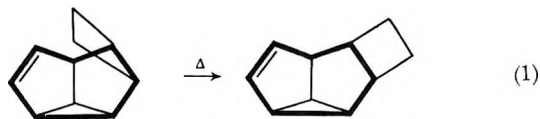
The stereochemistry of these adducts was deduced in the following way



(8) Other adducts of benzene to norbornene, if formed in this reaction, can be estimated to be less than 1% of the major adduct.

(9) R. Srinivasan, unpublished work.

Of the four 1,3 adducts that can be formed¹⁰ III and IV are interconvertible by breaking and reforming the 2,9 bond. V and VI form another such pair. Such reactions would be similar to the thermal transformation (reaction 1) of the endo-1,3 adduct of benzene to cyclobutene to the exo adduct.¹¹ A sample of the



minor adduct when heated to 280° for 20 min in a sealed tube was quantitatively transformed to the major adduct as shown by the retention time of the product and its infrared and nmr spectra. The major adduct was found to be stable under these conditions, although it underwent fragmentation at a higher (320°) temperature. Evidently, the two adducts that were obtained formed one of the pairs mentioned before.¹² The major adduct may be III or IV and there is little to choose between the two in terms of structural stability. Of the two possible structures, IV and VI for the minor adduct, molecular models show that IV should be significantly less strained than VI. Thus, in IV, the distance between the centers of C₇ and C₁₃ is 2.5 Å and between C₆ and C₁₂ is 2.3 Å. In VI, the distance between the centers of C₇ and C₁₁ is 1.9 Å and between C₆ and C₁₂ is 2.3 Å. Since the single bond distance between two carbons is only 1.54 Å and none of these pairs of carbon atoms is bonded, it is evident that VI would be much more strained than IV. The rigid, cage-like structures of both molecules would not allow any significant relief of this crowding by the distortion of the carbon skeleton. The closest approach between hydrogen atoms is more difficult to estimate from molecular models since CCH angles can undergo considerable distortion to avoid crowding between neighboring atoms. But the minimum distances between the centers of such neighboring hydrogen atoms in structures IV and VI (according to models) may be indicative of the distortion of the CCH angles necessary. These values in IV and VI are 2.0 and 1.0 Å, respectively. It seems therefore likely that IV may be the correct representation of the minor product in which case the major product would have structure III. According to the convention used in describing the 1,3 adducts of benzene^{1a} and the derivatives of norbornene, III and IV are the 2,9-exo,endo and 2,9-endo,exo structures, respectively.

The formation of the adducts and the dimers is shown as a function of time in Figure 1. Since the rates of formation of all four of these products were time dependent, only data obtained at conversions of 5% or less were used to calculate the quantum yields.

Quantum yields for the formation of the adducts and the dimers as a function of concentration are

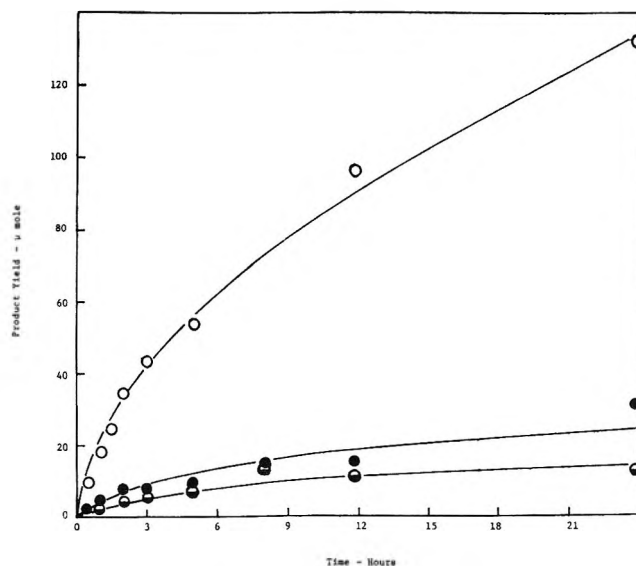


Figure 1. Product yields as a function of time; concentration of norbornene, 1.04 *M*; conversion after 24 hr, 15%: O, major adduct (III); ●, endo-trans-exo-norbornene dimer (I); ◐, minor adduct (IV) + exo-trans-exo-norbornene dimer (II).

given in Figures 2 and 3, respectively. A few runs in which undegassed solutions were used are also included.

Attempts were made to extend these results to very low concentrations of both benzene and norbornene by the use of cyclohexane as a solvent. Since the presence of cyclohexane led to a variety of new products some of which resulted from the addition of norbornene to cyclohexane, these experiments were abandoned.

Even under conditions of high resolution, a chromatographic column of silicone oil did not resolve the exo-trans-exo dimer (II) of norbornene from the endo-exo adduct (IV). Fortunately, at low concentrations of norbornene (<2 *M*) there was very little of this adduct formed and at high concentrations (~7 *M*), there was almost none of the dimer present. At intermediate concentrations it was possible to calculate the exact yields of these two products by first transforming the adduct IV to adduct III by heating and measuring the dimer II that was left behind. In this way it was found that the ratios of the yields of two dimers and of the two adducts were concentration independent.

The only quantitative data on the benzene-norbornene system that were previously available^{6b} were the ratios of the dimer II to I in 2.5, 0.5, and 0.2 *M* solutions. The radiation was from a medium-pressure mercury lamp filtered by Vycor. The ratios that

(10) Trans fusion at the 2,9-bond need not be considered since it has been shown^{1a} that the stereochemistry of the olefin is retained during the reaction.

(11) R. Srinivasan, *J. Amer. Chem. Soc.*, **92**, 7542 (1970).

(12) A referee has opined that from an adduct such as IV, fragmentation is likely to proceed with a smaller activation energy than an isomerization which involved the cleavage of the 2,9 bond. We have actually studied the thermal decompositions of III and IV quantitatively,⁹ and our data do not support this opinion.

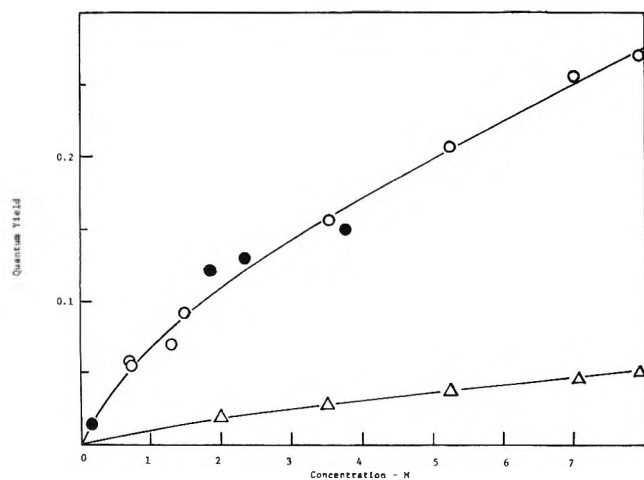


Figure 2. Quantum yields of adducts as a function of concentration: \circ , major adduct (III); Δ , minor adduct (IV); filled symbols correspond to irradiation of undegassed, unsealed samples.

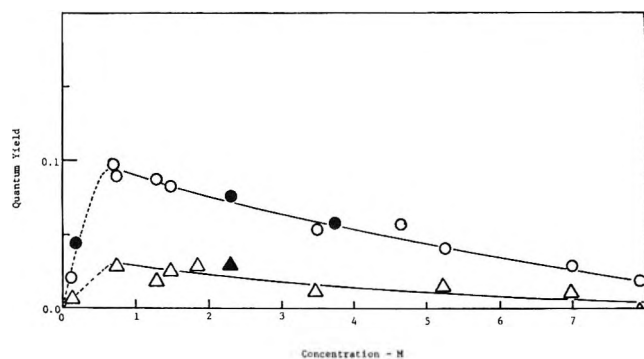


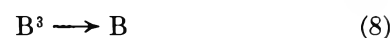
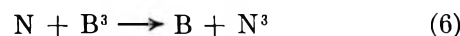
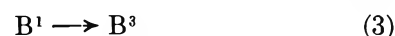
Figure 3. Quantum yields of dimers as a function of concentration: \circ , endo-trans-exo dimer (I); Δ , exo-trans-exo dimer (II); filled symbols correspond to irradiation of undegassed, unsealed samples.

were found were 0.30, 0.20, and 0.14, respectively. In this work, the ratio was found to be 0.3 and invariant with concentration. Since no importance was attached in the earlier work^{6b} to the change in the ratio that was observed at different concentrations, it is not possible to say if there is a discrepancy between the two studies. It may also be noted that the chromatographic column that was used by these workers was a "boiling-point" column.¹³ Therefore, the ratio of the dimer II to the dimer I would have shown an apparent increase with the concentration of norbornene because of the presence of adduct IV.

Discussion

Both the experimental work of Wilzbach and Kaplan¹ and the theoretical analysis that was conducted by Bryce-Smith and Longuet-Higgins^{2b} as well as by Bryce-Smith^{2d} on the photoaddition reactions of benzene suggest that the 1,3 addition takes place from the $^1B_{2u}$ state (which will hereafter be referred to as B^1) of benzene when the exciting radiation is of 253.7-

nm wavelength. Arnold and Abraitys^{6b} have proposed that the benzene-sensitized dimerization of norbornene involves the triplet state of benzene (B^3). A mechanism which incorporates both of these explanations is as follows (A = adduct; D = dimer; N = norbornene)



k_4 and k_7 which are the rate constants for the formations of the adducts and dimers, respectively, are actually sums of the individual rate constants for the formation of each isomeric product.

With the usual stationary-state approximations it can be derived that

$$\Phi_A = \frac{1}{(k_3 + k_5)/k_4[N] + 1} \quad (10)$$

and

$$\Phi_D = \frac{k_3 k_6 k_7 [N]^2}{(k_7[N] + k_9)(k_6[N] + k_8)(k_3 + k_5 + k_4[N])} \quad (11)$$

The specific tests which can be applied to this mechanism are the following.

(i) Equation 10 requires that a plot of $1/\Phi_{A(\text{III} + \text{IV})}$ vs. $1/[N]$ be linear and the intercept be unity. The plot of the experimental values fall on a satisfactory straight line from about 0.8 to 1.3 M . The extrapolated value at $[N] = \infty$ as determined by least-squares analysis corresponded to $\Phi = 0.52 \pm 0.12$ which indicates that step 4 leads to deactivation of the benzene singlet without any adduct being formed in about half of the collisions. The limiting quantum yield when compared to the corresponding value in the cyclobutene-benzene⁵ system of 0.8 suggests that there may be a correlation between the strain energy in the olefin and the efficiency of the addition.

The slope of the plot decreases with decreasing concentration at $[N] < 1.3 M$. This behavior is different from that observed in the case of cyclobutene. No explanation can be offered for this change at present.

(ii) Equation 11 requires that the quantum yields for the dimers *increase* steeply (as $[N]^2$) with concentration at low concentrations of norbornene and *decrease* with increasing concentration at high concentrations of the

(13) Reference 6b, p 36.

olefin. This is seen to be qualitatively true from Figure 3. Of more quantitative significance is the trend in the ratio Φ_A/Φ_D which is given by eq 12

$$\Phi_A/\Phi_D = k_4(k_7[N] + k_9)(k_6[N] + k_8)/k_3k_6k_7[N] \quad (12)$$

In the high concentration region in which Φ_A/Φ_D increases with an increase in $[N]$, the dependence would be a parabola according to (12) but would reduce to a linear dependence (eq 13) if k_9 (the unimolecular decay rate for N^3 , the triplet of norbornene) $\ll k_7[N]$

$$\Phi_A/\Phi_D = k_4[N]/k_3 + k_4k_8/k_3k_6 \quad (13)$$

The experimental values for Φ_A/Φ_D from 1 to 8 *M* actually fall on a parabola as indicated by eq 12. This shows that the addition of N^3 to itself to give dimers according to step 7 is an inefficient process even at high concentrations of norbornene.

It can be derived that at the minimum in the value of Φ_A/Φ_D

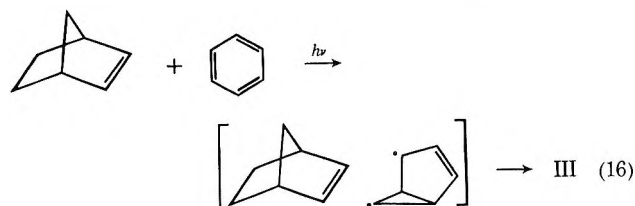
$$[N] = (k_8k_9/k_6k_7)^{1/2} \quad (14)$$

There are some data available¹⁴ on the unimolecular decay of the triplet state of benzene in the condensed phase, but a knowledge of k_6 would be needed to estimate the ratio of k_7 to k_9 , a quantity which would be useful in understanding the behavior of the triplet of the olefin in solution. However, eq 14 can be used to compare different olefins which undergo both 1,3 addition and dimerization in the presence of benzene. Studies are now in progress to obtain these data for several other olefins.

The stereochemistry of the 1,3-addition reaction offers an interesting contrast to that of the dimerization. Arnold and his coworkers⁶ have proposed the explanation that the major dimer from the sensitized dimerization, *i.e.*, I results from the attack of the norbornene by the sensitizer (*e.g.*, benzene in its triplet state) from the less-hindered exo side of the olefin so that the addition of the second norbornene takes place on the more-hindered



endo side. In the 1,3-addition reaction the major product corresponds to the attack of the norbornene from the more-hindered endo side by benzene in its singlet excited state. Two reasons may be offered for the dif-



ferent pathways that the encounters between the benzene and the norbornene follow. The reaction from the singlet state of benzene may be kinetically controlled whereas the reaction from the triplet state may be thermodynamically controlled. However, the small difference in energy between the two pathways (endo *vs.* exo with respect to the norbornene)¹⁵ is not necessarily a significant factor in determining a photochemical reaction. Further, the lifetime of the triplet of benzene in solution which may be comparable to that of the singlet¹⁴ makes it doubtful that thermodynamic control can be established in the former but not the latter. Alternatively, it is possible that the initial product of the addition is IV which corresponds to the attack on the norbornene from the exo side, but the product rearranges thermally to III. This explanation implies that adduct IV is formed in a "hot" ground state and undergoes rearrangement, a possibility that has not been widely encountered in photochemical studies in the condensed phase.

Data on the stereochemistry of these additions and dimerizations are needed in more instances in order that a definite pattern may be delineated among the various reaction pathways.

Acknowledgment. The assistance of Mrs. J. Picone in the early phase of this work is acknowledged.

(14) J. K. Thomas, *Ann. Rev. Phys. Chem.*, 21, 28 (1970).

(15) E. J. Corey, R. Hartmann, and P. A. Vatakencherry, *J. Amer. Chem. Soc.*, 84, 2611 (1962), and references therein.

Solute Radical Cation Yields in the Pulse Radiolysis of Solutions of Aromatic Amines in Chlorinated Hydrocarbons

by H. D. Burrows, D. Greatorex, and T. J. Kemp

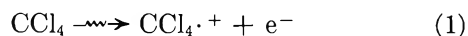
School of Molecular Sciences, University of Warwick, Coventry CV4 7AL, United Kingdom (Received August 11, 1971)

Publication costs assisted by the University of Warwick

G values for solute radical cation have been determined by microsecond pulse radiolysis of $10^{-2} M$ solutions of N -, N,N',N' -tetramethyl- p -phenylenediamine, p,p',p'' -tribromotriphenylamine, tritolyamine, triphenylamine, aniline, and 2,4,6-tri-*tert*-butylphenol in carbon tetrachloride and, in the cases of the first four solutes, also in chloroform, dichloromethane, and chlorocyclohexane. They are in most cases considerably higher than those previously reported. There is evidence for selective scavenging of $\text{RCl}\cdot^+$ by the trisubstituted triaryl amines while TMPD appears to scavenge a solvent radical in addition in the cases of CHCl_3 and CCl_4 . Extinction data have been independently determined for the solute radical cations by chemical oxidation.

Introduction

The radiolysis of chlorinated hydrocarbons (RCl) in the condensed phase has been studied extensively from several different points of view; in particular, attempts have been made to establish the nature of the primary species involved both by means of low-temperature matrix isolation¹⁻⁴ and by pulse radiolysis.⁵ Both of these physical methods indicate that an important primary species is $\text{RCl}\cdot^+$ formed in the initial act of ionization, *e.g.*, for CCl_4



This is capable of transferring its charge to a solute molecule, A, of lower ionization potential.



The importance of $\text{RCl}\cdot^+$ is particularly suggested by Hamill's demonstration of the facility of reaction 2 in rigid, polycrystalline CCl_4 ¹ and glassy *n*- and *sec*-butyl chloride matrices³ at 77°K following γ radiolysis, indicating a *mobile* oxidizing entity, such as $\text{RCl}\cdot^+$ which transfers its charge through a series of other RCl molecules until the charge reaches a solute molecule.

The optical spectra of a wide variety of solute radical cations $\text{A}\cdot^+$ have been obtained by the matrix isolation¹⁻⁴ and pulse radiolysis methods,^{6,7} and it is consequently surprising that few estimates of the yield of solvent radical cations are given. Shida and Hamill used N,N,N',N' -tetramethyl- p -phenylenediamine (TMPD) to scavenge $\text{RCl}\cdot^+$ in CCl_4 ⁷ and *s*-BuCl at 77°K obtaining G values of 1.9 and *ca.* 3, respectively,^{1,3} after utilizing a low-temperature extinction coefficient⁸ of $\epsilon_{\text{max}}(\text{TMPD}\cdot^+) 1.93 \times 10^4 \text{ l. mol}^{-1} \text{ cm}^{-1}$. Cooper and Thomas⁵ used aniline as a scavenger in liquid CCl_4 , relying on their extinction coefficient⁹ for $\text{C}_6\text{H}_5\text{NH}_2\cdot^+$ of $1.205 \times 10^4 \text{ l. mol}^{-1} \text{ cm}^{-1}$ obtained from a pulse ra-

diolysis examination of liquid aniline, obtaining $G(\text{CCl}_4\cdot^+) = 0.8$. This figure for $(\text{C}_6\text{H}_5\text{NH}_2\cdot^+)$ is, however, significantly greater than that of Land and Porter¹⁰ who give $\epsilon_{\text{max}} = 2.0 \times 10^3 \text{ l. mol}^{-1} \text{ cm}^{-1}$ from a flash photolysis study.

The problems of obtaining accurate G values from pulse radiolysis often stem from a lack of reliable extinction data for the transient species encountered, and we have thus conducted an examination of microsecond pulse radiolysis of several typical chlorinated hydrocarbons using solutes giving radical cations or radicals of reasonable stability, enabling reliable determination of their extinction coefficients by independent means. Such solutes include two tri-*para*-substituted triphenylamines, whose radical cations are stable for minutes, as established by Michaelis and colleagues,^{11,12} 2,4,6-tri-*tert*-butylphenol (which is oxidized to a blue phenoxyl radical) and TMPD. Triphenylamine was also examined but its radical cation, while of general interest, is much more reactive than its *para*-substituted analogs (undergoing rapid 4,4 coupling), and to this extent its use must be regarded with caution.

- (1) T. Shida and W. H. Hamill, *J. Chem. Phys.*, **44**, 2369 (1966).
- (2) T. Shida and W. H. Hamill, *ibid.*, **44**, 2375 (1966).
- (3) T. Shida and W. H. Hamill, *ibid.*, **44**, 4372 (1966).
- (4) P. W. F. Louwrier and W. H. Hamill, *J. Phys. Chem.*, **73**, 1702 (1969).
- (5) R. Cooper and J. K. Thomas, *Advan. Chem. Ser.*, **82**, 351 (1968).
- (6) S. Arai, H. Ueda, R. F. Firestone, and L. M. Dorfman, *J. Chem. Phys.*, **50**, 1072 (1969).
- (7) N. E. Shank and L. M. Dorfman, *ibid.*, **52**, 4441 (1970).
- (8) W. C. Meyer and A. C. Albrecht, *J. Phys. Chem.*, **66**, 1168 (1962).
- (9) R. Cooper and J. K. Thomas, *J. Chem. Phys.*, **48**, 5103 (1968).
- (10) E. J. Land and G. Porter, *Trans. Faraday Soc.*, **59**, 2027 (1963).
- (11) L. Michaelis, M. P. Schubert, and S. Granick, *J. Amer. Chem. Soc.*, **61**, 1981 (1939).
- (12) S. Granick and L. Michaelis, *ibid.*, **62**, 2241 (1940).

Experimental Section

Materials. TMPD and triphenylamine were purified by methods described previously.¹³ *p,p',p''*-Tribromotriphenylamine was prepared by the bromination of triphenylamine at -20° in benzene-chloroform mixture (cooled by a salt-ice mixture) and was purified by recrystallization from glacial acetic acid¹⁴ (mp 145°). *Anal.* Calcd for $C_{18}H_{12}Br_3N$: Br, 49.7. Found: Br, 49.5. Tritolylamine was prepared by means of an Ullman reaction¹⁵ and was purified three times by chromatography on neutral Al_2O_3 (eluent: benzene-chloroform), decolorized with charcoal and recrystallized successively from benzene and glacial acetic acid, mp 107° (lit. mp $110-117^\circ$). Mass spectral analysis showed a parent peak with $m/e = 287$. 2,4,6-Tri-*tert*-butylphenol, supplied by Koch-Light Laboratories Ltd., was recrystallized from *n*-hexane. Triphenylphosphine (B.D.H. reagent grade) was used without further purification. Aniline (Fison's analytical grade) was purified by the procedure given by Weissberger.¹⁶ Spectroscopic grade carbon tetrachloride was further purified by washing with ethanolic KOH (0.1%) and then several times with water, dried firstly over activated Al_2O_3 (type "H") and then with $CaCl_2$ and finally distilled from K_2CO_3 . Chlorocyclohexane (Koch-Light "pure" grade) was distilled from $CaCl_2$ and then passed down an activated Al_2O_3 column (type "H") to remove aromatic impurities detectable by uv absorption. Spectroscopic grade chloroform and dichloromethane were further purified by methods given by Vogel.¹⁷

Pulse Radiolysis. This was performed with 0.6- μ sec pulses of 3-MeV electrons of a few krad dose (except in those cases where the resulting absorption was very weak) delivered by a Van de Graaff accelerator at the Cookridge High Energy Radiation Research Centre of Leeds University at Cookridge Hospital, Leeds. The general experimental arrangement has been described before, as also have the methods of dosimetry, degassing of solutions and remote control of the flow system.¹³ Samples were normally protected from photolysis by the monitoring light by insertion of a filter cutting off just below the relevant transient absorption. Uv spectrophotometry was performed with a Cary 14 apparatus operated at ambient temperatures ($20 \pm 2^\circ$).

Results

Spectra and Extinction Coefficients of Amine Radical Cations. While chemical oxidation of several aromatic amines A to $A^{\cdot+}$ proceeds quantitatively in solvents such as water or alcohols, it has been noted¹⁸ that such an oxidation of TMPD does not go to completion in benzene and, in addition, $TMPD^{\cdot+}$ is rather unstable in benzene. The spectrum of $TMPD^{\cdot+}$ in benzene is somewhat different from that in methanol (although the marked doublet feature of the visible band is retained) and λ_{max} 570 nm, ϵ_{max} 1.08×10^4 l. mol⁻¹ cm⁻¹ in benzene¹⁸ compared with λ_{max} 565 nm, ϵ_{max} $1.247 \times$

10^4 l. mol⁻¹ cm⁻¹ in water.¹⁹ (The latter figures of Albrecht and Simpson¹⁹ are confirmed by those of Pettersson²⁰ who gives λ_{max} 564 nm, ϵ_{max} 1.24×10^4 l. mol⁻¹ cm⁻¹ and of Curzon²¹ who gives λ_{max} 563, ϵ_{max} 1.25×10^4 l. mol⁻¹ cm⁻¹.) In 8:2 methanol-water (v/v) Michaelis, *et al.*,¹¹ gave λ_{max} 560 nm, ϵ_{max} 1.22×10^4 l. mol⁻¹ cm⁻¹.

Absorption data for $TMPD^{\cdot+}$ are given for solutions in several nonpolar organic solvents at $77^\circ K$ ²² but these are inapplicable at room temperature where the doublet feature is less well resolved. Using TMPD solutions at room temperature, we have prepared $TMPD^{\cdot+}$ either by chemical or photochemical oxidation and have determined the oscillator strength of the resulting absorption. Extinction coefficients at $\lambda_{max} \simeq 560-565$ nm have then to be determined by comparison with the spectrum in water, using the very reliable data given above, after normalizing to "unit" oscillator strength.

Spectra of $TMPD^{\cdot+}$ in chlorinated hydrocarbon solvents are very similar to those in water and methanol as regards wavelength maxima ($C_6H_{11}Cl = 568$ nm, $CH_2Cl_2 = 567$ nm, $CHCl_3 = 570$ nm, and $CCl_4 = 572$ nm), prominence of the doublet feature, and half-width, and the resulting extinction coefficients ($10^{-4} \epsilon_{max}$, mol⁻¹ cm⁻¹: $C_6H_{11}Cl$, 1.251; CH_2Cl_2 , 1.220; $CHCl_3$, 1.160; CCl_4 , 1.187) are correspondingly similar (the optical data refer to the shorter-wavelength member of the doublet feature).

Few extinction data have been obtained for the other amines used in this study. Granick and Michaelis¹² partially oxidized tri-*p*-tolylamine (Me_3TPA) in 80% acetic acid-20% water with lead tetraacetate, obtaining $Me_3TPA^{\cdot+}$ with λ_{max} 665 nm, ϵ_{max} 1.087×10^4 l. mol⁻¹ cm⁻¹, based on measurement at a single solute concentration. We have determined spectral and extinction data for radical cations of all three compounds by chemical oxidation by Ce(IV) as follows.

Tri-*p*-tolylamine (Me_3TPA) and *p,p',p''*-Tribromotriphenylamine (Br_3TPA). Solutions (10^{-3} M) of amine in CH_2Cl_2 were oxidized with small quantities of a concentrated solution of ceric ammonium nitrate in acetonitrile dispensed from an "Agl" micrometer syringe (the final solvent composition was always at

(13) T. J. Kemp, J. P. Roberts, G. A. Salmon, and G. F. Thompson *J. Phys. Chem.*, **72**, 1464 (1968).

(14) H. Wieland, *Ber.*, **40**, 4260 (1907).

(15) R. I. Walter, *J. Amer. Chem. Soc.*, **77**, 5999 (1955).

(16) A. Weissberger and E. Strasser, *J. Prakt. Chem.*, **135**, 209 (1932); quoted in A. Weissberger, E. S. Proskawer, J. A. Riddick, and E. E. Toops, "Organic Solvents," Interscience, New York, N. Y., 2nd ed, 1955, p 442.

(17) A. I. Vogel, "Practical Organic Chemistry," Longmans, London, 3rd ed, 1964, p 176.

(18) J. Steigman and W. Cronkright, *J. Amer. Chem. Soc.*, **92**, 6736 (1970).

(19) A. C. Albrecht and W. T. Simpson, *ibid.*, **77**, 4454 (1955).

(20) G. Pettersson, *Acta Chem. Scand.*, **22**, 3063 (1968).

(21) G. Curzon, *Biochem. J.*, **103**, 289 (1967).

(22) T. Shida, *J. Phys. Chem.*, **74**, 3055 (1970).

least 98.5% CH_2Cl_2). The resulting spectra, which appeared on mixing the reactants, were recorded immediately (Figures 2 and 3) and their decays were monitored at the absorption maxima. The decays were comparatively slow ($t_{1/2} > 60$ sec) and a correction to zero time was applied from these decay kinetics for the interval between mixing and recording. The concentration of Ce(IV) was varied over a range 5×10^{-6} to 10^{-3} M (although at concentrations $> 2 \times 10^{-4}$ M, a substance precipitated from the solution of Br_3TPA), and plots of (optical density) vs. [Ce(IV)] yielded straight lines passing through the origin. Least-squares analysis yielded extinction data given below.

Triphenylamine (TPA). The above procedure could not be extended to this amine because the similarity of the rates of buildup and decay of $\text{TPA}\cdot^+$ prevented simple extrapolation of the decay curve to zero time. Accordingly 0.1 M ethanolic solutions of ceric ammonium nitrate were mixed with small quantities of ethanolic TPA administered from a 100- μl syringe to give [TPA] from 2×10^{-6} to 3×10^{-5} M. Under these conditions extremely rapid oxidation of TPA to $\text{TPA}\cdot^+$ was followed by a slower decay of $\text{TPA}\cdot^+$ and an extrapolation of optical density to zero time was readily performed. A complete spectrum of $\text{TPA}\cdot^+$ in ethanol was obtained by mixing together in a continuous flow system ethanolic solutions of TPA and ceric ammonium nitrate. At lower [Ce(IV)] the formation of $\text{TPA}\cdot^+$ was considerably slower and correction to zero time could not be effected. As before, a plot of optical density vs. [TPA] yielded a straight line passing through the origin. In another determination at [Ce(IV)] $\approx 10^{-2}$ M, using ethanol as solvent for both reactants, the "buildup" and "decay" curves for $\text{TPA}\cdot^+$ were analysed by means of a curve-fitting program devised in these laboratories.²³

The spectral and extinction data, which refer to $\text{CH}_2\text{-Cl}_2$ solution except for $\text{TPA}\cdot^+$ which was examined in ethanol, are as follows in Table I.

Table I: Spectral and Extinction Data

	$\text{TPA}\cdot^+$	$\text{Br}_3\text{TPA}\cdot^+$	$\text{Me}_3\text{TPA}\cdot^+$
λ_{max} , nm	660 ± 10	727	675
$10^{-3}\epsilon_{\text{max}}$, mol ⁻¹ cm ⁻¹	28.75 ± 0.4 (curve fitting program)	20.8 ± 0.6	21.9 ± 0.3
	30.50 ± 0.4 (high [Ce(IV)] conditions)		

The figure for $\text{Me}_3\text{TPA}\cdot^+$ is much higher than that due to Granick and Michaelis¹² of 1.087×10^4 l. mol⁻¹ cm⁻¹ but it is significant that their figure is based on a single measurement. The figure for $\text{TPA}\cdot^+$ seems singularly high compared with those for its trisubstituted derivatives, but it was readily reproducible.

Pulse Radiolysis Spectra

TMPD. Pulse radiolysis of 10^{-2} M solutions in all four solvents used yielded spectra identical with that of the radical cation prepared by chemical oxidation,¹² i.e., with an absorption extending from ca. 470 to ca. 650 nm with a weakly resolved doublet feature (λ_{max} 570 and 610 nm in CHCl_3). Details are collated in Table II.

Triphenylamine (TPA). The pulse radiolysis spectra in all four solvents are similar with a flattish peak in the region of 640 ± 10 nm and a weak shoulder at 575 ± 10 nm. A typical spectrum is shown in Figure 1. TPA does not form a stable radical cation, $\text{TPA}\cdot^+$ rapidly coupling with a second TPA molecule to produce tetraphenylbenzidine,²⁴ and we assign the pulse radiolysis spectra to $\text{TPA}\cdot^+$ on the basis of similarity with (i) the spectrum obtained by Hamill¹ on γ radiolysis of a solution of TPA in CCl_4 at 77°K, (ii) solution spectra obtained by both stopped-flow and continuous-flow oxidation of TPA by Ce(IV) in alcoholic and $\text{CH}_3\text{CN-CCl}_4$ media (Figure 1), and (iii) the insensitivity of the transient species obtained from the pulse radiolysis of a CCl_4 solution to the presence of O_2 , which rules out the possibility of assignment to an excited state of similar spectrum.¹³ Full details are given in Table II.

***p,p',p''*-Tribromotriphenylamine (Br_3TPA).** Similar spectra were obtained in all four solvents, a typical example being illustrated in Figure 2 together with a spectrum of $\text{Br}_3\text{TPA}\cdot^+$ obtained by chemical oxidation in the same solvent, CH_2Cl_2 . Complete data are given in Table II.

Tritolylamine (*p,p',p''*-Trimethyltriphenylamine or Me_3TPA). All four solutions displayed similar spectra

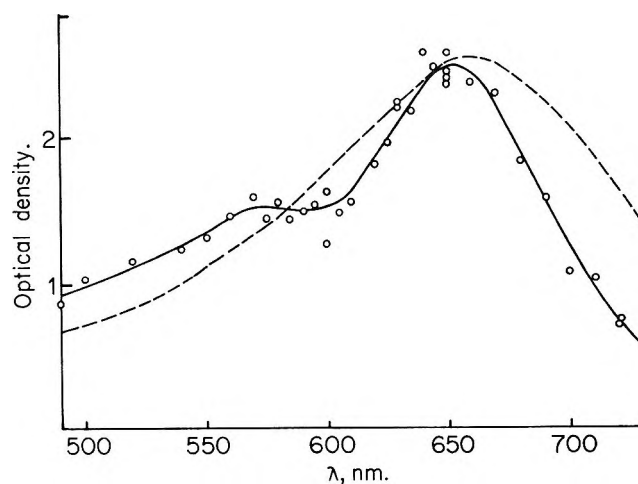


Figure 1. Key: —, pulse radiolysis spectrum of 10^{-2} M TPA in CH_2Cl_2 ; - - - -, spectrum obtained on mixing Ce(IV) and TPA in ethanolic solution in a continuous-flow system.

(23) N. W. Alcock, D. J. Benton, and P. Moore, *Trans. Faraday Soc.*, **66**, 2210 (1970).

(24) R. N. Adams, *Accounts Chem. Res.*, **2**, 175 (1969).

Table II: Values of λ_{\max} , $G\epsilon_{\max}$, and Decay Constants (k_2) for Pulse Radiolysis of Solutions at $10^{-2} M$ Solute Concentration^a

	Br ₃ TPA	Me ₃ TPA	TMPD	TPA	Aniline	2,4,6-Tri- <i>tert</i> -butylphenol	Ph ₃ P
				CCl ₄			
λ_{\max} , nm	700	675	575	630	~410	400	620
$10^{-4}G\epsilon_{\max}$	2.47 ± 0.14 (13)	3.24 ± 0.07 (5)	3.54 ± 0.39 (28)	2.18 ± 0.25 (25)	0.265 (2)	0.342 ± 0.029	0.087 ± 0.010 (6)
$10^{-6}k_2/\epsilon_{\max}$	Long-lived	Long-lived	Long-lived	1.39			
				CHCl ₃			
λ_{\max} , nm	705	680	570	650			
$10^{-4}G\epsilon_{\max}$	3.22 ± 0.08 (7)	3.46 ± 0.01 (2)	3.77 ± 0.39 (10)	1.59 ± 0.06 (7)
$10^{-6}k_2/\epsilon_{\max}$	Long-lived	Long-lived	0.117	Long-lived			
				CH ₂ Cl ₂			
λ_{\max} , nm	725	680	570	650			
$10^{-4}G\epsilon_{\max}$	7.30 ± 0.86 (5)	4.96 ± 0.29 (8)	3.19 ± 0.09 (7)	2.11 ± 0.10 (7)
$10^{-6}k_2/\epsilon_{\max}$	Long-lived	Long-lived	0.210	6.32			
				C ₆ H ₁₁ Cl			
λ_{\max} , nm	710	680	570	635			525 (sh)
$10^{-4}G\epsilon_{\max}$	2.17 ± 0.22 (13)	2.00 ± 0.04 (3)	1.61 ± 0.06 (6)	1.40 ± 0.03 (7)	0.355
$10^{-6}k_2/\epsilon_{\max}$	4.11	0.71	Long-lived	1.18			

^a The figures in parentheses refer to the number of separate estimations.

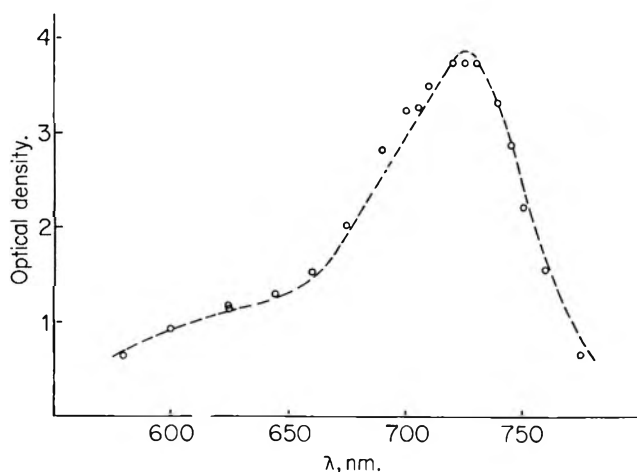


Figure 2. Key: O, pulse radiolysis spectrum of $10^{-2} M$ Br₃TPA in CH₂Cl₂; ---, spectrum obtained on chemical oxidation of Br₃TPA in CH₂Cl₂.

following pulse radiolysis with a peak at *ca.* 680 nm and a shoulder at *ca.* 590 nm. Typical is the spectrum shown in Figure 3 together with that of chemically prepared Me₃TPA^{•+}, the similarity again suggesting an identity. Complete data are given in Table II.

Aniline. Pulse radiolysis of a $10^{-2} M$ solution in CCl₄ gave absorptions in two spectral regions, *i.e.*, (i) a sharp peak at 405 ± 5 nm completely formed at the end of a 0.6- μ sec pulse with $G\epsilon_{\max} = 2650$ and decaying over a period of hundreds of microseconds and (ii) a broad absorption extending from 500 to 675 nm with λ_{\max} *ca.* 600 ± 20 nm and $G\epsilon_{\max} = 6500 \pm 500$; this absorption

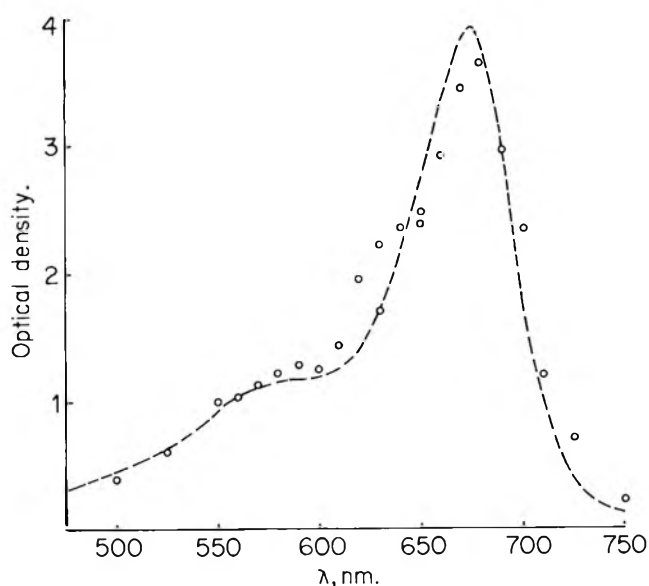


Figure 3. Key: O, pulse radiolysis spectrum of $10^{-2} M$ Me₃TPA in chlorocyclohexane; ---, spectrum obtained on chemical oxidation of Me₃TPA in CF₂Cl₂.

built-up after the end of the pulse over a period of *ca.* 7 μ sec and subsequently decayed over hundreds of microseconds. The 405-nm transient is assigned to C₆H₅-NH₂^{•+} in agreement with Cooper and Thomas⁵ and also Land and Porter¹⁰ who obtained $\lambda_{\max} = 423$ nm, $\epsilon_{\max} = 2000$ l. mol⁻¹ cm⁻¹ for this species in a flash photolysis study. Assignment of the 650-nm species is not readily made but it is presumably due to a coupling product of aniline.

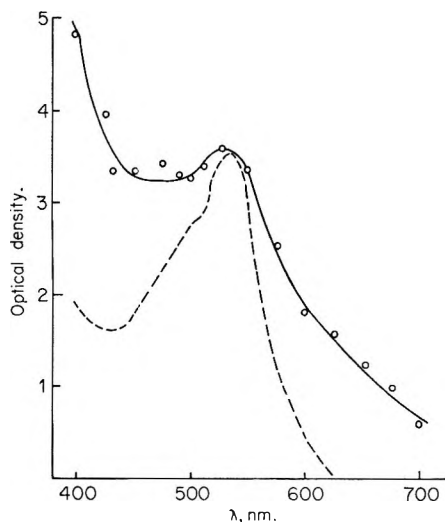


Figure 4. Key: —, pulse radiolysis spectrum of $10^{-2} M$ triphenylphosphine in chlorocyclohexane; - - -, spectrum obtained by Shida and Hamill¹ on γ radiolysis of a solution of triphenylphosphine in CCl_4 at 77°K .

Triphenylphosphine (TPP). While pulse radiolysis of a CCl_4 solution gave negligible absorption in the visible region, pulse radiolysis of $10^{-2} M$ TPP in chlorocyclohexane gave the spectrum exhibited in Figure 4, with $G_{\epsilon_{525}} = 3550$, which is compared with Hamill's solid-state spectrum of $\text{TPP}^{\cdot+}$ obtained by γ radiolysis of a CCl_4 matrix.¹ The agreement is rather poor, even allowing for the difference in temperature and phase, but it seems probable that the pulse radiolysis spectrum is due to $\text{TPP}^{\cdot+}$. Presumably $\text{TPP}^{\cdot+}$ reacts extremely rapidly with CCl_4 at ambient temperatures and can be stabilized in this solvent only at 77°K .

2,4,6-Tri-tert-butylphenol. This solvent produced absorptions in the uv and visible regions on pulse radiolysis in CCl_4 solution at *ca.* $10^{-2} M$ concentration (Figure 5). The similarity with the spectrum of the corresponding phenoxyl radical (ArO^{\cdot}) prepared by chemical oxidation (Figure 5)²⁵ suggests that we are observing either this species in pulse radiolysis or, possibly, its protonated form, $\text{ArOH}^{\cdot+}$.

Complete data on the last three solutes are given in Table II.

Yields

Values of $G\epsilon$ for $10^{-2} M$ solutions of the triarylamines and TMPD are collated in Table II, and the G values obtained from these by means of the extinction coefficients given in the text above are set out in Table III.^{26,27} An unusually large random error was found with this series of experiments and accordingly they have been repeated on several occasions over a period of 2 years. The bracketed figures refer to the number of separate estimations and the errors quoted were obtained by a least-squares procedure.

Examination of solutions of TPA at concentrations

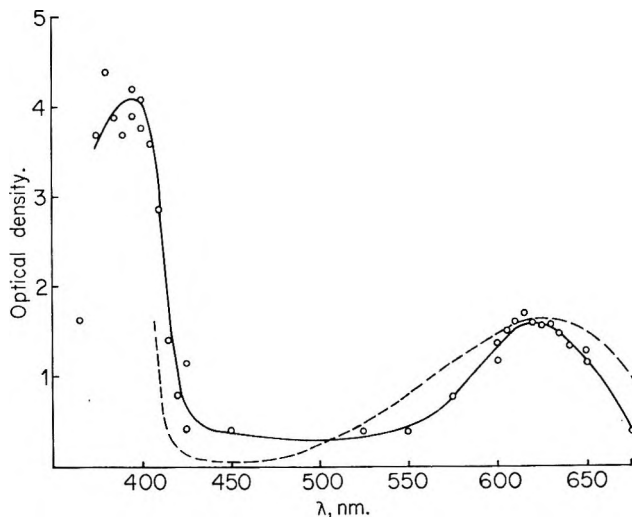


Figure 5. Key: —, pulse radiolysis spectrum of $10^{-2} M$ 2,4,6-tri-*tert*-butylphenol in CCl_4 ; - - -, chemically prepared spectrum of 2,4,6-tri-*tert*-butylphenoxyl radical.²⁵

Table III: G Values for Solute Radical or Radical Cation in Pulse Radiolysis of Halocarbon Solutions at $10^{-2} M$ Solute Concentration

	Br_3TPA	Me_3TPA	TMPD	TPA	Aniline ^a	2,4,6-Tri- <i>tert</i> -butylphenol ^a
CCl_4	1.19	1.48	2.98	0.71	1.3 ^a	2.05 ^a
CHCl_3	1.55	1.58	3.25	0.52
CH_2Cl_2	3.51	2.26	2.61	0.69
$\text{C}_6\text{H}_{11}\text{Cl}$	1.04	0.91	1.29	0.46

^a Figures based on $\epsilon_{\text{max}} 2.0 \times 10^3 \text{ l. mol}^{-1} \text{ cm}^{-1}$ for aniline positive ion²⁷ and $\epsilon_{400} 1.80 \times 10^3$, $\epsilon_{620} 0.40 \times 10^3 \text{ l. mol}^{-1} \text{ cm}^{-1}$ for phenoxyl radical.²⁵

of 3 and $7.5 \times 10^{-2} M$ revealed no perceptible increase in $G(\text{TPA}^{\cdot+})$ above that found at $10^{-2} M$.

Also in Table II are listed results for aniline and 2,4,6-tri-*tert*-butylphenol.

Kinetics

Many of the systems produced spectra which persisted for periods of several hundred microseconds, although ultimate decay was indicated by recovery of the transmitted light intensity, as recorded by the photomultiplier current, to its original value. This situation is described "long-lived" in Table II in which are collated the rate coefficients.

Discussion

That the solvent species scavenged by solute amine to give the amine radical cation in pulse radiolysis of

(25) C. D. Cook, D. A. Kuhn, and P. Fianu, *J. Amer. Chem. Soc.*, **78**, 2002 (1956).

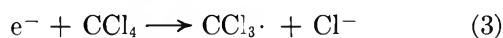
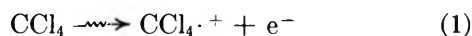
(26) C. D. Cook and B. D. Norcross, *ibid.*, **81**, 1176 (1959).

(27) E. J. Land, G. Porter, and E. Strachan, *Trans. Faraday Soc.*, **57**, 1185 (1961).

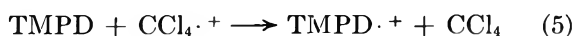
chlorinated hydrocarbon solutions is $\text{RCl}\cdot^+$ is indicated by the following evidence. First, nanosecond pulse radiolysis of pure CCl_4 yielded a transient with λ_{max} 475 nm, $t_{1/2} = 15 \pm 2$ nsec, assigned to $\text{CCl}_4\cdot^+$, which reacted with added aniline with $k_2 \simeq 10^{10} \text{ l. mol}^{-1} \text{ sec}^{-1}$ to give an optical spectrum of $\text{C}_6\text{H}_5\text{NH}_2\cdot^+$, scavenging of $\text{CCl}_4\cdot^+$ being complete at aniline concentrations of $10^{-2} M$.⁵ Second, Hamill's results with γ -irradiated solid matrices of chlorinated hydrocarbons containing various aromatic solutes at 77°K are rationalized only in terms of a positively charged entity transferring its charge through the matrix to a solute molecule of lower ionization potential.¹⁻⁴

With the exception of the rather atypical TPA as solute, the G values given in Table III for CCl_4 are considerably higher than that of 0.8 reported by Cooper and Thomas⁵ for pulse radiolysis of $10^{-2} M$ solutions of aniline in CCl_4 , a discrepancy clearly due in large part to the use of different extinction coefficients for the transient species. (Cooper and Thomas⁵ have not utilized their results for TMPD in CCl_4 to obtain $G(\text{TMPD}\cdot^+)$ and we can offer no comparison here.)

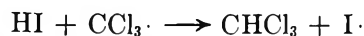
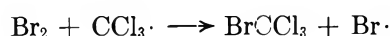
The solutes Br_3TPA , Me_3TPA , and 2,4,6-tri-*tert*-butylphenol, for each of which reliable extinction data are now available, all give G values of radical or radical cation in CCl_4 in the range 1.6 ± 0.4 , as does our figure for aniline. This value is also compatible with the figure of 1.9 of Hamill¹ using TMPD in CCl_4 at 77°K. The higher value for $G(\text{TMPD}\cdot^+)$ of 3 obtained in CCl_4 in the *liquid* phase suggests an additional path for the very facile oxidation of TMPD, for example, by $\text{CCl}_3\cdot$; oxidation of TMPD by solvent-derived radicals such as ethoxyl has been established by Bensasson and Thomas²⁸ in the pulse radiolysis of ethanolic TMPD with $G \simeq 1.0$. $\text{CCl}_3\cdot$ is known to be produced in the steady-state radiolysis of CCl_4 from product²⁹ and scavenging³⁰ studies, probably *via* the scheme



In the presence of TMPD further reactions are possible



Estimates for $G(\text{CCl}_3\cdot)$ come from radiolysis both of CCl_4 and its solutions; pure CCl_4 gives Cl_2 and C_2Cl_6 as sole products²⁹ in approximately equal yields of $G \simeq 0.75$. However, the use of Br_2 and HI as scavengers³⁰ for $\text{CCl}_3\cdot$, *viz.*



indicates $G(\text{CCl}_3\cdot) \simeq 7$. It appears that only a fraction, *i.e.*, $G \simeq 1.5$, of $\text{CCl}_3\cdot$ radicals formed recombine to give C_2Cl_6 and that this same fraction can be scavenged by TMPD to give a yield of $\text{TMPD}\cdot^+$ additional to that produced by reaction 5; *i.e.*, $G_6 = 1.4$ and $G_5 = 1.6$. The formation of C_2Cl_4 *only* in the presence of scavengers³⁰ may be due to formation and decomposition³¹ of CCl_3^- (reactions 6 and 7).

An alternative scavenger which has been employed in CCl_4 radiolysis is ferrocene, which is largely converted to ferricenium ion³² with a minimum figure of $G(-\text{ferrocene}) = 2.34 \pm 0.07$. This figure is much lower than that for $G(\text{CCl}_3\cdot)$ given by Bibler,³⁰ but is more compatible with our results if ferrocene scavenges both $\text{CCl}_4\cdot^+$ and $\text{CCl}_3\cdot$, each with an approximate yield of 1.5. We attempted the pulse radiolysis of CCl_4 solutions of ferrocene, but although ferricenium ion was produced at the end of the pulse, accurate estimations were frustrated both by the small optical density at the wavelength maximum (*ca.* 625 nm), due to the low extinction coefficient, and the deposition of small blue crystals after each pulse which could not be washed away using the automatic syringe system for filling the irradiation cell.

Chloroform behaves in a similar way to CCl_4 ; Br_3TPA and Me_3TPA give $G(\text{cation})$ of 1.57 ± 0.02 while TMPD gives a significantly higher yield of 3.25, suggesting additional scavenging either of $\text{CHCl}_2\cdot$ or of $\text{CCl}_3\cdot$ which is produced in CHCl_3 radiolysis by the process,³³ $\cdot\text{CHCl}_2 + \text{CHCl}_3 \rightarrow \text{CH}_2\text{Cl}_2 + \text{CCl}_3\cdot$, with a $G(\text{CH}_2\text{Cl}_2) = 1.9$.

The figures for dichloromethane fall in the range 2.8 ± 0.6 (excluding TPA) indicating approximate uniformity of behavior. A similar situation prevails with chlorocyclohexane with $G(\text{cation}) = 1.1 \pm 0.2$; here the solvent radical produced in the analog of reaction 3 is $\text{C}_6\text{H}_{11}\cdot$ which has no ability to oxidize TMPD.¹³

TPA and triphenylphosphine present some anomalies. Triphenylphosphine gives no transient on pulse radiolysis in CCl_4 despite its oxidation to the radical cation at 77°K in this solvent.¹ Presumably $\text{Ph}_3\text{P}\cdot^+$ reacts rapidly with CCl_4 and only in $\text{C}_6\text{H}_{11}\text{Cl}$ was an optical spectrum apparent (Figure 4) suggesting formation of the cation. TPA appears to give uniformly low cation yields in all the solvents studied. This may be due to difficulties in obtaining absolutely reliable

(28) R. V. Bensasson and J. K. Thomas, *Int. J. Radiat. Phys. Chem.*, **1**, 185 (1969).

(29) F. P. Abramson, B. M. Buckhold, and R. F. Firestone, *J. Amer. Chem. Soc.*, **84**, 2285 (1962).

(30) N. E. Bibler, *J. Phys. Chem.*, **75**, 24 (1971).

(31) J. D. Roberts and M. C. Caserio, "Basic Principles of Organic Chemistry," W. A. Benjamin, New York, N. Y., 1964, p 331.

(32) E. Collinson, F. S. Dainton, and H. Gillis, *J. Phys. Chem.*, **65**, 695 (1961).

(33) J. N. Baxter and N. E. Bibler, *J. Chem. Phys.*, **53**, 3444 (1970).

extinction data or, alternatively, to some systematic complexity concerning its use as a positive-ion scavenger in these particular systems.

Acknowledgments. We thank Miss Ruth Gibbons who devised the method for determining extinction coefficients for aromatic amine radical cations and for making some of the measurements as part of her under-

graduate research project in the School of Molecular Sciences. We acknowledge the help of our colleagues at the Cookridge High Energy Radiation Research Centre, particularly Dr. G. A. Salmon, and the access to the pulse radiolysis facility given by its Director, Professor Sir Frederick Dainton, F.R.S. H. D. B. and D. G. thank the S.R.C. for financial support.

Ion Yields and Ion Neutralization Processes in Pulse-Irradiated Acetone

by Shamim A. Chaudhri^{1a} and K.-D. Asmus*

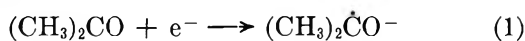
*Hahn-Meitner-Institut für Kernforschung Berlin GmbH, Sektor Strahlenchemie, Berlin, Germany
(Received June 7, 1971)*

Publication costs assisted by Hahn-Meitner-Institut für Kernforschung

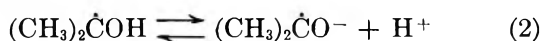
Ion yields and ion neutralization processes have been studied in pulse-irradiated acetone solutions using optical and conductivity methods. The yield of free $(\text{CH}_3)_2\dot{\text{C}}\text{O}^-$ ions has been determined to be $G_{fi} = 1.20 \pm 0.20$ by conductivity measurements. Tetranitromethane is reduced by $(\text{CH}_3)_2\dot{\text{C}}\text{O}^-$ ions to form $\text{C}(\text{NO}_2)_3^-$ ions with $k = 1.2 \times 10^{10} \text{ M}^{-1} \text{ sec}^{-1}$. Nitroform ions are neutralized by solvated protons with $k = 3.6 \times 10^8 \text{ M}^{-1} \text{ sec}^{-1}$, and $\text{C}(\text{NO}_2)_3\text{H}$ dissociates with $1.6 \times 10^3 \text{ sec}^{-1}$. The equilibrium constant of $\text{C}(\text{NO}_2)_3\text{H} \rightleftharpoons \text{C}(\text{NO}_2)_3^- + \text{H}_{\text{solv}}^+$ in acetone has been determined to be $4.5 \times 10^{-6} \text{ M}$. The yields of homogeneously distributed $\text{C}(\text{NO}_2)_3^-$ anions, anthracene anions, and chloride ions from the reduction of tetranitromethane, anthracene, and carbon tetrachloride, respectively, exceed $G_{fi}((\text{CH}_3)_2\dot{\text{C}}\text{O}^-)$. The influence of equilibrium conditions and possible activation energies on the neutralization process are discussed. Equivalent conductances have been determined for $\text{C}(\text{NO}_2)_3^-$ ions ($\Lambda = 130 \Omega^{-1} \text{ cm}^2 \text{ equiv}^{-1}$) and anthracene anions ($\Lambda = 135 \Omega^{-1} \text{ cm}^2 \text{ equiv}^{-1}$) in acetone.

Introduction

Acetone is known to be a good electron scavenger. The reaction^{1b,c}

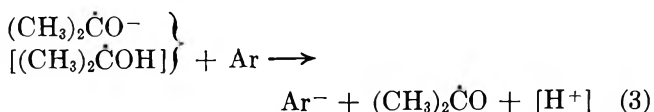


and the associated acid-base equilibrium²



have been studied in detail in irradiated aqueous solutions ($k_1 = 5.9 \times 10^9 \text{ M}^{-1} \text{ sec}^{-1}$ and $\text{p}K_{(2)} = 12.2$). Both the $(\text{CH}_3)_2\dot{\text{C}}\text{O}^-$ anion and the $(\text{CH}_3)_2\dot{\text{C}}\text{OH}$ radical were found to act as reducing species by transferring their radical electron to other solutes.³

The formation of a reducing species has also been observed when acetone was used as a solvent. Aromatic compounds such as naphthalene, anthracene, etc., for example, were shown to produce short-lived anions and triplets in irradiated acetone.⁴ The observed yield of aromatic anions in the electron-transfer reaction



has been associated with the yield of free ions produced upon irradiation of the solvent. Literature values of $G(\text{free ions})$, however, vary from 1.2 to 1.7 for the same system.⁴⁻⁶ This, presumably, is mainly due to uncertainties in the extinction coefficients and the very short lifetimes of the anions.

The aim of the present work has been to obtain information on ion formation and ion neutralization processes by combined optical and conductivity pulse radiolysis experiments. The conductivity method has been successfully applied in pulse radiolysis studies of aque-

(1) (a) Postdoctoral Fellow from the Pakistan Atomic Energy Commission, Karachi, with a grant from the Alexander von Humboldt-Stiftung, Bad Godesberg, Germany; (b) S. Gordon, E. J. Hart, M. S. Matheson, J. Rabani, and J. K. Thomas, *Discuss. Faraday Soc.*, **36**, 193 (1963); (c) E. J. Hart, S. Gordon, and J. K. Thomas, *J. Phys. Chem.*, **68**, 1271 (1964).

(2) K.-D. Asmus, A. Henglein, A. Wigger, and G. Beck, *Ber. Bunsenges. Phys. Chem.*, **70**, 756 (1966).

(3) See, for example, (a) K.-D. Asmus, A. Henglein, M. Ebert' and J. P. Keene, *ibid.*, **68**, 657 (1964); (b) K.-D. Asmus, A. Wigger' and A. Henglein, *ibid.*, **70**, 862 (1966).

(4) S. Arai and I. M. Dorfman, *J. Phys. Chem.*, **69**, 2239 (1965).

(5) E. Hayon, *J. Chem. Phys.*, **53**, 2353 (1970).

(6) M. A. J. Rodgers, *Trans. Faraday Soc.*, **67**, 1029 (1971).

ous solutions⁷ and recently also of alcoholic solutions.^{8,9} Acetone is expected to be quite a suitable solvent as well since equivalent conductances of ions are fairly high with *ca.* 180–200 $\Omega^{-1} \text{ cm}^2$ ¹⁰ per equivalent of an ion pair.

Experimental Section

Solutions. The experiments were carried out with acetone of "pro analysis" grade (Merck). Traces of water were removed by refluxing the solvent with anhydrous CaCl_2 and subsequently distilling under a constant flow of pure argon. A part of the column was heated to about 120° to avoid migration of ions. Tetranitromethane (Fluka purissimum p.a.) was purified by several washing procedures with triply distilled water. HClO_4 and NaOH were reagent grade and sodium isopropylate was prepared from sodium metal and isopropyl alcohol. The $\text{p}K$ of HClO_4 in acetone was determined to be 2.0 ± 0.2 by a conductivity method. In the concentration range used for our experiments, HClO_4 was therefore completely dissociated. Prior to the addition of solutes all samples (0.5–1 l.) were bubbled with specially pure argon (<2 ppm O_2) for *ca.* 1 hr.

The γ -ray experiments were carried out in a ⁶⁰Co source of *ca.* 2000 Ci and at an absorbed dose rate of 4×10^4 rads/hr. Pulse radiolysis experiments were done with a 1.5-MeV Van de Graaff (10 mA). The flow system, the optical and conductivity setup, and the associated electronic equipment have already been described in detail.^{7,11} All experiments were carried out at 18°.

For all optical experiments with tetranitromethane and carbon tetrachloride a filter, BG 12 (Schott), was used to cut off the light below 300 nm. Without the filter photolysis processes were observed which affected the stability of the solutes and also increased the background conductivity of the solutions.

Extinction Coefficients. The spectrum and the extinction coefficient of $\text{C}(\text{NO}_2)_3^-$ ions were determined using solutions of $\text{C}(\text{NO}_2)_3\text{K}$ in acetone. ($\text{C}(\text{NO}_2)_3\text{K}$ was prepared by the reaction of concentrated aqueous KOH with tetranitromethane and purified by several washing procedures with water and alcohol.) They were identical within the limits of error with the data in aqueous solutions: $\lambda_{\text{max}} = 350 \pm 2$ nm and $\epsilon_{350} = (1.50 \pm 0.05) \times 10^4 \text{ M}^{-1} \text{ cm}^{-1}$. For anthracene anions the literature value of $\epsilon_{720 \text{ nm}} = 1.0 \times 10^4 \text{ M}^{-1} \text{ cm}^{-1}$ was taken.¹²

Dosimetry. In the pulse radiolysis experiments the solutions were irradiated with pulses of 0.3–1.5- μsec duration. The absorbed dose (*ca.* 150 rads for the shortest pulse) was monitored with a secondary emission foil. Absolute dosimetry was based on simultaneous optical and conductivity measurements of $\text{C}(\text{NO}_2)_3^-$ ions which are produced with $G = 6.0$ in irradiated aqueous solutions of 10^{-3} M $\text{C}(\text{NO}_2)_4$ and 10^{-1} M isopropyl alcohol.^{7,8} Since dosimetry was carried out with

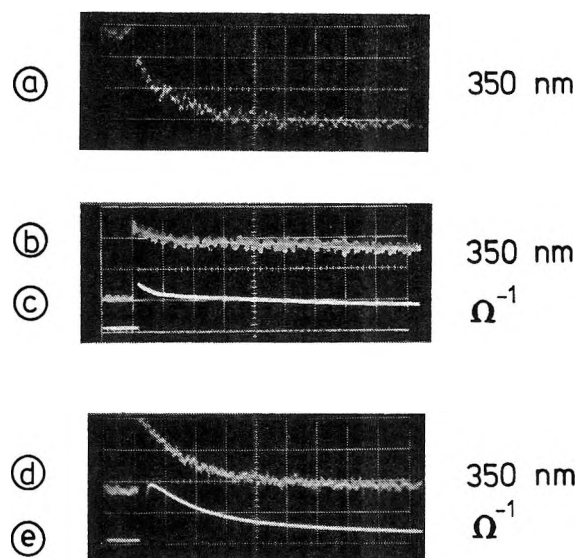


Figure 1. Changes in optical density and conductivity in pulse-irradiated solution of $\text{C}(\text{NO}_2)_4$ in argon-saturated acetone. (a) Formation of $\text{C}(\text{NO}_2)_3^-$ ions; λ 350 nm; $5.2 \times 10^{-6} \text{ M}$ $\text{C}(\text{NO}_2)_4$; pulse, 0.5 μsec ; time scale, 10 $\mu\text{sec}/\text{cm}$ (reversed signal). (b) Optical absorption at 350 nm; 10^{-3} M $\text{C}(\text{NO}_2)_4$; pulse, 1 μsec ; time scale, 100 $\mu\text{sec}/\text{cm}$. (c) Conductivity signal (same conditions as for 1b). (d) Optical absorption at 350 nm; 10^{-3} M $\text{C}(\text{NO}_2)_4$; $3.4 \times 10^{-6} \text{ M}$ HClO_4 ; pulse, 1 μsec ; time scale, 50 $\mu\text{sec}/\text{cm}$. (e) Conductivity signal (same conditions as for 1d).

aqueous solutions, appropriate corrections were made for the difference in density and electron density of acetone solutions.

Conductivity Experiments. Quantitative analysis of the conductivity data is based on eq I, which describes the observed voltage signal, ΔU_s , due to the conductivity changes in the pulse-irradiated solution⁷

$$\Delta U_s = \frac{U_b \times R_a}{10^3 \times k_z} \Delta \sum_i c_i |z_i| \Lambda_i \quad (\text{I})$$

U_b is the voltage between the electrodes (10–100 V), R_a (1 k Ω) is an operating resistance in series with the cell, k_z is the cell constant in reciprocal centimeters, c_i is the concentration of the charged species produced as a result of the irradiation, z_i is the charge number, and Λ_i is the equivalent conductivity in $\Omega^{-1} \text{ cm}^2 \text{ equiv}^{-1}$. The cell constant was determined with the aqueous tetranitromethane dosimetry solution for each set of experiments (average value $k_z = 0.7 \text{ cm}^{-1}$). Since k_z is a geometric parameter of the cell, the same value was applied for the acetone solutions. To avoid

(7) G. Beck, *Int. J. Radiat. Phys. Chem.*, **1**, 361 (1969).

(8) K.-D. Asmus, S. A. Chaudhri, N. B. Nazhat, and W. F. Schmidt, *Trans. Faraday Soc.*, **67**, 2607 (1971).

(9) P. Fowles, *ibid.*, **67**, 428 (1971).

(10) Landolt-Börnstein, "Zahlenwerte und Funktionen," Vol. 7/II, Springer-Verlag, West Berlin, 1960.

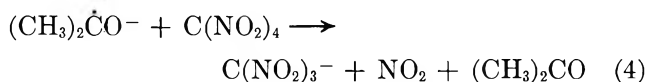
(11) A. Henglein, *Allg. Prakt. Chem.*, **17**, 296 (1966).

(12) D. Gill, J. Jagur-Grodzinski, and M. Szwarc, *Trans. Faraday Soc.*, **60**, 1424 (1964).

polarization effects at the electrodes the polarity of the dc voltage was changed with a frequency of 10 Hz.

Results

1. *Solutions of Tetranitromethane.* Tetranitromethane is reduced in irradiated acetone solutions to produce nitroform anions $C(NO_2)_3^-$. This process together with the neutralization of the nitroform anion is shown in Figure 1. Nitroform anions were identified by their optical spectrum and were found to be the only absorbing species at 350 nm. The formation of $C(NO_2)_3^-$ anions (Figure 1a) occurs *via* a one-step reaction which is attributed to the electron-transfer process

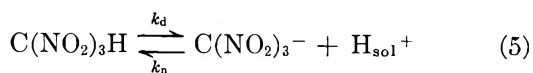


with the $(CH_3)_2\dot{C}O^-$ ion having been formed according to reaction 1. The reaction kinetics are of pseudo-first order since the $(CH_3)_2\dot{C}O^-$ concentration (*ca.* $5 \times 10^{-7} M/1\text{-}\mu\text{sec}$ pulse) is small compared with the tetranitromethane concentration used of 5×10^{-6} to $5 \times 10^{-5} M$. Consequently the half-life, $t_{1/2}$, of the electron-transfer process (reaction 4) is inversely proportional to the tetranitromethane concentration. The bimolecular rate constant for the $C(NO_2)_3^-$ ion formation is calculated to be

$$k_4 = \frac{\ln 2}{t_{1/2}[C(NO_2)_4]} = (1.2 \pm 0.2) \times 10^{10} M^{-1} \text{sec}^{-1}$$

Figures 1b and c show the partial neutralization of the nitroform anion in "neutral" solutions of $10^{-3} M$ TNM in acetone. Both the optical absorption signal at 350 nm and the conductivity signal which have been built up during the $1\text{-}\mu\text{sec}$ pulse decay to *ca.* $2/3$ of the initial yield. Addition of $3.4 \times 10^{-5} M$ $HClO_4$ leads to an almost complete neutralization of the $C(NO_2)_3^-$ ion as is shown in Figures 1d and e.

The dissociation constant of the acid-base equilibrium



may be obtained from a plot of the remaining optical absorption or conductivity after the partial neutralization of the $C(NO_2)_3^-$ ions as a function of H_{sol}^+ concentration.⁸ Since it is difficult to adjust the proton concentration in the interesting range below $10^{-5} M$ with the desired accuracy a second independent method using γ radiolysis was also applied to determine the dissociation constant K_5 .⁸ In irradiated solutions of tetranitromethane ($10^{-3} M$) the $C(NO_2)_3^-$ ion concentration equals the H_{sol}^+ concentration, so that the equilibrium (reaction 5) can be written in the form $[C(NO_2)_3^-]^2 = K_5[C(NO_2)_3H]$. The $C(NO_2)_3^-$ ion concentration can be measured directly, the $C(NO_2)_3H$ concentration after dilution with H_2O , *i.e.*, complete dissociation.

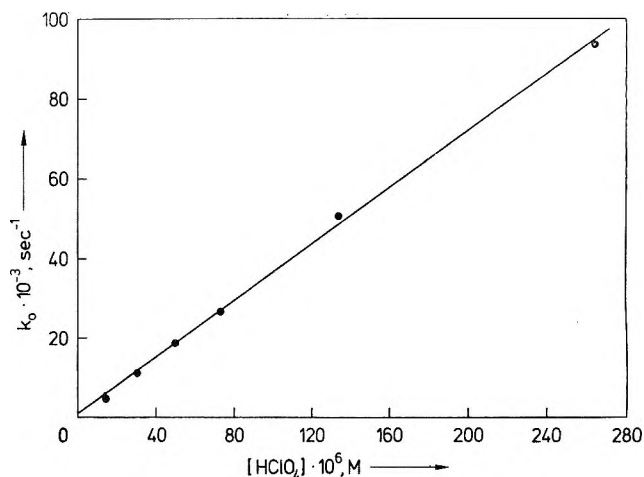


Figure 2. The observed first-order rate constants for the neutralization of $C(NO_2)_3^-$ ions *vs.* $HClO_4$ concentration.

From both the γ ray and the pulse radiolysis experiments $K_5 = 4.5 \times 10^{-6} M$ with an accuracy of $\pm 0.1 \times 10^{-6}$ and $\pm 0.8 \times 10^{-6} M$, respectively, *i.e.*, $pK_5 = 5.35 \pm 0.10$ was derived.

The quantitative kinetic analysis of the decay of the optical and conductivity curves in Figure 1 involve both the forward and the back reactions of the equilibrium given in reaction 5. Following a general kinetic treatment of a reversible reaction¹³ the rate constant for the observed pseudo-first-order disappearance of the anion in solutions with $[H_{sol}^+] > [C(NO_2)_3^-]$ is given by⁸

$$k_0 = k_n[H_{sol}^+] + k_d \quad (II)$$

Accordingly a plot of k_0 *vs.* $[H_{sol}^+]$ gives a straight line (Figure 2). From the slope the neutralization rate constant $k_n = 3.6 \times 10^8 M^{-1} \text{sec}^{-1}$ is derived. The rate constant for the dissociation, k_d , could be obtained from the intercept. Since it is very small, the error, however, is very large. It is calculated, therefore, from the known relationship

$$k_d = K \times k_n = 4.5 \times 10^{-6} \times 3.6 \times 10^8 = 1.62 \times 10^3 \text{sec}^{-1}$$

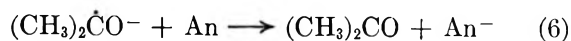
In pulse-irradiated solutions of $10^{-3} M$ tetranitromethane in acetone, nitroform ions are produced with an initial yield of $G(C(NO_2)_3^-) = 2.15 \pm 0.1$. This is calculated from the change in optical absorption immediately after the pulse (Figures 1b and d), the absorbed dose, and the known extinction coefficient of $C(NO_2)_3^-$.

From the initial change in conductivity and the $C(NO_2)_3^-$ concentration, and using eq I, the equivalent conductance of the $C(NO_2)_3^- + H_{sol}^+$ ion pair in acetone is calculated to be $\Delta_{C(NO_2)_3^- + H_{sol}^+} = 220 \pm 10 \Omega^{-1} \text{cm}^2 \text{equiv}^{-1}$. Since $\Lambda_{H_{sol}^+}$ in acetone is known to be $90 \Omega^{-1} \text{cm}^2 \text{equiv}^{-1}$,¹⁰ the equivalent conductance

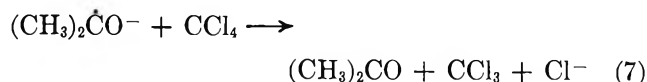
(13) A. A. Frost and R. G. Pearson in "Kinetics and Mechanism," 2nd ed, Wiley, New York, N. Y., 1963, Chapter 8, p 160.

of a nitroform ion is calculated to be $\Lambda_{C(NO_2)_3^-} = 130 \pm 10 \Omega^{-1} \text{ cm}^2 \text{ equiv}^{-1}$. This value is very similar to that of other large ions such as NO_3^- ($\Lambda = 120 \Omega^{-1} \text{ cm}^2 \text{ equiv}^{-1}$) or ClO_4^- ($\Lambda = 115 \Omega^{-1} \text{ cm}^2 \text{ equiv}^{-1}$) in acetone.¹⁰

2. *Solutions of Anthracene and Carbon Tetrachloride.* Both anthracene (An) and carbon tetrachloride are also reduced in irradiated acetone solutions. The electron-transfer processes



and



are followed by the neutralization of the An^- and Cl^- ions. The formation and disappearance of the anthracene anion could be observed simultaneously at 720 nm and by conductivity measurements. Using $\epsilon_{\text{An}^- 720\text{nm}} = 1.0 \times 10^4 \text{ M}^{-1} \text{ cm}^{-1}$ an initial yield of $G(\text{An}^-) = 1.7 \pm 0.2$ is calculated for a solution of $5 \times 10^{-3} \text{ M}$ anthracene in acetone. The true yield of An^- ions, however, might be considerably smaller than 1.7. As indicated in some recent work⁶ the absorption at 720 nm is due not only to negative but also to positive anthracene ions. From this and the observed conductivity signal the equivalent conductance $\Lambda_{\text{H}_{\text{sol}}^+ + \text{An}^-} = 225 \pm 20 \Omega^{-1} \text{ cm}^2 \text{ equiv}^{-1}$ is derived. The equivalent conductance of the anthracene anion of $\Lambda_{\text{An}^-} = 135 \pm 20 \Omega^{-1} \text{ cm}^2 \text{ equiv}^{-1}$ is, therefore, quite similar to that of the nitroform anion. The presence of some positive ions would have only little effect on the Λ values because all ions in acetone have quite similar equivalent conductivities.¹⁰

In solutions of CCl_4 in acetone only changes in conductivity could be observed. Similar to the tetranitromethane and anthracene solutions the conductivity is increased upon pulse irradiation due to the formation of Cl^- and H_{sol}^+ . The subsequent neutralization of Cl^- then causes the decay of the signal. The chloride ion yield can be calculated from the known equivalent conductances $\Lambda_{\text{H}_{\text{sol}}^+ + \text{Cl}^-} = 90 + 105 = 195 \Omega^{-1} \text{ cm}^2 \text{ equiv}^{-1}$ ¹⁰ and the change in conductivity extrapolated to the middle of the electron pulse. For solutions of $2.5 \times 10^{-3} \text{ M}$ CCl_4 , $G(\text{Cl}^-) = 1.40 \pm 0.10$ was obtained.

The neutralization processes of anthracene anions and chloride ions are much faster than that of the nitroform ions. The half-life of these ions is *ca.* 10–20 μsec in "neutral" solutions. The observed conductivity signals disappear upon addition of $<10^{-5} \text{ M}$ perchloric acid; *i.e.*, the lifetime of the ions becomes so short that they cannot be observed anymore. Since the H_{sol}^+ concentration cannot be determined with a reasonable accuracy and particularly since it is not possible to cover a wide enough H_{sol}^+ concentration range, the absolute determination of the involved reaction rate constants is

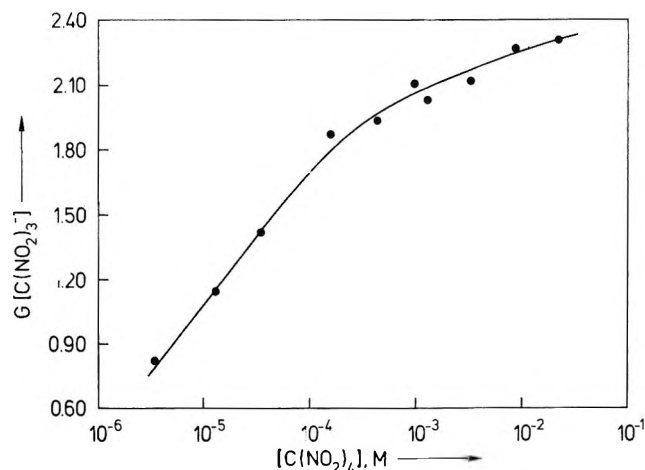
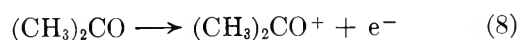


Figure 3. Initial yields of $\text{C}(\text{NO}_2)_3^-$ ions vs. $\text{C}(\text{NO}_2)_4$ concentration.

rather difficult. It can be said, though, that the neutralization rate constant is *ca.* two orders of magnitude higher than that for nitroform ions.

3. *The Concentration Dependence for the Scavenging of Reducing Species.* Figure 3 shows the yield of nitroform ions measured immediately at the end of the pulse as a function of the tetranitromethane concentration in the acetone solution. Over the entire concentration range of 3.5×10^{-6} to $2.2 \times 10^{-2} \text{ M}$, $G(\text{C}(\text{NO}_2)_3^-)$ is steadily increasing. Though the curve is leveling off at concentrations $>10^{-3} \text{ M}$, it apparently has not yet reached its final value. Similarly the yield of anthracene anions is increasing with increasing anthracene concentration.

4. *Pure Acetone.* In pure acetone ionization leads to the formation of electrons the majority of which are expected to react with the solvent to form $(\text{CH}_3)_2\dot{\text{C}}\text{O}^-$ ions before they can recombine with the positive ion. It is not possible to observe these ions or their neutralization product, $(\text{CH}_3)_2\dot{\text{C}}\text{OH}$ by optical pulse radiolysis measurements since both of the transient species absorb in the same region as the solvent itself. In pulse radiolysis conductivity experiments, however, a transient signal is observed which is shown in Figure 4. The strong negative signal in the first few microseconds has no chemical significance. It is due to changes in the double layers of the electrodes and the outflow of charges from the electron beam.⁷ The positive signal arises from the production of ions in the irradiated acetone. The transient conductivity disappears with a half-life of *ca.* 20 μsec , and no permanent conductivity remains after *ca.* 100 μsec . In the ionization process



electrons and positive acetone ions will be produced initially. The electron capture process (reaction 1) by the solvent molecules is expected to occur immediately after the e^- formation, *i.e.*, in a time less than the time resolution of the experimental method. The conduc-

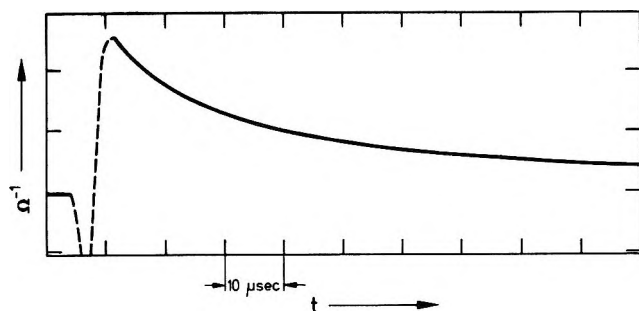
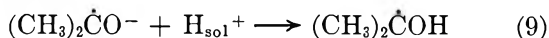


Figure 4. Changes in conductivity in pulse-irradiated pure acetone: pulse, 0.5 μsec ; time scale, 10 $\mu\text{sec/cm}$.

tivity signal, therefore, will be given by the acetone anion and the positive counterion. The latter is assumed to be the solvated proton resulting from a fast proton transfer from $\text{CH}_3\text{COCH}_3^+$ to acetone^{14,15} (analogous to the process in alcohols). The observed decay of the conductivity curve is explained by the neutralization process



This reaction is expected to occur quantitatively and fast since the dissociation constant of the isopropyl alcohol radical in acetone should be very small.

Kinetic analysis of the conductivity signal shows it to be of a mixed order. Upon addition of $10^{-5} M$ acid the $(\text{CH}_3)_2\dot{\text{C}}\text{O}^-$ ions become already so short-lived that they cannot be observed anymore. The rate constant for the neutralization process (reaction 9) can, therefore, only be estimated to be in the range 10^{10} to $10^{11} M^{-1} \text{sec}^{-1}$.

It is possible, however, to derive the yield of ion pairs produced during the pulse. Extrapolation to the middle of the 0.5- μsec pulse gave quite reproducible values for the product of the initial ion-pair concentration and the equivalent conductance (see eq I). $\Lambda_{\text{H}_{\text{sol}}^+}$ is known ($90 \Omega^{-1} \text{cm}^2 \text{equiv}^{-1}$). The equivalent conductance of the $(\text{CH}_3)_2\dot{\text{C}}\text{O}^-$ ion has not been reported yet. It should be similar, though, to that of other anions and can be estimated to be $105 \pm 20 \Omega^{-1} \text{cm}^2 \text{equiv}^{-1}$ giving a total of $195 \pm 20 \Omega^{-1} \text{cm}^2 \text{equiv}^{-1}$ for the $(\text{CH}_3)_2\dot{\text{C}}\text{O}^- + \text{H}_{\text{sol}}^+$ ion pair.

The yield of detectable ion pairs can, therefore, be calculated and was found to be $G = 1.20 \pm 0.20$. The uncertainty is mainly given by the unknown equivalent conductance of $(\text{CH}_3)_2\dot{\text{C}}\text{O}^-$ ions.

Changing the voltage between the two electrodes from 10 to 100 V did not change the yield. The observed yield of $G = 1.20$, therefore, is assumed to represent the yield of free ion pairs in acetone.

Discussion

The lifetime of the $(\text{CH}_3)_2\dot{\text{C}}\text{O}^-$ ions in pulse-irradiated acetone with respect to their neutralization has been shown to be long enough to attribute the bimolecular reaction rate constant for the $\text{C}(\text{NO}_2)_3^-$, An^- , and

Cl^- ion formation to an electron-transfer process from the acetone ion to tetranitromethane, anthracene, and CCl_4 , respectively. In all the cases the observed yields of the secondary ions at high solute concentrations are greater than the yield of free $(\text{CH}_3)_2\dot{\text{C}}\text{O}^-$ ions. The concentration dependence shown in Figure 3 suggests that a part of the so-called geminate ions can be observed in our pulse radiolysis experiments. This is an interesting observation since the lifetime of the ions which undergo geminate recombination generally was found to be so short that they could be observed only in the submicrosecond range.¹⁶ It is, therefore, appropriate at this point, to exclude other "homogeneous" reactions which could lead to the high ion yields. One possible reducing species in addition to $(\text{CH}_3)_2\dot{\text{C}}\text{O}^-$ ions is the hydrogen atom. From previous work^{17,18} on the radiolysis of acetone, it can be concluded, however, that $G(\text{H}\cdot)$ is essentially negligible. All the other species formed upon irradiation of acetone, *i.e.*, $(\text{CH}_3)_2\text{CO}^+$, $\dot{\text{C}}\text{H}_2\text{COCH}_3$, acetone triplet, etc., have not been found to have any reducing properties.^{3a,6} The higher yield of nitroform ions which become homogeneously distributed throughout the solution can be explained as follows. The rate constant for the neutralization of $\text{C}(\text{NO}_2)_3^-$ ions in acetone, as well as in other solvents,¹⁹ is much smaller than is expected for a merely diffusion-controlled process, thereby indicating that some activation energy might be involved. It is reasonable to assume that this activation energy and, therefore, a similar rate constant also applies for the recombination of those ion pairs which initially were produced within the range of their mutual Coulombic attraction. As a result of this the spectrum of the ion pair lifetime distribution will be shifted to longer times, and a much higher fraction of $\text{C}(\text{NO}_2)_3^-$ ions will be able to escape the geminate recombination process than of $(\text{CH}_3)_2\dot{\text{C}}\text{O}^-$ ions. Even if one argues that the neutralization process is faster and equilibrium conditions are different in the geminate range than in the bulk of the solution the result remains the same. A certain fraction of the geminate ions would still show up in the homogeneous system, since $\text{C}(\text{NO}_2)_3\text{H}$ molecules after diffusion into bulk of the solution will dissociate according to the prevalent equilibrium conditions. Both the Cl^- and An^- ion yields from the reduction of CCl_4 and anthracene, respectively, only slightly exceed $G((\text{CH}_3)_2\dot{\text{C}}\text{O}^-)$. This, however, is to be expected since the estimated rate constants for the neutralization of these ions by solvated protons is close to that for diffusion-controlled processes.

(14) T. Shida and W. Hamill, *J. Amer. Chem. Soc.*, **88**, 3683 (1966).

(15) M. S. B. Murton, *ibid.*, **87**, 5313 (1965).

(16) J. K. Thomas, K. Johnson, T. Klippert, and R. Lowers, *J. Chem. Phys.*, **48**, 1608 (1968).

(17) P. Ausloos and B. F. Paulson, *J. Amer. Chem. Soc.*, **80**, 5117 (1958).

(18) R. Barker, *Trans. Faraday Soc.*, **59**, 375 (1963).

(19) S. A. Chaudhri and K.-D. Asmus, *Trans. Faraday Soc.*, in press.

Our results, of course, raise a question about the meaning of the "free" ion yields as determined by chemical reactions in pulse radiolysis experiments on the μsec time scale and in the steady-state studies. In hydrocarbons the chemically determined data agree well with those obtained by direct conductivity measurements.²⁰ In all these cases the neutralization of ions both in the homogeneous and in the geminate range is essentially an irreversible process, since the equilibrium lies com-

pletely on the side of the undissociated form. If, however, the equilibrium conditions are such that the neutralization of the ions could be regarded as a reversible process, the observed "free" ion yield would entirely depend on the particular scavenger employed.

(20) See, for example, J. M. Warman, K.-D. Asmus, and R. H. Schuler, *Advan. Chem. Ser.*, No. 82, 25 (1968), and references cited therein.

Laser-Induced Gas Breakdown: Spectroscopic and Chemical Studies^{1a}

by Ph. de Montgolfier,^{*,1b,c} P. Dumont,^{1c} Y. Mille,^{1c} and J. Villermaux^{1c}

Theoretical Chemistry Institute, University of Wisconsin, Madison, Wisconsin 53706 and Centre de Cinétique Physique et chimique du CNRS, route de Vandoeuvre, 54 Villers les Nancy, France (Received July 7, 1971)

Publication costs assisted by Commissariat à l'Energie Atomique

In this paper we report the results of several investigations on laser-induced gas breakdown. These experiments included time-resolved spectroscopy, direct detection of H atoms with a TiO₂ probe, and chemical reactions; each of them provided insight into the behavior of the medium at different times. The spectroscopic study allowed us to isolate three effects contributing to the emission of light from the plasma: the bremsstrahlung radiation of the electrons, the line emission of the atoms or molecules, and a third peak which might correspond to an emission of light occurring in a supersonic blast in the direction of the laser. Comparison of the intensity of both the bremsstrahlung and line radiation with the number of H atoms, detected in a flow of hydrogen irradiated with the laser beam, showed that atoms were probably created during collisions with electrons. Chemical reactions and explosions have been initiated by the laser beam when a plasma was created. No primary multiphotonic absorption and no macroscopic chemical reactions were observed below the breakdown threshold.

I. Introduction

By focusing a Q switched laser beam, one can get an intense energy flux density ($\sim 10^{15}$ W/cm²). Above a threshold density there is a breakdown of air at the focus of the lenses;²⁻⁵ an intense blue-white ball appears accompanied by a clapping and a sharp reduction of the laser beam transmitted through the focal zone. There is also a pressure threshold, a function of the gas, under which nothing happens. The elementary processes are very complex and numerous: (1) creation of the first electrons; (2) heating of these electrons by inverse bremsstrahlung electron-neutral, or electron-ion; (3) emission of light by bremsstrahlung; (4) diffusion out of the focal zone; (5) ionizing collisions; (6) recombinations of ions and electrons; (7) elastic and inelastic collisions; (8) expansion of the plasma and shock waves: macroscopic movements of the plasma.

In order to analyze such a complex and rapidly evolving system, many different methods have been used. It is not our purpose to review here all the results obtained. We will recall only that, after an

initial period of time, there is a multiplication of electrons, in a very fast cascade, mainly by the mechanisms 2 and 5 above. Inverse bremsstrahlung is much more efficient in electron-ion collisions than in electron-neutral ones. Therefore, when the number of ions is sufficient there is a tremendous heating of the plasma, expansion, and often shock waves. After the extinction

* Address correspondence to this author at La Solitude, 07 Peaugres, France.

(1) (a) This research received financial support from: commissariat à l'Energie Atomique, Centre National de la Recherche Scientifique, and from the National Aeronautics and Space Administration Grant NGL 50-002-00; (b) Theoretical Chemistry Institute; (c) Centre de Cinétique Physique et Chimique.

(2) See, for example, L. V. Keldysh, *Soviet Phys. JETP*, **20**, 1307 (1965); H. B. Bebb and A. Gold, *Phys. Rev.*, **143**, 1 (1966); Y. Gontier and M. Trahin, *ibid.*, **172**, 83 (1968); Y. Mille, Thesis, Nancy, France, 1971.

(3) (a) R. G. Meyerand and A. F. Haught, *Phys. Rev. Lett.*, **11**, 401 (1963); (b) R. W. Minck, *J. Appl. Phys.*, **35**, 252 (1964).

(4) P. Agostini, J. P. Bonnal, C. Mainfray, and C. Manus, *C. R. Acad. Sci. Ser. B*, **266**, 1034 (1968).

(5) See, for example, W. F. Braerman, L. R. Stumpfel, and H. J. Kunze, *J. Appl. Phys.*, **40**, 2549 (1969).

of the laser beam, the plasma cannot increase its energy, and there is a dissipation of energy. By lowering the gas pressure, one can control the development of the cascade and hopefully study the primary processes creating the first electrons.

The different theories proposed in order to explain the primary processes of laser-induced gas breakdown² do not require that every atom or molecule excited to a discrete electronic level must be ionized later. In numerous studies, attempts have been made to measure at different pressures the number of electrons or ions created^{3,4} and the light emitted by the plasma.⁵ Recently, chemical reactions have been initiated by laser-induced gas breakdown,⁶⁻⁹ but unfortunately experimental conditions varied in all these experiments and it is difficult to compare the results.

In the following report we describe experiments, partially published elsewhere,¹⁰⁻¹² in which are compared the evolutions of different particles relevant in the medium's dynamics, including electrons, excited states, atoms, and products of reactions. By spectroscopy one can make conspicuous the radiation of bremsstrahlung of electrons and the radiative de-excitation of particular excited states. The hydrogen atoms created by interaction of the laser beam and a flow of molecular hydrogen are detectable with a semiconductor probe. Finally, some chemical reactions may be initiated.

Thus one can follow the evolution of the irradiated medium through time and know the origin of the excited species. The two last types of experiments can also be considered as means of detection giving an upper bound to the number of molecules dissociated by multiphotonic absorption.

II. Spectroscopic Study

A. Experimental Apparatus. We used a LASER CILAS VD 160 having the following characteristics: output energy = 3 J, λ 1.06 μ , FWHM time = 30 nsec, divergence of the beam = 5×10^{-4} radian. The electrical and optical setup (Figure 1) is fully described elsewhere.^{13,14} A double monochromator HUET M225 using two optical gratings with 610 lines per millimeter, blazed for 5000 Å, was coupled with a photomultiplier tube 56CVP or 53AVP (FWHM of output pulse = 5 nsec). The output pulses were monitored by an oscilloscope CRC 100 MHz which was triggered by a photocell CSF F9096. The photomultiplier was triggered *via* a coaxial line (50 Ω) to give the proper time delay. The spectral resolution was 5 Å and under our best conditions it was not possible to detect less than 10^3 photons per second at the focal point ($f = 8$ cm) of the laser beam.

B. Results. The spectral lines NII (4627 Å, 5007 Å) in nitrogen, HeI (5876 Å) and HeII (5686 Å) in helium, H α (6563 Å) in molecular hydrogen were studied in particular. In each case we observed an

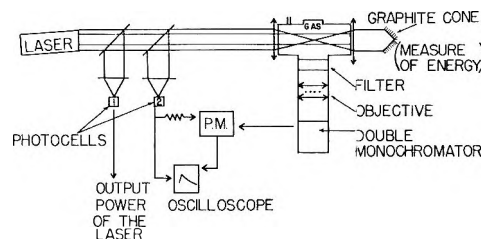


Figure 1. Block diagram of the apparatus. Photocell 2 triggers the oscilloscope and the photomultiplier P.M.

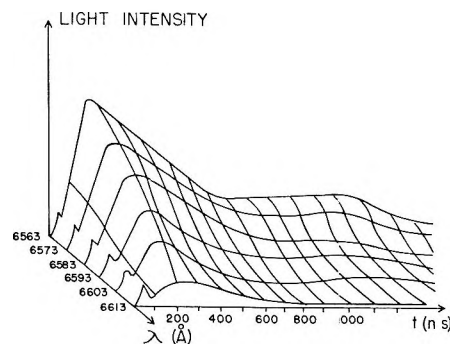


Figure 2. H α line; light intensity = $f(t, \lambda)$.

oscillogram showing three peaks corresponding to three luminous impulses appearing one after the other. In Figure 2 the results of H α line are reported.

The first peak appeared before the maximum impulse of the laser beam and earlier and earlier as the gas pressure was increased. It reached its maximum at the extinction of the laser beam and then decreased very rapidly. Since intensity also did not vary much with the wavelengths observed, it was concluded that this light was due to the bremsstrahlung radiation of the electrons. In Figure 3 the intensity of this peak is plotted against the gas pressure.

We have seen elsewhere^{10,13} that these results can be predicted by a model which ignores all inhomogeneities in the focal volume. Further simplifications give some insight on the differences of behavior of gases without any calculation: the evolution equation for the number of electrons has one term taking account of the rate of ionization (rate of energy increase by inverse brems-

(6) J. F. Verdick, *Nucl. Appl.*, **6**, 474 (1969).

(7) G. Porter, *Nature (London)*, **215**, 502 (1967).

(8) L. M. Epstein and K. H. Sun, *ibid.*, **211**, 1173 (1968).

(9) J. H. Lee and R. Knystautas, *AIAA J.*, **7**, 312 (1968).

(10) P. Dumont, Y. Mille, and P. de Montgolfier, to be published.

(11) P. Dumont and P. de Montgolfier, *J. Chim. Phys. Physicochem. Biol.*, **9**, 1284 (1971).

(12) P. Dumont and P. de Montgolfier, *ibid.*, accepted for publication.

(13) P. Dumont, Thesis, Nancy, 1970, Centre de Cinétique Physique et Chimique du CNRS, Route de Vandoeuvre, 54-Villers les Nancy, France.

(14) Y. Mille, Diplôme d'études approfondies, Nancy, 1968, Centre de Cinétique Physique et Chimique du CNRS, Route de Vandoeuvre, 54-Villers les Nancy, France.

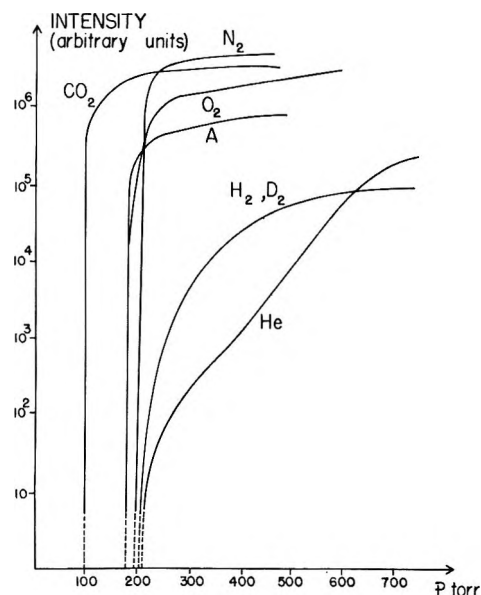


Figure 3. Bremsstrahlung light vs. gas pressure.

strahlung divided by a threshold energy ionization potential) and one other taking account of the losses by diffusion out of the focal volume. The diffusion constant is inversely proportional to the mass of the molecule, and therefore the losses are more important for helium than for argon or oxygen. Inverse bremsstrahlung cross sections increase with the energy of electrons much faster for heavy gases than for light ones,¹⁵ and as the ionization potential of helium is the highest, the rate of production of electrons by ionizing collisions will be low when compared to other gases and less sensitive to gas pressure.

A second peak, which appeared after the extinction of the laser beam, was centered on the spectral lines of the gas. Its decay time varied with the gas between several hundred and several thousand nanoseconds. By examining different points of the focal zone, we saw that the plasma was not homogenous and had two centers which were more intense. Nevertheless the decay time of the signal was the same at any part within the plasma, and one can assume that the processes giving rise to the excited states were identical throughout the plasma. We were able to compute the variations with time of the electron density N_e (electrons/cm³) and temperature T_e (°K) of the plasma by studying the line's shapes and their stark broadening: in Figure 4 we present the results for H_α line. One can see that T_e is stabilized for several microseconds while N_e is still decreasing. These results agree with those recently reported for helium.⁵

In the triparticular process, $H^+ + 2e \rightarrow H + e^*$, electrons increase their kinetic energy, and this gain can compensate for the losses in inelastic collisions for a time. During this period of time, collision cross sections were constant, and the decay of the second peak paralleled very closely the variation of N_e . Therefore

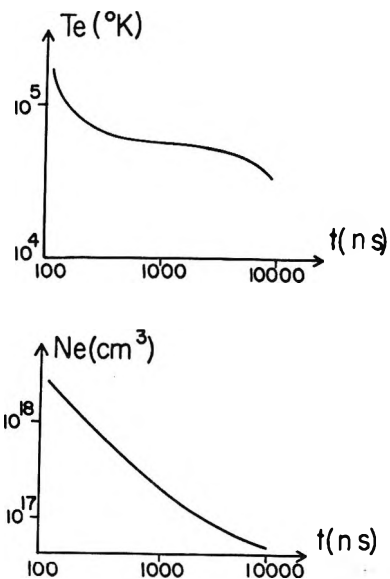


Figure 4. H_α line; electronic temperature and density at different times.

the corresponding excited states were probably produced in processes of first order with respect to electrons, such as: $H + e(\epsilon_1) \rightarrow H^* + e(\epsilon_2)$.

Numerous species and processes play a role in plasma's dynamics. In order to calculate T_e and N_e we supposed that the hypothesis of local thermodynamic equilibrium (LTE) applied. It could not be so if the process described above was predominant in the plasma's behavior. Actually we think that it plays a very small role and that evidence of the main processes could be investigated in the ultraviolet region.

The area under the second peak is plotted in Figure 5 vs. the gas pressure for the H_α and NII 4627 Å lines. At low pressures we could not see any inflection of the curves corresponding to the excited states created by multiphotonic absorption. In particular, for helium, the light emitted in the transition $3d \ ^3D \rightarrow 2p \ ^3P_0$, which is especially intense at ordinary pressure, did not show any irregularity at low pressures. This will be discussed in section V.

The third peak has been studied recently.^{16,17} It was centered on spectroscopic lines and appeared 300 nsec or several μ sec after the second signal, according to the part of the focal region examined: this result may be explained by assuming that the luminous zone was displaced toward the laser with a speed of 10^4 or 10^5 cm/sec. Its decay time is analogous to the decay time of the second peak, and the limit pressure of appearance is larger.

(15) Y. Zel'dovich and Yu P. Raizer, *Soviet Phys. JETP*, **20**, 772 (1965).

(16) V. Chalmeton, R. Rapouar, *C. R. Acad. Sci.*, **264**, 213 (1967).

(17) G. Lampis and S. C. Brown, *Phys. Fluids*, **11**, 1137 (1968).

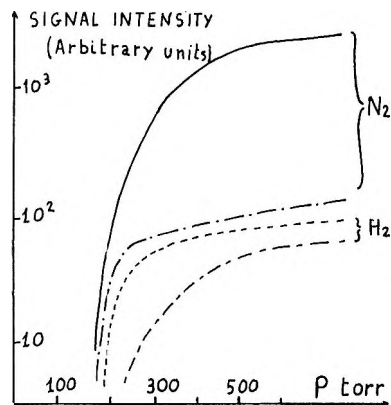


Figure 5. Intensity vs. pressure: —, NII 4627 Å; --, bremsstrahlung N₂; - · - ·, H_α line; · · · ·, bremsstrahlung H₂.

C. Sensibility of Detection and Breakdown's Threshold. The overall characteristics of the detection are: solid angle studied, 10^{-2} steradian; quantal efficiency of the photocathode, 10%; maximal gain, 10^6 ; time constant of the *Rc* circuit of charge, 0.7 nsec. In the most unfavorable case, *i.e.*, if a completely uniform distribution of excited states is created by direct multiphotonic absorption during the laser pulse, we would have been able to detect 10^6 deexcitations if the lifetime of excited states did not exceed 50 nsec.

Because of the very rapid increase with pressure in the intensity of the radiation emitted from the gas at fixed laser energy, we can define a threshold pressure of breakdown. This concept is very useful for comparing different gases but has no precise definition. As we define the threshold, it corresponds to the pressure at which the electronic cascade develops very rapidly. At constant pressure we can also define a power threshold.

III. Direct Detection of Hydrogen Atoms

A. Experimental Apparatus. The laser beam was focused in a glass bulb.¹¹ The focus of the lens ($f = 8$ cm) was on the axis of a glass tube (diameter = 2 mm) which served to introduce a large flow of H₂. A TiO₂ probe, whose distance to the focus can be varied and measured, was set on the same axis (Figure 6). The laser beam was directed perpendicular to this axis. The chemisorption of H atoms on TiO₂ has been extensively studied elsewhere;^{11,12} The change in conductivity of the probe due to the absorption is proportional to the local atomic concentration. One can show that H atoms created in the ionized volume and its vicinity were transported to the detector by the gaseous flow.^{11,13}

B. Results. Measuring the atomic concentration at different distances from the focus is equivalent to studying the homogeneous recombination of radicals at different times. Taking the usual value of the rate constant of this three particle process, 2×10^{-32} (cm³)² sec⁻¹, the recombination law is

$$\frac{1}{[H]} - \frac{1}{[H_0]} = 6 \times 10^{-3}t$$

A small part of the energy of the laser beam is absorbed by the plasma and later thermalized. This changes the constant of recombination negligibly, and we may neglect the effect of this absorption of energy from the laser.

The experimental law is

$$\frac{1}{[H]} - 1.75 \times 10^{-3}x = 0.5tx$$

where x is a constant which is a characteristic of the detector and whose value is unknown. But the comparison of these two expressions allows one to determine x , and therefore give an absolute measure of the local concentration of H atoms at different times.

In Figures 7 and 8 we have plotted the atomic concentration in the focal volume, just after the extinction of the plasma, as a function of the energy of the laser beam at 760 Torr and of the gas pressure at constant energy.

Below the breakdown's threshold we were not able to detect any H atoms. Under such conditions, taking account of the small focal volume (there is no plasma expansion), it would have been necessary to have 10^{11} dissociated molecules in order to detect any atoms.

IV. Chemical Reactions

Pyrex glass cells, of spherical or cylindrical shape, contained between 5 and 100 cm³ of the gas to be irradiated. The main product of reaction was analyzed

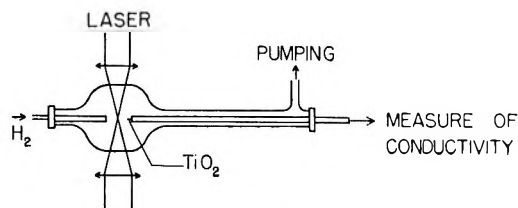


Figure 6. Direct detection of H atoms.

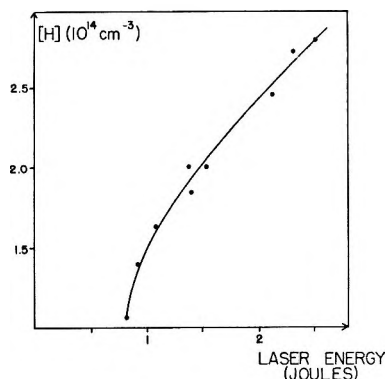


Figure 7. H concentrations in the focal volume just after the plasma extinction.

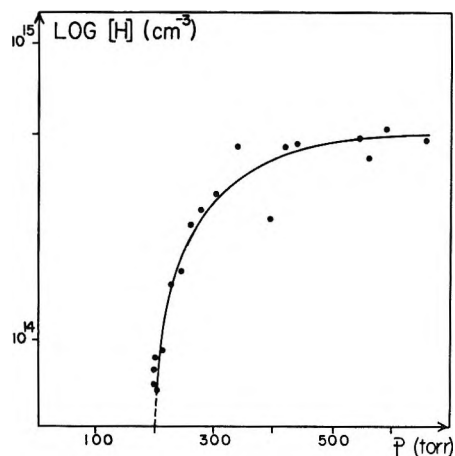


Figure 8. [H] concentrations at different pressures.

by gas phase chromatography or mass spectroscopy. We studied¹¹ the photolysis of acetaldehyde, the isotopic exchange between H_2 and D_2 , and some explosive mixtures: hydrogen and oxygen, hydrogen and chloride, acetone and oxygen, acetaldehyde and oxygen, propane and oxygen. Before the laser beam exposure, all the binary mixtures were equimolar.

Looking at the light emitted by the focal volume allowed us to determine the approximate development of the plasma at the time of the extinction of the laser beam.

We studied at first the reaction $H_2 + D_2 = 2HD$ by measuring the final concentration of HD. In Figure 9 this quantity is plotted at 760 Torr and 300°K against the laser beam energy. Below the threshold energy of 0.8 J we did not observe any HD. Analogous results were obtained for all other reactions.

Under the standard conditions of temperature and pressure the reaction $H_2 + Cl_2 = 2HCl$ can be initiated photochemically and is explosive. Porter⁷ observed this reaction below the breakdown threshold and interpreted it by assuming a dissociation of chloride by simultaneous absorption of two photons (ruby laser). With our laser (neodymium), one needs a three photon absorption to get the same result, and this mechanism is less probable. Nevertheless, if we compare this number to the ten photons necessary for the multiphotonic ionization of chloride, one could expect to see a photodissociation in spite of the selection rules.

The rate of branching of the reaction $2H_2 + O_2 = 2H_2O$ is small at standard T and P when compared to the rates of recombination of the radicals involved. Therefore one cannot initiate an explosion by creating locally a high atomic concentration. However an explosion occurred each time the mixture was irradiated with a laser beam whose energy was above the threshold; this is strong evidence for the important role played in the evolution of the reaction by the transformation of a part of the photonic energy of the laser beam into thermal energy of the gas.

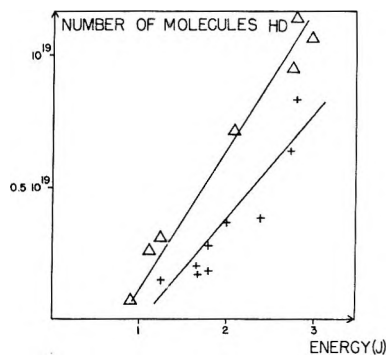


Figure 9. $HD = f(E)$: Δ , cell volume = 15 cm³; +, cell volume = 5 cm³.

When there is no breakdown, this energy transfer is negligible and we studied theoretically at 300°K and 600°K the progress of the reaction $H_2 + D_2 = 2HD$; the free radicals diffused from the center of the reactor and reacted together at the same time. Under our experimental conditions at least 10^{14} or 10^{15} molecules had to be dissociated in order to induce a detectable reaction. Optimizing all the physical parameters would lower this number to 10^{12} .

V. Discussion

All the experiments reported here might have given more precise results. This would have required very sophisticated apparatus and would have precluded the possibility of investigating more than a single aspect of the gas evolution.

Our results can be analyzed from several different points of view: chronometry, origin of the involved particles, multiphotonic absorption, chemical reactions.

The spectroscopic study allowed us to isolate three effects contributing to the emission of light from the plasma. The bremsstrahlung radiation from the electrons appeared first, reached its maximum at the extinction of the laser beam, and then decreased very rapidly. The radiative deexcitation of atoms became very important several hundred nanoseconds later. It is well known that during this interval the plasma expands greatly. The third peak might correspond to an emission of light occurring in a supersonic blast in the direction of the laser: this is the simplest interpretation of our results, but of course more detailed experiments are needed. In the case of molecular hydrogen, we determined the number of atoms present in the ionized volume after complete extinction of the plasma, *i.e.*, after a fraction of a millisecond. We followed the homogeneous recombination of these atoms and also the H_2 and D_2 exchange reactions. During these different moments of the evolution of the media, we had many evidences for macroscopic movements of the media.¹⁸

(18) P. de Montgolfier, WIS-TCI-442X, Theoretical Chemistry Institute, Madison, Wis., 1971.

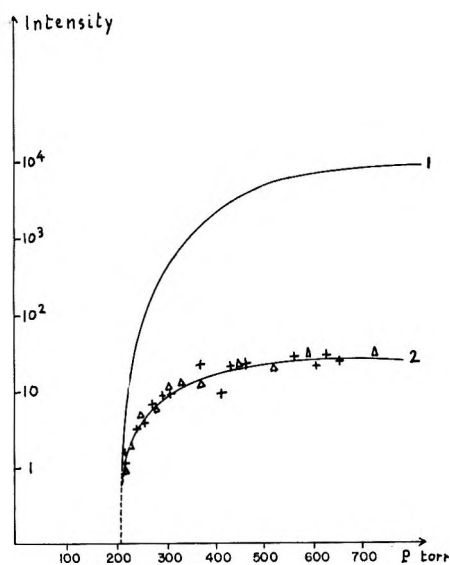
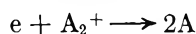


Figure 10. 1, I. bremsstrahlung; 2, square root of the I. bremsstrahlung intensity; X, [H]; Δ, H_{α} line intensity.

The bremsstrahlung effect is the emission of light occurring when electrons interact with ions or neutral particles. As a first approximation, ignoring the energy distribution of electrons, one can consider that the maximum intensity of this first peak is a measure of the square of the number of electrons in the plasma at the time of extinction of the laser beam. We have shown that the decrease in intensity of the spectral line H_{α} is of the first order with respect to the number of electrons, and concluded that the excited states involved were probably created by inelastic collisions between electrons and neutrals. In Figure 10 we have plotted the square root of the bremsstrahlung intensity, the H_{α} line intensity, and the number of atoms extrapolated from the measurements made with the TiO_2 detector against the gas pressure. One can see that it is impossible to distinguish the three curves. This result supports the interpretation given above for the origin of the excited states and also that the atoms are probably created by collisions of molecules with electrons, and not by such processes as



This concerns only hydrogen. The line $NII\ 4627\ \text{\AA}$ cannot be interpreted in the same way because its intensity varies more than the bremsstrahlung intensity with nitrogen pressure: actually this is not surprising because it corresponds to an emission from an ionic excited state and is proportional to a power of the electronic density greater than 2.

One can consider also that the excellent superposition of the three curves of Figure 10 demonstrates that the inhomogeneities and macroscopic movements are not important for the understanding of the light emission and of chemical reactions, in the domain of pressure studied.

The light emission by bremsstrahlung was a quasi continuum. Therefore at low pressure low spectral resolution would give the strongest signal. Under such conditions Agostini, *et al.*,⁴ have seen the beginning of the electronic cascade. It is obviously impossible to get the benefit of such conditions in the detection of spectral lines and we did not see any primary processes. As excitations of atoms and dissociations of molecules need many fewer photons than ionization one would expect these processes to be more probable. The results of our experiments showed that there were less than 10^{11} molecules of hydrogen dissociated by multiphotonic absorption just below the breakdown's threshold. It is more difficult to give a bound for the number of excited atoms because we studied only a few lines and because the efficiencies of the different processes of atomic deexcitation are not known. There were less than 10^5 photons emitted in each spectral line. A study of the ultraviolet region would give some information on the lower excited states but will encounter the same difficulty.

It seems impossible to initiate chemical reactions and explosions in the high pressure domain if there is no plasma. Under the best conditions 10^{12} molecules would have to be dissociated at the focus of the lens in order to observe an isotopic exchange between H_2 and D_2 at a macroscopic scale, but we have shown by direct detection that there are less than 10^{11} atoms and spectroscopic studies suggested this number is several orders of magnitude smaller.

It is known that, in the domain of pressure studied here, it is likely that the multiphotonic absorption involves impurities or collision-induced absorption; in such a case it should be normal not to have seen any excited state or atoms below the breakdown threshold. But at pressures lower than 1 Torr, multiphotonic absorption certainly involves the gas molecules, and therefore, one can perhaps see it; a molecular beam technique should be very interesting. Nevertheless Berezhetskaya, *et al.*,¹⁹ have reported that in H_2 at pressure as low as 10^{-4} to 10^{-5} Torr the leading process was the ionization of the molecule leading to the formation of the H_2^+ ion and not the dissociation process. Above the breakdown's threshold, the energy transfer between the laser beam and the gas plays an important role in the kinetics of the reaction. Unlike with many other techniques, it is possible by focusing a laser beam to achieve a very interesting spherical symmetry in the investigation of homogeneous reactions. Furthermore, the laser-induced gas breakdown can be very useful for studying the dynamics of explosions.

Acknowledgments. The experimental part of this work has been performed at the "Centre de Cinétique Physique et Chimique" du CNRS-Nancy-France,

(19) N. K. Berezhetskaya, G. S. Voronov, G. A. Delone, N. B. Delone, and G. K. Piskova, *Soviet Phys. JETP*, 31, 3, 403 (1970).

We would like to thank Professor P. Le Goff for his enthusiastic support, Dr. C. Rosenthal for discussions

on the cascade, and D. Chery for helpful discussions on the TiO_2 probe.

Studies of Surface Reactions of Nitric Oxide by Isotope Labeling. IV. The Reaction between Nitric Oxide and Ammonia over Copper Surfaces at 150–200°

by K. Otto* and M. Shelef

Fuel Sciences Department, Ford Motor Company, Dearborn, Michigan 48121 (Received May 28, 1971)

Publication costs assisted by the Ford Motor Company

Mixtures of ^{14}NO and $^{15}\text{NH}_3$, diluted by Ar, were circulated over unsupported cupric oxide in a closed reaction loop to study the product distribution as a function of oxidation state. The CuO was reduced along with the nitric oxide, and at first the only product in the gas phase besides water was mixed nitrogen $^{14}\text{N}^{15}\text{N}$. As the reaction proceeded, three other products were formed, $^{15}\text{N}^{14}\text{NO}$, $^{14}\text{N}_2$, and $^{14}\text{N}_2\text{O}$. Under steady-state conditions, using a slightly reducing mixture of the reactants, the ratio of nitrogen-containing products was $^{14}\text{N}^{15}\text{N} : ^{15}\text{N}^{14}\text{NO} : ^{14}\text{N}_2\text{O} : ^{14}\text{N}_2 = 54:16:9:21$. At this stage the catalyst is practically reduced to metallic copper, although some residual oxygen cannot be removed from the solid. A comparison with earlier results on Pt (*J. Phys. Chem.*, **75**, 875 (1971)) shows that the reaction rate at 200° per metal atom in the surface is 0.2 NO molecule/sec for Cu and 0.05 molecule/sec for Pt. The formation of unmixed nitrogen is more pronounced in the case of Cu than on a Pt catalyst. The experimental findings can be rationalized within the framework of the general mechanism proposed earlier for the reaction on Pt, with certain modifications.

Introduction

The catalytic interaction between ammonia and nitric oxide over supported Pt has been studied previously in this laboratory.^{1,2} The study of the same reaction was extended presently to a base metal, or metal oxide catalyst. It was motivated by the following reasons. First, there are several patents describing the use of this reaction for selective purification of NO containing effluents where base metal oxides are used as the catalysts.^{3–5} Therefore, it was of practical interest to compare the reaction mechanism on two different classes of catalysts. Second, it was deemed important to explore the effect of oxidation state changes, which base metal catalysts experience in the course of the reaction, on the reaction mechanism. Copper was chosen as a representative base metal.

Experimental Section

Catalyst, Purity of Gases, and Apparatus. In the majority of the experiments a single sample of 0.185 g of "specpure" cupric oxide (Johnson Matthey Chemicals, Ltd.) was used. The BET surface area before use was 0.88 m^2/g . It was determined by Kr adsorption at liquid nitrogen temperature. A few runs were carried out on copper metal powder (B & A, reagent grade) which had a very small surface area

(<0.1 m^2/g). With a few exceptions, the reaction conditions were reducing, using either 60 Torr of NO and 40 Torr of NH_3 or equimolar amounts (60 Torr) of both reactants. The purity of the reactants and the reaction apparatus are described in detail in ref 1.

Gas Analysis. Considerable effort was expended to improve the accuracy of the mass spectrometric gas analysis over that achieved previously.¹ The pressure of the inert gas, Ar, was lowered from 300 to 150 Torr to enhance the relative sensitivities of the other gas components. To minimize errors associated with the day-to-day changes in sensitivity the mass spectrometer was recalibrated daily with pure N_2 , N_2O , NO, Ar, NH_3 , and H_2 .

The evaluation of the mass spectra was modified to eliminate the dependence of the analysis on the secondary peaks m/e 14, 15, and 16 (see Table I, ref 1) which have contributions from several gas constituents. The involvement of these relatively small peaks in the

(1) K. Otto, M. Shelef, and J. T. Kummer, *J. Phys. Chem.*, **74**, 2690 (1970).

(2) K. Otto, M. Shelef, and J. T. Kummer, *ibid.*, **75**, 875 (1971).

(3) M. E. Griffing, F. W. Lamb, and R. E. Stephens, U. S. Patent 3,449,063 (1969).

(4) H. Nonnenmacher and K. Kartte, U. S. Patent 3,279,884 (1966).

(5) K.-H. Schmidt and V. Schulze, German Patent 1,259,298 (1968).

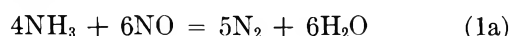
Table I: Initial Conditions of Experiments Performed on the First Copper Oxide Sample

Run no.	Reactants ^{a,b}	Temp. °C
1, 2, 3, 4, 5	60 ¹⁴ NO + 60 ¹⁵ NH ₃	201
6	60 ¹⁴ NO + 60 ¹⁴ NH ₃	201
7	60 ¹⁴ NO + 60 ¹⁵ NH ₃	201
8	60 ¹⁵ NO + 60 ¹⁴ NH ₃	201
9	60 ¹⁴ N ₂ O + 60 ¹⁵ NH ₃	201
10	72 ¹⁴ NO + 15 ¹⁵ NH ₃ + 30 H ₂	199
11	60 ¹⁴ NO + 60 ¹⁵ NH ₃	201
12	60 ¹⁵ NO + 60 ¹⁴ NH ₃	202
13 ^c	60 ¹⁴ NO + 25 ¹⁵ NH ₃	202+
14	60 ¹⁴ NO + 60 H ₂	200
15 ^c	60 ¹⁴ NO + 25 ¹⁵ NH ₃	157
16	60 ¹⁴ NO + 40 ¹⁵ NH ₃	157
17, 18, 19, 20	60 ¹⁴ NO + 40 ¹⁵ NH ₃	173
21, 22	60 ¹⁵ NO + 40 ¹⁴ NH ₃	173

^a The numbers in front of the reactants represent absolute initial pressures in Torr. ^b The reactants were always diluted by approximately 150 Torr of Ar. ^c These runs represent overall oxidizing conditions.

simultaneous equations employed to resolve the mass spectra introduces considerable error and limits the accuracy. To circumvent this limitation a method based on primary parent peaks only was devised as follows.

Ammonia and water, which can be adsorbed partially on catalyst and vessel walls, were evaluated indirectly by a material balance using the disappearance of NO and the appearance of reaction products according to the two overall reactions



and



Then, if the same four N-containing products observed previously on Pt² are the only ones to be considered, an analysis scheme based on primary peaks only can be devised. The products are $\bar{\text{N}}\text{N}$, N₂, $\bar{\text{N}}\text{NO}$, and N₂O, where $\bar{\text{N}}$ refers to a nitrogen atom introduced with the ammonia molecule and N to that introduced with the nitric oxide molecule.

Thus, it had to be verified that $\bar{\text{N}}\text{NO}$, $\bar{\text{N}}_2\text{O}$, and $\bar{\text{N}}_2$ are not important products. From the small fragmentation peak of *m/e* 31 arising from ¹⁴N¹⁵NO in the reaction between ¹⁴NO and ¹⁵NH₃ the upper limit of $\bar{\text{N}}\text{NO}$ was estimated at 4.5% of the total mixed nitrous oxide. This is low enough so as not to interfere with the analysis. Such a small degree of scrambling between the nitrogen atoms in nitrous oxide is not always the case as shown by Cooper, *et al.*,⁶ for liquid phase reactions. The peak corresponding to $\bar{\text{N}}_2\text{O}$ was completely absent. The limiting amount of $\bar{\text{N}}_2$ was estimated as below 0.1% of total nitrogen.

The possibility of ammonia formation in which the nitrogen atom is that introduced with the nitric oxide molecule was checked indirectly by the NO-H₂ reaction. In this case ammonia was not detected, not even when an equimolar mixture of NO and H₂ reacted at 200°. The ratio of the peaks *m/e* 17 and 18 remained at a constant value characteristic of the water mass spectrum. The appearance of NH₃ would have caused this ratio to increase. Material balances in the NO-H₂ reaction also indicate absence of ammonia formation.

Based on the above considerations the analysis for the reaction between ¹⁴NO and ¹⁵NH₃ is straightforward. There is a one-to-one relationship between the parent peaks *m/e* 28, 29, 30, 40, 44, and 45 and the molecules ¹⁴N₂, ¹⁴N¹⁵N, ¹⁴NO, Ar, ¹⁴N₂O, and ¹⁵N¹⁴NO, respectively.

In the reaction between ¹⁵NO and ¹⁴NH₃ the following mass peaks are considered: 28, 29, 30, 31, 40, 44, 45, and 46. These correspond to ¹⁴N₂ (from impurity), ¹⁴N¹⁵N, ¹⁴NO (impurity) and ¹⁵N₂, ¹⁵NO, Ar, ¹⁴N₂O, ¹⁴N¹⁵NO and ¹⁵N¹⁴NO (impurity), ¹⁵N₂O. The impurity contributions to peaks 30 and 45 were assessed from the known impurity levels in the reactants.

All the product distributions in the tables are corrected for impurities and refer to those that would have been obtained with isotopically pure reactants.

The analysis was checked by a total nitrogen material balance and by the material balance of the N isotope.² The improvement in the analysis accuracy is reflected in the material balances: whereas previously¹ these agreed to ±10%, the present balances agree to ±5%. The detection limit for a given constituent was lowered from ~1000 to ~100 ppm.

Experimental Results

The Reaction between NO and NH₃. The initial conditions of each run performed on the same sample of catalyst are listed in Table I. The listing is in chronological order to show the sample history. This is important because the sample changes composition in use. In some cases, such as in runs 13 and 15, the sample was deliberately reoxidized in part by the choice of an appropriate ratio of reactants.

Table II gives the product distributions in successive runs. These are expressed as the relative percentages of the four nitrogen-containing products which correspond to conversion intervals indicated by the extent of NO reaction. To conserve space only a selection of representative data is included.

The product distributions are strongly dependent on the oxidation state of the catalyst. A cursory examination of Table II indicates a continuous change in the distribution of products in consecutive runs. There is observed a gradual decrease of the $\bar{\text{N}}\text{N}$ content and

(6) J. N. Cooper, J. E. Chilton, Jr., and R. E. Powell, *Inorg. Chem.*, **9**, 2303 (1970).

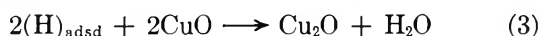
Table II: Product Distributions for NO- $\overline{\text{N}}\text{H}_3$ Reaction

Run no.	% $ \Delta\text{NO} $	% $\overline{\text{N}}$			
		NN	NNO	N ₂ O	N ₂
1	0.0-49.3	98.4	0.0	1.6	0.0
	6.7-98.0	98.5	0.2	0.9	0.4
	49.3-98.5	98.5	0.2	0.9	0.4
2	0.0-9.4	100.0	0.0	0.0	0.0
	0.0-66.5	97.6	0.0	2.4	0.0
3	0.0-10.5	94.2	1.3	4.5	0.0
	10.5-18.8	88.6	3.5	4.4	3.5
	10.5-96.7	78.3	7.0	3.9	10.8
	18.8-97.5	77.2	7.6	4.1	11.2
4	0.0-87.9	71.6	9.1	3.7	15.6
	0.0-96.9	72.6	9.0	3.5	15.0
5	0.0-47.7	70.1	9.5	3.8	16.5
	47.7-80.5	72.5	9.1	2.5	15.9
	80.5-96.2	73.3	9.8	2.1	14.8
7	0.0-42.7	68.5	10.8	4.0	16.8
	42.7-66.8	70.7	10.5	1.5	17.3
	66.8-91.5	75.8	10.9	2.6	10.7
8	55.8-83.5	68.0	10.8	3.7	17.5
	83.5-94.5	75.8	10.8	1.0	12.3
12	0.0-76.3	63.3	13.4	4.8	18.5
	76.3-97.3	66.8	13.2	3.8	16.1
13	0.0-35.4	62.9	15.7	5.0	16.3
	35.4-72.6	56.4	13.7	6.2	23.6
	0.0-76.2	58.3	14.4	5.9	21.4
15	0.0-19.0	65.8	16.3	8.4	9.5
	11.9-19.0	54.9	14.1	18.8	12.1
17	0.0-27.4	56.0	18.0	10.7	15.3
	27.4-49.7	55.8	18.8	9.8	15.6
	43.2-95.1	55.9	19.1	8.4	16.5
18	0.0-19.4	56.0	15.0	10.7	18.3
	19.4-41.0	55.5	16.2	9.5	18.7
	48.8-94.5	53.8	17.1	8.9	20.2
19	0.0-19.8	57.5	16.3	8.8	17.5
	19.8-42.5	54.7	17.8	10.3	17.2
	42.5-94.6	54.3	19.5	8.3	17.8
21	7.7-13.5	53.3	16.2	8.4	22.1
	27.3-42.6	57.7	15.2	9.3	17.9

an increase in $\overline{\text{N}}\text{NO}$ and N_2 . Strikingly, during the first two runs the reaction products are almost only mixed nitrogen and water. This behavior can be understood as follows. From the work on Pt, it is known that the only path leading to mixed nitrogen molecules is



As the adsorbed hydrogen is consumed in the reduction of the solid catalyst, initially CuO , according to



unmixed products cannot be formed. These reactions

fully describe the initial process on cupric oxide, where formation of mixed nitrous oxide is also almost absent.

The degree of the reduction of the solid sample can be assessed after each run by evaluating the amount of hydrogen which has not been consumed in the reduction of nitric oxide to products. This amount is assumed to be entirely used for stripping oxygen from the solid according to eq 3 and then for further reduction of the catalyst to metallic copper.

The general stoichiometric relationship is given by

$$x_1[\text{NO}] + x_2[\overline{\text{N}}\text{H}_3] = y_1[\overline{\text{N}}\text{N}] + y_2[\text{N}_2] + y_3[\overline{\text{N}}\text{NO}] + y_4[\text{N}_2\text{O}] + y_5[\text{H}_2\text{O}] \quad (4)$$

where x_i denotes the amounts of reactants which have disappeared and y_i the amounts of products formed. This relation can be split further into material balances for each of the species N, O, $\overline{\text{N}}$, and H.

$$\text{N: } x_1 = y_1 + 2y_2 + y_3 + 2y_4 \quad (4a)$$

$$\text{O: } x_1 = y_3 + y_4 + y_5 \quad (4b)$$

$$\overline{\text{N}}: x_2 = y_1 + y_3 \quad (4c)$$

$$\text{H: } 3x_2 = 2y_5 \quad (4d)$$

By inserting eq 4a, 4b, and 4c into 4d we obtain

$$\frac{H_1}{H_c} \equiv \frac{3x_2}{2y_5} = \frac{3y_3 + y_1}{2y_4 + 4y_2} \equiv \frac{3\overline{\text{N}}\text{NO} + \overline{\text{N}}\text{N}}{2\text{N}_2\text{O} + 4\text{N}_2} = 1 \quad (5)$$

This ratio between the surface hydrogen liberated in the formation of mixed products (H_1) and the hydrogen consumed in the formation of unmixed products (H_c) has been used previously to assess the consistency of the results on the Pt catalyst. The deviation of this ratio from unity serves as an index of the oxidation or reduction changes which the solid catalyst is undergoing. A large value indicates intensive reduction of the solid during the course of reaction. The values listed in Table III show the large extent of sample reduction during the first few runs characterized by the predominant formation of $\overline{\text{N}}\text{N}$.

Of the 2.3 mg-atom oxygen initially present in the sample, about 48% (1.1 mg-atom) has been removed in runs 1-3. At this stage, the extent of reduction corresponds roughly to an average oxygen content characteristic of Cu_2O . In the following four runs (4-7) about 10% of the original oxygen was removed from the sample each time. In subsequent runs, it is difficult to assess further reduction as it proved impossible to remove all the oxygen from the system. Even after several runs the H_1/H_c ratio is higher than unity without further improvement.

It was checked whether a part of the hydrogen desorbed as molecules into the gas phase in the course of reaction. Although some hydrogen was found in the gas phase (0.5-1.0 Torr), it was less than could account even for a H_1/H_c ratio of 1.1 (2.5 Torr). It is also known that the missing hydrogen could not have been

Table III: Relationships Derived from Product Distributions

Run no.	$ \Delta\text{NO} $, %	H_1/H_c	$\overline{\text{NN}} + \overline{\text{NNO}}$, %	$\overline{\text{NN}}/\overline{\text{NNO}}$	$\text{N}_2/\text{N}_2\text{O}$
1	0.0-49.3	30.8	98.4	∞	0.0
	6.7-98.0	29.1	98.7	493.0	0.44
	49.3-98.5	29.1	98.7	493.0	0.44
2	0.0-9.4	∞	100.0	∞	...
	0.0-66.5	20.3	97.6	∞	0.0
3	0.0-10.5	10.9	95.5	72.5	0.0
	10.5-18.8	4.35	92.1	25.3	0.80
	10.5-96.7	1.95	85.3	11.2	2.77
	18.8-97.5	1.89	84.8	10.2	2.73
4	0.0-87.9	1.42	80.7	7.87	4.22
	0.0-96.9	1.49	81.6	8.07	4.29
5	0.0-47.7	1.34	79.6	7.38	4.34
	47.7-80.5	1.45	81.6	7.97	6.36
	80.5-96.2	1.62	83.1	7.48	7.05
7	0.0-42.7	1.34	79.3	6.34	4.20
	42.7-66.8	1.42	81.2	6.73	11.53
	66.8-91.5	2.26	86.7	6.95	4.12
8	55.8-83.5	1.30	78.8	6.30	4.73
	83.5-94.5	2.11	86.6	7.02	12.30
12	0.0-76.3	1.24	76.7	4.72	3.85
	76.3-97.3	1.48	80.0	5.06	4.24
13	0.0-35.4	1.46	78.6	4.01	3.26
	35.4-72.6	0.91	70.1	4.12	3.81
	0.0-76.2	1.04	72.7	4.05	3.63
15	0.0-19.0	2.09	82.1	4.03	1.13
	11.9-19.0	1.13	69.0	3.89	0.64
17	0.0-27.4	1.33	74.0	3.11	1.43
	27.4-49.7	1.37	74.6	2.97	1.59
	43.2-95.1	1.37	75.0	2.93	1.96
18	0.0-19.4	1.07	71.0	3.73	1.71
	19.4-41.0	1.11	71.7	3.43	1.97
	48.8-94.5	1.07	70.9	3.15	2.27
19	0.0-19.8	1.21	73.8	3.53	1.99
	19.8-42.5	1.21	72.5	3.07	1.67
	42.5-94.6	1.28	73.8	2.78	2.14
21	7.7-13.5	0.97	69.5	3.29	2.63
	27.3-42.6	1.15	72.9	3.80	1.92

incorporated in the solid because copper hydride is unstable under the reaction conditions.⁷ Presumably, water vapor formed in the reaction, which is evacuated much slower than the permanent gases, was partially reoxidizing the solid during each outgassing period between runs. The Debye X-ray pattern taken after run 22 showed the lines of metallic Cu with very faint traces of Cu_2O .

For comparison one run was performed with Cu metal as the starting material. Due to the small surface area a large amount of sample (4.5 g) was employed and the reaction time was extended to ~ 5000 min. As seen

from Table IV the product distribution is similar to that obtained on the main sample in runs 8-12. Indeed, the metal sample contained some oxygen as evidenced by a weak Cu_2O pattern in the Debye X-ray picture. A complete prereduction of the metal was avoided to prevent additional shrinkage of the surface area.

Table IV: Product Distribution of $\text{NO}-\overline{\text{NH}}_3$ Reaction^a over Metallic Copper at 200°

% $ \Delta\text{NO} $	$\overline{\text{NN}}$	$\overline{\text{NNO}}$	N_2O	N_2
0.0-13.4	67.4	8.0	6.9	17.6
13.4-49.5	69.8	9.4	5.3	15.5
49.5-91.3	67.0	10.8	3.3	18.9

^a Initial conditions 60 Torr of ^{14}NO , 60 Torr of $^{15}\text{NH}_3$, and 150 Torr of Ar.

Apart from the product distribution, the reaction rate is also strongly influenced by the oxidation state of the catalyst. The rate at 200° (run 1) on a CuO surface was 2.3×10^{-3} mmol $\text{NO min}^{-1} \text{g}^{-1}$, while the rate in run 12 was 123×10^{-3} mmol $\text{min}^{-1} \text{g}^{-1}$. In addition, an overheating of $\sim 10^\circ$ due to nondissipated reaction heat was noted in run 13. Therefore the subsequent runs were carried out at lower temperatures (see Table I).

A typical reaction course is given in Figure 1, run 19. As in the case of Pt,² the decrease of NO and the increase of the products are linear with time during the initial stage of the reaction. The reproducibility on a stabilized surface is fair as shown in Figure 2 by repetitive runs 15 and 16 at 157°, and 17 and 22 at 173°. The change in the reactant ratio between runs 15 (oxidizing) and 16 (reducing) does not exert an effect on the initial rate. From the values of the hydrogen ratio in runs with oxidizing mixtures (13 and 15, Table III), it is seen that H_1/H_c tends to values below unity in the later periods indicating reoxidation of the surface. An apparent activation energy of 31 kcal mol^{-1} was derived from the rates shown in Figure 2 for the $\text{NO}-\overline{\text{NH}}_3$ reaction on a reduced Cu surface.

To compare the specific rates of the $\text{NO}-\overline{\text{NH}}_3$ reaction on Cu and Pt it is useful to characterize the rates by turnover numbers with respect to one surface atom at similar reaction conditions. At 200°, 60 Torr NO, and 60 Torr NH_3 the turnover on reduced Cu is 0.2 (molecule NO per surface Cu atom) sec^{-1} while on Pt it is 0.05 (NO molecule per surface Pt atom) sec^{-1} . Thus, the specific reaction rate is even faster on Cu than on Pt.

(7) W. Mueller, J. P. Blackledge, and G. G. Libowitz, "Metal Hydrides," Academic Press, New York, N. Y., and London, 1968, pp 546-549.

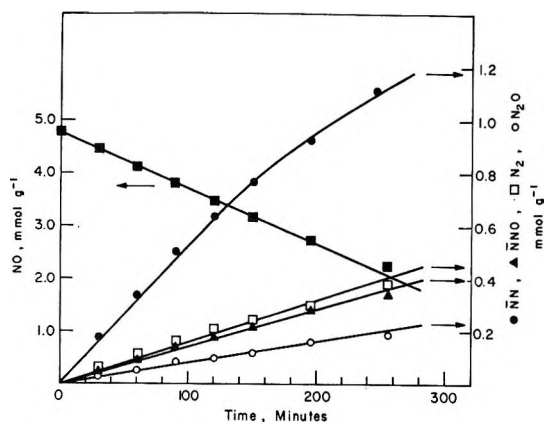


Figure 1. NO decrease and appearance of nitrogen containing products in the NO-NH₃ reaction as a function of time (run 19, 173°).

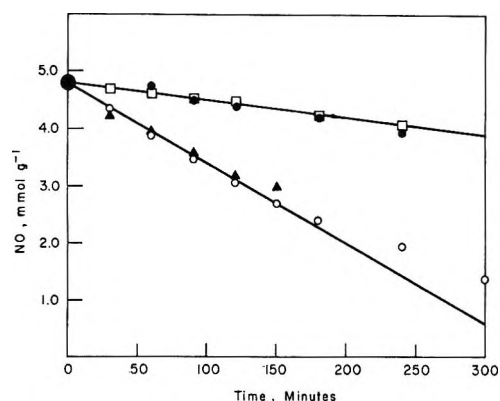


Figure 2. NO decrease during NO-NH₃ reaction at 157° (runs 15 (●) and 16(□)) and at 173° (runs 17 (○) and 22 (▲)).

The Influence of Additional Hydrogen. A mixture of 30 Torr of H₂, 72 Torr of ¹⁴NO, and 15 Torr of ¹⁵NH₃ reacted over the reduced sample at 199° (run 10). The product distribution is given in Table V and the decrease of NO as a function of time in Figure 3. For comparison the same figure contains also the NO decay in the reaction between 60 Torr of NO and 60 Torr of H₂ (run 14) and also the decay during a run (no. 8) between NO and NH₃ without H₂ under similar conditions. On a Cu surface the reaction between NO and H₂ turns out to be considerably slower than that between NO and NH₃. In run 10 initially a reaction rate is observed which is comparable to that of run 8 and can be ascribed to the predominant participation of the ammonia component. This is confirmed by the product distribution as given in Table V. The initial distribution agrees well with that observed in the NO-NH₃ reaction on an equivalent surface (runs 12 and 13, Table II). After most of the NH₃ is consumed, corresponding to the reaction of ~2.1 mmol of NO, the curve of run 10 inflects sharply to the lower reaction rate characteristic of the NO-H₂ reaction. In the period of slow reaction the main products are the unmixed ones, while some reaction with residual $\bar{\text{N}}\text{H}_3$

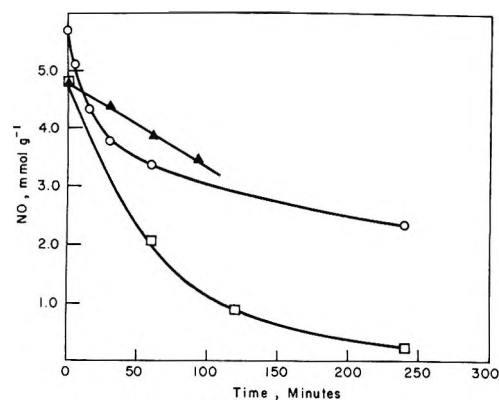


Figure 3. Comparison between reactions NO-NH₃, run 8 (□); NO-H₂, run 14 (▲); and NO-NH₃-H₂, run 10 (○), plotted as NO vs. time (200°).

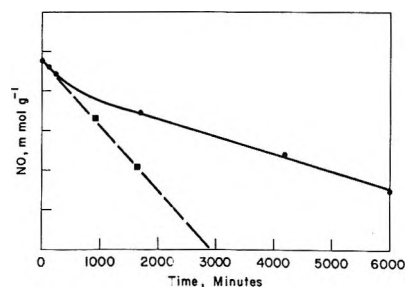


Figure 4. Comparison of NO-H₂ reaction, run 25 (●) and NO-NH₃ reaction, run 24 (■) on (low surface area) metallic Cu at 200°.

leads to the observed mixed products. The slowness of the NO-H₂ reaction with respect to the NO-NH₃ reaction was confirmed with the metallic, low surface area sample as shown on Figure 4. The initial steepness in the NO decrease in the NO-H₂ reaction is due to the fact that in the beginning the NO is reduced faster by the metallic surface than by hydrogen. It should be kept in mind that on Pt the NO-H₂ reaction was much faster than the NO-NH₃ reaction.

Table V: Product Distribution from Run 10

% ΔNO	% products				H ₁ /H ₀
	$\bar{\text{N}}\text{N}$	$\bar{\text{N}}\text{NO}$	N ₂ O	N ₂	
0.0-10.2	64.4	12.5	5.9	17.2	1.26
0.0-24.3	63.9	10.1	5.3	20.6	1.01
10.2-24.3	63.5	8.7	5.0	22.7	0.89
24.3-58.3	38.3	9.2	15.6	36.9	0.37
34.0-58.3	23.3	8.3	21.4	46.8	0.21

The Reduction of N₂O by Ammonia. The reduction of N₂O by ammonia (run 9) is exceedingly slow as is also the N₂O decomposition. At 200° (run 9) less than 1% of the N₂O was reduced after 2500 min. A control run of the N₂O-NH₃ reaction on a fresh CuO

sample showed that in this case the rate of N_2O reduction was even slower than in run 9.

Discussion

The increase in reaction rate with the sample reduction can be rationalized by the assumption that the dissociative chemisorption of ammonia: $(NH_3)_{ads} \rightarrow (NH_2)_{ads} + (H)_{ads}$ is rate controlling as is the case over a Pt catalyst.² As the dissociative chemisorption occurs predominantly on metallic surfaces it should rapidly increase with the reduction of the oxide. There are no direct measurements of the dissociative NH_3 chemisorption on Cu but there exists indirect evidence that on metallic Cu this process should be relatively rapid. The dissociative chemisorption is the first step in NH_3 decomposition⁸ and comparative tabulations^{8,9} of this decomposition on various metal surfaces indicate that on Cu it begins at relatively low temperatures.

On the contrary the dissociative chemisorption of hydrogen molecules on Cu is known to be much slower than on other metals as for instance—Pt. Below 0° there is a rapid nonactivated chemisorption of H_2 on Pt films but not on Cu films;¹⁰ on Cu powders the hydrogen chemisorption is activated¹¹ and slow. If the assumption of the rate-determining step of dissociative NH_3 chemisorption is extended to the dissociative chemisorption of hydrogen in the $NO-H_2$ reaction an explanation for the slowness of the last reaction on Cu is provided. To discuss the product distribution we reproduce here in a schematic form (Figure 5) the reaction paths leading to the four nitrogen containing products over Pt.¹ The boxed entities represent the postulated surface complexes I (top) and II (bottom), the thick arrows the major paths, and the thin, the minor ones. These reaction paths are proposed as a part of a possible reaction mechanism that, although hypothetical, is consistent with the experimental observations.

To examine the relative importance of the reaction paths and their applicability to the reaction over Cu surfaces, the data of Tables II and III are condensed into Table VI. Here, discrete (although somewhat arbitrary) bulk oxidation states have been defined and characteristic product distributions have been assigned to them.

The almost exclusive appearance of nitrogen as $\bar{N}N$ during the first two runs on a fresh CuO sample (Table II) is considered as being characteristic of a CuO surface.

After the same catalyst sample had been exposed to the $NO-\bar{N}H_3$ reaction for 22 times (*cf.* Table I) it was identified by X-ray diffraction as metallic copper, containing as impurity very faint traces of Cu_2O only. Runs 17 through 22 took place under the same experimental conditions (*cf.* Table I), and changes in the product distribution, if any, were small (*cf.* Table II).

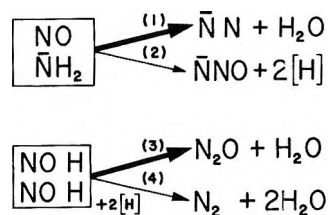


Figure 5. Schematic representation of paths leading to products on supported Pt (ref 1).

Table VI: Summary of Product Distributions for $NO-\bar{N}H_3$ Reaction

	CuO	Cu_2O	Cu	Pt
$\bar{N}N$ %	100	72.0	54.4	49.8
$\bar{N}NO$ %	0	9.3	15.9	12.7
N_2O %	0	3.1	9.1	31.6
N_2 %	0	15.6	20.6	5.9
H_1/H_0	∞	1.5	1.0	1.0
$\bar{N}N + \bar{N}NO$ %	100	81.3	70.3	62.5
$\bar{N}N/\bar{N}NO$	∞	7.7	3.4	3.9
N_2/N_2O	...	5.0	2.3	0.2

It can be assumed that the oxidation state of the catalyst bulk was in equilibrium with the catalyst surface under these conditions. Considering that there is an increase of the reaction rate with a decrease of the oxygen content of the solid and that the hydrogen balance of runs 18 and 21 is satisfied within about 10% (Table III) a representative, albeit idealized, product distribution for the reaction on metallic Cu is derived.

The definition of an intermediate oxidation state Cu_2O is somewhat more arbitrary. It is based on the amount of hydrogen which has been used for the reduction of the solid during the course of the reactions, as calculated from the hydrogen balance. As stated above, about 50% of the oxygen has been removed from the CuO sample after run 3. Assuming again equilibrium between bulk and surface, the product distributions of runs 4 and 5, which remain practically unchanged, should be typical for the reaction on Cu_2O . It must be emphasized that from the bulk phases it is not possible to deduce the surface compositions which are responsible for the observed product distributions. Table VI reflects thus, strictly speaking, only the general trend of the distribution changes with changes in the oxidation state of the solid. Corresponding data for Pt are included in Table VI for comparison.

The paths originating from Complex I are in essence the same on Pt and Cu, although initially on CuO ,

(8) R. E. Mardaleishvili, H. C. Hu, Zh. Ya. Smorodinskaya, *Kinet. Katal.*, **8**, 786 (1967).

(9) G. C. Bond, "Catalysis by Metals," Academic Press, London and New York, N. Y., 1962, pp 379-380.

(10) D. O. Hayward and B. M. W. Trapnell, "Chemisorption," Butterworths, Washington, D. C., 1964, p 75.

(11) Reference 10, pp 69, 181-183.

complex I splits cleanly along the major path only. As the reduction progresses the $\overline{NN}:\overline{NNO}$ ratio on Cu tends to the value noted on Pt.

The inspection of the internal ratio of the unmixed products in Tables III and VI shows that the lower part of the scheme of Figure 5 does not apply to Cu. There is more unmixed nitrogen than nitrous oxide and a modification of the mechanism is required. Knowing that the reduction of gaseous N_2O is a very slow process, we must exclude the possibility that gaseous N_2O formed in the reduction of NO is further reduced to N_2 . Besides such a mechanism would also increase the $\overline{NN}:\overline{NNO}$ ratio which is not observed. Therefore, we must assume that some form of Complex II, which contains two NO molecules, is reduced to a higher degree on Cu than on Pt.

Examining the various mutual ratios of the product distributions we have observed on Cu that the equality $2\overline{NNO} = N_2O + N_2$ holds in the majority of cases within 10%. Based on this observation and on the predominance of nitrogen in the unmixed products a model for the sequence leading to the experimental distribution is proposed. In this model, a surface Complex II*, which is the precursor of the unmixed products, involves 2NO molecules and only one hydrogen atom. Such an alternative, which is equivalent to $(HNO)_{\text{adsd}} + (NO)_{\text{adsd}}$ has been mentioned in ref 1. The aforementioned equality means that for every \overline{NNO} molecule released into the gas phase, two precursors

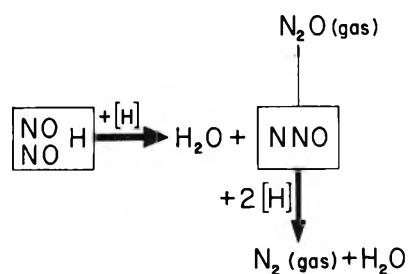


Figure 6. Schematic representation of paths leading to unmixed products on Cu.

(surface Complexes II*) of unmixed products are formed on the surface. The release of one \overline{NNO} molecule from Complex I generates two hydrogen atoms (process 2, Figure 5). These are incorporated into Complex II*, one atom per complex. We postulate further that these precursors are reduced stepwise first to unmixed N_2O and then to N_2 by the surface hydrogen generated in the dissociative chemisorption of the ammonia. On Cu, the probability of N_2O being released into the gas phase is smaller than the probability of being reduced further to N_2 . The schematic representation of major (thick) and minor (thin) paths leading to unmixed products according to this model is given in Figure 6.

Acknowledgment. We have profited from discussions with J. T. Kummer and we thank also H. Gandhi for the surface area measurements.

A Kinetic Study of *n*-Butene Isomerization over Supported Aluminum and Magnesium Sulfates

by Makoto Misono* and Yukio Yoneda

Department of Synthetic Chemistry, Faculty of Engineering, University of Tokyo, Bunkyo-ku, Tokyo, Japan
(Received October 4, 1971)

Publication costs assisted by the Kawakami Foundation

In order to examine the correlation between the selectivity of acid-catalyzed reactions and the acid strength of catalyst, the isomerization of three isomers of butene was studied kinetically at 40–100° over silica-supported aluminum and magnesium sulfate catalysts which were previously shown to be typical strong and weak acids, respectively. The activation energy differences between all paths and the relative rate constants have been determined for both catalysts, as well as the overall activation energies. The observed selectivity and the activity were shown to be determined principally by the differences in the energy barriers. For example, the increase in the 2-:1-butene ratio from one of 2-butenes with the increasing acid strength was quantitatively explained by the decrease in the height of energy barrier of 2-butene formation, relative to that of 1-butene formation. The activation energy difference was small between *cis*- and *trans*-2-butene formations, reflecting the *cis*:*trans* ratio close to unity. These results were interpreted by the stability of a common intermediate on the basis of carbonium ion mechanism and the principle of linear free energy relationships. The intermediate became more stable and long lived as the acid strength of catalyst increased.

Introduction

Stereoselectivity in the catalytic isomerization of 1-butene (*cis*:*trans* ratio in the products) has been a subject of several investigations.^{1–9} The selectivity between *cis*-*trans* isomerization and double-bond migration from 2-butene (2-:1-butene ratio) has also been studied. According to Foster and Cvetanovic,³ the 2-:1-butene ratio was high over acidic catalysts as the result of the rotation of a carbonium ion intermediate. The ratio was low for basic catalysts presumably because of the restricted rotation of carbanion.

We have previously demonstrated that 2-:1-butene ratio was markedly dependent on the acid strength of catalyst in the case of metal sulfate catalysts. The rate of isomerization and the selectivity of *cis*-*trans* isomerization over double-bond migration increased monotonously in the order of $H^+ > Fe^{3+} > Al^{3+} > Sc^{3+} > Cu^{2+} > Zn^{2+} \geq Ni^{2+} \geq Co^{2+} > Mn^{2+} > Mg^{2+}$.⁶ This order agreed with that in the acid strength which was estimated from the electronegativity of the constituent metal ion and tested by indicators.^{6,7} These trends found also for other metal salts were explained by the relative rates of proton addition and elimination, or the stability of protonated intermediate.^{6,8}

Hightower and Hall^{9,10} investigated the kinetics of *n*-butene isomerization over silica-alumina and explained the selectivity by the differences in the energy barriers interconnecting the carbonium ion and the products, assuming a *sec*-butyl carbonium ion as a common intermediate. The relative reactivities of three isomers were also explained on the same basis. Recently, Lombardo, Sill, and Hall¹¹ suggested that

the 2-:1-butene ratio increased with the acid strength of catalyst by the increase in the energy barrier between the carbonium ion and 1-butene, relative to that between the ion and 2-butene.

In the present work, we have studied the kinetics and energetics of *n*-butene isomerization, choosing aluminum sulfate as a typical strong-acid catalyst and magnesium sulfate as a typical weak-acid catalyst out of ten metal sulfates studied before.⁶ It was primarily intended in this work to examine how the kinetic parameters and the energy profile of reaction vary (Table I) with the acid strength of catalyst and to make clear the correlation between the selectivity and the acid strength. Since *n*-butene isomerization consists only of proton addition and elimination, it is expected that the present work will provide fundamental information about the rate and selectivity in acid catalysis.

- (1) W. O. Haag and H. Pines, *J. Amer. Chem. Soc.*, **82**, 387 (1960).
- (2) P. J. Lucchesi, B. L. Baeder, and J. P. Longwell, *ibid.*, **81**, 3235 (1959).
- (3) N. F. Foster and R. J. Cvetanovic, *ibid.*, **82**, 4274 (1960).
- (4) D. M. Brouwer, *J. Catal.*, **1**, 22 (1962).
- (5) H. P. Leftin and E. Hermana, *Proc. Int. Congr. Catal.*, 3rd, **1964**, 1064 (1965).
- (6) M. Misono, Y. Saito, and Y. Yoneda, *J. Catal.*, **9**, 135 (1967); **10**, 88 (1968).
- (7) M. Misono, E. Ochiai, Y. Saito, and Y. Yoneda, *J. Inorg. Nucl. Chem.*, **29**, 2685 (1967).
- (8) M. Misono and Y. Yoneda, *Bull. Chem. Soc. Jap.*, in press.
- (9) J. W. Hightower and W. K. Hall, *J. Phys. Chem.*, **71**, 1014 (1967).
- (10) J. W. Hightower and W. K. Hall, *J. Amer. Chem. Soc.*, **89**, 778 (1967).
- (11) E. A. Lombardo, G. A. Sill, and W. K. Hall, *J. Catal.*, in press.

Table I: Activation Energies and Differences in Activation Energies in the Isomerization of *n*-Butenes over Al-S and Mg-S, kcal mol⁻¹

1-Butene		Starting butene		Starting butene	
\bar{E}_t^a	$E_{t1} - E_{t2}^b$	\bar{E}_c^a	$E_{c1} - E_{c2}^b$	\bar{E}_t^a	$E_{t1} - E_{t2}^b$
		<i>cis</i> -2-Butene		<i>trans</i> -2-Butene	
Al-S					
7.2	0.0	7.5	1.5	8.0	1.4
7.0 ^c	(1.0) ^d		(6.9) ^d	8.5 ^c	(6.4) ^d
Mg-S					
9.5	0.3	10.0	0.2	11.8	0.3
8.5 ^c	(1.27) ^d		(1.22) ^d	11.2 ^c	(1.51) ^d

^a Overall activation energy obtained from the Arrhenius plot of the sum of two parallel reactions. ^b Difference in the activation energies between two parallel paths (eq 5). ^c The overall activation energy calculated by eq 7, where those for *cis*-2-butene were from Arrhenius plots of the rate. ^d Selectivity ratio at 60°.

Experimental Section

Equipment. The equipment was a closed circulating system (124 or 300 ml in volume, including a reactor) connected to a conventional vacuum line, similar to that described before.⁶ A U-type reactor (Pyrex, 10 mm in o.d.) was connected to the circulating system with a 4-way stopcock. The temperature of the catalyst bed which was maintained within $\pm 0.5^\circ$ was measured by a thermocouple set in a well installed inside the reactor. The reaction gas prepared as described below was circulated at a velocity of 120–150 ml/min through the catalyst bed whose top was filled with clean quartz wool for preheating. The amount of catalyst (30–300 mg) was chosen depending on the catalyst and the reaction temperature, so that sufficient gas circulation, relative to the reaction rate, was attained. Satisfactory gas circulation was confirmed by the invariance of the specific activity and the selectivity upon increasing twice or decreasing one-half the amount of catalyst and the circulation rate. Secondary isomerization during diffusion in micropores may be neglected because (i) good agreement between experiment and calculation was obtained (Figure 3, see later section) and (ii) only a trace of multideuterated species was observed in the products which were mainly monodeuterated species in case of the isomerization over deuterated catalysts.¹² The fact that the selectivity ratio became higher or lower than the equilibrium ratio depending on catalyst^{6,8} denies the possibility that the ratio was determined by secondary isomerization. Therefore, under the present experimental conditions, the reactions were considered not to be diffusion controlled.

Materials. Silica-supported metal sulfates were prepared as described elsewhere.⁶ Al-S and Mg-S denote aluminum and magnesium sulfates supported

on silica gel, respectively. Butenes (Matheson, at least 99.5% pure) were used after dehydration by the passage through a calcium chloride column and distillation at liquid nitrogen temperature.

Procedure. Catalysts were evacuated for 1 hr at 100° in the reactor prior to run. This pretreatment enabled reproducible rate measurement. Reaction gas was prepared by mixing measured amounts of butene and deoxygenated nitrogen in the circulating system. The reaction was started by the introduction of gas to the reactor by 4-way stopcock operation. The reaction temperature and butene pressure studied ranged from 40 to 100° and from 4 to 22 cm. The total pressure was always kept higher than the atmospheric pressure, so that gas sampling with a syringe through a serum cap did not contaminate the system. About 0.5 ml of gas was sampled at appropriate intervals and submitted to glc analysis. Reaction was usually followed until the initial selectivity ratio and rate constant could reasonably be determined (see Figures 1 and 3).

Results

Figure 1 shows the progress of the reactions of *cis*-2-butene over Al-S and Mg-S plotted according to the first-order rate equation

$$\ln(x_e - x) = -kt + \ln x_e \quad (1)$$

where x and x_e represent the conversion at time t and at equilibrium, respectively. Although this equation is an approximate one for this reaction,¹⁰ a practically straight line was obtained up to 98% attainment of equilibrium conversion, when $\ln(x_e - x)$ computed using rate constants given in Table II in the exact rate equation¹³ was plotted against time. Therefore, this equation is useful for practical purpose. Over Mg-S, the reaction followed this rate equation, except initial slight deactivation. Over Al-S, after initial rapid deactivation, the rate gradually decreased showing a slow, time-dependent poisoning, until an apparently stationary stage was reached. The rates measured with varied butene pressure indicated that the reaction order was 0.6–0.8. However, if deactivation which was larger in the experiments with higher butene pressure is taken into account, the reaction order seems close to first order. First-order plots (Figure 1) and the

(12) M. Misono, N. Tani, and Y. Yoneda, *Ann. Symp. Catal., Sapporo (Japan)*, 1971.

(13) The exact rate equation for parallel, reversible first-order reactions among three butene isomers have been derived by Haag and Pines.¹ The rate constants in this paper are defined as

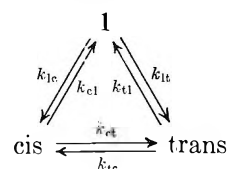


Table II: The Relative Rate Constants of *n*-Butene Isomerization over Al-S and Mg-S

Temp, °C	Relative rate constants						Selectivity ratio ^a		
	k_{1c}	k_{1t}	k_{ct}	k_{ct}	k_{tc}	k_{t1}	k_{1c}/k_{1t}	k_{ct}/k_{ct}	k_{tc}/k_{t1}
Al-S									
60	1.0	1.020	1.242	0.184	0.469	0.071	0.98 (1.0)	6.75 (6.9)	6.6 (6.4)
80	1.0	1.020	1.294	0.216	0.537	0.091	0.98 (1.0)	6.0 (6.2)	5.9 (5.6)
Mg-S									
60	1.0	0.794	0.222	0.184	0.083	0.055	1.26 (1.27)	1.21 (1.22)	1.52 (1.51)
80	1.0	0.813	0.257	0.216	0.107	0.071	1.23 (1.24)	1.19 (1.20)	1.46 (1.46)

^a Selectivity ratios were slightly modified for calculation, so that eq 2 holds exactly. The original ones are given in parentheses.

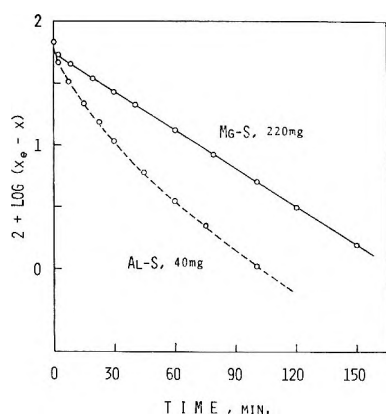


Figure 1. First-order-rate plots of the isomerization of *cis*-2-butene over Al-S and Mg-S at 80°.

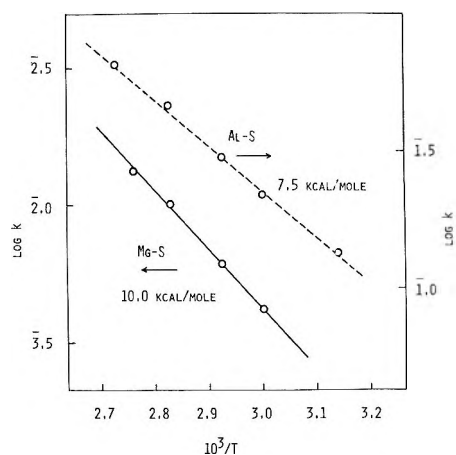


Figure 2. Log k vs. $1/T$ plots for the isomerization of *cis*-2-butene over Al-S and Mg-S.

validity of the exact first-order equation¹³ (Figure 3, see later section) also supported the idea that all reactions were almost first order.

In Figure 2, the logarithm of rate constant obtained from the first-order plot is plotted against $1/T$. For Al-S, the mean rate constants at the initial ten minutes were used. The activation energies thus obtained (\bar{E}_c , etc., Table I) were about 7 and 10 kcal mol⁻¹ for Al-S and Mg-S, respectively. Among the selectivity ratios for each catalyst obtained by the extrapolation of the product ratios to zero conversion, the next relationships were confirmed as in other metal sulfate catalysts⁶

$$(\text{trans}/1)(1/\text{cis})(\text{cis}/\text{trans}) \simeq 1 \quad (2)$$

$$(\text{trans}/1) \simeq (\text{cis}/1), (\text{cis}/\text{trans}) \simeq 1 \quad (3)$$

where $\text{trans}/1$, for example, represents the initial *trans*-2-butene to 1-butene ratio from *cis*-2-butene. Equation 2 supports that the reaction orders of all six paths were approximately the same and the selectivity ratios were the ratio of rate constants, e.g.

$$(\text{trans}/1) = k_{ct}/k_{c1} \quad (4)$$

Assuming first-order reactions, the six relative rate constants were calculated for each catalyst as summarized in Table II, following the ordinary method.^{1,9} In calculation, the selectivities were slightly modified, so that eq 2 held exactly. In Figure 3, the composition changes computed using these rate constants and the exact first-order equation¹³ are compared with the experimental ones. Good agreement shown in this figure between the calculated lines and the experimental points justifies the assumption that the reactions were all parallel, reversible, and nearly first order, and that the selectivity ratios were equal to the ratios of rate constants (eq 4).

The temperature dependences of the selectivity ratios are shown in Figure 4. The $\text{trans}/1$ ratio, for example, being equal to k_{ct}/k_{c1} , is related to the activation energy difference between the two parallel paths from *cis*-2-butene by the following equation⁹

$$\ln (k_{ct}/k_{c1}) = \frac{1}{RT}(E_{c1} - E_{ct}) + \text{constant} \quad (5)$$

where E_{ct} and E_{c1} are the activation energy of *trans*-2-

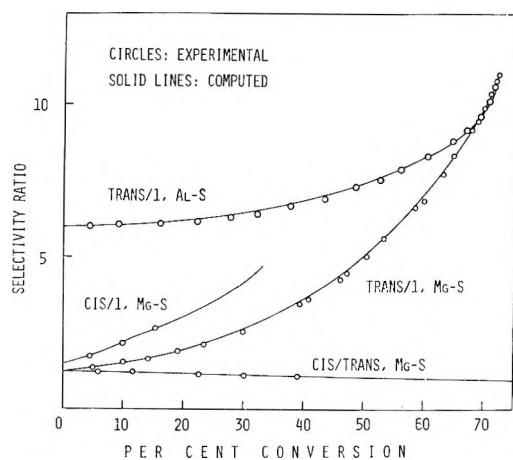


Figure 3. Experimental and computed product ratios plotted against conversion. Reaction temperature: 80°.

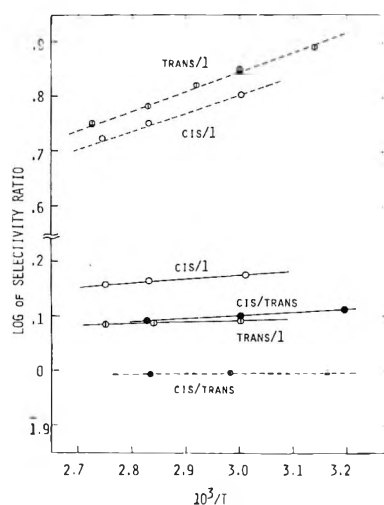


Figure 4. Temperature dependence of selectivity ratios; ---, Al-S; —, Mg-S.

butene formation and that of 1-butene formation, respectively. Analogous equations are derived for the other selectivity ratios, as well. The activation energy differences thus obtained from the slopes in Figure 4 are given in Table I. The difference between *trans*-2-butene and 1-butene formations and between *cis*-2-butene and 1-butene formations were larger for Al-S (1.4–1.5 kcal mol⁻¹) than for Mg-S (0.2–0.3). They were reported to be 0.8 kcal mol⁻¹ for silica-alumina.⁹ The difference, $E_{1c} - E_{1t}$, was small for both catalysts, as it was for silica-alumina.⁹ These trends may be compared with eq 3. The following relation which is expected from eq 2 is to be noted among the activation energy differences.

$$(E_{c1} - E_{ct}) + (E_{1c} - E_{1t}) + (E_{1t} - E_{1c}) \simeq 0 \quad (6)$$

The relative rates of the isomerization of three isomers were roughly 1:*cis*:*trans* = 3:2:1 over Al-S and 10:2.5:1 over Mg-S at 60°. These ratios agreed with those calculated from the relative rate constants

given in Table II as 3.7:2.8:1 for Al-S and 13:3:1 for Mg-S.

Discussion

Correlation between Selectivity and Energy Barrier. It was previously reported for *n*-butene isomerization catalyzed by supported metal sulfates that the rate of isomerization and the selectivity of *cis*-*trans* isomerization over double-bond migration increased monotonously, as the acid strength increased from MgSO₄ to H₂SO₄.⁶ Present results demonstrate that this change in the selectivity has its origin in the variation of the energy barriers of the parallel paths. Increase in *trans*/1 ratio from Mg-S to Al-S was

$$\frac{(\text{trans}/1) \text{ for Al-S}}{(\text{trans}/1) \text{ for Mg-S}} = \frac{6.9}{1.2} = 5.7 \quad (\text{at } 60^\circ)$$

This ratio agrees within experimental error with that calculated from the activation energy difference as

$$\exp\left[\frac{(E_{c1} - E_{ct})_{\text{Al-S}} - (E_{c1} - E_{ct})_{\text{Mg-S}}}{RT}\right] = \exp\left[\frac{(1.5 - 0.2)}{RT}\right] = 7$$

Similarly, for *cis*/1 ratio it was 6.4/1.5 = 4.2, as compared with $\exp[(1.4 - 0.3)/RT] = 5.2$. Consequently, the 2-/1-butene ratio increased with the acid strength, as the height of energy barrier to 2-butene became lower, relative to that to 1-butene. The *cis*/*trans* ratio, on the other hand, was nearly unity for both catalysts, where $E_{1t} - E_{1c} \leq 0.3$ kcal mol⁻¹. Table III shows the activation energy differences expected from the selectivity ratios and the observed ones. Considering the experimental error and the simple assumption of the neglect of the entropy terms, the agreement is good in general.

Table III: Comparison of the Observed Activation Energies with those Expected from the Selectivity Ratios, kcal mol⁻¹

	Al-S		Mg-S	
	Calcd ^a	Found	Calcd ^a	Found
$E_{c1} - E_{ct}$	1.3 (2.0)	1.5	0.15 (0.9)	0.2
$E_{1t} - E_{1c}$	1.2 (1.9)	1.4	0.25 (1.0)	0.3
$E_{1t} - E_{1c}$	0 (0)	0.0	0.15 (0.15)	0.3

^a Calcd, for example, as $\text{trans}/1 = \exp\{(E_{c1} - E_{ct})/RT\}$. Figures in parentheses were calcd as $\text{trans}/1 = (1/3)\exp\{(E_{c1} - E_{ct})/RT\}$, considering equivalent three hydrogen atoms in 1-butene formation.

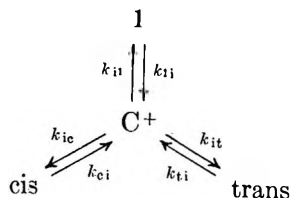
The relative reactivities are also explained by the activation energies. Smaller activation energy for Al-S was reflected in its higher activity. The difference in the overall activation energies calculated independently

using the temperature dependence of the relative rate constants in the following approximate equation

$$\ln (k_{ct} + k_{ci}) / (k_{tc} + k_{ti}) = (\bar{E}_t - \bar{E}_c) / RT + \text{constant, etc.} \quad (7)$$

generally agreed with those from Arrhenius plots as shown in Table I. The differences among isomers were smaller for Al-S (0.8–1.5 kcal mol⁻¹) than for Mg-S (2.3–2.7), as the natural consequence of the smaller activation energy differences between parallel paths for Mg-S (0.2–0.3). Those observed activation energies were in accord with the observed reactivity order of 1-butene > *cis*-2-butene > *trans*-2-butene and the larger difference in reactivity over Mg-S than over Al-S.

Energy Profile of Butene Isomerization Correlated with the Acid Strength of Catalyst. Although discussion given above is valid regardless of the kind of mechanism, the present results are better understood if one considers a common *sec*-butyl carbonium ion intermediate.^{14,15} If a *sec*-butyl carbonium ion (C⁺) is a common intermediate, the reaction scheme may be written as



According to this scheme, the selectivity ratios become the ratios of rate constants of the parallel paths from the ion, *viz.*, (trans/1) = k_{it}/k_{i1} , etc. The activation energy differences, $E_{c1} - E_{ct}$, etc., are then attributed to those between two parallel paths from the ion. The initial rate of the isomerization of each butene may be expressed by the next equations on the assumption of first-order reaction and a stationary concentration of carbonium ion.

$$v = \frac{d(\text{cis-2-butene})}{dt} = \frac{k_{ci}(k_{it} + k_{i1})}{k_{i1} + k_{ic} + k_{it}} \cdot p \cdot s_a, \text{ etc.} \quad (8)$$

where p and s_a are the butene pressure and the acid content, respectively.

Upon the basis of this mechanism, the energy profiles of butene isomerization *via* a carbonium ion may be drawn as in Figure 5, following Hightower and Hall.⁹ In this figure, possible weakly adsorbed states of butenes were added, although their stability is unknown. The overall activation energies, \bar{E}_c , etc., give the height of the transition state measured from the starting butene, because eq 8 becomes $v \doteq (1/2) k_{ci} p s_a$ for Al-S since $k_{ic} \simeq k_{it} \gg k_{i1}$ (experimentally, $6.9 \simeq 6.4 \gg 1.0$ at 60°) and that for Mg-S is $v \doteq (2/3) k_{ci} p s_a$ (experimentally, $1.5 \simeq 1.2 \simeq 1.0$). The heights of transition states were estimated from $\bar{E}_{c1} - E_{ct}$, etc.

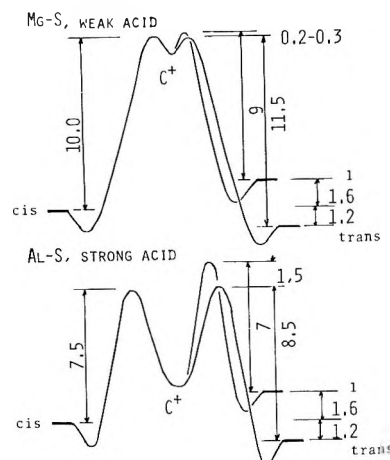


Figure 5. Schematic energy profiles of *n*-butene isomerization *via* carbonium ion intermediate over Al-S and Mg-S, kcal mol⁻¹.

According to Hammond¹⁶ and Leffler and Grunwald,¹⁷ the transition state bears greater resemblance to the less stable state between the initial and final ones. In other words, the transition state more nearly resembles the initial state as the reaction becomes more exothermic. The extent of the resemblance can be represented by α in LFER, $\delta G^\ddagger = \alpha \delta G$, where δG^\ddagger and δG denote small variations in the free energy (or enthalpy) of the transition state in either the initial or final state, respectively.^{17,18}

If one applies this postulate in the present case, it is expected that the transition state more nearly resembles the carbonium ion as the acid strength of catalyst decreases, since the ion must be less stable over a weak acid than over a strong acid. Little differences among $E_{c1} - E_{ct}$, etc., observed for Mg-S (0.2–0.3 kcal mol⁻¹, therefore, $\alpha \simeq 0.1$) agreed with this expectation. Large differences for Al-S (1.4–1.5 kcal mol⁻¹, $\alpha \simeq 0.7$) may be explained as the transition state reflecting the energy difference in butenes. Since the double-bond migration and the *cis*–*trans* isomerization would sometimes be dissimilar reactions, LFER is applied here, not in rigorous meaning, but for convenience of better understanding.

Similarly, the fact that difference among isomers in the overall activation energies was greater for Mg-S (2.3–2.7 kcal mol⁻¹) than for Al-S (0.8–1.5) can be explained as the ion formation was more exothermic

(14) Several studies have suggested a carbonium ion mechanism for *n*-butene isomerization over solid acids such as silica–alumina and nickel sulfate.^{9–11,15} The result that deuteration of products, similar to the former investigations,^{10,15} was observed for the isomerization over deuterated Al-S and Mg-S provides an evidence of protonic acid sites.¹² The observed deuterium distribution indicated a carbonium ion mechanism.

(15) A. Ozaki and K. Kimura, *J. Catal.*, **3**, 395 (1964).

(16) G. S. Hammond, *J. Amer. Chem. Soc.*, **77**, 334 (1955).

(17) O. A. Leffler and E. Grunwald, "Rates and Equilibria of Organic Reactions," Wiley, New York, N. Y., 1963.

(18) Y. Yoneda, *Int. Congr. Catal.*, **4th**, (1968).

over Mg-S. The stability of carbonium ion is also speculated upon the same basis. According to the above discussion, the ion is at least $10.0 - 7.5 = 2.5$ kcal more stable over Al-S. Further, if one should assume α to be 0.5 in $\delta_C \bar{E} = \alpha \delta_C H$, where suffix C means stabilization concerning the catalyst,¹⁸ the ion would be $(10.0 - 7.5)/0.5 = 5$ kcal more stable over Al-S.

In conclusion, over a strong acid the carbonium ion intermediate was rather stable and the energy barrier of 2-butene formation was lower than that of 1-butene formation, probably because the transition states reflected the energy difference in butene isomers. Therefore, the high 2-:1-butene ratio, as well as the high rate of isomerization and the small difference in the reactivities of three isomers, was observed over Al-S. On the contrary, low activity, low 2-:1-butene ratio and larger difference in the reactivities of butenes were observed over Mg-S. Over a weak acid, the

intermediate must be less stable and would bear less resemblance to butene, effecting little difference in the energy barriers between parallel paths. It seems also probable in this case, by analogy with the variation of the elimination mechanism from E1 to E2, *e.g.*,¹⁹ that the reaction appears more concerted, proton addition becoming slower and the elimination more rapid.^{6,8} A concerted mechanism would also favor the double-bond migration.²⁰ These two explanations for weak-acid catalysts may not be mutually exclusive as suggested by Lombardo, *et al.*¹¹

Acknowledgement. The authors are indebted to Dr. W. K. Hall of Gulf Research and Development Company and Professor Y. Saito of the University of Tokyo for their helpful suggestions.

(19) J. F. Bunnett, *Surv. Progr. Chem.*, **5**, 353 (1969).

(20) J. Turkevich and R. K. Smith, *J. Chem. Phys.*, **16**, 466 (1948).

Electron Spin Resonance Spectroscopy of the

Bisdithiooxalatonitrosyl Iron Anion

by W. V. Sweeney and R. E. Coffman*

Chemistry Department, University of Iowa, Iowa City, Iowa 52240 (Received July 19, 1971)

Publication costs assisted by the National Science Foundation

Liquid and rigid solution electron spin resonance studies were conducted on the bisdithiooxalatonitrosyl iron dianion. The rigid solution spectrum was matched using an efficient FORTRAN IV simulation program. The magnetic symmetry is axial, with spin-Hamiltonian parameters: $g_{||} = 2.0162$, $g_{\perp} = 2.0345$, $A_{||} = 0.00156$ cm⁻¹, $A_{\perp} = 0.0127$ cm⁻¹. These parameters were found to be both temperature and solvent dependent. On addition of anhydrous SnCl₄, a ligand perturbation effect leads to the conclusion that the unpaired electron is in an orbital of symmetry a₁ or a₂ in the point group C_{2v}. Consideration of evidence from previous studies on related complexes indicates that the half-filled orbital has d_{z²} character.

The study of the esr spectroscopy of pentacoordinate sulfur-bonded iron nitrosyls is interesting because of the known delocalization of the unpaired electron over the Fe-NO group and because the spin-Hamiltonian g values give information concerning the relative ordering of the one-electron MO's in relation to the MO containing the unpaired electron. Previous studies of molecules of this type¹⁻⁶ have not yet resulted in agreement concerning the ordering of the predominantly Fe-3d MO's.^{3,6} The dithiocarbamates and dithioenes, for example, are so similar that one would expect that one set of Fe-3d molecular orbitals should suffice for both. Accordingly, the dithiooxalate complex should be interesting for purposes of comparison.

We report here a study of the esr spectroscopy of the benzyltriphenylphosphonium salt of the bisdithiooxalatonitrosyl iron dianion, Fe(DTO)₂NO²⁻, in liquid and rigid solution. The synthesis and structure of this molecule have been reported by Coucouvanis, *et al.*⁷

(1) J. Gibson, *Nature*, **64**, 196 (1962).

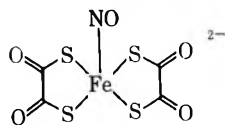
(2) A. McDonald, W. D. Phillips, and H. F. Mower, *J. Amer. Chem. Soc.*, **87**, 3319 (1965).

(3) J. A. McCleverty, N. M. Atherton, J. Locke, E. J. Wharton, and C. J. Winscom, *ibid.*, **89**, 6082 (1967).

(4) N. S. Garif'yanov and S. A. Luchkina, *Dokl. Akad. Nauk SSSR*, **189**, 779 (1969).

(5) J. A. McCleverty and B. Ratcliff, *J. Chem. Soc. A*, 1627 (1970).

(6) B. A. Goodman, J. B. Raynor, and M. C. R. Symons, *ibid.*, 2572 (1969).



The results reported here indicate that the $\text{Fe}(\text{DTO})_2\text{-NO}_2^-$ dianion has apparent magnetic axial symmetry and that the g values are affected by solvation, temperature, and ion-pairing effects. A ligand perturbation effect is interpreted to imply that the unpaired electron is in a molecular orbital which transforms as the a_1 or a_2 irreducible representations of the point group C_{2v} . This information, when taken into consideration with evidence from previous studies on similar iron nitrosyls, is helpful towards establishing the character of the molecular orbital occupied by the unpaired electron.

Experimental Section

Esr spectra were measured using a Varian VA-4500-10A system with 9-in. electromagnet. DPPH was used as a g -value standard,^{8,9} and the linearity of the field sweep was calibrated against the peroxyamine disulfonate free radical in aqueous solution.^{10,11} All solvents were reagent grade and were usually used without further purification. Methylene chloride was purified according to the method of Perrin, Armarego, and Perrin.¹²

Rigid glass line shapes were calculated using resonance field values, for arbitrary magnetic field direction, calculated to second order in perturbation theory^{13,14} using the spin-Hamiltonian

$$\mathcal{H} = \beta \mathbf{H} \cdot g \cdot \mathbf{S} + \mathbf{S} \cdot \mathbf{A} \cdot \mathbf{I} \quad (1)$$

where we assume the tensors g and A to be diagonal in the same (molecular) reference frame, and $S = 1/2$, $I = 1$. The derivative line shape

$$I'(H) = \sum_i \int P_i(\theta, \phi) G_i'(H, \theta, \phi) d\Omega / 4\pi \quad (2)$$

function was evaluated taking the intensity factor¹⁵ $P_i(\theta, \phi) = 1$ (small g -value anisotropy) and using $G_i'(H, \theta, \phi) =$ the derivative of a Lorentzian line shape, which peaks at the resonant field value $H_0(\theta, \phi)$ determined by (1) and the microwave frequency. The summation index " i ," which sums over all transitions, was set equal to m_I , since I , m_I are good quantum numbers for $S = 1/2$ systems for large values of the magnetic field. Integration over one octant of the unit sphere used the variables $t = \cos \theta$ and ϕ . The t integration was performed by the method of Gaussian quadrature,¹⁶ while the ϕ integration was done by subdivision of the range of ϕ . Thus, (2) becomes

$$I'(H) = (2/\pi) \sum_i \int_0^{\pi/2} F_i(H, \phi) d\phi \quad (3)$$

where

$$F_i(H, \phi) = \int_{t_-}^{t_+} P_i(t, \phi) G_i'(H, t, \phi) dt \quad (4)$$

The limits of integration over t ($0 \leq t_- \leq t_+ \leq 1$) were determined for each value of (H, ϕ) with a "LIMITS" subroutine which determined two values of t such that $H - H_0(t, \phi) = \pm 4\Delta$, where $H_0(t, \phi)$ is the resonance line center for given t and ϕ , and Δ is the Lorentzian half-width. It is necessary to restrict the range of the t integration in order to achieve maximum benefit of the Gaussian quadrature method, which is one of the most accurate of the quadrature formulas in ordinary use.¹⁷ Relative integration accuracy and efficiency was verified by comparison with other numerical routines.

Results and Discussion

The average g values measured in solution at 25° in methanol-glycerol and methylene chloride are given in Table I. Since the crystal structure is not yet known, it was decided to extract g_x, g_y, g_z and A_x, A_y, A_z from the experimental spectra of rigid solutions (glasses) by calculation of the rigid solution line shape. The g tensor and hyperfine splitting (hfs) tensor components so found are also given in Table I. A comparison of experimental and calculated spectra for a 1:1 (v/v) methanol-glycerol glass at 77°K is given in Figure 1. An axially symmetric spin-Hamiltonian was found to be suitable. Calculations using a rhombic symmetry spin-Hamiltonian showed that the deviation of the g values from axial symmetry, $|g_x - g_y|$, was less than 0.003. Good general agreement with the experimental glass spectrum was obtained, but with some significant differences: a noticeable line width anisotropy is present (an isotropic line width was used in the calculations), and there are three recognizable bumps to the high-field side of the three hyperfine lines distributed about $H_{\perp} = h\nu/\beta g_{\perp}$. Lowering the symmetry to rhombic in the line-shape calculation changes the perpendicular hyperfine components of the line shape in a different way than observed, *i.e.*, as $|g_x -$

(7) D. Coucouvanis, R. E. Coffman, and D. Piltingsrud, *J. Amer. Chem. Soc.*, **92**, 5004 (1970).

(8) A. N. Holden, C. Kittel, F. R. Merritt, and W. A. Yager, *Phys. Rev.*, **77**, 147 (1950).

(9) C. P. Poole, Jr., "Electron Spin Resonance," Interscience, New York, N. Y., 1967, p 589.

(10) G. E. Pake, J. Townsend, and S. I. Weissman, *Phys. Rev.*, **85**, 682 (1952).

(11) R. J. Farber and G. K. Fraenkel, *J. Chem. Phys.*, **47**, 2462 (1967).

(12) D. D. Perrin, W. L. F. Armarego, and D. R. Perrin, "Purification of Laboratory Chemicals," Pergamon Press, Elmsford, N. Y., 1966.

(13) W. Low, "Paramagnetic Resonance in Solids," Academic Press, New York, N. Y., 1960, p 60.

(14) A. Abragam and B. Bleaney, "Electron Paramagnetic Resonance of Transition Ions," Clarendon Press, Oxford, 1970.

(15) J. R. Pilbrow, *Mol. Phys.*, **16**, 307 (1969).

(16) P. J. Davis and I. Polonsky, "Handbook of Mathematical Functions," M. Abramowitz and I. A. Stegun, Ed., NBS Applied Mathematics Series, No. 55, Washington, D. C., 1964.

(17) J. B. Scarborough, "Numerical Mathematical Analysis," 4th ed, Johns Hopkins Press, Baltimore, Md., 1958.

Table I: Magnetic Resonance Parameters

	T , °C	$\langle g \rangle$	$g_{ }$	g_{\perp}	$\langle A \rangle$, $\text{cm}^{-1} \times 10^4$	$A_{ }$, $\text{cm}^{-1} \times 10^4$	A_{\perp} , $\text{cm}^{-1} \times 10^4$
Fe(DTO) ₂ NO ²⁻ in Methanol-Glycerol, 1:1 (v/v)							
Soln	25	2.0333 ± 0.0010			12.6 ± 0.1		
Rigid soln	-160	2.0284 ± 0.0010	2.0162 ± 0.0005	2.0345 ± 0.0015	13.7 ± 0.1	15.6 ± 0.1	12.7 ± 0.1
Fe(DTO) ₂ NO ²⁻ in Methylene Chloride							
Soln	25	2.0337 ± 0.0010			12.8 ± 0.1		
Soln	-50	2.0322 ± 0.0010			13.2 ± 0.1		
Fe(DTO) ₂ NO · 2SnCl ₄ ²⁻ in Methylene Chloride							
Soln	25	2.0359 ± 0.0010			11.6 ± 0.1		
Rigid soln	-160	2.0305 ± 0.0010	2.0150 ± 0.0005	2.0383 ± 0.0015	11.9 ± 0.1	14.0 ± 0.1	10.9 ± 0.1

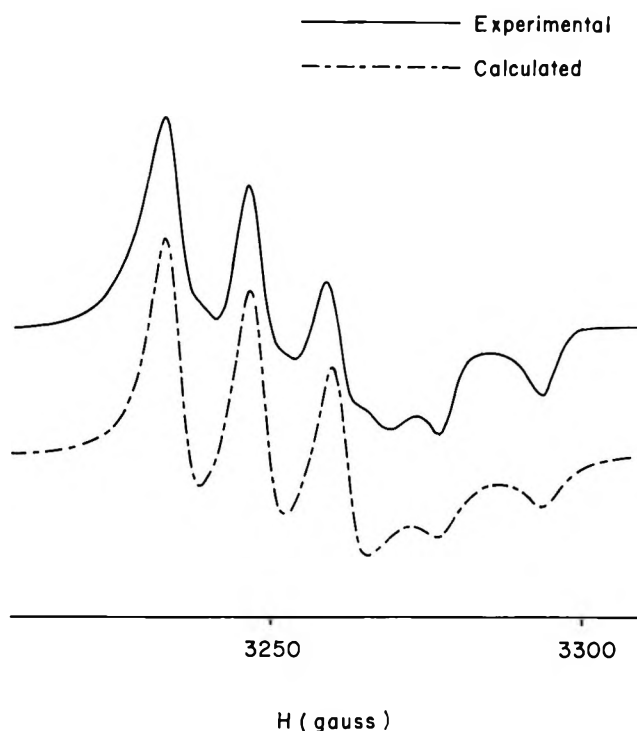


Figure 1. The calculated and experimental absorption derivative spectra of Fe(DTO)₂NO²⁻ at 9.248 GHz, in a rigid solution of methanol-glycerol, 1:1 (v/v) at -160°. The calculated spectrum was obtained using the parameters given in Table I.

g_y is increased, the perpendicular hyperfine "lines" split into two components each, each component having equal intensity. Therefore we conclude that this anomaly is due to about 10% of another species. Since repeated purification has no effect on the bumps and they appear to be related to some property of the solvent, we tentatively assign them to a small fraction of molecules which are ion-paired with the benzyltriphenylphosphonium counterion. Alternately, there could be solvent coordination with the oxygens of the dithiooxalate group (assuming that the Fe atom is bonded to the S atoms). A somewhat analogous situation to the latter case has been identified by Guzy,

et al.,¹⁸ in the form of solvation of the oxygen atom of the vanadyl group in vanadyl acetylacetonate.

The average values $\langle g \rangle$ and $\langle A \rangle$ were found to depend slightly on temperature and solvent. From Table I, we find $\partial\langle g \rangle/\partial T = 2.0 \times 10^{-5} \text{ deg}^{-1}$ and $\partial\langle A \rangle/\partial T = -5.3 \times 10^{-7} \text{ cm}^{-1} \text{ deg}^{-1}$ in methylene chloride. This is similar to an effect found by Guzy, *et al.*,¹⁹ for a dithiocarbamate nitrosyl iron. They interpreted this effect as due to solvent coordination with the sixth (vacant) site of the iron in the limit of fast exchange. That similar perturbation effects exist which involve perturbation of the ligand was demonstrated by the following experiment suggested by Coucouvanis:²⁰ addition of a small amount of anhydrous SnCl₄ to a dry solution of Fe(DTO)₂NO²⁻ results in a color change and an associated shift of the g values and hfs constants; see Table I. It was found that $\langle g \rangle$ and $\langle A \rangle$ vary with temperature and solvent as before. However, the bumps found earlier in the spectrum are now missing from the rigid solution spectrum. This may be interpreted as due to SnCl₄ blocking solvent or counterion interaction with the dithiooxalate ligands.

The analysis of the effect of SnCl₄ on the g values is helpful towards identifying the symmetry character of the half-filled molecular orbital. By reference to Table I, it is seen that on addition of SnCl₄ $g_{||}$ is changed by 0.001, g_{\perp} is changed by 0.004. Now, the SnCl₄ probably affects the g values through the π system of the dithiooxalate ligand. The only metal orbitals of the correct symmetry to interact with the dithiooxalate π system are d_{xz} and d_{yz} , which transform as b_1 and b_2 .²¹ Using the first-order perturbation theory result for g shifts in a molecule²² and calculating only

(18) C. M. Guzy, J. B. Raynor, and M. C. R. Symons, *J. Chem. Soc. A*, 2791 (1969).

(19) C. M. Guzy, J. B. Raynor, and M. C. R. Symons, *ibid.*, 2987 (1969).

(20) D. Coucouvanis, *J. Amer. Chem. Soc.*, **92**, 707 (1970).

(21) This may be seen by considering the iron and only the dithiooxalate ligands under symmetry D_{3h} .

(22) A. Carrington and A. D. McLachlan, "Introduction to Magnetic Resonance," Harper and Row, New York, N. Y., 1967.

those terms which group theory allows to be nonzero, it is seen that there are only two possible symmetry orbitals for the unpaired electron that are consistent with the observed effects. If an orbital of symmetry a_1 or a_2 is half-filled, then a destabilization (raising in energy) of the $b_1(d_{xz})$ and $b_2(d_{yz})$ orbitals by the SnCl_4 would result in a positive shift in g_{\perp} , g_{\parallel} remaining approximately constant.

An analysis of the nitrogen hyperfine splitting of the type described by Symons²³ gives further information on the nature of the lowest unfilled MO in the vicinity of the N atom. Let us analyze the hyperfine data of Table I by introducing the customary definitions

$$A_{\parallel} = T_{\parallel} + A_{\text{iso}} + A_d \quad (5a)$$

$$A_{\perp} = T_{\perp} + A_{\text{iso}} - (1/2)A_d \quad (5b)$$

Then, ignoring the pseudo-Fermi-contract (spin-orbit) and 1s-spin-polarization contribution to A_{iso} , the fraction of 2s character (actually a charge density since only one orbital is involved) is A_{iso}/A_{2s} , and the 2p charge density (p character) is T_{\parallel}/A_{2p} . Here, A_{2s} and A_{2p} are the values, in gauss, for A_{iso} and T_{\parallel} for a single electron in pure 2s or 2p orbitals:²³ $A_{2s} = 550$ G, $A_{2p} = 34.1$ G. The principal contribution to the electron-nucleus dipolar interaction may be written¹⁴ $A_d(2I_zI_x - I_xS_x - I_yS_y)$, where $A_d = g_e g_n \beta_n / R^3$ with R equal to the iron-nitrogen bond distance. Then using²⁴ $R = 1.56$ Å, $A_d/g_e \beta$ is found to equal 0.5 G. (Note that the validity of the point dipole approximation rests on the condition that R is much greater than the average radius of the iron orbital containing the unpaired electron. Using the radial function for 3d orbitals on Fe^I of Richardson, *et al.*,²⁵ we find $\langle r \rangle = 0.25$ Å. Thus, the dipolar approximation seems reasonably accurate.)

Using this value of A_d and the data of Table I, we may now find the percentage of nitrogen 2s and 2p character of the half-filled MO. The s character of the dianion in a rigid solution is 2.63% and the p character is 2.72%. On addition of SnCl_4 (in slight excess—it is not critical) the s character changes to 2.28% and the p character becomes 3.36%. Thus the p character has gone up and the s character has gone down. Consideration of configuration interaction affords a plausible explanation. First, consider the Fe-NO bond angle. Although this bond is probably slightly bent,²⁴ it should still be possible, as an approximation, to discuss the nitrosyl orbitals in terms of the irreducible representations of the point group C_{2v} . Now the d_{xz} and d_{yz} orbitals have the correct symmetry to mix with the $\pi^*(\text{NO})$ orbitals. If the d_{xz} and d_{yz} orbitals are raised in energy (due to SnCl_4 addition), the energy difference $E_{\pi^*(\text{NO})} - E_{d_{xz}, d_{yz}}$ grows smaller. This will increase the NO character of the $b_1(d_{xz})$ and $b_2(d_{yz})$ orbitals. Since the bent Fe-NO bond allows configuration interaction with excited states which have the unpaired electron in the $b_1(d_{xz})$ and

$b_2(d_{yz})$ orbitals, the $\pi^*(\text{NO})$ character of the "unpaired electron's" orbital should increase. A corresponding small decrease in the $\sigma(\text{NO})$ and $\sigma^*(\text{NO})$ character of the unpaired electron would be expected because of the normalization condition. This will then change the ratio of p/s character in the manner observed.

Knowledge of the magnitude and sign of the ^{57}Fe hyperfine splitting tensor would aid considerably in assigning the irreducible representation of the half-filled MO. The results of Goodman, *et al.*,⁶ concerning the ^{57}Fe hyperfine splittings of $\text{Fe}(\text{NO})(\text{S}_2\text{CNMc}_2)_2$ indicate that T_{\parallel} , the anisotropic contribution to A_{\parallel} , must have the opposite sign to $A_{\text{iso}} = \langle A \rangle$ of ^{57}Fe . Direct calculation of T_{\parallel} with the operator²⁶

$$T_{\parallel}/2P' = (3 \cos^2 \theta - 1)s_z + \frac{3}{2} \sin \theta \cos \theta r^{-3} (e^{-i\phi} s_+ + e^{+i\phi} s_-)$$

where $P' = g_e g_n \beta \beta_n$, shows that T_{\parallel} is positive for d_{z^2} , d_{xz} , and d_{yz} ($4/7$, $2/7$, $2/7$, respectively, in units of $P' \langle r^{-3} \rangle$), while T_{\parallel} is negative for $d_{x^2-y^2}$ and d_{xy} ($-4/7$, $-4/7$). In the point group C_{2v} , the d orbitals transform as $a_1(d_{z^2}, d_{x^2-y^2})$, $a_2(d_{xy})$, $b_1(d_{xz})$, and $b_2(d_{yz})$. We have shown that the MO of the unpaired electron must be of symmetry a_1 or a_2 , so a positive value of A_{iso} (^{57}Fe) implies T_{\parallel} negative, and therefore the MO must be of the $x^2 - y^2$ or xy type. Now, $a_2(3d_{xy})$ will not mix with an $a_1(4s)$ orbital in C_{2v} , so it appears unlikely that an unpaired electron in an xy orbital would contain enough 4s character to make A_{iso} positive. The $3d_{x^2-y^2}$ orbital is of a_1 type, so this is a reasonable assignment for positive A_{iso} . Similarly, it follows that the half-filled MO must be of d_{z^2} type if A_{iso} is negative.

Thus, there are two possible assignments of symmetry character for the MO containing the unpaired electron depending on the sign of A_{iso} . Unfortunately, the sign of $\langle A \rangle$ is unknown, at present, for any Fe^I , $3d$,⁷ system, and studies of the isoelectronic low spin $\text{Co}^{II27-29}$ show that $A_{\text{iso}}(\text{Co}^{II})$ can be either negative or positive. For this reason, we are unable to deduce the sign of $A_{\text{iso}}(\text{Fe}^I)$ from available experimental information. We are currently attempting to determine its sign experimentally.

Conclusions

Our analysis leads to the conclusion that the unpaired electron is in an orbital of either d_{z^2} or $d_{x^2-y^2}$ character.

(23) M. C. R. Symons, "Advances in Physical Organic Chemistry," V. Gold, Ed., Academic Press, New York, N. Y., 1962.

(24) A. I. M. Rae, *Chem. Commun.*, 1245 (1967).

(25) J. W. Richardson, W. C. Nieuwpoort, R. R. Powell, and W. F. Edgell, *J. Chem. Phys.*, **36**, 1057 (1962).

(26) B. R. McGarvey, "Transition Metal Chemistry," Vol. 3, R. L. Carlin, Ed., Marcel Dekker, New York, N. Y., 1966.

(27) B. R. McGarvey, *J. Phys. Chem.*, **71**, 51 (1967).

(28) A. O. Caride, S. I. Zanette, and J. Danon, *J. Chem. Phys.*, **52**, 4911 (1970).

(29) R. B. Bentley, F. E. Mabbs, W. R. Smail, M. Gerloch, and J. Lewis, *J. Chem. Soc. A*, 3003 (1970).

The sign of the isotropic (Fermi-Dirac) coupling is needed in order to choose between these two. We are presently considering both theoretical and experimental means of determining the sign of the isotropic coupling. It seems *probable* that the correct choice for $\text{Fe}(\text{DTO})_2\text{NO}_2^-$ is d_{z^2} , by comparison with the work of McNeil, *et al.*,³⁰ on $\text{Mn}(\text{CN})_5\text{NO}_2^-$. In that case, the electron is assigned to a d_{xy} type orbital for which no N hyperfine splitting ($A_{\text{iso}}(\text{N}) < 1.9 \text{ G}$) could be detected, and one would expect a similarly small N hfs for the unpaired electron in a $d_{x^2-y^2}$ orbital for symmetry reasons.

An ordering of the energy levels cannot be obtained with the available information if the electron is contained in the orbital with d_{z^2} character. The shift of g_{\parallel} from the free electron value is due to spin-orbit interactions on the ligand atoms (d_{z^2} has no angular momentum in the z direction). Thus, the magnitude of $g_{\parallel} - g_e$ in relation to $g_{\perp} - g_e$ cannot be used to determine an ordering.

Further experiments are planned for determining both the extent of delocalization of the free electron and the extent of localization on the Fe atom by isotopic substitution. The magnitude of the contribution by the S ligands to the molecular g values is also of great theoretical and practical interest due to the relatively large value of the spin-orbit coupling of the valence electrons of the sulfur atom.

Acknowledgments. The authors wish to acknowledge partial support of this research under National Science Foundation Grant GP-9559. W. V. S. received support under a National Defense Education Act, Title IV, fellowship. The authors are highly indebted to Professors Dimitri Coucouvanis and Robert G. Kooser and Mr. Douglas Piltingsrud for valuable discussions.

(30) D. A. C. McNeil, J. B. Raynor, and M. C. R. Symons, *J. Chem. Soc.*, 410 (1965).

Nuclear Magnetic Resonance Studies of Quadrupolar and Dipolar Relaxation Effects. Complexes of Lithium Halides with Pyridine in Aqueous Solution

by David W. Larsen

Department of Chemistry, University of Missouri-St. Louis, St. Louis, Missouri 63121 (Received May 10, 1971)

Publication costs borne completely by The Journal of Physical Chemistry

A study was conducted of the effects of lithium halides on α -proton line shapes and spin-lattice relaxation times of pyridine. Addition of the chloride to aqueous pyridine was found to broaden the multiplet substantially while addition of the bromide or the iodide was found to have little effect upon the multiplet. All lithium salts added to neat pyridine were found to sharpen the multiplet. The α -proton multiplet line shapes are governed by the rate of ^{14}N quadrupolar relaxation, and the results are interpreted in terms of an anisotropic rotational diffusion mechanism. The proton T_1 values are also interpreted in terms of an anisotropic rotational diffusion mechanism. The experimental parameters were satisfactorily accounted for in terms of geometric models for the complexes: linear $\text{Li}^+\text{Cl}^- \text{py}$ for LiCl in aqueous pyridine, linear $\text{Li}^+(\text{H}_2\text{O})\text{py}$ for LiBr in aqueous pyridine, and tetrahedral $\text{Li}^+\text{Cl}^- \text{py}_3$ for LiCl in neat pyridine.

Introduction

Complex formation in aqueous solution between lithium ion and pyridine has been studied¹ using nmr chemical shifts. It was found that addition of LiCl to a pyridine-water mixture caused the water protons to exhibit a slight low-field displacement and the pyridine protons to exhibit almost no displacement. The former observation was attributed to solvation pro-

cesses and the latter to weak interaction of the salt with pyridine resulting from stronger interaction of the salt with water. It was also concluded that anions are involved in structure-breaking processes and are not solvated to any appreciable extent.

(1) A. Fratiello and E. G. Christie, *Trans. Faraday Soc.*, **61**, 306 (1965), and references contained therein.

We present the results of a study of the effect of lithium halides on the proton nmr line shapes and relaxation times of pyridine. These studies indicate that the salts interact strongly with pyridine both in neat pyridine solution and in aqueous pyridine solution and that the nature of the lithium-pyridine complex depends on the anion present in solution.

Experimental Section

Lithium Salts. Commercially available salts were used after drying in an oven. Lithium iodide was synthesized by the reaction of metallic lithium with iodine in ether solution.

Solutions. The aqueous electrolyte solutions were prepared by addition of the salts to 5% (v/v) pyridine in aqueous solution. The electrolyte solutions in neat pyridine were prepared by vacuum distilling pyridine into nmr tubes containing the dry salts. The samples used for proton T_1 measurements were degassed by repeated use of the freeze-pump-thaw technique.

Nmr Measurements. Proton nmr line shapes of pyridine were recorded using a Perkin-Elmer R-20 nmr spectrometer operating at 60 MHz. The resolution was carefully adjusted before recording each spectrum. Line widths were estimated by comparing the observed line shapes with those calculated using literature peak positions and intensities.² Each peak in a multiplet was assumed to be Lorentzian, and all peaks in a given multiplet were assumed to have the same line width. Multiplet line shapes were thus calculated using an IBM 1130 computer with component line width ($\Delta\nu_{1/2}$) as the single independent parameter. An error is introduced by this procedure since proton-proton coupling constants and chemical shifts are known to change slightly with complexation of pyridine;³ however, in this case, these changes and the associated errors are very small.

Proton spin-lattice relaxation times, T_1 , were obtained by the direct method.⁴

Viscosity Measurements. Relative viscosities were determined using an Ostwald viscosimeter.⁵

Experimental Results

The lithium halides which are soluble in aqueous media, LiCl, LiBr, and LiI, were added to 5% (v/v) pyridine in aqueous solution. It was found that the chloride caused a substantial broadening of the α -proton nmr multiplet, while the β - and γ -proton multiplets were broadened only very slightly. The bromide and iodide salts caused a slight sharpening of the α multiplet relative to the β and γ multiplets. Figure 1 shows the α -proton spectra of aqueous pyridine and aqueous pyridine in the presence of LiCl, LiBr, and LiI. The concentration of lithium salt is 5 M in each case. Since the features of interest are similar for LiBr and LiI but quite different for LiCl and LiBr, we

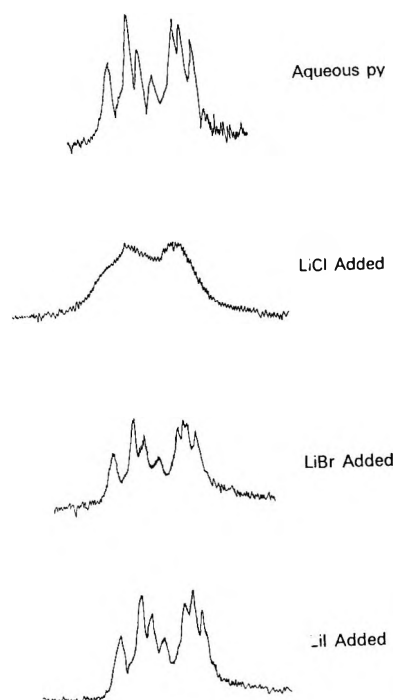


Figure 1. The α -proton spectra of aqueous pyridine and aqueous pyridine with added LiCl, LiBr, and LiI at 35°.

will focus upon the differences between LiCl and LiBr. The line widths of the α components as a function of concentration of added lithium salt are presented in Table I. The line widths are presented as $\Delta\nu_{1/2} - \Delta\nu_{1/2}^0$, where $\Delta\nu_{1/2}$ is the observed α -component line width and $\Delta\nu_{1/2}^0$ is the α -component natural line width, which is expected to increase slightly with viscosity increase. The value of $\Delta\nu_{1/2}^0$ was taken to be equal to the line width of the γ -multiplet components. Also presented in Table I are the experimental T_1 values for the α protons in pyridine and the experimental values of η/η_0 , where η is the viscosity of the solution and η_0 is the viscosity of water.

A second type of study was conducted in which a variety of lithium salts were added to neat pyridine, and the nmr lines shapes were recorded. It was found that all the salts caused a sharpening, to a greater or lesser extent, of the α -proton multiplet relative to that of neat pyridine. Figure 2 shows the α -proton spectra of neat pyridine and a saturated solution of LiCl in pyridine. This salt was chosen because it is fairly soluble in pyridine and has a relatively large effect on the line shape. Further consideration of the neat pyridine results will be deferred until the aqueous solutions have been fully considered.

(2) S. Castellano, C. Sun, and R. Kostelnik, *J. Chem. Phys.*, **46**, 327 (1967).

(3) J. B. Merry and J. H. Goldstein, *J. Amer. Chem. Soc.*, **88**, 5560 (1966).

(4) A. L. Van Geet and D. N. Hume, *Anal. Chem.*, **37**, 983 (1965).

(5) D. P. Shoemaker and C. W. Garland, "Experiments in Physical Chemistry," McGraw-Hill, New York, N. Y., 1967, pp 278-285.

Table I: Line Widths and Proton T_1 Values for Pyridine in the Presence of Aqueous Lithium Salts

Solution	$(\Delta\nu_{1/2} - \Delta\nu_{1/2}^0)^a$ Hz	$T_{1\alpha}^b$ sec	η/η_0
5% pyridine in D ₂ O	0.30	27.3	1.12
2.5 M LiCl	1.05	7.4	1.48
5.0 M LiCl	1.65	4.9	2.01
7.5 M LiCl	1.65	3.6	2.68
10.0 M LiCl	1.75	2.2	4.67
2.5 M LiBr	0.30	21.2	1.42
5.0 M LiBr	0.30	14.0	1.86
7.5 M LiBr	0.25	7.5	2.65
10.0 M LiBr	0.25	5.5	4.29

^a Experimental error, ± 0.05 . ^b Experimental error, $\pm 10\%$.

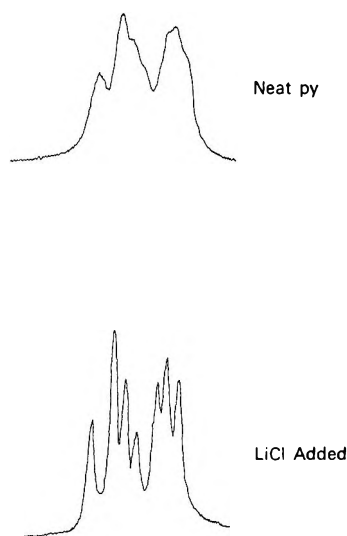


Figure 2. The α -proton spectra of neat pyridine and neat pyridine with added LiCl at 35°.

Theory

Kintzinger and Lehn⁶ have shown that the broadening of pyridine α -proton spectra is due to incomplete washing out of the coupling to ^{14}N ($I = 1$). The nitrogen spin-lattice relaxation time, $T_{1\text{N}}$, is governed by the quadrupole relaxation mechanism⁷ according to

$$(T_{1\text{N}})^{-1} = \frac{3}{8}(QCC)^2\tau q \quad (1)$$

where QCC is the quadrupole coupling constant, eQq/\hbar , Q is the nuclear electric quadrupole moment of ^{14}N , q is the fluctuating electric field gradient, and τq is the correlation time for the relaxation mechanism. Allerhand and Thiele⁸ have shown that when the quadrupole multiplet collapses to a single line, an approximately Lorentzian line shape is obtained, with line width given by

$$\Delta\nu_{1/2} = \Delta\nu_{1/2}^0 + \frac{8}{3}\pi J_{\text{N}\alpha}^2 T_{1\text{N}} \quad (2)$$

where $\Delta\nu_{1/2}$ is the observed line width, $\Delta\nu_{1/2}^0$ is the

natural line width (that in the absence of quadrupolar broadening), and $J_{\text{N}\alpha}$ is the spin-spin coupling constant between ^{14}N and the α protons. The value of $\Delta\nu_{1/2}$ is applicable to each component in the α -proton multiplet arising from coupling with the β and γ protons.

We will interpret our experimental results in terms of a two-site case with rapid chemical exchange between the two sites. The two sites will correspond to free pyridine and pyridine complexed by the salt. The two sites are separated by a very small chemical shift¹ and exchange is rapid enough to eliminate exchange broadening.

Gore and Gutowsky⁹ have shown that for the two-site case, in the limit of $p_A \gg p_B$, where p_A and p_B are mole fractions in each site, eq 2 may be generalized for $I = 1$ to read

$$(\Delta\nu_{1/2} - \Delta\nu_{1/2}^0)^{-1} = \left(\frac{8}{3}\pi\right)^{-1} \left(\frac{p_A}{T_{1\text{N}}^A} + \frac{p_B}{T_{1\text{N}}^B}\right) (p_A J_{\text{N}\alpha}^A + p_B J_{\text{N}\alpha}^B)^{-2} \quad (3)$$

We have made computer simulations of line shapes in the collapsed multiplet region to which eq 3 applies using the complete expressions of Gore and Gutowsky. These simulations show that the difference between the simulated line widths and those predicted by eq 3 is $< 8\%$ over the entire mole fraction range. Thus the restriction $p_A \gg p_B$ may be removed for our purposes since this error is not much larger than our estimated experimental error. In addition, we expect to obtain useful numbers from eq 3 only in the limit of $p_A \gg p_B$.

An expression analogous to eq 3 can also be written for the observed α -proton T_1 values¹⁰

$$\frac{1}{T_1} = \frac{p_A}{T_1^A} + \frac{p_B}{T_1^B} \quad (4)$$

where T_1 is the observed proton spin-lattice relaxation time for the solution, and T_1^A and T_1^B are the T_1 values in the A and B sites, respectively.

The values of $T_{1\text{N}}^A$ and $T_{1\text{N}}^B$ may be interpreted in terms of anisotropic rotational diffusion.¹¹ In the present case, the field gradient is expected to lie along the C_2 axis of pyridine, and the complex expression of Huntress¹¹ reduces to

$$\frac{1}{T_{1\text{N}}^i} = \frac{(OCC)^2}{32} \frac{D_x^i + D_y^i + 4D_z^i}{D_x^i D_y^i + D_y^i D_z^i + D_x^i D_z^i} \quad (5)$$

where D_j^i is the rotational diffusion constant about the j th axis in the internal molecular coordinate system. In this case, the C_2 axis lies in the z direction.

(6) J. P. Kintzinger and J. M. Lehn, *Mol. Phys.*, **14**, 133 (1968).

(7) J. A. Pople, *ibid.*, **1**, 168 (1958).

(8) A. Allerhand and E. Thiele, *J. Chem. Phys.*, **45**, 902 (1966).

(9) E. S. Gore and H. S. Gutowsky, *J. Phys. Chem.*, **73**, 2515 (1969).

(10) H. G. Hertz, *Progr. NMR Spectrosc.*, **3**, 159 (1967).

(11) W. T. Huntress, *Advan. Magn. Resonance*, **4**, 1 (1970).

The values of T_1^A and T_1^B may also be interpreted in terms of anisotropic rotational diffusion.¹² In the present case with the solvent D_2O , the relaxation mechanism for the α proton is expected to be intramolecular dipolar interaction with the β proton. Relaxation by interaction with other ring protons will be negligibly small. The internuclear axis between the α and β proton is parallel to the C_2 axis of pyridine and Woessner's expression¹² reduces to

$$\frac{1}{T_1^i} = \frac{3}{4} \frac{\gamma^4 \hbar^2}{r^6} \left[\frac{D_z^i}{D_x^i D_y^i + D_y^i D_z^i + D_x^i D_z^i} \right] \quad (6)$$

where r is the distance between α and β protons.

If we let the A and B sites refer to free pyridine and pyridine complexed by the salt, respectively, and with the definition

$$F(\Delta\nu) \equiv \frac{(\Delta\nu_{1/2} - \Delta\nu_{1/2}^0)^{-1}_{\text{py-salt(aq)}}}{(\Delta\nu_{1/2} - \Delta\nu_{1/2}^0)^{-1}_{\text{py(aq)}}}$$

where the numerator refers to the aqueous pyridine solution with salt and the denominator to aqueous pyridine with no salt, then eq 3 can be rewritten

$$F(\Delta\nu) = \frac{\left(\frac{p_F}{T_{1N}^F} + \frac{p_C}{T_{1N}^C} \right) J_{N\alpha}^2}{\left(\frac{1}{T_{1N}} \right) (p_F J_{N\alpha}^F + p_C J_{N\alpha}^C)^2} \quad (7)$$

where T_{1N}^F , T_{1N}^C , and T_{1N} refer to free pyridine in the salt solution, complexed pyridine in the salt solution, and pyridine in aqueous solution containing no salt. In the presence of excess salt in the solution, it is expected that $p_C \approx 1$ and $F(\Delta\nu) \approx F(\Delta\nu)_C$, where (from eq 7)

$$F(\Delta\nu)_C = \frac{\left(\frac{1}{T_{1N}^C} \right) \left(\frac{J_{N\alpha}}{J_{N\alpha}^C} \right)^2}{\left(\frac{1}{T_{1N}} \right)} \quad (8)$$

Equations 5 and 6 indicate that T_1 and T_{1N} values are related to D_j^i , and this quantity is given by¹¹

$$D_j^i = \frac{kT(\tau_j)_j^i}{I_j^i}$$

where $(\tau_j)_j^i$ and I_j^i are the effective collision time and the moment of inertia about the j th axis. Since $(\tau_j)_j^i$ is not a directly measurable quantity, an alternate expression for D_j^i is necessary. We will interpret our results using the assumption $D_j^i \propto (I_j^i \eta)^{-1}$, where η is the macroscopic shear viscosity. One then obtains, from eq 5 and 8

$$F(\Delta\nu)_C F(\eta) = \frac{(QCC)_C^2 \left(\frac{J_{N\alpha}}{J_{N\alpha}^C} \right)^2}{(QCC)^2} F_I^{\Delta\nu} \quad (9)$$

where

$$F(\eta) = (\eta/\eta_0)_C^{-1}/(\eta/\eta_0)^{-1}$$

and

$$F_I^{\Delta\nu} = \left(\frac{4I_x I_y + I_y I_z + I_x I_z}{I_x + I_y + I_z} \right)_C / \left(\frac{4I_x I_y + I_y I_z + I_x I_z}{I_x + I_y + I_z} \right)$$

Equation 6 may be rewritten in analogous manner

$$F(T_1)_C F(\eta) = F_I^{T_1} \quad (10)$$

where

$$F(T_1)_C = \left(\frac{1}{T_1^C} \right) / \left(\frac{1}{T_1} \right)$$

and

$$F_I^{T_1} = \left(\frac{I_x I_y}{I_x + I_y + I_z} \right)_C / \left(\frac{I_x I_y}{I_x + I_y + I_z} \right)$$

Figure 3 shows the experimental plots of $F(\Delta\nu)F(\eta)$ vs. concentration for LiCl and LiBr, and Figure 4 shows the experimental plots of $F(T_1)F(\eta)$ vs. concentration. The plots are consistent with formation of a complex following the law of mass action (two-site case) and with the assumed expression for D_j^i . Above 5 M, the pyridine is essentially completely complexed ($p_C \approx 1$). Values of $F(\Delta\nu)_C F(\eta)$ and $F(T_1)_C F(\eta)$ can be estimated from Figures 3 and 4. These are presented in Table II.

Equation 10 indicates that $F(T_1)_C F(\eta)$ is a function of geometry only, whereas eq 9 indicates that $F(\Delta\nu)_C F(\eta)$ is a function of geometry and factors affecting QCC and $J_{N\alpha}$. Thus $F(T_1)_C F(\eta)$ provides a direct test for possible geometric models of the complex (within the context of our assumptions).

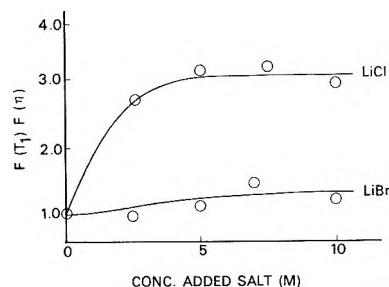


Figure 3. Plot of $F(\Delta\nu)F(\eta)$ vs. concentration of LiCl and LiBr in aqueous pyridine at 35°.

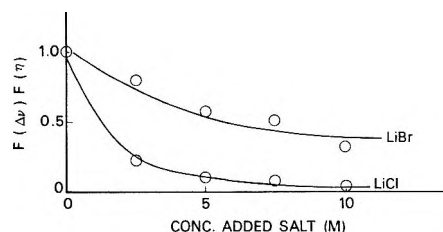


Figure 4. Plot of $F(T_1)F(\eta)$ vs. concentration of LiCl and LiBr in aqueous pyridine at 35°.

Table II: Estimated Values of Line Width and Relaxation Time Functions for Pyridine-Salt Complexes

	LiCl	LiBr
$F(\Delta\nu)_c F(\eta)$	0.04 ± 0.02	0.36 ± 0.03
$F(T_1)_c F(\eta)$	3.0 ± 0.3	1.4 ± 0.3

Discussion

Geometric Models. Two complexes with stoichiometry LiCl·py and LiCl·3py have been isolated.^{13,14} Thermodynamic data¹⁵ and the crystal structure¹⁶ of the LiCl·py complex have also been reported. In addition, the crystal structure of a complex with stoichiometry LiCl·H₂O·2py has been reported.¹⁷ These crystal structures indicate that Li⁺ is tetrahedrally coordinated; thus, a tetrahedral model for the complex in solution should be investigated. However, nmr results have been rationalized¹⁸ in terms of formation of a linear complex Li⁺·2CH₃CN in the case of LiClO₄ in CH₃CN solution; thus, a two-coordinated linear model should also be investigated.

Two anion-containing models were used to calculate the geometric factors in eq 9 and 10 as follows: (a) tetrahedral coordinated Li⁺ with stoichiometry Li⁺Cl⁻py(D₂O)₂, and (b) linear two-coordinated Li⁺ with stoichiometry Li⁺Cl⁻py. Bond lengths used were those reported¹⁷ for the crystal structure of LiCl·H₂O·2py: Li-Cl, 2.33 Å; Li-O(H₂O), 1.94 Å; Li-N(py), 2.05 Å. The stoichiometry for model a was assumed because water is present in large excess with respect to pyridine. Two additional models which exclude anions were also used in the calculations: (c) tetrahedrally coordinated Li⁺ with stoichiometry Li⁺py(D₂O)₃, and (d) linear two-coordinated Li⁺ with stoichiometry Li⁺py(D₂O). These models will be referred to as (a) ion-paired tetrahedral (IPT), (b) ion-paired linear (IPL), (c) ionic tetrahedral (IT), (d) ionic linear (IL).

The moment of inertia factors were calculated for the four models, a-d, for each of the two salt complexes with pyridine. The calculated values of $F_I^{T_1}$ and $F_I^{\Delta\nu}$ are presented in Table III. The value of the Li-Br bond length was assumed to be 2.38 Å, consistent with the larger ionic radius for Br⁻. The model used for aqueous pyridine was py·D₂O.

It can be seen from the data in Table III that there is excellent agreement between $F_I^{T_1}$ and $F(T_1)_c F(\eta)$ with the IPL model for the LiCl complex and with the IL model for the LiBr complex. It is worthwhile to emphasize at this point that the calculation is quite sensitive to the hydration of the complex at the cation site. For the LiBr complex, $F_I^{T_1}$ values show a substantial difference between IT (three waters) and IL (one water). A complex involving no water can be ruled out since this model gives $F_I^{T_1} = 0.5$. Replace-

ment of a hydrogen-bonded water molecule with a lighter Li⁺ decreases $F_I^{T_1}$ (tending to increase T_1); thus, the effect of the salt is to coordinate a specie heavier than the specie which is coordinated in aqueous pyridine (presumably a hydrogen-bonded water). Comparison between $F_I^{\Delta\nu}$ and $F(\Delta\nu)_c F(\eta)$ for the two complexes shows that there is poor agreement between the two functions for any of the models used. This indicates that there is a substantial decrease in the ratio $(QCC)^2/J_{N\alpha}^2$ when pyridine forms a complex with the salts. We will now consider the factors which affect the changes in the $(QCC)^2/J_{N\alpha}^2$ ratios.

Table III: Calculated Moment of Inertia Functions for Aqueous Pyridine-Salt Complexes

Model	$F_I^{T_1}$				Observed $F(T_1)_c F(\eta)$
	IPT	IPL	IT	IL	
LiCl complex	2.38	2.81	2.04	1.71	3.0
LiBr complex	3.20	4.38	2.04	1.71	1.4
Model	$F_I^{\Delta\nu}$				Observed $F(\Delta\nu)_c F(\eta)$
	IPT	IPL	IT	IL	
LiCl complex	2.55	2.62	2.15	1.64	0.04
LiBr complex	3.35	4.03	2.15	1.64	0.36

Spin-Spin Coupling Constants. It has been shown⁶ that $J_{N\alpha}$ for neat pyridine is not much affected by dissolution in water; thus, $J_{N\alpha}$ for py·H₂O can be set equal to 7.9 Hz. Protonation of pyridine has been shown⁶ to decrease $J_{N\alpha}$ to 1.45 Hz. These two values may be considered the upper and lower limits for $J_{N\alpha}$ for the complex, the former representing a weak interaction between pyridine and Li⁺ and the latter a strong enough interaction to form a covalent bond. A semiquantitative estimate of $J_{N\alpha}^c$ can be made if one takes note that while protonation of pyridine decreases $J_{N\alpha}$ substantially, it also increases $J_{N\beta}$ substantially. This makes it possible to estimate J values by comparing line widths of both α and β components. Thus for any given complex, from eq 8, one may write

$$R_{\alpha\beta} \equiv \frac{(\Delta\nu_{1/2} - \Delta\nu_{1/2}^{\circ})_c^{\alpha}}{(\Delta\nu_{1/2} - \Delta\nu_{1/2}^{\circ})_c^{\beta}} = \left(\frac{J_{N\alpha}^c}{J_{N\beta}^c} \right)^2 \quad (11)$$

If it is assumed that J varies linearly with quaternization

- (13) S. Halut-Desportes, *C. R. Acad. Sci., Ser. C*, **263**, 403 (1966).
- (14) H. Brusset and S. Halut-Desportes, *Bull. Soc. Chim. Fr.*, 459 (1967).
- (15) S. Halut-Desportes, *ibid.*, 2283 (1967).
- (16) F. Durant, J. Verbist, and M. van Meerssche, *Bull. Soc. Chim. Belg.*, **75**, 806 (1966).
- (17) F. Durant, P. Piret, and M. van Meerssche, *Acta Cryst.*, **22**, 52 (1967).
- (18) T. T. Bopp, *J. Chem. Phys.*, **47**, 3621 (1967).

$$J_{N\alpha}^{\text{obsd}} = J_{N\alpha}^{\text{Q}}F_q + J_{N\alpha}(1 - F_q) \quad (12)$$

where $J_{N\alpha}$ and $J_{N\alpha}^{\text{Q}}$ refer to pyridine and quaternized pyridine, and F_q is the fraction of quaternary character in the N-Li⁺ bond, then using an expression analogous to eq 12 for $J_{N\beta}^{\text{obsd}}$ and rearranging eq 11, one obtains

$$F_q = \frac{J_{N\alpha} - J_{N\beta}R_{\alpha\beta}^{1/2}}{(J_{N\beta}^{\text{Q}} - J_{N\beta})R_{\alpha\beta}^{1/2} - (J_{N\alpha}^{\text{Q}} - J_{N\alpha})} \quad (13)$$

Equating $J_{N\alpha}$ and $J_{N\beta}$ with the coupling constants for pyridine, 7.9 and 1.0 Hz, respectively, and equating $J_{N\alpha}^{\text{Q}}$ and $J_{N\beta}^{\text{Q}}$ with the coupling constants for pyridinium ion, 1.45 and 3.2 Hz, respectively,⁶ one can estimate F_q from eq 13. The values of F_q so estimated from line width data for pyridinium ion and the LiCl complex are given in Table IV.

Table IV: Multiplet Line Widths and Fractions of Quaternary Character

	$\frac{(\Delta\nu_{1/2} - \Delta\nu_{1/2}^{\circ})C^{\alpha}}{\text{Hz}}$	$\frac{(\Delta\nu_{1/2} - \Delta\nu_{1/2}^{\circ})C^{\beta}}{\text{Hz}}$	R_{α}	F_q
Pyridinium ion	1.3	2.7	0.48	0.91
LiCl complex	1.75	0.45	3.9	0.55

These F_q values suggest the N-Li⁺ bond in the complex is only about one-half covalent, taking the N-H⁺ bond to be completely covalent. The chemical shifts of the α and β protons for the LiCl complex of pyridine also reflect the low covalent character of the N-Li⁺ bond. The α and β multiplets are well separated for the LiCl complex (as they are in uncomplexed pyridine) whereas the multiplets partially overlap for the pyridinium ion.³

Quadrupole Coupling Constants. The value of $J_{N\alpha}$ for the LiCl complex as estimated from eq 12 with $F_q = 0.55$ is $J_{N\alpha}^{\text{C}} = 4.4$ Hz. Thus $(QCC)_C/(QCC)$ for the LiCl case can be estimated from eq 9 to be 0.07. The value of $(QCC)_C/(QCC)$ for the LiBr case can be only roughly estimated by assuming a value for $J_{N\alpha}^{\text{C}}$, since the line widths are too small in this case to use the above procedure. If $J_{N\alpha}^{\text{C}}$ for the LiBr complex is assumed to equal that for the LiCl complex, then $(QCC)_C/(QCC)$ for the LiBr complex is 0.26. However, the effects of D₂O and Cl⁻ on the N-Li⁺ bond could be quite different, which would result in different $J_{N\alpha}^{\text{C}}$ values for the two complexes.

Thus both the LiCl and LiBr complexes with pyridine have much smaller QCC values than that for aqueous pyridine. In addition, the LiBr complex appears to have a somewhat larger QCC value than the LiCl complex. The QCC value is related to the nitrogen atom p electron unbalance (U_p) according to the Townes-Dailey¹⁹ theory. The presence of a nonbonding pair on pyridine results in a nonzero U_p ,

whereas coordination of the nonbonding pair by Li⁺ is expected to greatly reduce U_p . The small, nonzero U_p for the complexes and the difference in U_p values for the two complexes thus reflect varying ionic character in N-Li⁺ bonds as well as several other factors possibly including different hybridizations for the two complexes.²⁰

Neat Pyridine Spectra. A brief consideration of the neat pyridine spectra and their relationship to the aqueous pyridine spectra will now be given. The pertinent data are given in Table V. Consider first the differences between neat pyridine and aqueous pyridine. There is a problem associated with analysis of these data; the intramolecular contribution to T_1 must be extracted from the observed T_1 for neat pyridine. The intramolecular T_1 for neat pyridine has been reported by Zeidler,²¹ and this value is given in the table. Comparison of proton T_1 values obtained with different instruments is not in general reliable; however, these data do at least provide a rough basis for comparing the two cases at hand. The geometric models used to calculate moments of inertia were py·D₂O, used previously for aqueous pyridine, and the simple py for neat pyridine. The functions introduced previously are as follows.

System	$\frac{F(\Delta\nu)_C}{F(\eta)}$	$\frac{F(T_1)_C}{F(\eta)}$	$F_I\Delta\nu$	$F_I T_1$
Py-5% in D ₂ O	2.7	3.2	3.1	3.8

In this case, $F(\Delta\nu) \equiv (\Delta\nu_{1/2} - \Delta\nu_{1/2}^{\circ})^{-1}_{\text{py}\cdot\text{H}_2\text{O}} / (\Delta\nu_{1/2} - \Delta\nu_{1/2}^{\circ})^{-1}_{\text{py}}$. The agreement between $F(T_1)_C F(\eta)$ and $F_I T_1$ is remarkable considering the uncertainties in T_1 stated previously. The close agreement $F(\Delta\nu)_C F(\eta)$ and $F_I \Delta\nu$ indicates that the change in the factor $(QCC)^2/J_{N\alpha}^2$ due to coordination of water is very small. Since the values of $J_{N\alpha}$ for neat pyridine and aqueous pyridine are identical,⁶ the conclusion that may be drawn is that coordination of a water molecule by pyridine does not appreciably affect QCC , and thus the observed sharpening of the spectrum is due primarily to the increase in the moments of inertia.

Let us now consider the differences between neat pyridine and neat pyridine saturated with LiCl. There are several problems associated with analysis of these data: (a) a geometric model must be constructed; (b) $F(T_1)_C F(\eta)$ and $F(\Delta\nu)_C F(\eta)$ are not readily determinable; (c) the intramolecular contributions to T_1 are not available. This latter difficulty makes analysis of the proton T_1 data useless in this case.

The geometric model can be formulated by considering the reported studies¹³⁻¹⁷ on LiCl-pyridine com-

(19) C. H. Townes and B. P. Dailey, *J. Chem. Phys.*, **17**, 782 (1949).

(20) T. M. Sudgen and C. N. Kenney, "Microwave Spectroscopy of Gases," Van Nostrand, Princeton, N. J., 1965, pp 111-143.

(21) M. D. Zeidler, *Ber. Bunsenges. Phys. Chem.*, **89**, 659 (1965).

Table V: Data for Comparison of Neat Pyridine with Aqueous Pyridine

System	$\frac{(\Delta\nu_{1/2} - \Delta\nu_{1/2}^0)}{\text{Hz}}$	T_1 , sec	η/η_0
Pyridine-5% in D ₂ O	0.30	27.3	1.12
Pyridine-neat	0.90	22.6, ^a 100 ^b	0.99
Pyridine-satd with LiCl	0.25	13.3	2.10

^a Experimental value, this work. ^b Estimated intramolecular value (see ref 21).

plexes. A tetrahedral configuration with stoichiometry $\text{Li}^+\text{Cl}^- \text{py}_3$ is the most likely model. The value of $F(\Delta\nu)_C F(\eta)$ cannot be obtained directly, but eq 7 can be rearranged to read

$$F(\Delta\nu)F(\eta) = \left[p_F + p_C \frac{(QCC)_C^2}{(QCC)^2} F_I^{\Delta\nu} \right] \left[p_F + p_C \frac{J_{N\alpha}^C}{J_{N\alpha}} \right]^{-2} \quad (14)$$

The above equation assumes that moment of inertia functions and $J_{N\alpha}$ values are identical for the free pyridine in the salt solution and for neat pyridine.

Mole fractions of free and complexed pyridine are needed for use in eq 14. These can be estimated from solubility data¹⁴ and the proposed model. The values obtained are $p_F = 0.23$ and $p_C = 0.77$. Assuming a value of $J_{N\alpha}^C$ between 4.4 and 7.9 Hz, with $F_I^{\Delta\nu} = 17.0$, one estimates $0.20 < (QCC)_C/(QCC) < 0.34$. The value 4.4 Hz should be a lower limit for $J_{N\alpha}$ since an Li^+ complexed to three py should not affect $J_{N\alpha}$ as much as Li^+ complexed to a single py. The value of $(QCC)_C/(QCC)$ for the tetrahedral $\text{Li}^+\text{Cl}^- \text{py}_3$ is larger than the values for the complexes in aqueous solution; this also reflects the weaker interaction for a Li^+ complexed to three py molecules as opposed to a Li^+ complexed to a single py.

The observed effects reported herein are indicative of longer correlation times for pyridine due to the presence of lithium salts. These longer correlation times will presumably be caused by interaction of the nitrogen nonbonding pair in pyridine with Lewis acids as well as concentration-dependent behavior of the solvent. Pyridine is a large enough molecule that the rotational diffusion mechanism should be correct. Our expression for D_j^i is probably oversimplified; however, it does allow the results to be explained in a self-consistent way assuming complex formation between pyridine and the salts. If it is assumed that no salt complexes are present, then the results must be rationalized in terms of "microviscosity" effects. This explanation does not allow for changes in QCC , $J_{N\alpha}$, or $J_{N\beta}$, and thus the proton T_1 values would indicate longer correlation times for the LiCl solutions, whereas the nitrogen T_1 values would indicate longer correlation times for the LiBr solutions. This inconsistency, as well as the observed dependence of $R_{\alpha\beta}$ values on salt concentration are strong evidence in favor of complexing of the salts by pyridine.

We have demonstrated that in cases when proton T_1 values are governed by an intramolecular anisotropic rotational diffusion mechanism, the experimental results provide a possible test for geometric models. In addition, the line width measurements, because of their relationship to QCC values, provide insight into the hybridization in pyridine, the ionic character in the $\text{N}-\text{Li}^+$ bond in the complex, and the effects of counterions and water on the electronegativity of the metal ion. This is potentially an important tool for structure determination of complexes in solution. The effects herein reported for the Li salts can be observed for the group Ia salts in general. We are at present systematically investigating the interaction of a large number of alkali halides with aqueous pyridine in order to extend the scope of the present studies.

Bisdifluoraminoalkanes: the Mass Spectral Decomposition of Isomeric Propanes

by Martin Hertzberg,

Safety Research Center, Bureau of Mines, Pittsburgh, Pennsylvania 15213

George White,

Atlantic Research Corporation, Alexandria, Virginia 22314

R. S. Olfky, and F. E. Saalfeld*

Naval Research Laboratory, Washington, D. C. 20390 (Received March 11, 1971)

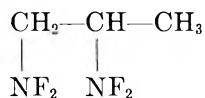
Publication costs assisted by the Naval Research Laboratory

The abundance of positive ions in the mass spectra of several bisdifluoraminoalkanes has been measured. The most abundant ions observed were the methylene fluoroimmonium ion $(\text{CH}_2\text{NF})^+$ from the 1,2-propane and the 1,3-propane, and hydrocarbon-type ions from the 2,2-propane. The identities of the ions were verified by exact mass measurements. Mechanisms are postulated to account for the observed fragmentation patterns. Some of the observed ionization products originate *via* rearrangement reactions having a ringlike intermediate configuration. The ions observed in greatest abundance are those that proceed through the minimal energy path for the overall ionic reaction process. Appearance potentials were measured for the more abundant ions formed from the three isomeric propanes studied. These data have been used to estimate differences in bond strengths within the isomeric series.

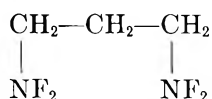
Introduction

Mass spectral measurements have been made on the following compounds

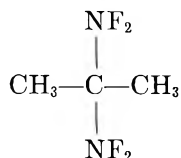
1,2-bis(*N,N*-difluoramino)propane (1,2-DP)



1,2-bis(*N,N*-difluoramino)propane (1,3-DP)



2,2-bis(*N,N*-difluoramino)propane (2,2-DP)



These compounds, which contain the $-\text{NF}_2$ functional group, are relatively new and potentially significant because their high-energy content could make them useful as propellants.

Experimental and Results Section

The sample of 1,2-DP was obtained from the DuPont Eastern Laboratories as a 20% solution in methylene chloride; the 1,3-DP compound was acquired from Aerojet Laboratories in Azusa, Calif., as a 15% solution in

methylene chloride; while the 2,2-DP sample was received as a 10% solution in *sym*-tetrachlorethane from the Rohm and Haas Redstone Arsenal Laboratory. Each of the samples was separated from its solvent by vacuum fractionation immediately prior to initiating the mass spectral study. The studies were not begun until no solvent was detected with the mass spectrometer. These bis(difluoramino) compounds decompose slowly to their more stable products (HCN , C_{solid} , CH_3CN , N_2 , and HF)¹ at 200–280°, while at higher temperatures, 280–500°, they decompose explosively.¹ The explosive sensitivity of these compounds in the gaseous phase has been reported elsewhere.^{1,2}

The mass spectral data for the positive ions from the bis(difluoramino)propanes are shown in Table I. The empirical formulas assigned to the various ions are given in column 2. These empirical formulas are based on exact mass measurements made on a high-resolution mass spectrometer (AEI MS-9 using 70-V electrons for the ionization process). The low-energy spectral data presented in Table I were obtained with a modified³ Bendix Corp. Model 12-107 time-of-flight mass spectrometer and compared with abundances measured with

(1) G. von Elbe, J. B. Levy, and G. White, "A Study of the Explosion Limits of Simple Difluoramino Compounds," Final Report, ONR Contract No. Nonr-4065(00), June 1969.

(2) G. von Elbe and G. White, "Branched-chain Mechanism of Bis-difluoroaminoalkane Explosions," 13th Symposium (International) on Combustion, The Combustion Institute, Pittsburgh, Pa., 1971, in press.

(3) F. E. Saalfeld and M. V. McDowell, *Inorg. Chem.*, **6**, 96 (1967).

Table I: Identity, Abundance, and Appearance Potential of Ions from the BisdifluoraminoPROPANES (in % Total Ion Current)^a

Mass, amu	Positive ion identity ^b	1,2-DP			1,3-DP			2,2-DP		
		A, %	B, %	C, eV	A, %	B, %	C, eV	A, %	B, %	C, eV
15	CH ₃	2	10	16.4 ± 0.4	2	8	14.6 ± 0.3	21	25	14.7 ± 0.2
27	HCN	6	12		6	9		1	5	
28	H ₂ CN	7			12	21		9	5	
30	C ₂ H ₆	0.5	0.5		25	4	13.1 ± 0.2
33	NF	0.5	3		2	3	13.0 ± 0.3	13	9	13.9 ± 0.3
41	CH ₃ CN, C ₂ H ₅	2	9		11	7		2	5	
42	C ₃ H ₆	0.5	12		5	9		1	3	
47	H ₂ CNF	74	31	11.5 ± 0.2	45	23	11.9 ± 0.2	2	2	
52	NF ₂	...	0.5		...	0.5	14.8 ± 0.4	...	1	13.9 ± 0.4
56	C ₃ H ₆ N	...	3	15.6 ± 0.3	...	1	15.6 ± 0.4	2	9	15.4 ± 0.3
61	CH ₃ CNF	...	0.5		...	2	16.8 ± 0.4	
65	CHNF ₂	0.5	1		4.5	3	13.7 ± 0.3	19	14	13.2 ± 0.3
66	CH ₂ NF ₂	1	7	13.1 ± 0.2	3	6	13.6 ± 0.3	1	0.5	
75	CH ₂ NFCH ₂ CH ₃	1	2	14.6 ± 0.3	...	0.5		...	1	
94	C ₂ H ₆ NF ₂	...	2	10.8 ± 0.2	...	1	11.8 ± 0.3	...	8	11.1 ± 0.3

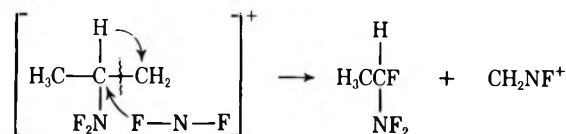
^a A, low voltage mass spectrum (15 V, uncorrected); B, conventional mass spectrum (70 V, uncorrected); C, appearance potential in electron volts; error limits are estimates of the measurement's accuracy—see text. ^b Determined from exact mass measurements with an AEI MS-9 high-resolution mass spectrometer.

an Electronic Associates, Inc. quadrupole mass spectrometer. The Bendix instrument was preferred for the ionization studies because of its relatively cool ion source ($35 \pm 5^\circ$) and the fact that the mass spectral data (fragmentation patterns and ionization efficiency curves) could be obtained rapidly. Rapid recording of the data immediately after turning on the mass spectrometer filament reduces the chance of products formed by decomposition on the hot filament from diffusing into the ion source and interfering with the recorded mass spectrum. In these studies the ionization efficiency curves for two ions (an ion from the sample of interest and the internal standard used to calibrate the voltage scale, either Kr, Xe, or Ar) were obtained simultaneously in less than 1 min. The disadvantage of obtaining data this rapidly is that statistical fluctuations in the ion currents are emphasized, resulting in larger error limits. To estimate the accuracy of appearance potential (AP) measurements, a second rare gas was introduced into the mass spectrometer with the standard and sample, its ionization potential measured immediately following the determination of the AP of the sample and compared to the spectroscopic ionization potential of the rare gas. The accuracy of the AP measurements determined in this manner is shown with the AP's in columns 5, 8, and 11 of Table I; the precision of the AP measurements was better than ± 0.2 V in all cases. A fresh sample of the compound being investigated was introduced into the mass spectrometer for each AP measurement. It was impossible to determine whether or not the ions reported possessed excess kinetic energy; therefore, the AP potentials reported here may be greater than the true potentials.

Discussion

a. Mass Spectra. 1,2-Bis(N,N-difluoramino)propane.

The most abundant ion over the energy range of 12 to 70 V in the 1,2-DP spectrum is the methylene fluoroimmonium ion, $[\text{CH}_2\text{NF}]^+$, $m/e = 47$. The simplest mechanism for its formation involves the cleavage of the 1,2 C-C bond with simultaneous F-atom displacement. The formation of the C-F bond during the



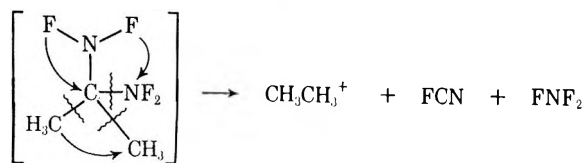
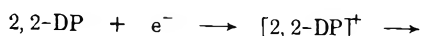
dissociative decomposition of the $[\text{1,2-DP}]^+$ ion provides a low-energy decomposition path to the $[\text{CH}_2\text{NF}]^+$ ion. Another plausible decomposition mechanism involves the establishment of an H-F bond during the decomposition of the parent ion, or a stepwise mechanism which involves the reestablishment of only a C-F bond in the neutral fragments. This latter mechanism is similar to the one proposed by Ross, Mill, and Hill⁴ to account for the rates of the low-pressure pyrolysis of these compounds. It is not possible to distinguish between these schemes and our data.

The spectrum of 1,2-DP observed at 70 V is remarkably simple; namely, the ion current observed at $m/e = 47$ is dominant in spite of the fact that its formation involves the cleavage of at least two bonds of the parent ion. The abundance of the parent ion is negligibly low, and even ions formed by the cleavage of only one bond, such as the $\text{C}_2\text{H}_6\text{NF}_2^+$ ion (which has the lowest appearance potential) are significantly lower in abundance, even at low electron energies, than $m/e = 47$.

(4) D. S. Ross, T. Mill, and M. E. Hill, "The Very Low Pressure Pyrolysis of Some Difluoramino Compounds," American Institute of Aeronautics and Astronautics, Aerospace Sciences Meeting, New York, N. Y., Paper No. 68-147, Jan 1968.

1,3 - Bis(N,N - difluoramino)propane. The most abundant ion is again observed at m/e 47. The fragmentation pattern is similar to the mass spectrum of the 1,2 isomer. The similarity in the patterns of 1,2-DP and 1,3-DP suggests that the 47 ion is formed from the end $-\text{CH}_2\text{NF}_2$ group in both isomers. The close similarity of the two appearance potentials supports this supposition. There are also some significant differences between the spectra of the 1,2-DP and 1,3-DP compounds, the most notable being the increased intensity of the m/e 28 ion. Part of the increased intensity of this ion current can be explained by the increased number of CH_2NF_2 groups in the 1,3-DP isomer compared to the 1,2 isomer. However, this explanation cannot be the full explanation of this difference because the intensity of the m/e 47 ion current has not changed in a similar manner.

2,2 - Bis(N,N - difluoramino)propane. There is a drastic change between the spectrum of 2,2-DP isomer compared to that of the 1,2- and 1,3-DP isomers. At low electron energies, a rearranged hydrocarbon ion, C_2H_6^+ , is the dominant ion. The H_2CNF^+ ion, which was the most abundant ion in the spectra of the other isomers, is observed, but only in a very low abundance (2%), in the 2,2-DP spectrum. The major decomposition paths appear to involve the formation of the hydrocarbon ions CH_3^+ , C_2H_6^+ , C_2H_4^+ , C_3H_5^+ , and C_2H_6^+ . The CH_3^+ , C_2H_5^+ , and C_2H_6^+ ions can be produced by simple bond cleavages of the $[2,2\text{-DP}]^+$ ion. However, the most abundant ion at low electron energies, C_2H_6^+ , can be formed only through a rearrangement mechanism involving complex ion formation with cleavage of both the original C-C bonds and subsequent reestablishment of a bond between the 1 and 3 carbon atoms. It is plausible to suggest that the ethane ion is formed *via* a triangular ring intermediate



Of course, the identity of the neutrals is speculation; however, such a mechanism would provide a low-energy path for the formation of C_2H_6^+ . This mechanism involving the initial cleavage of methyl groups and their simultaneous re-formation to form the C_2H_6^+ ion is analogous to a postulated mechanism for the formation of ethane in the unimolecular decomposition of azo-methane.^{5,6}

It is interesting to consider the variation in the percent total ion current of the ions as a function of electron energy. The data (obtained with the quadrupole instrument) for the 2,2-DP isomer is shown in Figure 1. There is a decline in the abundance of the C_2H_6^+ ion

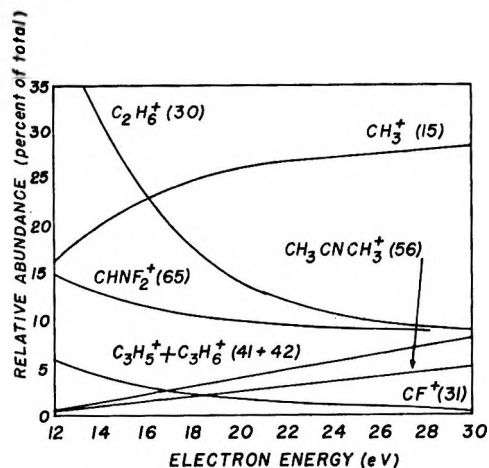


Figure 1. The relative abundance of various ions from 2,2-DP as a function of excitation energy.

with increasing electron energy. Similar declines are observed for the ions HCNF_2^+ and CF^+ . Other ion currents, particularly those formed by the simple bond cleavage, show moderate increases with increasing electron energy. This behavior is explicable in terms of the relative significance of rearrangement ion formation *vs.* direct dissociative ionization as a function of the total energy available to the ion. The former process appears to be favored at low electron energies whereas the latter is favored at higher electron energies. In general the ions from these propane isomers which are produced by a rearrangement mechanism decrease in abundance with increasing electron energy. This observation can be explained by the quasi-equilibrium theory of mass spectra.⁷ Since the unimolecular rate constant for the decomposition of these is proportional to the energy of the system, at lower energies the rate is slower and therefore the rearrangement has sufficient time to occur. However, at higher electron energies, the rate constant is larger, and there is insufficient time available for rearrangement before decomposition.

The shape of the curve of m/e 65 from the 2,2-DP in Figure 1 and the shape of the curves of m/e 47 for the 1,2-DP and 1,3-DP (not shown, but similar to the CHNF_2 curve in Figure 1), *i.e.*, decreasing abundance with increasing electron energy, suggests that in these ions a rearrangement process has occurred. This most probably has been the migration of an F atom from the nitrogen atom to the carbon atom.

b. Bond Energies. The appearance potential data shown in Table I have been used to estimate bond dissociation energies. It has been assumed that the appearance potential measured for a fragment ion is the minimum energy necessary to break the bond in ques-

(5) H. C. Ramsperger, *J. Amer. Chem. Soc.*, **49**, 912 (1927).

(6) H. C. Ramsperger, *ibid.*, **49**, 1495 (1927).

(7) H. M. Rosenstock, M. B. Wallenstein, A. L. Wahrhaftig, and H. Eyring, *Proc. Nat. Acad. Sci. U. S.*, **38**, 637 (1952).

tion and to ionize the radical precursor of the observed ion. Thus, the appearance potential (AP) for the X^+ fragment ion produced from the molecule $X-Y$ is the sum

$$AP(X^+) = D(X-Y) + I(X\cdot) \quad (1)$$

where $D(X-Y)$ is the $X-Y$ bond dissociation energy and $I(X\cdot)$ is the ionization potential of the $X\cdot$ free radical. This equation assumes that no excess kinetic or electronic energy is contained in either the ion or neutral fragments.

Equation 1 can be used with the AP obtained for the mass 94 ions of the propane isomers to estimate the bond energies from the 1,2-DP isomer (where the superscripts 1 and 2 denote primary and secondary fragments, respectively)

$$AP(\text{CH}_2\text{NF}_2\text{CHCH}_3)^+ = I(\text{CH}_2\text{NF}_2\text{CHCH}_3) + D_{1,2}(^2\text{C-NF}_2) = 10.8 \text{ V} \quad (2)$$

and from the 1,3-DP isomer

$$AP(\text{CH}_2\text{NF}_2\text{CH}_2\text{CH}_2)^+ = I(\text{CH}_2\text{NF}_2\text{CH}_2\text{CH}_2) + D_{1,3}(^1\text{C-NF}_2) = 11.8 \text{ V} \quad (3)$$

Since the mass 94 ions from the 1,2 and 1,3 isomers are formed from radicals that are probably tautomers of one another, it is plausible to assume that their ionization potentials are nearly identical, and hence

$$D_{1,3}(^1\text{C-NF}_2) - D_{1,2}(^2\text{C-NF}_2) = 1.0 \text{ V} = 23.1 \text{ kcal mol}^{-1} \quad (4)$$

Similar data for the 2,2 compound cannot be reliably estimated because the ionization potential of the radical is probably different than the one produced from 1,3- and 1,2-DP.

Consider the mass 52 ion formed from the 1,3 and 2,2 compound. Applying eq 1 for the 1,3-DP isomer

$$AP(\text{NF}_2^+) = I(\cdot\text{NF}_2) + D_{1,3}(^1\text{C-NF}_2) = 14.8 \text{ V} \quad (5)$$

and for the 2,2-DP isomer

$$AP(\text{NF}_2^+) = I(\cdot\text{NF}_2) + D_{2,2}(^2\text{C-NF}_2) = 13.9 \text{ V} \quad (6)$$

hence

$$D_{1,3}(^1\text{C-NF}_2) - D_{2,2}(^2\text{C-NF}_2) = 0.9 \text{ V} = 20.8 \text{ kcal mol}^{-1} \quad (7)$$

and by subtracting eq 7 from eq 4

$$D_{2,2}(^2\text{C-NF}_2) - D_{1,2}(^2\text{C-NF}_2) = 2.3 \text{ kcal mol}^{-1} \quad (8)$$

Thus, the following order of bond energies is obtained

$$D_{1,2}(^2\text{C-NF}_2) \sim D_{2,2}(^2\text{C-NF}_2) < D_{1,3}(^1\text{C-NF}_2)$$

The two secondary carbon-nitrogen bond energies are of comparable magnitude, while the primary C-NF_2

bond is stronger than the secondary by about 23 kcal mol^{-1} .

The appearance potential of the mass 56 peak, corresponding to the $\text{C}_2\text{H}_6\text{N}^+$ ion, may be used to estimate the N-F bond energy order, if we again assume that the ionization potentials for the isomeric radicals are equal and that the neutral products produced in the electron bombardment of the propanes are identical. The order of N-F bond strengths, obtained in a manner similar to that employed to estimate the C-NF_2 order and using the previously determined order of the C-NF_2 bond energies, is

$$D_{1,3}(^1\text{N-F}) \sim D_{2,2}(^2\text{N-F}) < D_{1,2}(^1\text{N-F})$$

This is the inverse of the order of C-NF_2 bond strengths. This reversal of orders can be explained as the effect of "induction" or inductive bond polarization. These data are significant for the explosion kinetics problem²

The difference between appearance potentials measured for the mass 66 ion (CH_2NF_2^+) formed from the 1,2 and 1,3 compounds suggests that vicinal substitution of an NF_2 group weakens the $\alpha\text{-C-C}$ bond by 11.5 kcal mol^{-1} , as compared with β substitution of the NF_2 group. While this difference is only slightly greater than our estimated accuracy, we feel it to be real and significant because the accuracy value applies to the absolute value of the measurement, whereas when using only differences in AP values the precision is the limiting factor. The CH_3^+ appearance potential from the 1,3-DP and 2,2-DP are essentially equal (14.6 and 14.7 V, respectively); however, the $AP(\text{CH}_3^+)$ from 1,2-DP is 16.0 V, considerably greater than the AP of CH_3^+ from the other two isomers. This difference is larger than the experimental error in these measurements. Using eq 1 and the data for 1,2-DP and 2,2-DP, it is seen that the substitution of a second NF_2 moiety lowers C-C bond energy by nearly 30 kcal mol^{-1} . This is approximately twice the bond energy reduction observed for the first NF_2 substitution. The low value of $AP(\text{CH}_3^+)$ from the 1,3 compound is puzzling since the 1,3 compound does not contain an end methyl group. This value can be rationalized, however, by noting that some energy must be returned to the system when the $\text{CH}_2\text{-H}$ bond recombines *via* a rearrangement process. Thus, one would expect a lower appearance potential for a rearrangement process compared to a process which involves only bond cleavage. Low values for $AP(\text{CH}_3^+)$ have also been observed from diketene⁸ and azetidine.⁹

Because rearrangement ions dominate the low-voltage spectra, it is not possible to correlate the ion current intensities observed in these spectra with the bond en-

(8) F. A. Long and L. Friedman, *J. Amer. Chem. Soc.*, **75**, 2837 (1953).

(9) J. L. Franklin, J. G. Dilard, H. M. Rosenstock, J. T. Herron, K. Draxl, and F. H. Field, *Nat. Stand. Ref. Data Ser., Nat. Bur. Stand., No. 26*, 30 (1969).

ergy orders reported. This means that the energy gained by the molecule in the formation of new bonds is more influential in determining the low-voltage spectra of these bisdifluoraminoalkanes than the bond dissociation orders in the original molecules.

Acknowledgments. The authors acknowledge the assistance of R. L. Hanson, the ONR Project Monitor,

who was able to provide the disubstituted difluoramino compounds, and to thank Mr. Richard Lee for his assistance in the construction and operation of the experimental equipment. Finally, the authors gratefully acknowledge Drs. H. M. Fales and G. W. A. Milne of the National Institutes of Health for their cooperation in obtaining the high-resolution mass measurements used in this study.

Restricted Rotation about the Exocyclic Carbon-Nitrogen Bond

in Cytosine Derivatives

by Regitze R. Shoup, H. Todd Miles, and Edwin D. Becker*

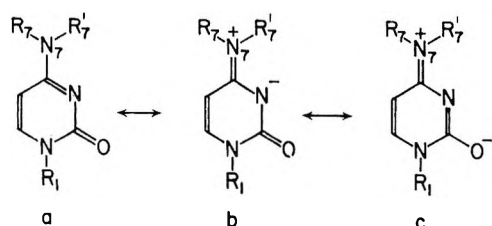
National Institute of Arthritis and Metabolic Diseases, National Institutes of Health, Bethesda, Maryland 20014
(Received August 9, 1971)

Publication costs assisted by the National Institutes of Health

Rotational barriers of methyl-substituted amino groups in cytosine derivatives have been examined by nmr spectroscopy. Total line shape analysis of the spectra of dimethylamino derivatives gave activation energies in the range 15–18 kcal/mol. Qualitative measurements showed that the rotation in monomethylamino derivatives is restricted and that the predominant conformer ($\sim 95\%$ at -19°) has the N_7 -methyl group *syn* to N_3 .

Introduction

It is generally assumed that the amino group hydrogens of the nucleic acid bases are essentially coplanar with the heterocyclic rings, both in hydrogen-bonded complexes and in the unassociated molecules. The amino group is considered to have significant amide character as a result of contributions of such forms as a-c to the resonance hybrid.



The question of rotational barriers for the amino groups of the bases is important to our understanding of the configurations and interactions of the polynucleotides. When the amino groups are unsubstituted (*i.e.*, $R_7 = R_7' = H$) either coplanar conformation is capable of base pairing, and when $R_7 = R_7' = CH_3$ neither conformation is capable of pairing. A special interest, however, arises in the case of mono-

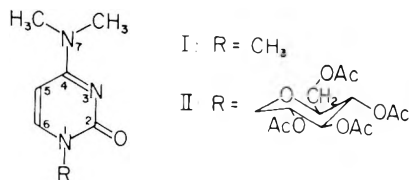
methyl substitution ($R_7 = H$, $R_7' = CH_3$) since in this case one rotamer is capable of pairing and one is not. Rotational restrictions which exist in the monomeric units would also exist in the polymers, but the equilibrium between the two rotamers may be changed by helix formation.

It is therefore important to establish the equilibrium conformations of monomethylamino derivatives of the bases and obtain information on the rates of rotation. In view of the amide character of the amino group in cytosine derivatives, the energy barrier for the rotation about the C-N bond should fall in the range commonly observed for amides (*i.e.*, 15–25 kcal/mol) and should therefore be subject to study by nuclear magnetic resonance.

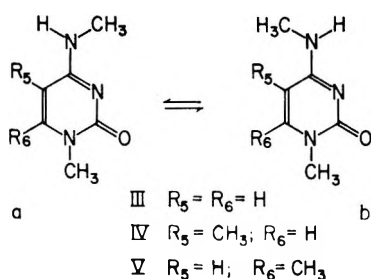
We recently reported¹ the observation of restricted rotation of the amino group in 1-methylcytosine in dimethylformamide solution. For this molecule, however, it was not feasible to obtain an accurate measure of the energy barrier by the use of total line shape (TLS) analysis because of the low signal/noise ratio and competitive chemical exchange processes. We

(1) R. R. Shoup, E. D. Becker, and H. T. Miles, *Biochem. Biophys. Res. Commun.*, **43**, 1350 (1971).

present here the result of a measurement of the rotational barrier in the related dimethylamino cytosine derivatives I and II, which are experimentally more tractable.



In addition we demonstrate that the rotation in the mono-*N*-methyl derivatives III, IV, and V is slow on the nmr time scale, and we present semiquantitative data on the equilibrium populations of the conformers a and b.



Experimental Section

1,7,7-Trimethylcytosine (I) was prepared from 1-methyl-4-methoxypyrimidone-2 and aqueous dimethylamine.² It was recrystallized from ethyl acetate with a small amount of methanol, yielding white prisms, mp 181–182°. 7,7-Dimethyl-1-(2',3',4',6'-tetraacetyl-D-glucopyranosyl)cytosine (II) was prepared according to Miles,³ and recrystallized from 95% ethanol, yielding white prisms, mp 283–284°. Both compounds were dried *in vacuo* at 80° over P₂O₅ before use; 0.4 M solutions were prepared in the nmr tube by weighing 0.2 mmol of material and adding solvent to a predetermined height equivalent to 0.5 ml of solution. A small amount of tetramethylsilane (TMS) was added and the samples were thoroughly degassed by the usual freeze-thaw technique and sealed under vacuum.

1,7-Dimethylcytosine² (III) and 1,5,7-trimethylcytosine⁴ (IV) were prepared as described previously. 1,6,7-Trimethylcytosine was prepared from 4-methoxy-1,6-dimethyl-1,2-dihydro-2-oxo-pyrimidine⁵ and aqueous methylamine, yielding white prisms, mp 248.5°. *Anal.* Calcd for C₇H₁₁N₃O: C, 54.89; H, 7.24; N, 27.43. Found: C, 55.42; H, 7.05; N, 26.45. Nmr spectra of these compounds in dimethylformamide-*d*₇ solution were recorded on a Varian HR-220 spectrometer.

The nmr spectra of I and II were obtained as a function of temperature on a Varian A-60 spectrometer. The spectra were recorded at a sweep rate of 0.1 Hz/sec using a filter bandwidth of 0.4 Hz, conditions which

were demonstrated not to cause distortion of the line shape.⁶ The rf power level was minimized to avoid saturation, and particular care was used in the adjustment of the phase at each temperature. Several scans were recorded at each temperature to assure that temperature equilibrium had been reached. The temperature was measured before and after each set of spectra had been obtained using the standard methanol and ethylene glycol samples. New calibration curves⁷ were used for the relation between temperature and chemical shift of these samples. A more detailed discussion of the calibration curves is included in the following paper.⁸

The rotational rate constants were obtained from the digitized nmr spectra by total line shape (TLS) analysis using the equation of Gutowsky and Holm⁹ for an equally populated, uncoupled two-site system. Calculations of the rate constants were performed using a modified version of a least-squares fitting program by Jonas, *et al.*¹⁰ The necessary input parameters—chemical shift, $\Delta\nu$, and line width, W , both in the absence of exchange—were observed to be temperature dependent. $\Delta\nu$ was obtained by extrapolation from values obtained at lower temperatures, and W was obtained by interpolation between values observed above and below the region of exchange. Activation energies were obtained from a least-squares fit to the Arrhenius equation. A detailed discussion of the procedure and its attendant errors is reported separately.⁸

Rates of Rotation and the Rotational Barrier in Dimethylamino Cytosine Derivatives

The activation parameters obtained for I and II by total line shape analysis are listed in Table I. Figure 1 shows the Arrhenius plots of the rate constants *vs.* inverse absolute temperature. The activation energies in Table I are listed without the customary statistical error limits, since we feel that systematic errors have not been eliminated to the extent that random errors dominate. Based on the analysis of the procedure presented in the following paper,⁸ we apply confidence limits of about 1.5–2.0 kcal/mol to

(2) G. W. Kenner, C. B. Reese, and A. R. Todd, *J. Chem. Soc.*, 855 (1955).

(3) H. T. Miles, *J. Amer. Chem. Soc.*, **79**, 256 (1957).

(4) R. R. Shoup, H. T. Miles, and E. D. Becker, *ibid.*, **89**, 6200 (1967).

(5) L. J. Rabinowitz and S. Gurin, *ibid.*, **75**, 5758 (1953).

(6) A. Allerhand, H. S. Gutowsky, J. Jonas, and R. A. Meinser, *ibid.*, **88**, 3185 (1966).

(7) A. L. Van Geet, Abstracts of the 10th Experimental NMR Conference, Pittsburgh, Pa., 1969; A. L. Van Geet, *Anal. Chem.*, **42**, 679 (1970).

(8) R. R. Shoup, E. D. Becker, and M. McNeel, *J. Phys. Chem.*, **76**, 71 (1972).

(9) H. S. Gutowsky and C. H. Holm, *J. Chem. Phys.*, **25**, 1228 (1956).

(10) J. Jonas, A. Allerhand, and H. S. Gutowsky, *ibid.*, **42**, 3396 (1965).

Table I: Activation Parameters for the Rotation of the Dimethylamino Group in 1,7,7-Trimethylcytosine (I) and 7,7-Dimethyl-1-(2',3',4',6'-tetraacetyl-D-glucopyranosyl)-cytosine (II)

Compound	Solvent ^a	E_a , ^b kcal/mol	k_{298} , sec ⁻¹	t_c , °C	$(\Delta\nu)_c$, ^c Hz	ΔS^\ddagger , eu	ΔF^\ddagger_{298} , kcal/mol	ΔF_c^\ddagger , ^d kcal/mol
I	CDCl ₃	17.6	90	10	8.6	7.5	14.8	14.9
I	CD ₃ CN	15.1	123	-3	4.0	-0.5	14.6	14.6
I	CD ₃ OD	15.7	48	5	3.4	0.2	15.2	15.1
I	SO ₂	11.5	1050	-39	2.8	-8.1	13.3	12.7
II	CDCl ₃	17.3	4.5	37	7.2	0.5	16.6	16.5
II	CD ₃ CN	18.1	8.8	22	3.0	4.4	16.2	16.2

^a All solutions are 0.4 M. ^b Estimated error in E_a is 1.5–2.0 kcal/mol (see text). ^c Extrapolated from lower temperature values. ^d Free energy of activation at coalescence, accurate to 0.1 kcal/mol.

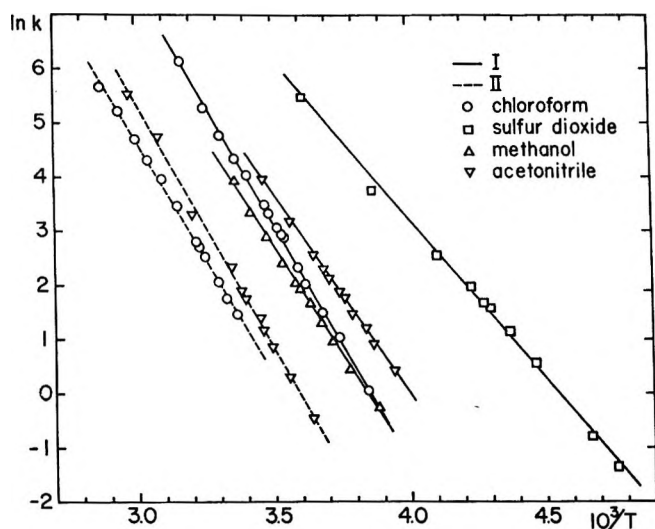


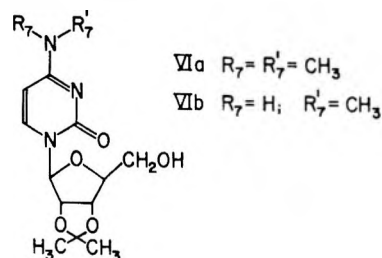
Figure 1. Arrhenius plot for the hindered rotation of the dimethylamino group in 0.4 M solutions of cytosine derivatives I and II.

the activation energies. This uncertainty is considerably larger than the ones quoted in recent TLS studies^{11–14} of restricted rotation in amides and results from the combination of a less favorable signal/noise ratio in the spectra of 0.4 M cytosine solutions, low coalescence temperatures, and relatively small chemical shifts between the dimethylamino protons.

With one exception, the SO₂ solution of I, which is discussed later, the range of activation energies is 15–18 kcal/mol. These values are somewhat lower than the ones recently obtained from total line shape studies of the restricted rotation in dimethylformamide¹⁴ (20.5 kcal/mol) and dimethylacetamide¹³ (19.6 kcal/mol). The difference seems reasonable if one considers the heteroaromatic amines as an intermediate case between true amides and anilines. Only in special cases, (e.g., through substitution with several nitro groups) do the latter molecules show restricted rotation.¹⁵ The values observed for the cytosine derivatives are similar to those obtained for dimethylcarbamoyl chloride¹² (16.9 kcal/mol) and dimethyltrichloroacetamide¹⁶ (16.2 kcal/mol) in recent total

line shape studies. In such cases electron delocalization has been postulated¹⁷ to reduce the double bond character of the C–N bond in comparison with the simple amides.

The activation energies found for I and II in this study are twice that (8.6 kcal/mol) reported by Martin and Reese¹⁸ for 2',3'-O-isopropylidene-7,7-dimethylcytidine (VIa). Considering that the difference in



activation energy between I and II is only of the order of 2–3 kcal/mol, it appears unlikely that a change in the sugar moiety can account for the difference between their results and ours. Since Martin and Reese¹⁸ did not describe the method by which this number was obtained, however, and since it has been demonstrated⁶ that the commonly used approximate methods for obtaining rate constants from nmr spectra usually give much too low activation energies, we feel the values obtained in the present study are more reliable.

For further consideration of the results in Table I, we can focus on several properties: the coalescence temperature, t_c , and the associated rate constant, k_c ; the activation energy, E_a ; and the entropy of

- (11) H. S. Gutowsky, J. Jonas, and T. H. Siddall, III, *J. Amer. Chem. Soc.*, **89**, 4300 (1967).
- (12) R. C. Newmann, Jr., D. N. Roark, and J. Jonas, *ibid.*, **89**, 3412 (1967).
- (13) R. C. Neumann, Jr., and J. Jonas, *ibid.*, **90**, 1970 (1968).
- (14) M. Rabinowitz and A. Pines, *ibid.*, **91**, 1585 (1969).
- (15) J. Heidberg, J. A. Weil, G. A. Janusonis, and J. K. Anderson, *J. Chem. Phys.*, **41**, 1033 (1964).
- (16) R. R. Shoup, unpublished results.
- (17) M. T. Rogers and J. C. Woodbrey, *J. Phys. Chem.*, **66**, 540 (1962).
- (18) D. M. G. Martin and C. B. Reese, *Chem. Commun.*, 1275 (1967).

activation, ΔS^\ddagger . Of these quantities t_c is in general quite well determined, and the rate, k_c , at coalescence can be determined with high accuracy. However, rate constants should be compared only at the same temperature, say 25° (298°K). The accuracy of k_{298} then depends on the accuracy of E_a and the magnitude of the difference between 25° and t_c . In the present study the error in E_a can be as large as 1.5–2.0 kcal/mol,³ and therefore the larger the extrapolation from the coalescence point the greater the uncertainty in k_{298} . The value of ΔS^\ddagger is subject to the greatest uncertainty, since several systematic errors may be included in this quantity. Values of ΔS^\ddagger very different from zero for systems of the sort studied here are usually suspect and suggest the presence of systematic errors in the measurements.

It is apparent that I in SO_2 gives values for all of these parameters that are quite different from those for the other systems. We defer further discussion of I in SO_2 to the section on solvent effects. The values of k_{298} and t_c for I do not vary significantly among the other three solvents but are quite different from the values for II; in fact, the values of k_{298} for II are more than an order of magnitude smaller than the values for I, and II has a correspondingly higher coalescence temperature. The origin of this pronounced effect of the substituent at the 1-position is not entirely clear. It seems most likely that it is attributable to the increase in double bond character of the $\text{C}_4\text{-N}_7$ bond as electrons are withdrawn from the cytosine ring by the more strongly electronegative sugar substituent and nonbonding electrons drawn from N_7 into the $\text{C}_4\text{-N}_7$ bond. The change in E_a itself that would be expected to accompany this process is less easy to discern with the limited accuracy (1.5–2 kcal/mol) of E_a . Alternatively, the difference in rates between I and II might be related to intermolecular solute-solute interactions, which are known to increase rotational barriers in some dimethylamides. However, we have no evidence of such specific interactions. (II does form a gel in CD_3CN below $\sim 0^\circ$, but the solution of II in CDCl_3 remained nonviscous over the whole temperature range.)

Solvent Effects

Table I and Figure 1 show that the rotational rate of I varies with solvent, increasing in the order $\text{CD}_3\text{OD} < \text{CDCl}_3 < \text{CD}_3\text{CN} \ll \text{SO}_2$. The rate in SO_2 at 25° is an order of magnitude greater than that in the other solvents. Since SO_2 is known to interact strongly with electron-rich centers such as amines,¹⁹ it seems likely that the solvent in this case plays a major role in determining the rotational parameters. Support for this proposal comes from the observation of a distinct yellow color for solutions of I and other cytosine derivatives in SO_2 . These compounds give colorless solutions in other solvents. The color is absent from

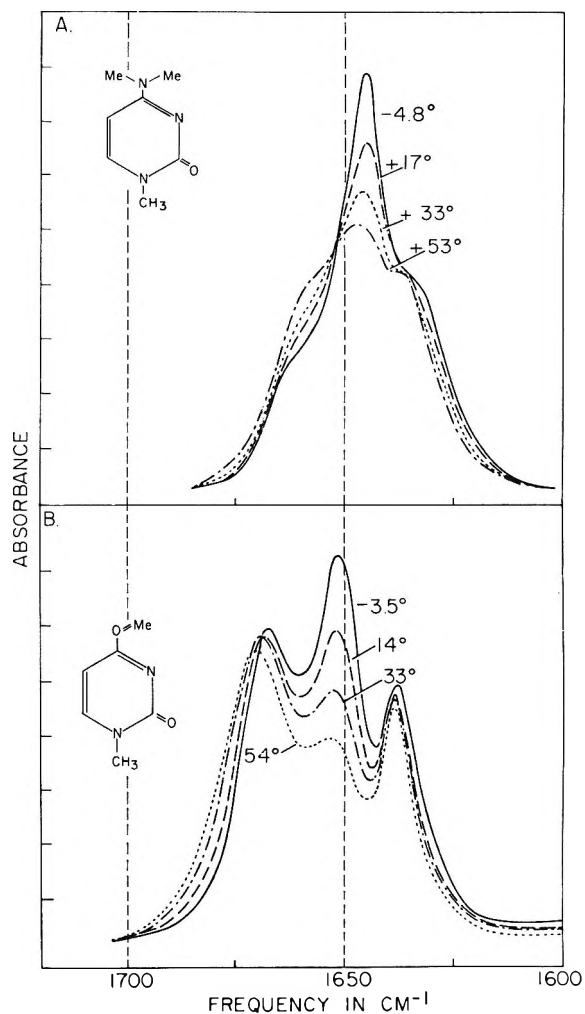


Figure 2. Infrared spectra in chloroform solution at different temperatures. A, 1,7,7-Trimethylcytosine. At low temperature the most intense band (1646 cm^{-1}) is assigned to vibration of the carbonyl group, which is hydrogen bonded to chloroform. With increasing temperature the bonded carbonyl band decreases in intensity, and the unbonded at ~ 1659 (sh) increases in intensity. The ring vibration at ~ 1638 (sh) shows little influence of temperature. B, 1-Methyl-4-methoxypyrimidone-2. The clearer resolution of the bands in this case support the similar interpretation of the spectra of the cytosine derivative shown above. The hydrogen bonded carbonyl band is at 1651 cm^{-1} at -3.5° , the unbonded band at 1670 cm^{-1} at 54° , and a ring vibration at 1638 cm^{-1} .

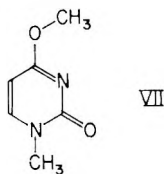
SO_2 solutions of protonated cytosines. These observations suggest the presence of a charge-transfer complex¹⁹ involving nonbonding electrons on one of the nitrogen atoms in cytosine, but determination of the exact nature of the complex is beyond the scope of the present paper.

The order of variation of rotational rate of I in the other three solvents suggests that hydrogen bonding from the solvent to the $\text{C}=\text{O}$ group or to N_3 might play a role by increasing resonance forms Ib and Ic

(19) T. C. Waddington, "Non-Aqueous Solvent Systems," Academic Press, New York, N. Y., 1965, pp 253-284.

and thus increasing the double bond character of the C₄-N₇ bond. Hydrogen bonding between the C=O group of I (and that of related compounds) and the solvents CDCl₃ and CD₃OD does indeed exist; we digress briefly from discussion of the nmr results to present infrared spectroscopic data which provide independent evidence of such hydrogen bonding.

Figure 2 shows ir spectra in the C=O stretching region of I and the related compound VII in CDCl₃



as a function of temperature. In the noninteracting solvent CCl₄ the C=O stretching band is at 1671.5 cm⁻¹ with a weaker ring vibration at 1636 cm⁻¹. Addition of 5% ethanol to this solvent leads to a peak at 1647 cm⁻¹ with a strong shoulder at ~1667 cm⁻¹ and an unchanged ring vibration at 1637 cm⁻¹. In pure ethanol hydrogen bonding leads to a single strong carbonyl vibration at 1646 cm⁻¹. Hydrogen bonding by the solvent chloroform is weaker than that by ethanol, and the spectra in chloroform (Figure 2) show temperature-dependent equilibria between bonded ($\nu_{\max} = 1645$ cm⁻¹) and unbonded ($\nu_{\max} \sim 1660$ cm⁻¹(sh)) species, which are entirely in accord with the bands observed in carbon tetrachloride and in ethanol. The infrared spectrum of II in CDCl₃ displays only one C=O stretching band, at 1658 cm⁻¹, quite similar to that of II in CCl₄, suggesting that the bulky sugar sterically prevents hydrogen bonding to the C=O oxygen.

The presence of hydrogen bonding to the solvent, then, may account for the variation shown in k_{298} in Table I and Figure 1. The systematic errors⁸ that limit the absolute accuracy of the values found for E_a should be nearly equal for I in the three solvents under consideration, and with due caution we can discuss differences in E_a . In accord with the slower rotational rate found in CD₃OD, E_a in this solvent is somewhat larger than that in CD₃CN, but the difference is barely significant. The value of E_a in CDCl₃ is, surprisingly, about 2 kcal/mol larger than that in CD₃OD, whereas the rotational rate is larger, indicating less hydrogen bonding. This anomaly may be explained by the temperature-dependent equilibrium between hydrogen bonded and nonbonded forms (compare Figure 2). Thus E_a might be expected to vary somewhat with temperature, and k would increase as the proportion of nonbonded molecules increases. Experimental limitations prevent our testing the data of Figure 1 for nonlinearity in the Arrhenius plot, but consideration of the effect of the equilibrium indicates that fitting rate constants to a linear

Arrhenius plot would result in too steep a slope, thereby accounting for the high value calculated for I in CDCl₃. As in the case of the SO₂ results, the large value of ΔS^\ddagger for I in CDCl₃ (7.5 eu) also indicates a substantial systematic error in E_a .

We have little comment on the data for II. The ir spectra of II in chloroform indicate that hydrogen bonding of the solvent should be of little consequence. The rates of rotation in CDCl₃ are slower than those in CD₃CN, although the activation energy in CDCl₃ is almost 1 kcal/mol lower than that calculated for II in CD₃CN. The temperature range was, however, limited for the acetonitrile solution of II due to gel formation, and the large value for ΔS^\ddagger suggests error in the calculated activation energy. We attempted to elucidate further the effect of solvent on both I and II by making studies in water, dimethyl sulfoxide, and dimethylformamide, but low solubility and the limited temperature range available with the high-melting solvents water and DMSO prevented successful completion of these experiments.

Conformation of 7-Methyl Substituted Derivatives

Spectra at 220 MHz of the *N*-monomethylated cytosine derivatives III, IV, and V are shown in Figures 3 and 4. At 21° all three compounds show the presence of only one set of sharp lines, for which the assignments are included in the figures. At -19° small additional peaks from a less abundant conformer appear in the spectra of III and V, but not in the spectrum of IV, the 5-methyl derivative. The small peaks are found at slightly lower field than the stronger signals from the more abundant conformer.²⁰

Assuming that the rotation of the methylamino group is slow enough at -19° not to broaden the minor lines, the relative concentrations of the conformers can be obtained from the peak heights. By measuring these, we found relative concentrations of 4.0/96.0 and an associated free energy difference $\Delta F = 1.6$ kcal/mol at -19° for the conformers of III, and corresponding values of 5.3/94.7 and 1.5 kcal/mol for V.

The absence of additional peaks in the low-temperature spectrum of IV shows that this compound exists almost exclusively (at least >99%) in one conformation, almost certainly the one with the 7-methyl *syn* to N₃. Steric considerations suggest that the more abundant conformers of III and V are also the ones with the *N*-methyl group *syn* to N₃ (*i.e.*, IIIa and Va), in accord with studies of *cis-trans* isomerism in simple *N*-alkylamides. Mizushima²¹ showed, using

(20) The width of the NH peak prevents detection at low concentration, and for the 7-methyl signal the spectral region is obscured by solvent signals and spinning side bands from the 1- and 6-methyl groups. A careful check of the frequencies of all small peaks was made to identify spinning side bands (at $\sim \pm 95$ Hz).

(21) S. Mizushima, "Structure of Molecules and Internal Rotation," Academic Press, New York, N. Y., 1954, p 18.

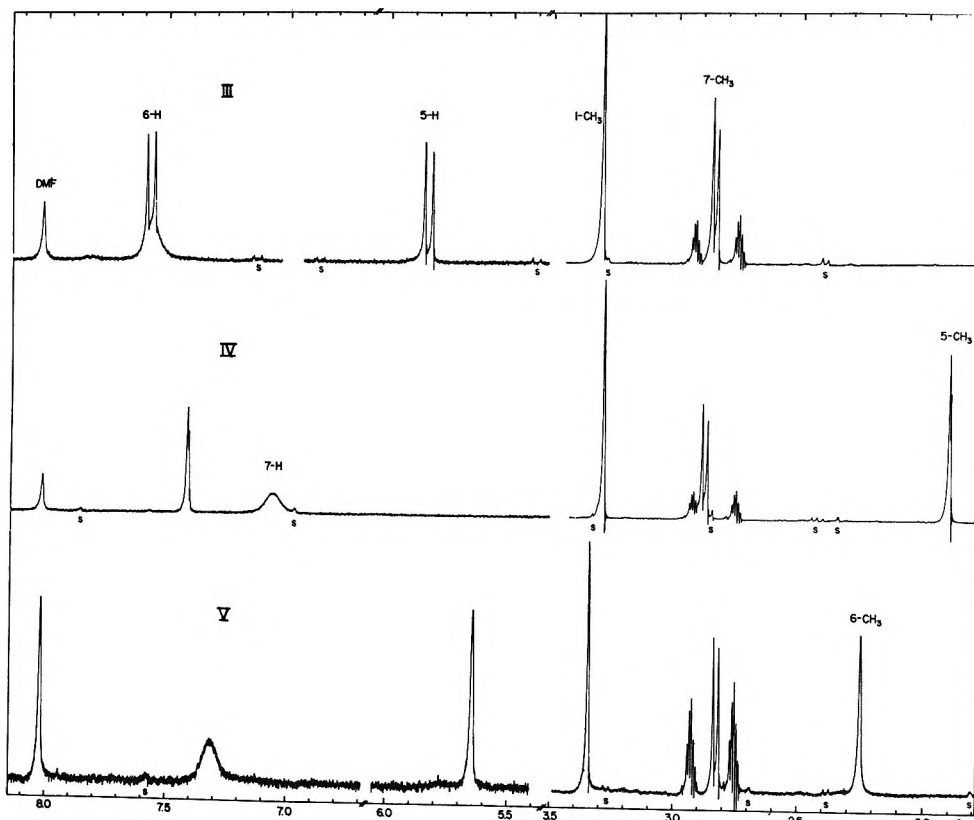


Figure 3. The 220-MHz proton nmr spectra of cytosine derivatives III, IV (0.2 *M*), and V (0.1 *M*) in dimethylformamide-*d*₇ at 21°. The abscissa (δ) is given in ppm relative to internal tetramethylsilane. Spinning side-bands (at $\sim \pm 95$ Hz) are labeled *s*. Gain settings differed for different spectral regions.

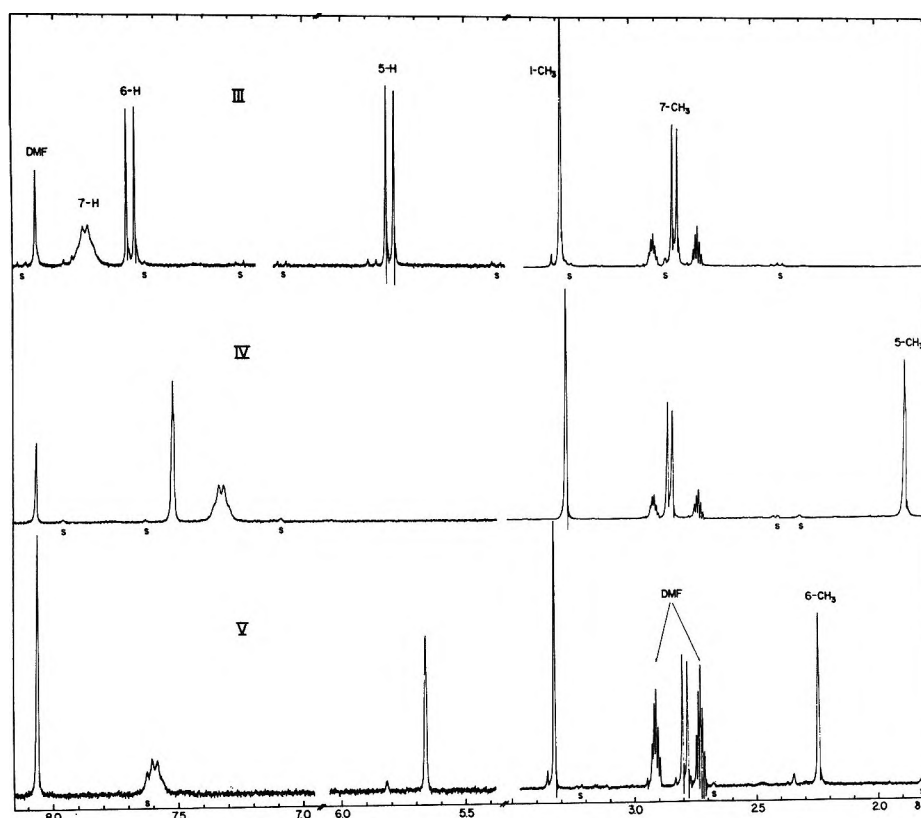
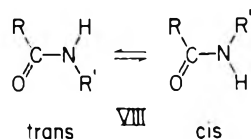


Figure 4. The 220-MHz proton nmr spectra of III, IV, and V in dimethylformamide-*d*₇ at -19° . Spectral parameters are the same as in Figure 3. Note in the spectra of III and V the small peaks to the low-field side (by 0.03–0.16 ppm) of the major peaks labeled 5-H, 1-CH₃, and 6-CH₃.

Raman and infrared spectra, that *N*-methylacetamide (VIII, R = R' = CH₃) exists mainly as the *trans* isomer.



LaPlanche and Rogers²² found from nmr spectra that the rotation in simple *N*-alkylamides is strongly restricted and that only in *N*-alkyl formamides could some (~20%) *cis* isomer be detected. Their spectra of higher *N*-alkylamides (VIII: R = CH₃, C₂H₅, etc.) showed only one *N*-alkyl signal, and they concluded from solvent shifts and coupling constants that the conformation was 100% *trans*. More recently, Barker and Boudreaux,²³ and Sandström and Uppström²⁴ observed that an aqueous solution of *N*-methylacetamide contains 3% of the *cis* isomer.

Inasmuch as a proton in the 5-position in the cytosine derivatives III and V can be expected to contribute an amount of steric interference similar to that of the acetyl methyl group in *N*-methylacetamide, the observed 4% and 5% abundance of IIIb and Vb are in qualitative agreement with the data reported for *N*-methylamides.

We recently observed that the rotation of the unsubstituted amino group in 1-methylcytosine is also restricted, and a rate constant $k \approx 138 \text{ sec}^{-1}$ was obtained at room temperature for a 0.02 *M* solution in dimethylformamide-*d*₇.¹ Thus there is qualitative agreement between this rate and the rates obtained for the dimethylamino compound I at 25° in chloroform ($k = 95 \text{ sec}^{-1}$), methanol ($k = 50 \text{ sec}^{-1}$) and acetonitrile ($k = 122 \text{ sec}^{-1}$). No rotational rates have been obtained for the monomethylamino derivatives III and V, since the low abundance of one isomer makes total line shape analysis quite inaccurate. However, closer inspection of the room temperature spectra of III and V reveals that low-intensity broad bands are present in the regions expected for observation of the less abundant isomers (see Figure 3). The rotation of the methylamino group is consequently still slow on the nmr time scale at this temperature.

This observation is in obvious contrast to the conclusions drawn by Martin and Reese,¹⁸ who stated without presenting data that the rotation of the methylamino group of VIb is fast at -60° and above. It seems likely that they actually observed the predominant conformer and failed to detect the less abundant conformer.

Conclusion

The present study has shown that the rotation about the exocyclic C-N bond in cytosine derivatives is restricted by an energy barrier $E_a \approx 15 \text{ kcal/mol}$. It was further concluded that the 7-*N*-monomethyl-substituted derivatives exist predominantly in the configuration with the 7-*N*-methyl group *syn* to N₃. These results may help to explain the interaction behavior observed for 7-*N*-methylated polycytidylic acids. Brimacombe and Reese²⁵ found that polycytidylic acid completely substituted with 7-*N*-methyl groups (poly 7N-MeC) showed no detectable interaction with polyinosinic acid (poly I), whereas the copolymer (60:40) of C and 7N-MeC did interact with poly I. The stoichiometry was suggestive of pairing to 7N-MeC as well as to C residues. From the present data on cytosine monomers one can estimate a lifetime of the order of 10⁻³ sec for the conformation with the amino proton in the position capable of base pairing. This lifetime may be too short to allow interaction of fully *N*-methylated poly C, but long enough, once helix formation has been initiated by unsubstituted C residues, to allow pairing also of the *N*-methylated C residues. The energetic advantage of helix formation may then be enough to overcome the steric interference between the *N*-methyl group and the 5 proton.

(22) L. A. LaPlanche and M. T. Rogers, *J. Amer. Chem. Soc.*, **86**, 337 (1964).

(23) R. H. Barker and C. J. Boudreaux, *Spectrochim. Acta*, **A23**, 727 (1967).

(24) J. Sandström and B. Uppström, *Acta Chem. Scand.*, **21**, 2254 (1967).

(25) R. L. C. Brimacombe and C. B. Reese, *J. Mol. Biol.*, **18**, 529 (1966).

An Evaluation of the Nuclear Magnetic Resonance Total Line Shape

Analysis of Uncoupled, Exchanging Two-Site Systems

by Regitze R. Shoup, Edwin D. Becker,*

National Institute of Arthritis and Metabolic Diseases, National Institutes of Health, Bethesda, Maryland 20014

and Mildred L. McNeel

Division of Computer Research and Technology, National Institutes of Health, Bethesda, Maryland 20014

(Received August 9, 1971)

Publication costs assisted by the National Institutes of Health

The use of nmr total line shape (TLS) analysis to determine rates and activation energies of internal rotation has been critically examined. A study of the barrier to internal rotation of the dimethylamino group in two cytosine derivatives has been used as a specific example. In these systems (0.4 *M* solutions) a moderate signal to noise ratio and a limited temperature range combine to make the temperature dependence of both chemical shift and line width uncertain, and the resulting uncertainty in the calculated rate constants is especially serious above the coalescence temperature. Estimates have been made of the possible systematic errors in E_a by a numerical analysis of theoretical line shapes. Additional errors in E_a may result from the use of incorrect standard calibration charts for temperature measurements. It is concluded that the statistical error limits of 1–2% often quoted for E_a 's obtained by TLS analysis should be applied only in the most favorable cases.

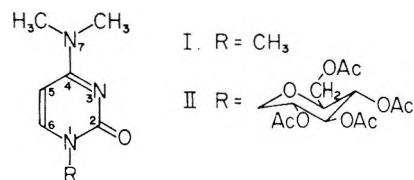
Several papers^{1–3} published during the past few years have been devoted to the examination of the proper use of high-resolution nuclear magnetic resonance (nmr) spectroscopic methods for studying chemical exchange. One excellent review article⁴ gives a thorough discussion of the theoretical concepts and experimental methods. The surge in literature on this subject was prompted, first, by the realization that grave errors are introduced by the commonly used approximate methods and, second, by the availability of computer facilities which permitted the undertaking of total line shape (TLS) analysis of nmr spectra. The comparative success of the TLS methods has resulted in activation energies being quoted with statistical limits of error of the order of 0.2–0.5 kcal/mol for typical energy barriers of ~ 20 kcal/mol. Many investigators seem to believe that systematic errors have been completely eliminated. Yet, as Johnson⁴ emphasizes, "large systematic errors are sometimes introduced because site frequencies and linewidth corrections are assumed to be constant where in fact they depend on temperature."

We recently undertook a TLS analysis of the restricted rotation of two dimethylamide type molecules, the results of which were reported in the preceding paper. During the course of this work it became obvious that it was all too easy to introduce serious systematic errors. These could arise from (i) insufficient knowledge of the temperature dependence of the chemical shifts between the two exchanging sites, (ii) neglect of line width changes over the temperature

range, and (iii) improper temperature calibration. The present paper is intended to demonstrate the kind of problems one can encounter under conditions often found in practice. Our results are presented in terms of data for cytosine derivatives, but we believe that the factors discussed are of wide applicability.

Description of Procedure

The nmr spectra of 0.4 *M* solutions of 1,7,7-trimethylcytosine (I) and 7,7-dimethyl-1-(2',3',4',6'-tetraacetyl-D-glucopyranosyl)cytosine (II) were obtained with a Varian A-60 spectrometer. Both I



and II were studied in chloroform and acetonitrile; in addition I was studied in sulfur dioxide and methanol. The sample temperature was measured using standard samples of methanol and ethylene glycol in combination with revised calibration curves.⁵ The

(1) A. Allerhand, H. S. Gutowsky, J. Jonas, and R. A. Meinzer, *J. Amer. Chem. Soc.*, **88**, 3185 (1966).

(2) P. T. Inglefield, E. Krakover, L. W. Reeves, and R. Stewart, *Mol. Phys.*, **15**, 65 (1968).

(3) F. A. L. Anet and A. J. R. Bourne, *J. Amer. Chem. Soc.*, **87**, 5250 (1965).

(4) C. S. Johnson, Jr., *Advan. Magn. Res.*, **1**, 33 (1965).

(5) A. L. Van Geet, *Anal. Chem.*, **42**, 679 (1970).

temperature measurements and the effect of errors in these will be discussed below. Other experimental details were included in the preceding paper.

The rotation of the dimethylamino group about the exocyclic C-N bond was treated as an exchanging, equally populated, uncoupled two-site system. For this simple system Gutowsky and Holm⁶ provided the solutions to the Bloch equations modified to include the effect of chemical exchange. The resulting line shape equation has been extensively used in TLS analysis of simple systems like the dimethylamides. It expresses transverse magnetization as a function of frequency and the three, usually unknown, parameters: (i) the chemical shift between the two sites, $\Delta\nu = \nu_A - \nu_B$, (ii) the line width in the absence of exchange, $W = 1/\pi T_2$, and (iii) the exchange rate constant, $k = 1/2\tau$. In principle, the use of a least-squares fitting program⁷ allows the simultaneous determination of all three parameters from the comparison of the theoretical curve with experimental data. In practice, however, inconsistent values of $\Delta\nu$ and W often arise, both from experimental errors⁸ and from the inherently low sensitivity of the TLS method to change in individual parameters. In addition, certain assumptions must be made to allow the use of this equation, namely that the spin-spin relaxation time T_2 is the same for the two sites A and B (*i.e.*, $T_{2A} = T_{2B}$) and that no scalar coupling exists between the exchanging nuclei. If these assumptions are not valid the quality of the fit to the theoretical Lorentzian line shapes will be lowered. In the present case of the cytosine derivatives the T_2 's should be nearly equal, but we cannot completely rule out a very small four-bond $\text{CH}_3\text{-N-CH}_3$ coupling and long-range couplings to other protons in the molecules. Under such conditions it may be necessary to use predetermination of one or both $\Delta\nu$ and W in order to obtain reliable rate constants by the TLS method.

In the present study the fitting of the nmr spectra to the Gutowsky-Holm equation was performed using a modified version of the program originally described by Jonas, *et al.*⁹ This program was rewritten for the IBM 360 and it provides for the generation of theoretical curves and a least-squares fitting of these to the digitized experimental spectra by a stepwise variation of k , $\Delta\nu$, and W within certain limits. This program consumes a large amount of computer time, but it allowed us to evaluate the sensitivity of the method to the choice of $\Delta\nu$ and W , both in the actual treatment of the experimental data and in a numerical analysis of the sensitivity of the TLS method to changes in the individual parameters.

The activation energies were obtained as usual from the rate constants by a linear least-squares fit to Arrhenius' equation. The plots of $\ln k$ vs. inverse absolute temperature were included in the preceding paper.

Line Width in the Absence of Exchange

Our preliminary attempts to use a three-parameter model fitting program for the spectra of I and II resulted in inconsistent values for $\Delta\nu$, W , and k , and showed that preselection of the line width was necessary before $\Delta\nu$ and k could be obtained. Such a procedure was adopted in other studies of restricted rotation of amides.¹⁰⁻¹³ Some investigators¹⁰ used a constant-input line width, determined below the slow exchange limit, throughout the temperature range. An error in the input line width is only important in the high- and low-temperature limits, so the use of a low-temperature value is especially justified when measurements are not extended into the very fast exchange region. Neumann, *et al.*,^{11,12} showed that magnetic field inhomogeneity was the principal cause of the line broadening in their studies and used the line width of TMS as observed at each temperature. Neither of these approaches was justified for the calculations of rate constants for the cytosine derivatives.

The full line width of the methyl peaks in the absence of exchange can be expressed as

$$W = 1/\pi T_2 = 1/\pi T_2^{\text{inh}} + 1/\pi T_2^{\text{sc}} + 1/\pi T_2^{\text{dd}}$$

These three terms arise from magnet inhomogeneity, scalar coupling to ¹⁴N in the dimethylamino group, and dipole-dipole interactions.¹⁴ Additional contributions to the line width may come from unresolved long-range proton-proton couplings. The magnitude of the inhomogeneity term, $1/\pi T_2^{\text{inh}}$ can be obtained from the observed line width of internal TMS, since the natural line width for TMS is negligible. The TMS line width fell in the range 0.35-0.40 Hz for these experiments except for I in SO₂ below -50°, where magnetic field homogeneity deteriorated.

The contribution to the proton line width from scalar coupling of ¹⁴N in the dimethylamino group is a function of the ¹⁴N spin-lattice relaxation time T_{1N} and given by¹⁵

(6) H. S. Gutowsky and C. H. Holm, *J. Chem. Phys.*, **25**, 1228 (1956).

(7) We are grateful to Mr. R. I. Shrager of the Division of Computer Research and Technology at N.I.H. for adapting his Least-Squares Model Fitting Program to TLS Analysis.

(8) The filtering level necessary in the present study (for 0.4 M solutions we used a filter band width of 0.4 Hz at a scanning speed of 0.1 Hz/sec) should not be excessive according to Allerhand, *et al.*¹

(9) J. Jonas, A. Allerhand, and H. S. Gutowsky, *J. Chem. Phys.*, **42**, 3396 (1965).

(10) H. S. Gutowsky, J. Jonas, and T. H. Siddall III, *J. Amer. Chem. Soc.*, **89**, 4300 (1967).

(11) R. C. Neumann, Jr., D. N. Roark, and V. Jonas, *ibid.*, **89**, 3412 (1967).

(12) R. C. Neumann, Jr., and V. Jonas, *ibid.*, **90**, 1970 (1968).

(13) M. Rabinovitz and A. Pines, *ibid.*, **91**, 1585 (1969).

(14) Other relaxation mechanisms can be ignored in these molecules.

(15) A. Abragam, "The Principles of Nuclear Magnetism," Oxford University Press, Oxford, 1961, p 309.

$$1/\pi T_2^{\text{sc}} = 4/3\pi J^2 S(S+1)T_{1N} \times \left\{ 1 + \frac{1}{1 + (\omega_H - \omega_N)^2 T_{1N}^2} \right\}$$

Here $(\omega_H - \omega_N)^2 T_{1N}^2 \gg 1$ so that substitution of $S = 1$ and $J \simeq 0.8$ Hz¹⁶ yields

$$1/\pi T_2^{\text{sc}} \simeq 5.4 T_{1N}$$

This shows that T_{1N} must be ~ 20 msec to contribute 0.1 Hz to the proton line width. ¹⁴N relaxation times this long have been observed only for molecules with much more spherical electron distribution around ¹⁴N.¹⁷ The ¹⁴N relaxation times for more typical small (mol wt <150) organic molecules have been found to fall in the range ~ 1 –5 msec.¹⁷ For larger molecules and at lower temperatures T_{1N} will be correspondingly shorter, and scalar coupling can therefore be assumed to make negligible contributions to the *N*-methyl line widths for the cytosine derivatives.

The third term, $1/\pi T_2^{\text{dd}}$ arises from dipole-dipole interaction between individual protons in the molecule. For liquids of low viscosity the contribution to the transverse relaxation rate $1/T_2^{\text{dd}}$ equals the spin-lattice relaxation rate $1/T_1$. For sufficiently small molecules, the dipolar term is negligible in comparison with the magnetic field inhomogeneity, the justification for using the TMS line width in kinetic studies of simple amides.^{11,12} The spin-lattice relaxation rate does, however, increase rapidly with molecular size, since $1/T_1$ is proportional to τ_c , the correlation time for molecular reorientation. For compounds with some similarity to the present case, Nogrady and Burgen¹⁸ observed spin-lattice relaxation rates of 0.351 and 0.702 sec⁻¹ for the methyl protons in phenyl- and benzyltrimethylammonium ions, respectively, in aqueous solution at 25°. This corresponds to line width contributions of 0.11 and 0.22 Hz, and at lower temperatures where molecular reorientation gets slower, the line broadening from dipolar interactions in molecules of this approximate size should become increasingly apparent. This effect was observed in the width of the proton lines for both I and II. Except for the SO₂ solution, the spectra of I all showed a line broadening of 0.2 Hz for all protons at the lowest temperatures (-40 to -48°). The field homogeneity remained satisfactory (TMS line width ~ 0.35 – 0.45 Hz) in this range, whereas the spectra of I in SO₂ at lower temperatures showed the effect of deteriorating field homogeneity, resulting in a TMS line width of 0.9 Hz at -63° . The effect of dipolar broadening on the line width of II (mol wt = 469) was much more pronounced. Between $+68^\circ$ and -26° a line width change of 0.4 to 1.7 Hz was observed for both the *N*-methyl protons and nonexchanging protons of II in chloroform. The acetonitrile solution of II formed a gel below 0° and complete line broadening prevented measurements at lower temperatures.

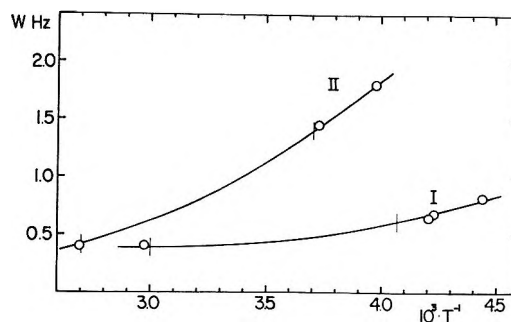


Figure 1. Temperature dependence of nonexchange line width for I and II in chloroform. The markers refer to temperatures for which exchange contributions to the line width were less than 0.05 Hz.

Since these observations made it clear that the use of a constant temperature line width was not justified, we interpolated between values observed in the high- and low-temperature limit. The interpolation was done graphically from plots such as the ones in Figure 1. Considering the uncertainty regarding contributions from long-range couplings, we felt it inappropriate to generate a mathematical relationship between *W* and temperature.

The high-temperature limit was determined as the temperature for which approximate calculations⁴ showed that the line width contribution from the exchange $\pi(\Delta\nu)^2/2k < 0.05$ Hz. The observed limiting value was for all samples very close to the TMS line width, 0.4 Hz. Similarly, the nonexchange line widths in the low-temperature limit were obtained from spectra recorded below the temperature for which $k/\pi = W_{\text{ex}} - W < 0.05$. Where possible the line width was measured at several temperatures. Our interpolated values seem reasonable but could suffer from an overestimate of the dipolar contribution in the high-temperature region. For I in SO₂ solution the limiting low temperature ($\sim -67^\circ$) could not be reached with our spectrometer, but since *W* seemed to be determined by the inhomogeneity contribution in this temperature region, the observed TMS line width was used as the basis for the interpolation. Consequently, the data for I in SO₂ are less reliable.

These considerations demonstrate the difficulties one can encounter in trying to obtain accurate rate constants if insufficient line width data are available in the low-temperature region. If dipolar broadening had been ignored and the TMS line width had been used throughout, too low activation energies would have been obtained. Activation parameters for I in

(16) The magnitude of J^{14N-CH_3} can be estimated from the known $J^{15N-CH_3} = 1.2$ Hz in 1,7-dimethyl-7-¹⁵N-cytosine: E. D. Becker, H. T. Miles, and R. B. Bradley, *J. Amer. Chem. Soc.*, **87**, 5375 (1965).

(17) W. B. Moniz and H. S. Gutowsky, *J. Chem. Phys.*, **38**, 1155 (1963).

(18) T. Nogrady and A. S. V. Burgen, *J. Amer. Chem. Soc.*, **91**, 3390 (1969).

Table I: Activation Parameters for the Rotation of the Dimethylamino Group in Cytosine Derivatives I and II

Compound	Solvent	t_c^a °C	$\Delta\nu_c^a$ Hz	ΔF_c^a kcal/mol	Method ^b	E_a		E_a , diff, %	ΔS , eu
						kcal/mol	rms dev, kcal/mol		
I	CDCl ₃	10	8.6	14.9	A	17.6	0.19		7.5
					B	16.9	0.15	7	4.7
					A'	15.5	0.22	12	0.0
I	CD ₃ CN	-3	4.0	14.6	A	15.1	0.25		-0.5
					B	14.2	0.24	6	-4.0
					A'	13.3	0.18	12	-6.8
I	CD ₃ OD	5	3.4	15.2	A	15.7	0.28		-0.2
					B	14.2	0.23	10	-5.6
					A'	14.3	0.21	9	-5.2
I	SO ₂	-39	2.8	12.7	A	11.5	0.27		-8.1
					B	10.0	0.48	13	-15.0
II	CDCl ₃	37	7.2	16.5	A	17.3	0.45		0.5
					B	16.1	0.46	7	-3.6
II	CD ₃ CN	22	3.0	16.2	A	18.1	0.42		4.4

^a Temperature, chemical shift, and free energy of activation at coalescence. ^b A and B refer to results obtained using as input the chemical shift values from curves A and B in Figure 2. The results labeled A' were obtained using curves A for $\Delta\nu$ and a temperature-independent line width of 0.4 Hz.

chloroform, acetonitrile, and methanol obtained from a TLS analysis with a constant input line width of 0.4 Hz are included in Table I under the subheading A'. A comparison of these values with the values under A shows discrepancies as large as 2.1 kcal/mol. The alternative procedure of using the low-temperature value has not been included in Table I. It would have led to too high values for the activation energy, but provided that the line shape analysis is not extended much above the coalescence temperature, the systematic error encountered would have been much smaller. This is due to the fact that the TLS calculation is insensitive to W in the region of coalescence provided $\Delta\nu \gg W$.

The Chemical Shift in the Absence of Exchange

In order to carry out an accurate line shape analysis it is desirable to predetermine the chemical shift, $\Delta\nu$, between the exchanging sites as a function of temperature. Early investigators of restricted rotation in *N,N*-disubstituted amides often assumed that $\Delta\nu$ remained constant throughout the exchange region. This assumption resulted in serious systematic errors in the activation energy,¹ since $\Delta\nu$ often varies with temperature because of changes in the degree of molecular association. Recent papers^{13,19} have provided more quantitative insight into the nature of the self-association and solvent interactions of dimethylamides.

Provided that the chemical shift is large enough, these true amides have the advantage of having coalescence take place considerably above room temperature, due to activation energies of the order of 20–25 kcal/mol for the rotation. Under such circumstances the temperature dependence of $\Delta\nu$ can be measured over a wide temperature range below the slow exchange limit, assuring more accurate extrap-

olation to higher temperatures. Gutowsky, *et al.*,¹⁰ successfully used this approach in the study of the rotation in *N*-methyl-*N*-benzylformamide. The temperature dependence of the chemical shift between the formyl protons in the two isomers could be fitted to a simple mathematical expression below the slow exchange limit, and the extrapolated values were found to agree well with the best fit $\Delta\nu$ values obtained from TLS calculations at higher temperatures.

The activation energy for the rotation of the dimethylamino group in I and II was found to be ~ 5 kcal/mol lower than in the true amides. The resulting lower coalescence temperatures (see Table I) severely limited the accurate determination of the temperature dependence of the chemical shifts between the methyl groups. The situation is depicted in Figure 2, where observed peak separation (solid circles) is plotted as a function of inverse absolute temperature. For all cases except I in SO₂ and II in CD₃CN a sufficiently large temperature range was accessible below the low exchange limit to permit a curve to be traced through several points.²⁰ The value of $\Delta\nu$ at higher temperatures might be estimated by extrapolation, as indicated by the curves labeled A in Figure 2. Alternatively, the values of $\Delta\nu$ obtained from the TLS analysis can be used. In the region below and near the coalescence temperature the TLS program usually yielded minima sharp enough to extract values of $\Delta\nu$, while at higher temperatures the minima were so shallow that we could not select values of $\Delta\nu$. The values of $\Delta\nu$ from

(19) A. Calzolari, F. Conti, and C. Franconi. *J. Chem. Soc. B*, 555 (1970).

(20) Gel formation of II in CD₃CN prevented studies below 0°. For I in SO₂ even at the lowest temperature obtainable, -63°, exchange affected the observed peak separation.

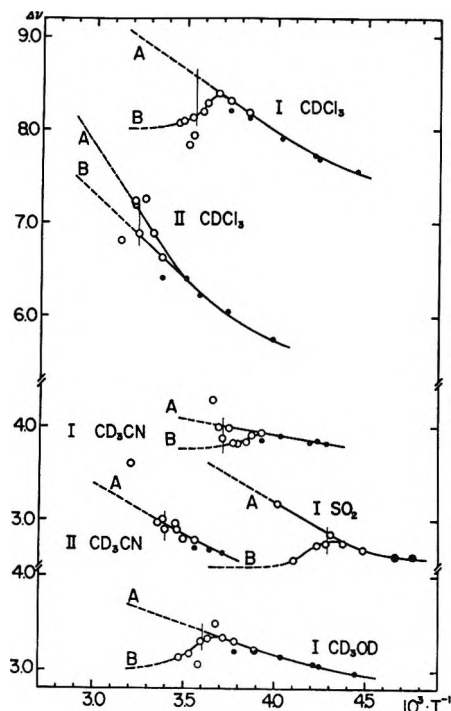


Figure 2. Temperature dependence of best-fit chemical shifts $\Delta\nu$ (open circles) and observed peak separation (solid circles). Curves A and B (see text) are extended to the highest temperature at which the samples were studied. The coalescence temperatures are indicated by vertical markers.

the TLS analysis, shown as open circles in Figure 2, scatter somewhat, largely as a result of limitations in signal to noise ratio and in deviation from Lorentzian line shape, but also as a result of limitations in the TLS treatment, as we show in the following section. For II, $\Delta\nu$ seems to increase monotonically with temperature, but for I in all four solvents, $\Delta\nu$ from the TLS analysis appears to exhibit a maximum just below the coalescence temperature, t_c . (t_c 's are indicated by the vertical markers in Figure 2.) This maximum could be real and result from competitive self-associations and solvent effects, but such an interpretation is highly speculative. Nevertheless, in order to take the TLS values of $\Delta\nu$ into account, we have made the extrapolations labeled B in Figure 2. Using the values of $\Delta\nu$ thus obtained and the interpolated values of W from curves like those in Figure 1, we repeated the TLS analysis and calculated a complete set of rate constants for each solution. The activation parameters obtained from these by least-squares fitting to Arrhenius' equation are listed in Table I. It is apparent that the three methods of treating the data lead to differences in activation energy of about 1–2 kcal/mol, which are far larger than the rms deviations of about 0.2–0.4 kcal/mol.

Numerical Analysis of Theoretical "Spectra"

Further insight into the TLS analysis can be obtained by examining an ideal case, with no noise and

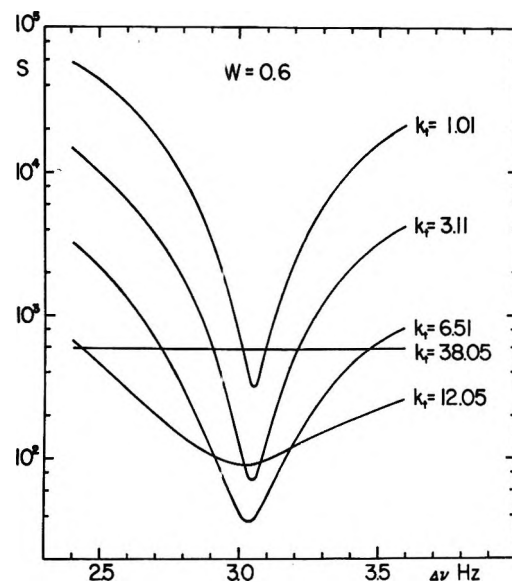


Figure 3. Minimum sum-squared deviation, S (in arbitrary units), obtained as a function of input values of chemical shift, $\Delta\nu$, in TLS fitting of theoretical spectra with $\Delta\nu_t = 3.06$ Hz, $W_t = 0.59$ Hz, and five different rate constants. The input line width was 0.60 Hz. The small difference in position of the curve minima is due to round off errors in the calculations.

perfect Lorentzian line shape. We generated two sets of artificial "ideal spectra" from the Gutowsky-Holm equation⁶ with theoretical input parameters $\Delta\nu_t = 0.59$ Hz and rate constants, k_t , representative of very fast, fast, medium, slow, and very slow exchange. The theoretical chemical shifts, $\Delta\nu_t$, were chosen as 3.06 and 8.06 Hz in order to resemble the situations existing for the cytosines. The TLS program was then allowed to fit these "spectra" by varying k , using selected input values of $\Delta\nu$ and W , and the associated minimum sum-squared deviation, S . In Figure 3, S is plotted for the case $\Delta\nu_t = 3.06$ Hz as a function of $\Delta\nu$. The input line width, W , was 0.6 Hz, very close to the true value $W_t = 0.59$ Hz. For this system coalescence occurs at a rate $k_c = \pi\Delta\nu_t/\sqrt{2} \simeq 6.8 \text{ sec}^{-1}$. It is obvious from Figure 3 that for $k > 2k_c$, the determination of $\Delta\nu_{\text{min}}$ becomes very uncertain, since no minimum was obtained for S at $k_t \sim 5k_c$, and for $k_t \sim 2k_c$ the minimum is quite shallow. For real data containing noise and experimental errors the observed minimum in S at this rate of exchange could easily be shifted by a substantial amount. Since the relationship between $\Delta\nu$ and k is such that a $\pm 10\%$ uncertainty in $\Delta\nu$ results in approximately a $\pm 20\text{--}25\%$ uncertainty in k , the calculations demonstrate the fact that TLS calculations should not be extended into the fast exchange region unless a good *a priori* knowledge of $\Delta\nu$ is available.

A similar set of curves was obtained for the case

$\Delta\nu_t = 8.06$ Hz. A figure has not been included since qualitatively they show the same phenomenon: above $k_t \simeq 2k_c$ the curves become too shallow to allow an accurate determination of $\Delta\nu$. However, in this case $k_c \simeq 17.8$ sec⁻¹, and the larger chemical shift thus extends the range of temperature over which both $\Delta\nu$ and k can be determined from the TLS analysis.

If, in addition, a range of input line widths has to be considered, the determination $\Delta\nu$ (and k) becomes less accurate. This is illustrated in Figure 4 for $\Delta\nu_t = 3.06$ Hz, where S is plotted vs. $\Delta\nu$ for input line widths between 0.4 and 0.8 Hz. In the slow exchange case ($k_t = 3.1$ sec⁻¹) $\Delta\nu_{\min}$ ranges from 2.9 to 3.2 Hz and the associated uncertainty in k is $\sim \pm 20\%$. For the fast exchange case ($k_t = 12.05$ sec⁻¹) the range of $\Delta\nu_{\min}$ is larger (2.5–3.5 Hz). An uncertainty in k of $\pm 20\%$ is still associated with this larger range, but we should include, say, a 10% confidence limit in $\Delta\nu_{\min}$ due to the shallowness of the minima. The resulting uncertainty in k is $\sim \pm 40\%$, and at higher rates the situation would be even more serious. In Table II best-fit values of chemical shift, $\Delta\nu_{\min}$, and

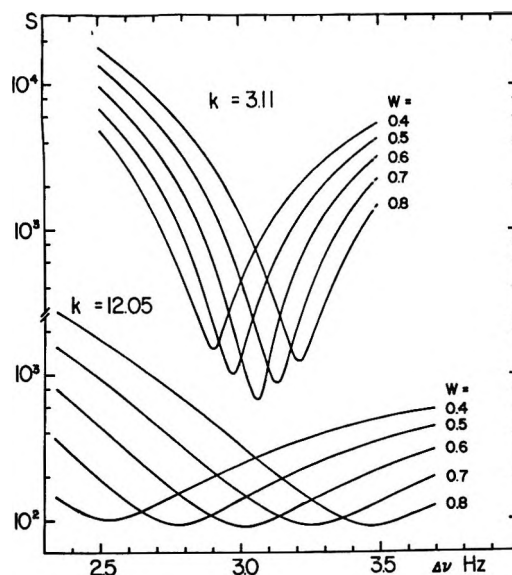


Figure 4. The minimum sum-squared deviation, S , for the same theoretical system as in Figure 3 for five different input line widths at two theoretical rate constants.

This is, of course, to be expected, since in this region the lines are already narrow and their width $W_{\text{ex}} \cong W + k$ is close to the nonexchange width.⁴ An incorrect input line width will therefore have a profound effect on k .

The magnitude of the possible systematic error in the activation energy can now be estimated from the maximum and minimum slopes in the Arrhenius plots. The per cent deviation in E_a can be expressed as

$$\Delta E_a (\%) = \frac{\ln k_f - \ln k_s - (\ln k_{tf} - \ln k_{ts})}{\ln k_{tf} - \ln k_{ts}} \times 100$$

where the subscripts t, f, and s refer to true, fast, and slow exchange rates. Including a $\pm 10\%$ confidence limit in $\Delta\nu$ at fast rates and combining the worst possible values, *i.e.*, too high k_f with too low k_s , one obtains $\Delta E_a = \pm 46\%$ and $\pm 21\%$ for the small and large $\Delta\nu_t$ cases, respectively.

Temperature Measurements

Up to this point we have been concerned with the systematic errors introduced in the energy of activation from incorrect rate constants, but systematic errors can also be introduced by improper measurement of the sample temperature. The temperature of a sample in the nmr probe is most often measured by the sample substitution technique, *i.e.*, the one which utilizes the known temperature dependence of the internal chemical shifts of standard samples of methanol and ethylene glycol. The correctness of the Varian calibration curves for these samples was recently challenged by Van Geet.^{5,21} In addition, Neumann and Jonas¹²

(21) A. L. Van Geet, Abstracts of the 10th Experimental NMR Conference, Pittsburgh, Pa., March 1969.

Table II: Output Values of $\Delta\nu_{\min}$ and k for Different Input Line Widths^a

k_t , sec ⁻¹	Range of $\Delta\nu_{\min}$ Hz	Range of k , sec ⁻¹	Δk , %
$\Delta\nu_t = 3.06$ Hz ^b			
$\sim k_c/7$	3.15–3.00	1.6–0.4	± 60
$\sim k_c/2$	3.20–2.90	3.7–2.4	± 21
$\sim k_c$	3.35–2.75	7.7–5.3	± 18
$\sim 2k_c$	3.50–2.50	14.0–9.3	± 20
$\sim 2k_c^c$	3.85–2.25	16.8–7.0	± 41
$\Delta\nu_t = 8.06$ Hz ^b			
$\sim k_c/8$	8.10–8.00	2.6–1.4	± 30
$\sim k_c/2$	8.20–7.90	9.1–7.8	± 8
$\sim k_c$	8.30–7.80	18.6–16.6	± 6
$\sim 2k_c$	8.40–7.60	31.8–28.8	± 5
$\sim 2k_c^c$	9.20–6.80	38.4–22.8	± 25

^a Input line width $W = 0.60 \pm 0.20$ Hz. ^b True line width $W_t = 0.59$ Hz. ^c Range of calculated rate constants when an additional uncertainty of $\pm 10\%$ is included in determination of $\Delta\nu_{\min}$ (see text).

the associated best-fit rate constants are listed for different input values of W . Situations corresponding to fast, medium, slow, and very slow exchange are included for $\Delta\nu_t = 3.06$ Hz and $\Delta\nu_t = 8.06$ Hz. The values in this table show that whereas a ± 0.2 Hz variation in W results in a $\pm 20\%$ range for k in the case $\Delta\nu_t = 3.06$ Hz, the same line width variation results in only a ± 5 – 8% uncertainty in k for $\Delta\nu_t = 8.06$ Hz. It should also be noted that the range of best-fit rates increases dramatically (to $\pm 60\%$ and $\pm 30\%$, respectively) at very slow exchange rates.

Table III: Activation Energies (E_a in kcal/mol) Obtained Using Temperature Calibration Curves by Varian and Van Geet⁶

	I (CDCl ₃)	I (CD ₃ CN)	I (CD ₃ OD)	I (SO ₂)	II (CDCl ₃)	II (CD ₃ CN)
Van Geet	17.6	15.1	15.7	11.5	17.3	18.1
Varian	16.2	13.7	13.9	12.3	17.1	17.8
Difference, %	8	9	11	7	1	2

found deviations from the ethylene glycol curve by measuring sample temperatures with a thermocouple.

Calibration measurements performed by us on methanol agreed in detail with Van Geet's curve.⁵ We measured the internal chemical shift of a methanol sample over the range -65 to $+40^\circ$, calibrating each spectrum with audio side bands in order to eliminate errors due to changes in the sweep width with decreasing temperatures. A minimum of three scans were recorded at each temperature and the variation in chemical shift was rarely larger than 0.1 Hz. The temperature of the sample was measured immediately before and after these scans by lowering a copper-constantan thermocouple into the spinning sample to the level of the receiver coil.²² In order to get an idea of the magnitude of temperature gradients over the sample the thermocouple was moved ~ 10 mm above and below the receiver coil. No measurable difference was observed between the three positions over the temperature range. A temperature gradient over the sample could affect the line shape and result in the calculation of incorrect rate constants.

The direct use of a temperature-sensing device—the thermocouple or thermistor⁵—inserted in the sample is, of course, advantageous since the substitution method requires very careful temperature equilibration and introduces other possibilities for errors through the measurement of chemical shifts. However, when degassed, sealed tubes are used the sample temperature cannot be measured directly, and the substitution method becomes the desirable alternative. Provided that reasonable care is taken to assure temperature equilibrium, random errors which result from uncertainty in sweep width can be reduced to less than $\pm 1^\circ$. At 200°K this means a relative uncertainty of 0.5%.

Much more serious is the systematic error that can be introduced in the activation energy, E_a , by using a temperature calibration curve with an incorrect slope. The same effect occurs if sweep width changes of the spectrometer at low temperatures are ignored. Above room temperature, where the ethylene glycol sample is used, the difference between Varian's and Van Geet's⁵ curves is not very large. This is fortunate since the restricted rotation of many simple dimethylamides has been studied in this temperature region. However, in the low-temperature region the use of the old methanol calibration curve can introduce a temperature

error of as much as 4° . The effect on E_a can be substantial, as demonstrated in the present study. The values of E_a for the cytosine derivatives obtained using the same rate constants and the two methanol calibration curves are listed in Table III. The largest effect was observed for I in methanol, where a difference of 1.7 kcal/mol (11%) was found. The greater similarity between new and old ethylene glycol curves is reflected in the smaller differences observed for II, which was studied at higher temperatures.

Conclusions

In arriving at the possible systematic errors by the numerical analysis we took into account a $\pm 10\%$ uncertainty in the determination of $\Delta\nu$ in the fast exchange region and a line width variation of ± 0.2 Hz. The $\pm 10\%$ uncertainty in $\Delta\nu$ was chosen to cover roughly the differences in $\Delta\nu$'s obtained from the curves A and B in Figure 2 and used in the TLS analysis of the experimental data. However, the input line widths obtained from plots such as Figure 1 probably come much closer to the true values of W than the ± 0.2 Hz used in the numerical analysis. Limiting the range for W to the accuracy with which the line widths could be measured outside the exchange region and retaining the $\pm 10\%$ uncertainty in $\Delta\nu$ in the fast exchange region decreases the maximum error in E_a to ± 19 and $\pm 14\%$ for the small and large chemical shift cases, respectively. A comparison with the values (± 46 and $\pm 21\%$) obtained above demonstrates the importance of knowing the nonexchange line width, especially when $\Delta\nu$ is small.

The experimental energy barriers (see Table I) calculated by the use of the chemical shift curves A and B are seen to differ by 7–13%, well within the maximum systematic errors calculated above. The larger differences occur when $\Delta\nu$ is small, in agreement with the theoretical calculations, demonstrating the importance of using the highest possible magnetic field for systems with low activation energy. One then has the additional advantage of an increase in coalescence temperature.

The differences shown in Table I between the energy barriers calculated by methods A, B, and A' are ob-

(22) The position of the receiver coil in the A-60 insert was easily determined by moving a spherical micro cell filled with benzene until maximum peak height was obtained.

vously much larger than the standard deviations listed for E_a , thus emphasizing the often-made point that linearity of the Arrhenius plot in itself is no guarantee that the data are accurate. The use of these standard deviations as a measure of the reliability of E_a is valid only if one is certain that systematic errors have been eliminated.

The entropy of activation, as usual, shows the highest sensitivity to systematic errors. An error of $\pm 15\%$ in the enthalpy of activation $\Delta H = E_a - RT \sim 15$ kcal/mol would result in an error in the entropy of ± 7.5 eu. The differences in entropy of activation

found in the study of the cytosine derivatives fall in this range.

The present study has reemphasized that TLS analysis of exchanging systems should not be extended much above the coalescence temperature, where uncertainties in the determination of $\Delta\nu$ provide the principal limitation on the accurate calculation of k . It has furthermore been demonstrated that k is subject to appreciable error if line widths in the absence of exchange are not well known. This condition is likely to exist for moderate size molecules if the line width variation with temperature is ignored.

Raman Spectra of Tetrafluoroberyllate Ion in Molten Sodium Fluoride and Lithium Fluoride to 686°

by Arvin S. Quist,* John B. Bates, and George E. Boyd

Oak Ridge National Laboratory, Oak Ridge, Tennessee 37830 (Received July 29, 1971)

Publication costs assisted by Oak Ridge National Laboratory

The expected four normal vibrational modes of the tetrahedral BeF_4^{2-} ion have been observed in the Raman spectra of molten Li_2BeF_4 , Na_2BeF_4 , and 17 mol % BeF_2 in NaF-LiF (53:30 mol %, respectively) to 686°. Raman spectra of aqueous $(\text{NH}_4)_2\text{BeF}_4$ and of solid $^6\text{Li}_2\text{BeF}_4$ and $^7\text{Li}_2\text{BeF}_4$ also were measured, and the infrared spectra of the latter two compounds were recorded. Force constants for the BeF_4^{2-} ion were calculated from the observed vibrational frequencies. The symmetric stretching force constants, F_{11} , for the isoelectronic series BeF_4^{2-} , BF_4^- , and CF_4 were correlated with the anion charge and the M-F bond distance (M = Be, B, C).

Introduction

The predominantly covalent chemistry of beryllium, in contrast to the ionic behavior of the other group II elements, makes it unique in its chemical behavior as compared with the other members of this series. Beryllium-fluorine compounds are of particular interest because in them the smallest divalent cation is combined with the most electronegative anion. Although beryllium-fluorine compounds are often isomorphous with silicon-oxygen compounds, some tetrafluoroberyllates are more similar to sulfates in their crystal chemistry and solubility behavior. Among the alkali metal tetrafluoroberyllates, Li_2BeF_4 is of importance because it is the solvent for fissionable and fertile components of homogeneous molten salt thermal breeder nuclear reactors. The BeF_4^{2-} ion is of interest also because it is the first member of the isoelectronic series BeF_4^{2-} , BF_4^- , and CF_4 , in which the valence shell of the central atom is limited to eight electrons, and consequently no double bond formation is possible.

The vibrational frequencies of BeF_4^{2-} in melts have not been reported, although infrared and Raman spectra of solid¹⁻⁴ and aqueous⁵ tetrafluoroberyllates have been measured. Raman spectral studies are particularly well-suited for investigations on this anion as all of the four normal modes of vibration of the tetrahedral BeF_4^{2-} anion are Raman active whereas only two modes are infrared active.

Most of our measurements have been with molten Li_2BeF_4 because of the local interest in this salt. Molten Na_2BeF_4 was also studied to obtain information on the effect of the cation on the vibrational spectrum of BeF_4^{2-} . Molten Na_2BeF_4 and Li_2BeF_4 contain

- (1) R. D. Peacock and D. W. A. Sharp, *J. Chem. Soc.*, 2762 (1959).
- (2) J. LeComte, C. Duval, and C. Wadier, *C. R. Acad. Sci.*, 149, 1991 (1959).
- (3) A. I. Grigorev, Y. V. Orlova, V. A. Sipachev, and A. V. Novoselova, *Dokl. Akad. Nauk USSR*, 152, 762 (1963) (Eng. transl.).
- (4) E. Funck, *Ber. Bunsenges. Phys. Chem.*, 68, 617 (1964).
- (5) R. E. Mesmer and C. F. Baes, Jr., *Inorg. Chem.*, 8, 618 (1969).

only the minimum fluoride ion concentration necessary for complete four-coordination of all beryllium to form BeF_4^{2-} ; hence, it was of interest to measure the spectrum of BeF_4^{2-} in an excess of F^- ion where the likelihood of dimer formation ($\text{Be}_2\text{F}_7^{3-}$) is minimized. Accordingly, a solution of 17 mol % BeF_2 in NaF - LiF (53:30 mol %, respectively) also was studied. Additional measurements were made with aqueous $(\text{NH}_4)_2\text{BeF}_4$ solutions at 25° to obtain the spectrum of BeF_4^{2-} ion under conditions of reduced interionic interactions. Solid Li_2BeF_4 was of interest, and the vibrational spectra of the isotopically substituted $^6\text{Li}_2\text{BeF}_4$ and $^7\text{Li}_2\text{BeF}_4$ forms are included in this report.

Experimental Section

Fluoride melts are generally corrosive towards the usual optical window materials; therefore, special techniques have been developed to contain and study these systems. A modification of the captive-liquid or "windowless" nickel cell, previously employed to measure the visible absorption spectra of fluoride melts,⁶ was developed for use with laser light sources to measure the Raman spectra of the BeF_4^{2-} -containing melts. This cell has been described,⁷ as has the furnace used with it.⁸

The $^7\text{Li}_2\text{BeF}_4$ examined in these studies was purified in an all-nickel apparatus by treatment with a mixture of HF and H_2 at 600° and filtered through fritted nickel under H_2 . The $^6\text{Li}_2\text{BeF}_4$ was prepared from the reaction of ^6LiF (99.6% ^6Li) with vitreous BeF_2 . The Na_2BeF_4 and the mixture containing 53, 30, and 17 mol % NaF , LiF , and BeF_2 , respectively, were prepared from Harshaw single crystal NaF and LiF (Harshaw Chemical Co., Cleveland, Ohio) and from a clear BeF_2 glass which had been vacuum distilled in a nickel apparatus.

The windowless cells were filled in a vacuum drybox in which the water content was maintained at less than 3 ppm. Subsequent transfers of the sample-containing cells also were carried out in this drybox. The aqueous solution of 2.5 M $(\text{NH}_4)_2\text{BeF}_4$ in 2 M NH_4F was prepared from reagent grade materials and filtered through an F-porosity Pyrex filter. A complete description of the experimental procedures for loading and manipulating the cells is given elsewhere.⁷⁻⁹ Briefly, the windowless cells are loaded, placed in a quartz tube, heated to 150 - 200° under vacuum for about 1 hr, and then the sample is melted under an atmosphere of dry helium. The cells are cooled, transferred to another quartz tube having an optical flat fused to one end, again heated under vacuum, and finally sealed in this latter quartz tube under a helium pressure of about 0.3 atm. The initial melting process ensures that the cell will be filled with an appropriate quantity of melt. The final arrangement whereby the cell is sealed in a quartz tube takes advantage of the desirable optical features of a quartz cell and also completely

encloses the sample in an inert atmosphere. Sample containment is of particular importance because of the toxicity of beryllium. It should be noted that the molten fluoride does not come into contact with the quartz tube.^{7,9}

Raman spectra were recorded with a Jarrell-Ash Model 25-300 spectrophotometer (Jarrell-Ash Co., Waltham, Mass.) using $4880\text{-}\text{\AA}$ radiation from a Spectra-Physics Model 141 argon ion laser (Spectra-Physics, Mountain View, Calif.) to excite the spectra. The optical system for focusing and collecting the light has been described.⁷⁻⁹

The infrared spectrum of Li_2BeF_4 at 25° was measured with a Perkin-Elmer 621 spectrophotometer. A small crystalline sample was ground onto the surface of a AgBr plate which was placed at the focus of a $4\times$ beam condenser. By using a cover plate of AgBr and sealing the edges between the two plates, the powdered sample of Li_2BeF_4 was prevented from escaping into the air.

Results

Raman spectra of molten Li_2BeF_4 (melting point 459^{10}) were obtained from 487 to 640° . A typical spectrum measured at 533° is shown in Figure 1. Three of the four bands are visible at frequencies near 390 , 550 , and 800 cm^{-1} . The expected fourth band is located near 260 cm^{-1} , but it is somewhat obscured in Figure 1 by the steeply rising background; this band may be observed more readily in other spectra, such as in Figure 2 for molten Na_2BeF_4 at 616° . The Raman and infrared spectra of solid Li_2BeF_4 at 25° are presented in Figures 4 and 5, respectively. Table I summarizes the vibrational frequencies observed for molten Li_2BeF_4 at several temperatures. The results for solid $^7\text{Li}_2\text{BeF}_4$ and $^6\text{Li}_2\text{BeF}_4$, for molten Na_2BeF_4 (mp 595^{11}), for a melt containing 17 mol % BeF_2 in NaF - LiF , and for aqueous BeF_4^{2-} in excess F^- also are reported.

Frequency Assignments

The polarization and intensity of the band at $550 \pm 3\text{ cm}^{-1}$ in the Raman spectra of molten tetrafluoroberyllates (Figures 1-3) make it logical to assign it to the totally symmetric stretching mode, $\nu_1(a_1)$, of the tetrahedrally coordinated BeF_4^{2-} anion. Its frequency does not vary significantly (within experimental error) with temperature or when the cation is changed from lithium to sodium. The $\nu_1(a_1)$ frequency

(6) J. P. Young, *Anal. Chem.*, **36**, 390 (1964).

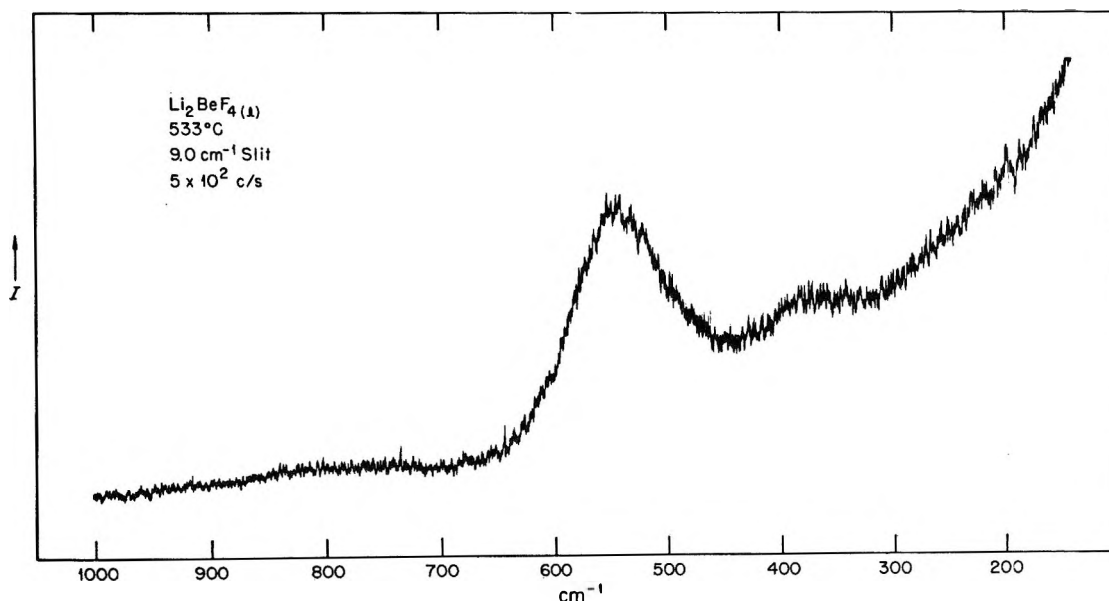
(7) A. S. Quist, *Appl. Spectrosc.*, **25**, 80 (1971).

(8) A. S. Quist, *ibid.*, **25**, 82 (1971).

(9) A. S. Quist, J. B. Bates, and G. E. Boyd, *J. Chem. Phys.*, **54**, 4896 (1971).

(10) K. A. Romberger and J. Braunstein, Reactor Chemistry Division Annual Progress Report, ORNL-4586, July 1970, p 3.

(11) D. M. Roy, R. Roy, and E. F. Osburn, *J. Amer. Ceram. Soc.*, **36**, 185 (1953).

Figure 1. Raman spectrum of molten Li_2BeF_4 at 533° .**Table I:** Vibrational Frequencies Observed in the Raman Spectra of BeF_4^{2-} in Melts, in Solid Li_2BeF_4 , and in Aqueous Solution (Frequencies in cm^{-1})

Li ₂ BeF ₄ melts at			Molten Na ₂ BeF ₄ at 616°	NaF-LiF-BeF ₂ (53:30:17) mol % at 645, 686°	2.5 M (NH ₄) ₂ BeF ₄ in 2 M NH ₄ F at 25°	Li ₂ BeF ₄ (s) at 25°				Assignment	
487°	533°	640°				Raman		Ir			
					⁷ Li	⁶ Li	⁷ Li	⁶ Li			
255	240	260	265	255	...	257 295	257 297	$\nu_2(e)$	
385	390	390	385	380	380	348 377	354 377	333 360 372	340 361 380		$\nu_4(f_2)$
						402 440 475	...	405 435 463 500	417 456 486 520	(?)	
547	550	545	550	552	548	563 775	563	$\nu_1(a_1)$	
800	800	800	800	800	795	795 850	...	775 805 860	772 808 862	$\nu_3(f_2)$	

^a Vibrations from Li-F stretching modes in crystalline Li_2BeF_4 .

is essentially the same in aqueous solution as in the melts; only in solid Li_2BeF_4 does it occur at a different (higher) frequency. The observed frequency and assignment are consistent with previously reported values for the Raman spectra of solid alkali metal tetrafluoroberyllates³ and for aqueous solutions.⁵ Although the position of the ν_1 band in the melt does not vary greatly with temperature or cation, its half-bandwidth decreases considerably when lithium is replaced by sodium. Thus, in molten Li_2BeF_4 at 582° , the ν_1 half-bandwidth is about 100 cm^{-1} , whereas in molten Na_2BeF_4 at 616° this value is *ca.* 50 cm^{-1} .

The triply degenerate $\nu_3(f_2)$ and $\nu_4(f_2)$ vibrational

modes of tetrahedral ions are both Raman and infrared active. Infrared studies with solid alkali metal fluoroberyllates have resulted in the assignment of bands near 800 cm^{-1} to the ν_3 vibration¹⁻⁴ and of the bands near 380 cm^{-1} to ν_4 .²⁻⁴ The Raman spectrum of solid Li_2BeF_4 exhibits three bands in each of these regions, consistent with a lowering of the T_d symmetry of the BeF_4^{2-} ions which occupy sites of C_1 symmetry in the hexagonal unit cell lattice.¹² In molten and aqueous tetrafluoroberyllates, only single bands at 800 ± 10 and $385 \pm 5 \text{ cm}^{-1}$ are observed for the ν_3 and ν_4 vibra-

(12) J. H. Burns and E. K. Gordon, *Acta Cryst.*, **20**, 135 (1966).

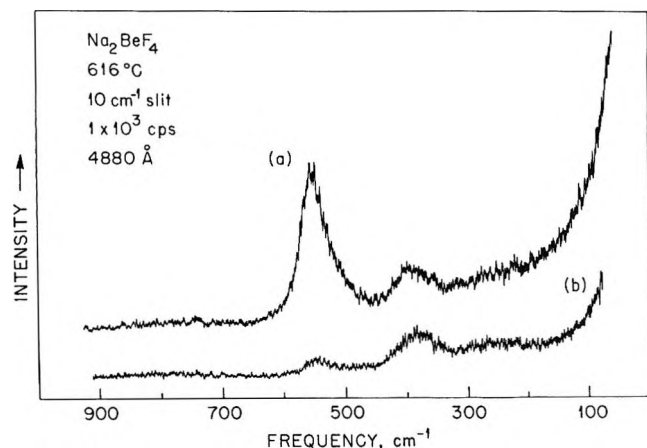


Figure 2. Raman spectrum of molten Na_2BeF_4 at 616° : (a) incident light polarized perpendicular to plane containing slit and laser beam; (b) parallel polarization.

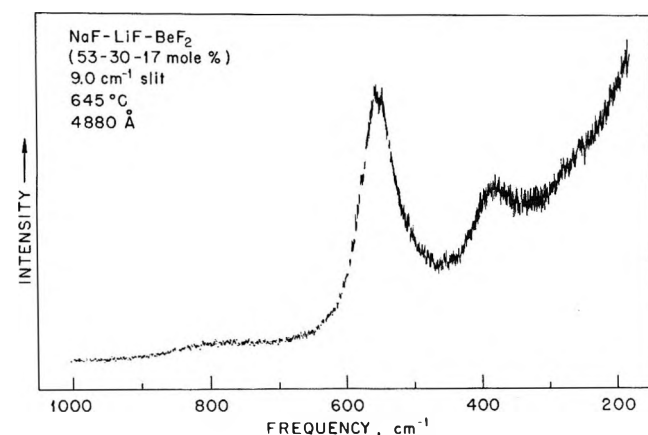


Figure 3. Raman spectrum of molten BeF_4^{2-} (17 mol %) in NaF-LiF (53:30 mol %, respectively) at 645° .

tions, respectively, indicating a symmetric environment for BeF_4^{2-} (no complexing) in these solutions. Half-bandwidths for ν_3 and ν_4 in Na_2BeF_4 melts are approximately 110 and 75 cm^{-1} , respectively.

The doubly degenerate $\nu_2(\text{e})$ vibration has not been reported previously. In solid Li_2BeF_4 , bands at 257 and 295 cm^{-1} (Figure 4) are assigned to this vibrational mode. In melts, ν_2 exhibits a single band at $255 \pm 10\text{ cm}^{-1}$, and the half-bandwidth was approximately 90 cm^{-1} in molten Na_2BeF_4 . The ν_2 mode was not detected in aqueous BeF_4^{2-} because of the high background in the spectra.

No additional bands were found in Raman spectra of the melts. In the Raman spectrum of solid $^7\text{Li}_2\text{BeF}_4$, however, weak bands were observed near 402, 440, and 475 cm^{-1} . These bands correspond to the strong absorptions observed in the infrared spectrum of $^7\text{Li}_2\text{BeF}_4$ in the region between 550 and 400 cm^{-1} (Figure 5 and Table I). The corresponding bands in the infrared spectrum of $^6\text{Li}_2\text{BeF}_4$ shifted 12 to 23 cm^{-1} higher in frequency. The assignment of these bands to the stretching vibrations of the Li^+F^- sublattice in crys-

talline Li_2BeF_4 (Table I) is supported by the observed isotopic shifts. Similar bands observed in the 500- to 400-cm^{-1} region of Li_2CO_3 also were found to shift to *ca.* 17 to 34 cm^{-1} higher frequencies when ^6Li was substituted for ^7Li , while the modes due to CO_3^{2-} showed either a very small ($<5\text{ cm}^{-1}$) or no change in frequency.¹³ Since the Li-F bonds in Li_2BeF_4 are mainly ionic in character, their stretching modes should exhibit relatively strong infrared bands but weak Raman bands as observed (Figures 4 and 5). As shown in Table I, some of the bands assigned to components of the $\nu_4(\text{f}_2)$ mode of BeF_4^{2-} also exhibited relatively small ($<10\text{ cm}^{-1}$), positive frequency shifts in the Raman and infrared spectra of polycrystalline $^6\text{Li}_2\text{BeF}_4$. This suggests that motions of the Li^+ sublattice may be involved to a small degree in the low-frequency internal vibrations of the BeF_4^{2-} sublattice.

Force Constant Calculations

The force constants of the general valence force field (GVFF) of BeF_4^{2-} were calculated with the approximation method of Krebs, *et al.*,¹⁴ and the ν_1 , ν_2 , ν_3 , and ν_4 frequencies observed in molten Li_2BeF_4 at 487° . The Be-F bond distance of 1.56 \AA used in calculating the G matrix was taken from crystallographic data of ref 12. The calculated frequencies and force constants for BeF_4^{2-} are given in Table II. The number of significant figures to which the force constants are reported is not justified on the basis of the uncertainties reported in the measurement of peak frequencies for ν_2 , ν_3 , and ν_4 (see above, "Frequency Assignments"). The force constants given in Table II should be considered as those values which must be used to obtain the calculated frequencies reported in Table II. The bond stretching constant, f_d , for Be-F was computed to be 3.17 mdyn/\AA using the values of F_{11} and F_{33} from Table II and the formula $f_d = 1/4(F_{11} + 3F_{33})$ (ref 14).

Table II: Calculated Frequencies and Force Constants for Tetrahedral BeF_4^{2-} Using the Melt Data at 487°

Mode	Frequency cm^{-1}		Force constants, ^a mdyn/ \AA
	Observed	Calculated	
$\nu_1(\text{a}_1)$	547	547	$F_{11} = 3.342$
$\nu_2(\text{e})$	255	255	$F_{22} = 0.242$
$\nu_3(\text{f}_2)$	800	800	$F_{33} = 3.115$
			$F_{34} = 0.689$
$\nu_4(\text{f}_2)$	385	385	$F_{44} = 0.355$

$$f_{\text{Be-F}} = 1/4(F_{11} + 3F_{33}) = 3.172\text{ mdyn/\AA}$$

^a The number of significant figures reported for the force constants does not imply a commensurate accuracy in the observed frequencies.

(13) P. Tarte, *Spectrochim. Acta*, **20**, 238 (1964).

(14) B. Krebs, A. Müller, and A. Fadini, *J. Mol. Spectrosc.*, **24**, 198 (1967).

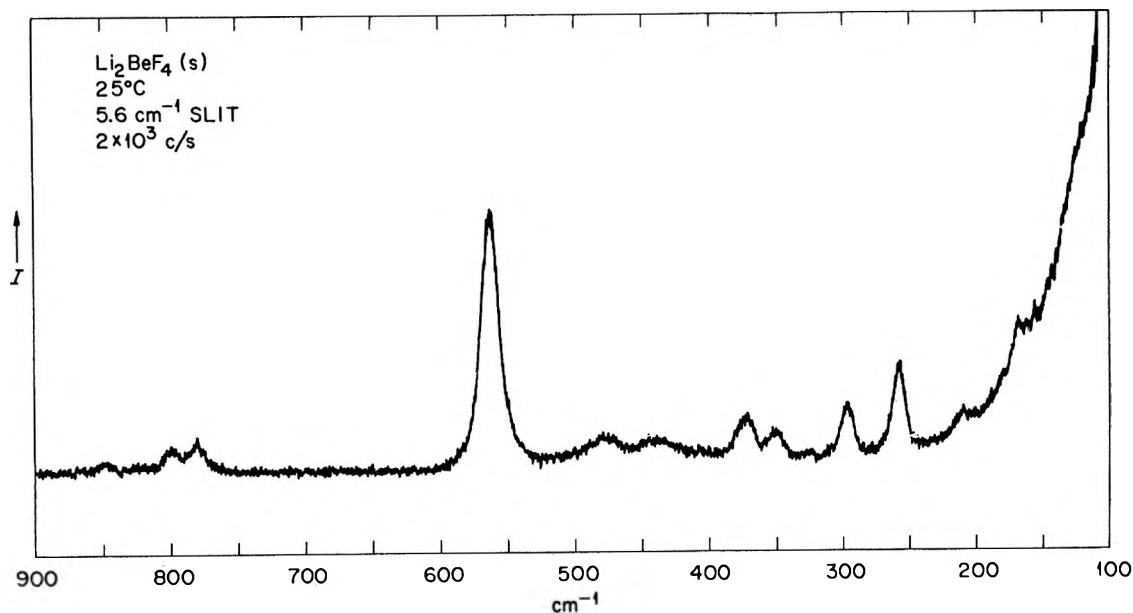


Figure 4. Raman spectrum of polycrystalline Li_2BeF_4 near 25° .

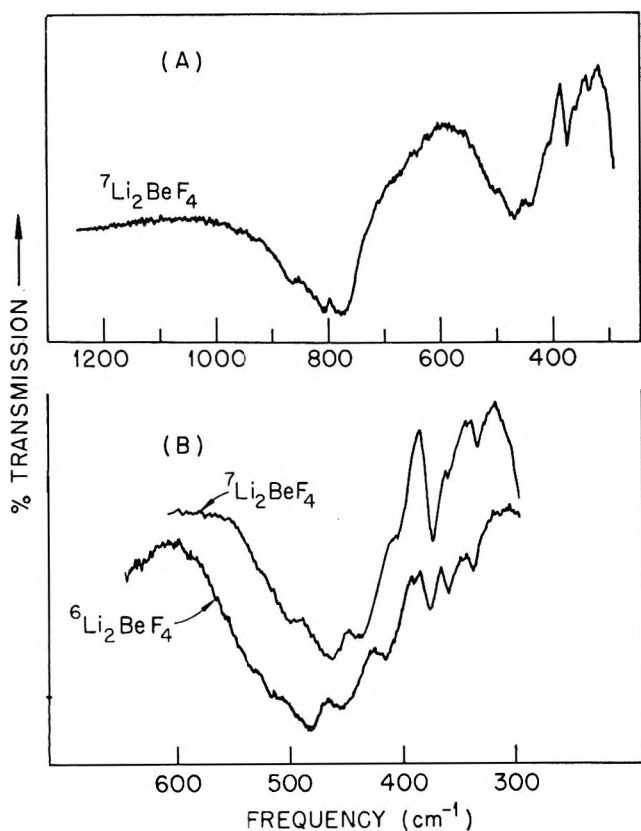


Figure 5. Infrared spectrum of polycrystalline ${}^7\text{Li}_2\text{BeF}_4$ and ${}^6\text{Li}_2\text{BeF}_4$ near 25° .

As pointed out above, BeF_4^{2-} , BF_4^- , and CF_4 are isoelectronic, and it is thus of some interest to compare the bond stretching constants for these three species. Values of f_d for BF_4^- and for CF_4 have been calculated as 4.41⁹ and 6.70¹⁴ mdyn/Å, respectively, using the same method of computation described above. In

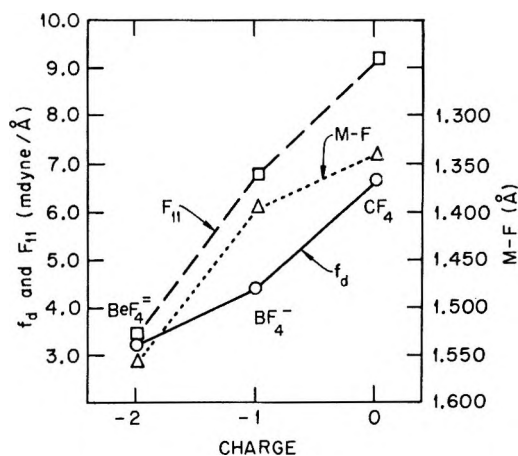


Figure 6. Plots of F_{11} (---) and f_d (—) force constants and M-F (---) bond distances (M = C, B, Be) vs. anion charge for BeF_4^{2-} , BF_4^- , and CF_4 .

Figure 6 the bond stretching constants and the F_{11} symmetrized force constants for BeF_4^{2-} , BF_4^- , and CF_4 are plotted vs. the charge on the anion. The values of F_{11} for CF_4 ⁹ and BF_4^- ¹⁴ were previously calculated to be 9.25 and 6.75 mdyn/Å, respectively.^{9,14} A plot of the M-F bond distance (M = Be, B, C) vs. anion charge is also included in Figure 6. A |C-F| = 1.34 Å bond distance was obtained from electron diffraction data,¹⁵ while the |B-F| and |Be-F| bond distances were taken from X-ray crystal data on NaBF_4 ¹⁶ and Li_2BeF_4 ,¹² respectively.

Discussion

The frequencies of the BeF_4^{2-} vibrations observed from Raman spectral measurements on the molten salts

(15) H. J. M. Bowen, *Trans. Faraday Soc.*, **50**, 444 (1954).

(16) G. Brunton, *Acta Cryst.*, **B24**, 1703 (1968).

described above are relatively insensitive (within experimental error) to temperature and composition. As shown in Table I, the frequency of the ν_1 vibration does not vary appreciably in going from the molten state (for a variety of compositions and temperatures) to aqueous $(\text{NH}_4)_2\text{BeF}_4$.

The most significant change observed in the Raman spectra of BeF_4^{2-} in the molten state was the narrowing of ν_1 on substituting Na^+ for Li^+ . The half-bandwidth (δ) of ν_1 decreased by a factor of 2 in molten Na_2BeF_4 compared with the δ observed in molten Li_2BeF_4 at the same temperature. The origin of this effect appears to be primarily cation dependent since it is expected that any significant change in anion-anion interaction would be observed as a frequency shift of ν_1 . Similar results were obtained from measurements of δ for $\nu_1(a_1)$ of NO_3^- in molten alkali metal nitrates.¹⁷ At a given melt temperature, it was observed that the δ 's of ν_1 followed the order $\text{Li} > \text{Na} > \text{K} > \text{Rb} > \text{Cs}$. The explanation advanced for the change of $\delta(\nu_1)$ in molten nitrates¹⁷ may be applicable to the case of the change in δ observed for the ν_1 mode of BeF_4^{2-} . An increase in the potential barrier for hindered rotation of BeF_4^{2-} ions in molten Li_2BeF_4 compared with the barrier height in molten Na_2BeF_4 results in an increase in δ for ν_1 . Because of their comparatively smaller size, the Li^+ ions are able to get closer to the center of the BeF_4^{2-} anions than are the Na^+ ions; the closer proximity of Li^+ to BeF_4^{2-} produces a larger barrier to anion libration. On this basis, the change in $\delta(\nu_1)$ for molten K, Rb, and Cs fluoroberyllates may be expected to follow the trends observed in molten nitrates. Additional experiments are required, however, to test these assumptions.

The correlation between bond force constants and anion charge for a number of isoelectronic tetrahedral species was discussed previously by Woodward.¹⁸ The trends exhibited by the series BeF_4^{2-} , BF_4^- , and CF_4 (Figure 6) follow the expected general pattern of increasing f_d and F_{11} and decreasing M-F bond length as the anion charge varies from -2 to 0 . Both the covalent M-F bond strength and the coulombic attraction between the M and F atoms increase in the series from BeF_4^{2-} to CF_4 .¹⁸ An interesting feature shown in Figure 6 is that, while the graphs of bond lengths, M-F, and symmetrized force constants, F_{11} , exhibit the largest rate of increase from BeF_4^{2-} to BF_4^- , the plot of f_d vs. anion charge shows the greatest rate of increase from BF_4^- to CF_4 . The potential constants, f_d , are related to the restoring force for a single M-F bond, while the F_{11} constants are related to the restoring force for simultaneous, symmetric stretching of all four M-F bonds. Thus, it seems reasonable that the varia-

tion of F_{11} with anion charge should be similar to that exhibited by the graph of bond length vs. anion charge while, for the single bond M-F force constants, similar reasoning does not hold. Both the equilibrium bond lengths and the resistance to stretching of four M-F bonds simultaneously and with equal displacements (symmetric stretching mode) are influenced by the mutual interactions of the M-F bonds. The effects of bond-bond interaction have been removed (within the approximation of the calculations described above) in the computation of f_d .

The Raman and infrared spectra of crystalline Li_2BeF_4 (Figures 4 and 5 and Table I) were surprisingly simple in view of the number of formula weights (18) of Li_2BeF_4 in the primitive unit cell. All atoms occupy sites of general symmetry;¹² hence, a total of 18 Raman-active and 18 infrared-active internal modes (derived from motions of the BeF_4^{2-} ions) are allowed. The observed spectra appear to be those of noninteracting BeF_4^{2-} tetrahedra located on sites of low symmetry in which degeneracy is completely removed in the e and f_2 modes by the static field. Correlation field effects were only weakly apparent from the small differences observed between the frequencies of the infrared and Raman components of a given internal mode (Table I).

Conclusions

The BeF_4^{2-} anion appears to retain its tetrahedral symmetry in aqueous solution and in molten Li_2BeF_4 and Na_2BeF_4 . Both the frequencies and force constants of "free" BeF_4^{2-} were well characterized from these studies. A comparison of the frequencies and half-bandwidths for ν_1 in molten Li_2BeF_4 and in molten Na_2BeF_4 showed that cation-anion interactions may be important, while effects of anion-anion interactions were not apparent. Further studies of the effects of cation size and charge on the band shape of ν_1 would be helpful in determining the nature of the cation-anion interaction.

Acknowledgments. The authors would like to thank K. Romberger and B. Hitch of the ORNL Reactor Chemistry Division for supplying high-purity samples of Li_2BeF_4 and BeF_2 , and D. E. LaValle of the Analytical Chemistry Division for preparing the samples of $^6\text{Li}_2\text{BeF}_4$. This research was sponsored by the U. S. Atomic Energy Commission under contract with the Union Carbide Corporation.

(17) N. A. Ponyatenco and I. V. Radchenko, *Opt. Spectrosc.*, **26**, 353 (1969).

(18) L. A. Woodward, *Trans. Faraday Soc.*, **54**, 1271 (1958).

Near-Infrared Spectral Studies on the Effects of Perchlorate and Tetrafluoroborate Ions on Water Structure

by S. Subramanian and Harvey F. Fisher*¹

Veterans Administration Hospital, Kansas City, Missouri 64128, and the Department of Biochemistry, University of Kansas Medical Center, Kansas City, Kansas (Received August 5, 1971)

Publication costs assisted by the Veterans Administration Hospital

The effect of perchlorates of sodium, magnesium, zinc, and aluminum, and sodium tetrafluoroborate on the structure of water has been studied with respect to the anion effect, cation effect, concentration, and temperature effects. All of these salts split the 1.45- μ band of water, an effect which is ascribed to their special water-structure-breaking effect. The anions play the predominant role and the effect of cations is found to be only of secondary importance. The effects of the anions and increase of temperature seem to be complementary. It is reasoned that the perchlorate and tetrafluoroborate ions are not significantly hydrated in aqueous solutions.

I. Introduction

The structure of water and the effect of electrolytes on the structure of water have been widely studied by several physico-chemical techniques. In view of the prevailing uncertainty over the structure of water, the molecular nature of the electrolyte-water interactions is also not completely understood. The importance of solute-water interactions in determining biopolymer conformations has been realized lately. The effects of neutral salts on the structure of water and protein conformation have been reviewed² recently. Except for the perchlorate ion, no direct quantitative correlation has been found³ between the effect of ions on water structure and their protein denaturing potential. The effect of perchlorate ion on water structure has been studied recently^{4,5} by ir and raman spectroscopy. In continuation of our studies^{6,7} on the structure of water and hydration of alkali halides in aqueous solutions in the near-infrared region, we investigated the effect of perchlorate and tetrafluoroborate ions on water structure, their hydration, if any, and the influence of cations and temperature on the tendency of perchlorate ion in disrupting water structure, by studying the 1.45 μ , ($\nu_1 + \nu_3$) combination band of water.

II. Experimental Section

The water used in this study was deionized tap water which was found in this laboratory to be equivalent to glass-distilled water. NaClO_4 (as $\text{NaClO}_4 \cdot \text{H}_2\text{O}$, purified) and $\text{Mg}(\text{ClO}_4)_2$ were obtained from Fisher Scientific Company. $\text{Zn}(\text{ClO}_4)_2 \cdot 6\text{H}_2\text{O}$ and $\text{Al}(\text{ClO}_4)_3 \cdot 9\text{H}_2\text{O}$ were obtained from K & K Laboratories, Inc. These were used as such. NaBF_4 was purchased from Alfa Inorganics and was recrystallized from aqueous solution; the insoluble residue present was filtered off. The sodium tetrafluoroborate solution was made just

prior to recording the spectra in order to minimize the effect of hydrolysis on the spectra recorded. Sodium trifluoroacetate was made by titrating trifluoroacetic acid (Eastman Organic Chemicals) with NaOH to neutral pH and crystallizing the salt from the solution.

All spectra were recorded using a Cary Model 14R double-beam recording spectrophotometer. The spectra recorded were the average of three or four scans; the averaging was done with the help of a Varian Spectro System 100 computer linked to the Cary 14 spectrophotometer. The absorption cells were of the insert type with a pathlength of 0.05 ± 0.0001 cm. The temperature of the contents in the cells was controlled to $\pm 0.02^\circ$ using a Lauda thermostat.

The direct spectra were recorded by using water (or solution) in the sample cell against a matched empty cell in the reference compartment. The difference spectra were obtained by placing water in the reference cell and solution in the sample cell and maintaining appropriate temperatures.

The pH's of the solutions were measured using a Radiometer PHM26 pH meter.

III. Results and Discussion

A. *The Absorption Spectra of Water and Solutions in the 1.45- μ Region.* The spectra of H_2O and 2 M

(1) Address correspondence to this author at the Veterans Administration Hospital.

(2) P. H. von Hippel and T. Schleich, "Structure and Stability of Biological Macromolecules," S. N. Timasheff and G. D. Fasman, Ed., Marcel Dekker, New York, N. Y., 1969, Chapter 6.

(3) T. Schleich and P. H. von Hippel, *Biochemistry*, **9**, 1059 (1970).

(4) (a) P. Dryjanski and Z. Kecki, *Rocz. Chem.*, **43**, 1053 (1969); (b) G. E. Walrafen, *J. Chem. Phys.*, **52**, 4176 (1970).

(5) G. Brinck and M. Falk, *Can. J. Chem.*, **48**, 3019 (1970).

(6) W. C. McCabe and H. F. Fisher, *J. Phys. Chem.*, **74**, 2990 (1970).

(7) W. C. McCabe, S. Subramanian, and H. F. Fisher, *ibid.*, **74**, 4360 (1970).

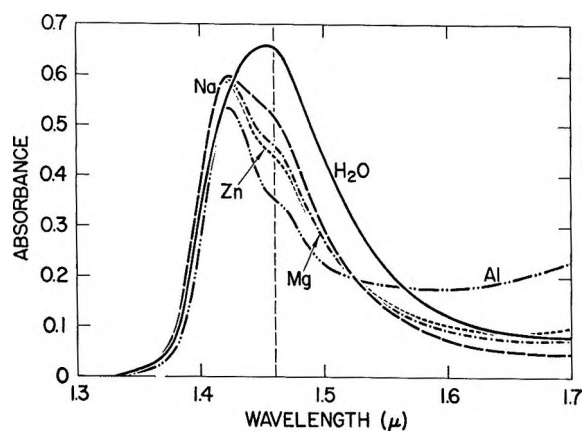


Figure 1. The near-infrared absorption spectra of water and aqueous solutions (salt concentration = 2 M) of sodium, magnesium, zinc, and aluminum perchlorates at 20° measured vs. the empty cell. The cell pathlengths were 0.05 cm.

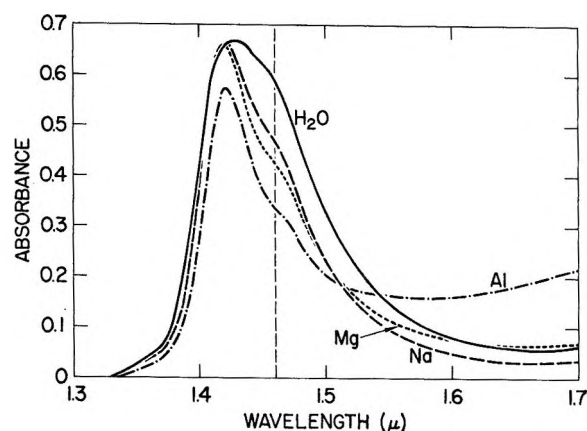


Figure 2. The spectra of water and aqueous perchlorate solutions (concentration = 2 M) at 60°. The cell pathlengths were 0.05 cm.

solutions of Na, Mg, Zn, and Al perchlorates at 20° are shown in Figure 1. The electrolytes do not have any absorption of their own in the spectral region studied. The spectrum of water in the various aqueous perchlorate solutions is shifted toward higher frequencies (shorter wavelength) relative to that of pure water, the maxima being almost the same for the different perchlorates. The spectrum of water itself shifts to higher frequencies with increase of temperature as shown in Figure 2, suggesting a similarity in the effects of temperature and perchlorate salts in disrupting water structure. At 20°, the spectra of water in aqueous perchlorate solutions show a splitting into (1) a high-frequency peak ($\sim 1.42 \mu$) and (2) a low-frequency shoulder (1.46μ). The spectra of water in the same solutions at 60° (Figure 2) are not significantly different from those at 20°. In Figure 3 are shown the spectra of water in aqueous sodium tetrafluoroborate at 20°. Here again the changes are similar to those in aqueous perchlorate solutions. A cursory examination of Figures 1–3 reveals certain character-

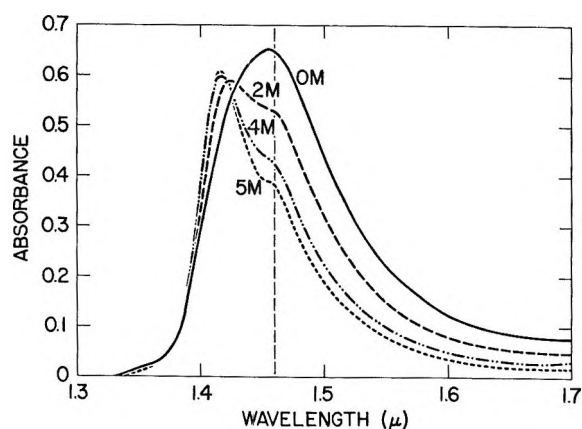


Figure 3. The spectra of aqueous sodium tetrafluoroborate solutions at 20°. The cell path lengths were 0.05 cm. The vertical dotted line in Figures 1–3 refers to the position of the shoulder at $\sim 1.46 \mu$.

istic features. The high-frequency peak of water in aqueous perchlorates and tetrafluoroborate indicates an extensive breakdown of the water structure. The shoulder in the solutions spectra at 1.46μ is seen only with perchlorates and tetrafluoroborate and not in the presence of other common anions.⁸ The shoulder at 1.46μ is also seen in the spectra of water at high temperatures.⁷ The position of the shoulder in the solutions spectra does not appear to shift measurably when the temperature is increased from 20° to 60°. Furthermore, the position of the shoulder has very little dependence on the species of cation. These features demonstrate that the major effect in the spectra is due to the anions and that their effects are similar to that of a temperature increase. We had also noticed earlier⁷ that the intensity, but not the frequency, of the high-frequency peak is dependent on the concentration of perchlorate.

B. Difference Spectra of Aqueous ClO_4^- , BF_4^- vs. Water at 20°. The difference spectra of 2 M solutions of Na, Mg, Zn, and Al perchlorates (Figure 4) and 2 M, 4M, and 5 M solutions of NaBF_4 (Figure 5) measured vs. water at 20° consist, in general, of a negative component arising from excluded volume⁶ for water in the sample cell, with a positive peak in the $1.42\text{-}\mu$ region superimposed. The difference spectra for aqueous solutions of alkali halides consisted⁶ of similar curves with the positive peak centered at 1.43μ . The difference spectra for Al and Zn perchlorates also show positive absorbances at wavelengths greater than 1.57 and 1.65μ , respectively. In these two cases and possibly for $\text{Mg}(\text{ClO}_4)_2$, the positive absorbance could be due to partial hydrolysis of the solutions resulting in acidic or basic solutions. It is known^{9–11} that hy-

(8) Unpublished results of this laboratory.

(9) G. E. Walrefan, *J. Chem. Phys.*, **36**, 1035 (1962).

(10) T. T. Wall and D. F. Hornig, *ibid.*, **47**, 784 (1967).

(11) W. R. Busing and D. F. Hornig, *J. Phys. Chem.*, **65**, 284 (1961)

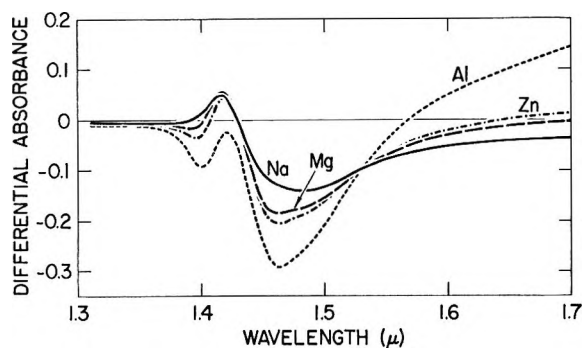


Figure 4. Difference spectra of the 2 *M* aqueous perchlorate solutions measured *vs.* water at 20°. The cell path lengths were 0.05 cm.

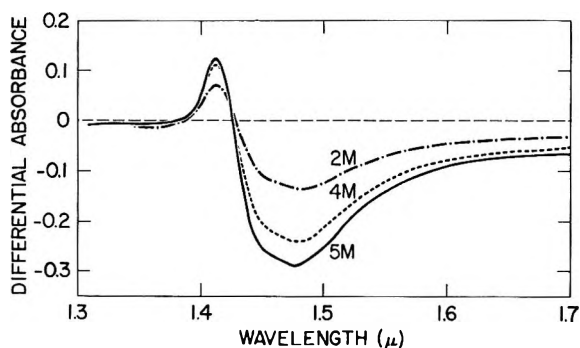


Figure 5. Difference spectra of aqueous sodium tetrafluoroborate solutions measured *vs.* water at 20°. The cell path lengths were 0.05 cm.

dronium and hydroxide ions have broad absorption bands in the long wavelength region of the water spectrum. We measured the pH's of the 2 *M* perchlorate solutions and they were: Al, 1.0; Zn, 4.0; Mg, 8.1; while NaClO₄ solution was nearly neutral. Hence, instead of the negative component, being proportional to the excluded volume, increasing in the order Al > Zn > Mg > Na throughout the spectral region the reverse sequence is obtained in the longer wavelength region. The high-frequency positive peak is only slightly affected by the cation change. The position of the peak is 1.416 μ (7063 cm⁻¹) for Na and Mg perchlorates and 1.419 μ (7049 cm⁻¹) for Zn and Al perchlorates. The change in frequency (~15 cm⁻¹) for a change in the cationic charge (+1 to +3) is negligible enough to be nothing more than a secondary effect due to the cations. The difference spectra for the tetrafluoroborate solutions are similar to NaClO₄ difference spectrum except for the fact that the high-frequency positive peak is at 1.412 μ (7081 cm⁻¹) instead of the 1.416 μ.

C. Temperature and Concentration Difference Spectra for Aqueous NaClO₄. In Figure 6 are shown the difference spectra obtained by varying the concentration of NaClO₄ in the sample cell while keeping the reference solution at a constant concentration. The effect of concentration is not to change the features but

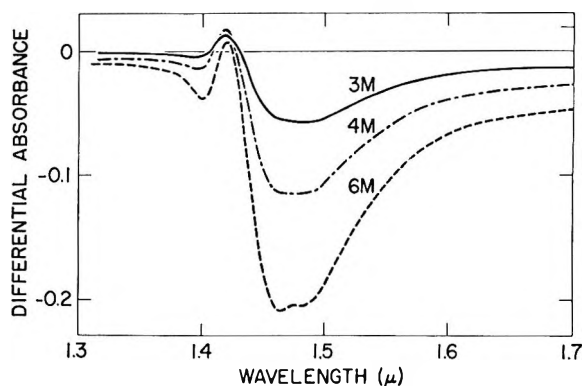


Figure 6. Effect of change in concentration on the difference spectra of aqueous sodium perchlorate at 20°. The reference cell contained a 2 *M* solution and the sample cell, 3, 4, and 6 *M*. The cell path lengths were 0.05 cm.

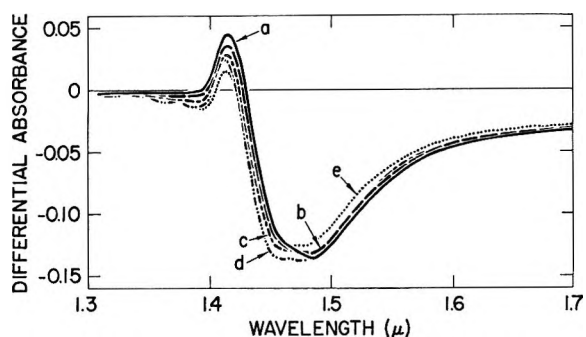


Figure 7. Effect of temperature on the difference spectrum of 2 *M* sodium perchlorate solution *vs.* water: a, 20°; b, 30°; c, 39.6°; d, 49.2°; e, 59.8°. The cell path lengths were 0.05 cm. The sample and reference cells were maintained at the same temperature in each case.

only to intensify or diminish the changes. The positive peak at 1.416 μ is invariant with concentration. Figures 7 and 8 show the simultaneous effect of temperature and perchlorate addition. With the same or different temperatures in reference and sample cells, addition of perchlorate is seen to complement the effect of temperature. While there are intensity changes, no frequency change is noticed. This suggests that the perchlorate anion disrupts water structure in the *same* manner as temperature does. This would also suggest that bonding interactions between ClO₄⁻ and water are very weak.

D. Analysis and Assignments. The most important question we address ourselves to is the nature of the interaction between the ClO₄⁻ and BF₄⁻ ions and water. To determine this we need a parameter which represents such interactions directly. In an earlier study,⁶ we made use of the concept of "excluded volume" in determining the hydration of alkali halides in aqueous solutions. Using the same approach, we attempted to derive "hydration spectra" for the ClO₄⁻ and BF₄⁻ salts. The hydration of halide anions and several cations is well established. However, it

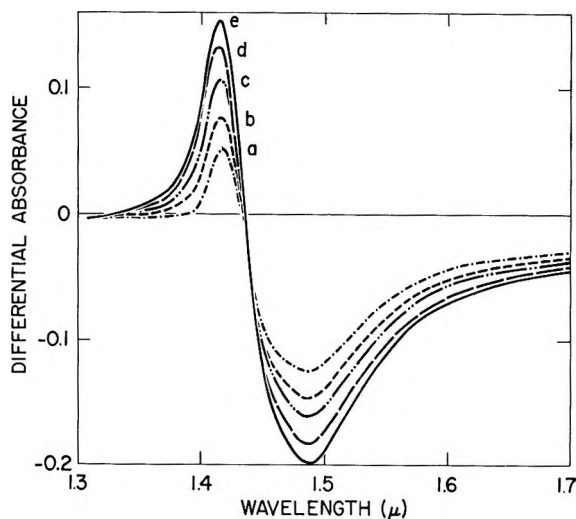


Figure 8. Difference spectra of 2 M sodium perchlorate solutions at several temperatures vs. water at 20°. The cell path lengths were 0.05 cm. Key: a, 20°; b, 30.1°; c, 40.1°; d, 51.2°; e, 60°.

is still not clear whether or not the ClO_4^- and BF_4^- are hydrated.^{4,5,12,13} An examination of the difference spectra and pH measurement of all the solutions indicate that except for NaClO_4 , all other solutions studied were either acidic or basic, thereby contributing some absorption in the long wavelength tail of the difference spectra. It is difficult to evaluate such absorption quantitatively and hence we have derived "hydration spectrum" only for NaClO_4 . We will use the hydration spectrum of NaClO_4 to draw inferences with regard to other solutions. The positive peak in the high-frequency region of the difference spectra of perchlorates (Figure 4) could arise either from hydration of perchlorate or from an excess production of singly bonded water.⁷

Figure 9 describes the resolution of the difference spectrum for 2 M NaClO_4 , curve a, into two arbitrary component spectra, one (curve b) representing the net contribution of the absorption by water in the reference cell. This was effected with the help of the Varian Spectro System 100 Computer and a duPont Model 310 Curve Resolver. Curve b has the same shape as the spectrum of normal water and by definition it is the excluded volume spectrum. Curve c is the hydration spectrum.¹⁴ We shall define curve c as the "apparent hydration spectrum" pending the settlement of the question whether the perchlorate ion is hydrated or not.

In Figure 10 we have shown the resolution of the "apparent hydration spectrum" for 2 M NaClO_4 into component Gaussian curves B and C. The appropriate Gaussian distribution parameters are as follows: curve B (1) absorption maximum, ν_0 , equal to $7050 (\pm) 5 \text{ cm}^{-1}$ (1.419μ), (2) absorbance at ν_0 , $A\nu_0$, equal to 0.27; and (3) half-band width $\Delta\nu_{1/2}$, $225 \pm 10 \text{ cm}^{-1}$; curve C (1) ν_0 equal to $6816 \pm 5 \text{ cm}^{-1}$ (1.467μ); (2)

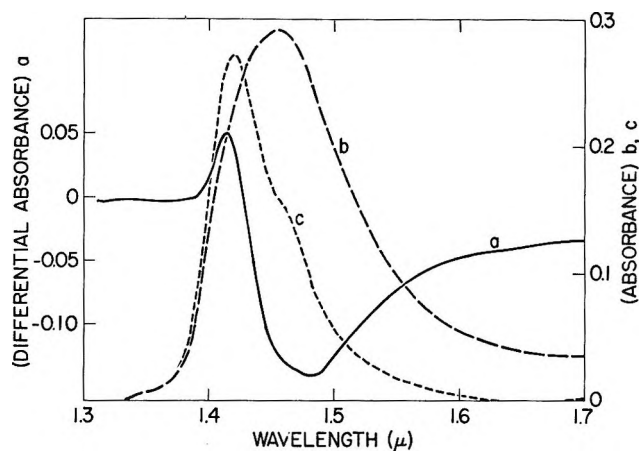


Figure 9. Determination of the excluded volume and "apparent" hydration spectrum for 2 M NaClO_4 . Curve a is the difference spectrum for 2 M NaClO_4 measured vs. water; the optical path length was 0.05 cm and the cells were thermostated at 20°. Curve b is the normalized water spectrum determined by normalizing the spectrum for water measured vs. empty cell (curve H_2O in Figure 1) to curve a at 1.68μ . Curve c is the "apparent" hydration spectrum for 2 M NaClO_4 . Curve b is negative but plotted in the positive sense. The algebraic sum of curves c and b produces curve a.

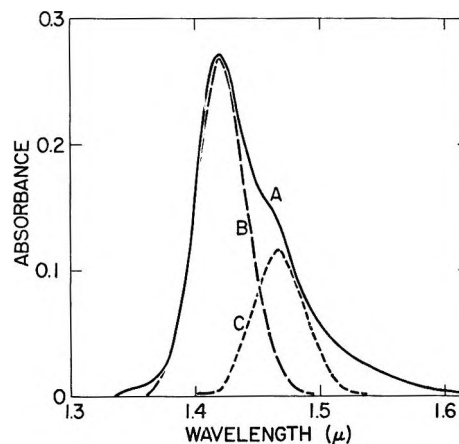


Figure 10. The resolution of the "apparent" hydration spectrum for 2 M NaClO_4 into two components. Curve A is the hydration spectrum for 2 M NaClO_4 ; it is the same as curve c in Figure 9. The appropriate Gaussian distributions of absorption parameters are listed in the text.

$A\nu_0$ equal to 0.116, and (3) half-band width $\Delta\nu_{1/2} = 214 \pm 10 \text{ cm}^{-1}$. These curves have been compared with the absorption parameters for anion and cation hydrates,⁶ singly bonded water in acetone and the high frequency peak of water in the temperature difference spectra for water⁷ in Table I. The "C" curve in the present study is in agreement with sodium ion hydrate in the previous study⁶ and hence we assign it to sodium ion hydrate. The "B" curve

(12) K. A. Hartman, Jr., *J. Phys. Chem.*, **70**, 270 (1966).

(13) P. Dryjanski and Z. Kecki, *Rocz. Chem.*, **44**, 1141 (1970).

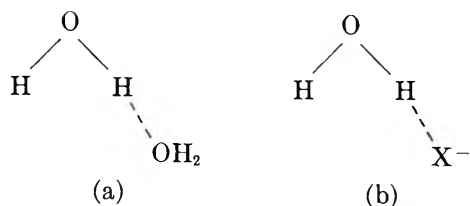
(14) For more details regarding the procedure, see ref 6.

has absorption parameters closely similar to the singly bonded water in acetone with regard to frequency and bandwidth and resembles the halide anion hydrate in bandwidth while differing in frequency.

Table I: Absorption Parameters for Some Spectral Component Curves

Spectral component	Cm ⁻¹		Reference
	Absorption maximum ν_0	Half-band width $\Delta\nu^{1/2}$	
Water in acetone peak	7075	200	7
High-frequency peak in temperature difference spectra for water ("B" curves)	7081 ± 5	216 ± 10	7
Halide anion hydrate	6997	212	6
Sodium ion hydrate	6800	200	6
Sodium perchlorate hydration spectrum			
"B" curve	7050 ± 5	225 ± 10	This work
"C" curve	6818 ± 5	214 ± 10	This work

On the basis of this comparison, one could assign the "B" curve in Figure 10 to singly bonded water produced by the perchlorate addition or to water weakly H-bonded⁵ to the perchlorate anion. We have assigned⁷ the following structures for the singly bonded water (a) absorbing at 7080 cm⁻¹ (in comparison with singly bonded water in acetone absorbing at 7075 cm⁻¹) and halide anion hydrate (b) absorbing at 6997 cm⁻¹. The lower frequency of absorption of b relative



to a is easy to reconcile since it is known from the Raman spectral studies of Kecki, *et al.*,¹⁵ that halide anions form stronger bonds with water than water molecules do between each other. Kecki, *et al.*,¹⁵ also give an order for the strength of the water-anion bonds: I⁻ > Br⁻ ≈ CCl₃COO⁻ > Cl⁻ > NO₃⁻ > F⁻ ≈ H₂O > ClO₄⁻. It is clear from the above series that water-perchlorate H bonds are weaker than water-water H bonds and hence the "B" curve in Figure 10 with absorption maximum at 7050 cm⁻¹ cannot arise from water-perchlorate H bonds since such bonds would result in the shifting of the frequency of absorption maximum of the "B" curve to greater than 7075 cm⁻¹. On the other hand, if one considers that the effect of perchlorate is to convert doubly bonded water into singly bonded water, the "B" curve would account for this. The "B" curve differs in frequency from that of

singly bonded water by 25 cm⁻¹ toward the lower frequency side. This can be explained as a medium effect arising from the electrostatic field of the Na⁺ and ClO₄⁻ ions. It must be emphasized however, that the delimitation between ion-dipole interaction and hydrogen bond is not sharp.

Brinck and Falk⁵ have favored assigning the high-frequency peak in their studies of the effect of perchlorate on HDO in liquid water to a weak ClO₄⁻ H₂O H-bond in analogy with studies of NaClO₄·H₂O in the solid state, wherein the water-perchlorate interactions seem to satisfy the geometric criteria of hydrogen bonding.¹⁶ There are other evidences which indicate that the perchlorate ion is not H-bonded to the water in aqueous solution. Walrafen's Raman spectral studies⁴ indicate that the ClO₄⁻ ion is a strong structure-breaker and that it is not hydrated appreciably. Walrafen concludes⁴ that "nondirected ionic interactions between ClO₄⁻ and water would thus be consistent with the failure to observe Raman bonds characteristic of hydrated ClO₄⁻ ions." Samoilov reports¹⁷ that the Cl-O stretching frequency is 1085 cm⁻¹ in NaClO₄·H₂O (where the water is H bonded to the ClO₄⁻ ion) whereas in both anhydrous NaClO₄ and in aqueous solution of NaClO₄ the frequency is 1115 cm⁻¹, suggesting that the ClO₄⁻ ion in aqueous solution is not H-bonded to water. It is interesting to note that so far no complex of a transition metal with perchlorate as the ligand has been reported.¹⁸ Inasmuch as the tendencies to function as a ligand in complex formation and as an acceptor in an H-bond are interrelated we conclude that ClO₄⁻ does not form an H-bond with water in solution.

It was suggested by Kecki and Dryjanski¹³ that the high-frequency peak in the infrared spectrum of HOD in liquid water in the presence of NaClO₄ could be due to water molecules trapped between anion and cation without H bonding to the anion. From our studies it is evident that the high-frequency peak in the difference spectra (Figure 4) shifts only by 15 cm⁻¹ as the charge on the cation is increased from 1 to 3. It is known¹⁹ that highly charged cations form partially covalent bonds with water molecules which are most likely to produce significant effects on the OH and OD stretching frequencies. The reasoning of Kecki and Dryjanski would be valid only if the water molecule is trapped between the cation and perchlorate physically

(15) Z. Kecki, J. Witanowski, K. Akst-Lipszyc, and S. Minc, *Rocz. Chem.*, **40**, 919 (1966).

(16) G. Brinck and M. Falk, *Can. J. Chem.*, **43**, 2096 (1970).

(17) O. Ya Samoilov, "Water in Biological Systems," L. P. Kayushin, Ed., Consultants Bureau, New York, N. Y., 1969, p 25.

(18) F. A. Cotton and G. Wilkinson, "Advanced Inorganic Chemistry: A Comprehensive Text," Interscience, New York, N. Y., 1962, p 450.

(19) (a) D. E. Irish, B. McCarroll, and T. F. Young, *J. Chem. Phys.*, **39**, 3436 (1963); (b) R. E. Hester, R. A. Plane, and G. E. Walrafen, *ibid.*, **38**, 249 (1963).

without getting involved in a chemical interaction. It is difficult to see how that can be so.²⁰

We have also studied CF_3COONa solutions. The difference spectra lacked the feature of a high-frequency positive peak, found in the perchlorate and tetrafluoroborate solutions. Kecki and Dryjanski reported¹³ that the ClO_4^- , BF_4^- , and CCl_3COO^- ions behave in a similar manner in affecting water structure, since these three ions give rise to very strong acids. Our studies agree with this conclusion except for the fact that with CF_3COO^- ions, the effect is not very predominant as is the case with ClO_4^- and BF_4^- . The size of the ions may be a factor insofar as the sizes of ClO_4^- and BF_4^- are almost the same, and they would be expected to behave similarly; also both the ions have a low surface charge density.

In the absence of knowledge about the hydronium and hydroxyl absorption contribution in the long-wavelength region of the spectra, we are not reporting the hydration spectra for NaBF_4 and CF_3COONa . However, we made qualitative resolutions and the two component curves, as in the case of NaClO_4 (Figure 10) were obtained. The sodium ion hydrate curve is common in all the three cases at the same frequency and with the same bandwidth while the "B" curve not differing in bandwidth from that for NaClO_4 , changes in frequency. The ν_0 for CF_3COONa "B" curve is 7042 cm^{-1} and for NaBF_4 it is 7075 cm^{-1} . These differences could arise from small differences in the ionic fields.

Mention must be made about the causes of the appearance of the shoulder in the direct spectra of the perchlorate and tetrafluoroborate solutions. Since the shoulder does not shift observably in frequency with increase of temperature and change of cation

and it does appear in a high-temperature pure water spectrum,⁷ it must be a property of water structure influenced but not caused by the ClO_4^- and BF_4^- anions. It is not due to a cation hydrate since highly charged cations shift²¹ the OH stretch frequencies of the hydrated water molecules in addition to the effect due to H bonding of the hydrated water with anions. This effect of the cations is also observed in the nmr study of the aqueous solutions of highly charged cations where separate resonances for bulk and hydrated water are obtained,²² the hydrated water resonance appearing at a lower field than the bulk water resonance. In our studies⁷ on the effect of temperature on the structure of water, we could not assign a spectral component centered at $1.46\ \mu$ to any specific species. It was a temperature-invariant component and in accordance with the observation of Luck²³ we assign the shoulder component at $1.46\ \mu$ to some energetically unfavorable H bonded species of water. The shoulder appears only in solutions containing non-H-bonding anions since, if the anions H bond with water, the absorption maxima are shifted towards longer wavelength with concomitant disappearance of the shoulder.

Acknowledgment. This work was supported in part by a Public Health Service research grant (GM15188) from the National Institutes of Health and a National Science Foundation grant (GB29023).

(20) (a) S. Subramanian and H. F. Fisher, *Rocz. Chem.*, **45**, 933 (1971); (b) Z. Kecki and P. Dryjanski, *ibid.*, **45**, 937 (1971).

(21) I. Gamo, *Bull. Chem. Soc. Jap.*, **34**, 760 (1961).

(22) A. Fratiello, R. E. Lee, V. M. Nishida, and R. E. Schuster, *J. Chem. Phys.*, **48**, 3705 (1968).

(23) W. A. P. Luck, "Physico-Chemical Processes in Mixed Aqueous Solvents," F. Franks, Ed., Heinemann, London, 1968, Chapter 2.

The Ion-Product Constant of Water to 350°¹

by James R. Fisher² and H. L. Barnes*

*Department of Geochemistry and Mineralogy, Pennsylvania State University, University Park, Pennsylvania 16802
(Received July 9, 1970)*

Publication costs assisted by the Ore Deposits Research Section, Pennsylvania State University

The ion-activity product of water, K_w^0 , has been determined to 350° along the liquid-vapor curve from conductance measurements made between 100 and 350° on aqueous solutions in the system acetic acid-ammonium acetate-ammonia. Derivation of K_w^0 requires data on the limiting equivalent conductivities of acetic acid, ammonia, and ammonium acetate, the ionization constants of acetic acid and ammonia, and of the conductivities of pairs of these solutes at a series of concentrations. The limiting equivalent conductivities were indirectly obtained from literature data on the limiting equivalent conductivities of HCl, NaCl, NaOH, NH₄Cl, and NaOAc. The ionization constants of acetic acid were obtained from our conductance measurements combined with literature data; constants for ammonia were obtained from the literature. From our conductivities, values of K_w^0 were obtained between 100 and 350°; these were combined with well established literature values and the combined set analytically smoothed to provide a consistent set of molal constants from 25 to 350°; respective p*K*'s at 150, 250, and 350° are: for H₂O, 11.64, 11.05, and 11.42; for HOAc, 5.22, 5.95, and 7.68; and for NH₄OH, 5.11, 5.91, and 7.30.

Introduction

Interest has developed in recent years in the properties of aqueous solutions at elevated temperature and pressure and in the interactions of these solutions with gases and solids. In addition to their basic physico-chemical interest, the properties of hydrothermal solutions are pertinent to saline water conversion technology, steam power generation, the problems of water-cooled and homogeneous nuclear reactors, growth of crystalline materials for solid-state research, and to the geologic processes of metamorphism and formation of ore deposits.

The object of this study was to reinvestigate the temperature dependence of the ion-activity product of pure water, K_w^0 , using electrical conductance measurements on aqueous solutions along the liquid-vapor curve between 100 and 350°, and to combine these results with other well established values to provide a consistent set of constants from 0 to 350°.

Previous Investigations. At the turn of the century, Noyes³ and his coworkers used electrical conductance measurements to explore hydrolytic equilibria in the system acetic acid-ammonium acetate-ammonia and to extract from these data values for K_w^0 at several temperatures between 100 and 306°. Great pains were taken in the collection and analysis of their data, but reduction to limiting equivalent conductivities and ionization constants was impaired by the lack, at that time, of a consistent and well grounded theory of electrolytic solutions.

Three decades later, Harned and his students⁴ derived K_w^0 from emf measurements on solutions of the halogen acids and alkali halides in cells without liquid junction. Their measurements between 0 and

60° have been reviewed and a consistent set of K_w^0 values presented by Harned and Robinson.⁵

Ackermann⁶ measured the heat capacity of solutions of HCl, NaOH, and NaCl between 10 and 120°, from which he was able to derive the sum of the partial molal heat capacities of the hydrogen and hydroxyl ions. These, combined with the heat capacity of liquid water, permit calculation of the temperature variation of ΔC_p^0 of ionization. Using Harned and Robinson's values of $\Delta H^0(298)$ and $\Delta S^0(298)$ of ionization as base values, he then calculated $\Delta H^0(T)$, $\Delta S^0(T)$, and so K_w^0 to 120°.

The low-temperature data of Harned and Robinson and Ackermann are in excellent agreement and together form an adequate set of K_w^0 values from 0 to 100°. Clever⁷ has recently reviewed the thermodynamics of water ionization, discussing these results in more detail.

We have used the same basic methods as in the early work of Noyes: the conductance of solutions of ammonium acetate and in ammonium acetate-acetic acid mixtures was measured at six temperatures be-

(1) Contribution No. 69-64, College of Earth and Mineral Sciences, The Pennsylvania State University. This research was supported by the Office of Saline Water, U. S. Department of the Interior, under Grant No. 14-01-0001-408.

(2) U. S. Geological Survey, Washington, D. C. 20242.

(3) A. A. Noyes, *et al.*, "The Electrical Conductivity of Aqueous Solutions," Publication 63, Carnegie Institution of Washington, Washington, D. C. 1907.

(4) H. S. Harned and B. B. Owen, "The Physical Chemistry of Electrolytic Solutions," 3rd ed, Reinhold, New York, N. Y., 1958.

(5) H. S. Harned and R. A. Robinson, *Trans. Faraday Soc.*, **36**, 973 (1940).

(6) T. Ackermann, *Z. Elektrochem.*, **62**, 411 (1958).

(7) H. L. Clever, *J. Chem. Educ.*, **45**, 231 (1968).

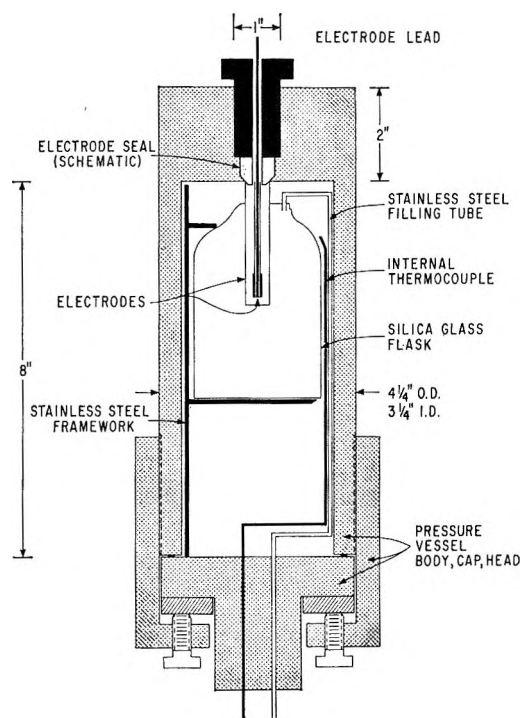


Figure 1. Design of the pressure vessel used to contain the silica glass flask and platinum electrodes for conductance measurements. During measurements, the vessel is operated in a vertical position with the electrodes at the top.

tween 25 and 350°. These data are interpreted here to derive K_w^0 using our data plus literature values for the limiting equivalent conductivities of acetic acid, ammonia, and ammonium acetate, as well as the ionization constants of acetic acid and ammonia.

Experimental Methods

The 1-l. pressure vessel (Figure 1) is constructed of stainless steel, chrome-plated within. Two concentric electrodes, described below, are sealed into the center of the upper end of the vessel. An internal thermocouple and a filling tube enter through two ports in the base of the vessel and are sealed using conventional high-pressure, cone-in-cone fittings. Externally, the filling tube is connected to a two-way valve which permits sequential evacuation of the vessel and introduction of solution. To minimize contamination, solutions are contained within the vessel in a 250-ml silica glass flask, supported on a stainless steel framework. The electrodes project from the top of the vessel through the neck of the flask into the solution. The end of the filling tube projects over the lip of the flask and so discharges solution directly into it.

Electrode Assembly. The electrode assembly (Figure 2) consists of an outer cylinder of 90 Pt-10 Ir alloy in contact with the body of the vessel, maintained at ground potential. It is supported on a 316 ss. piece sealed by the outer thrust bolt.

The central electrode post, of dense, high-purity

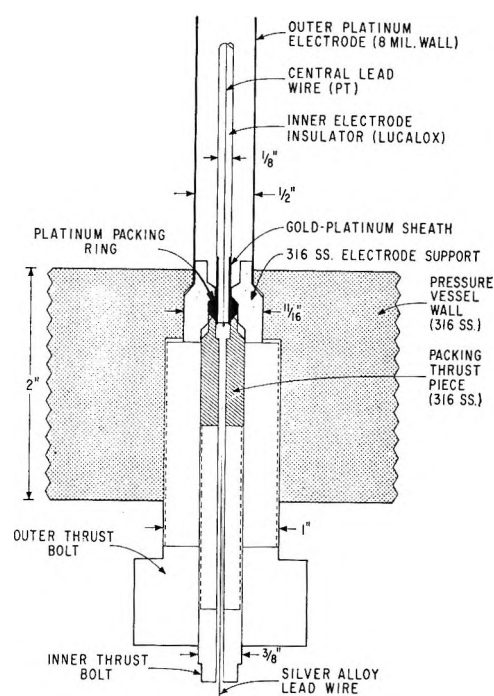


Figure 2. Detailed configuration of the platinum electrode assembly and pressure seal. The assembly as shown here is inverted with respect to actual operating position.

alumina (General Electric Lucalox) is partially sheathed at each end by platinum tubing. The sheath at the end inside the vessel is welded to a central platinum lead wire and serves as the inner electrode; the sheath at the other end serves as a bearing surface for the platinum packing ring. The electrode is assembled by first swaging half-inch lengths of 10-mil-wall gold tubing over each end of the Lucalox tube; the tube is encapsulated in close-fitting platinum tubing, and the ends of the tubing crimped and welded. The sealed assembly is placed in a pressure vessel and heated to 1150° under a hydrostatic gas pressure of about 5000 bars. The gold, molten under these conditions, alloys with the platinum and is forced into surface irregularities in the Lucalox, thereby bonding the platinum to the insulator. The central section of platinum tubing, around the waist of the post, is next cut away, leaving the gold-bonded sheaths at each end. A length of platinum wire, to act as a lead to the exterior of the vessel, is crimped to the basal end of the central platinum lead and insulated by a hollow ceramic tube.

The electrodes are sealed into the vessel wall in two stages. The shoulder of the outer electrode support piece is forced against the internal chamfer in the vessel wall by advancing the outer thrust bolt. The inner bolt is then advanced, causing the packing thrust piece to bear against the platinum packing ring. The transmitted force seals the outside of the packing against the outer electrode support piece and also causes it to seize and seal around the basal sheath. The electrodes are lightly platinized to eliminate

polarization at their surfaces and the resulting dependence of conductance on frequency.

The cell constant was determined by measurement of the conductance at 25° of solutions of KCl of several concentrations. The measured conductances were reduced to equivalent conductivities using known solution concentrations and the equation of Lind, Zwolenik, and Fuoss;⁸ the mean cell constant was $0.0870 \pm 0.0009 \text{ cm}^{-1}$. The calculated effect of the thermal expansion of platinum on the cell constant was less than 0.5% at 350°; therefore, the 25° cell constant was used throughout.

The impedance bridge used in this work was a General Radio Type 1608-A in combination with a variable frequency R-C oscillator and a tuned amplifier with null detector (General Radio Types 1210-C and 1232-A). Conductance measurements were made at 10 kHz; at this frequency, the uncertainty is stated in the manufacturer's specifications to be less than 0.5%.

Temperature Measurement. Temperature was measured using two chromel-alumel thermocouples, an external one inserted in a well in the cap of the vessel and an internal one as shown in Figure 1. The output of these thermocouples was fed to a multichannel recorder on which the approach to temperature and thermal equilibration could be continuously monitored; the internal sensor provided the temperatures of the conductance measurements. Thermocouple output was measured using a precision potentiometer, associated guarded dc power supply, null detector (Honeywell, Models 2784, 2890-11, and 104W1-G, respectively), and newly calibrated standard cell.

The internal thermocouple was calibrated at 28 points between 20 and 400° against a four-lead platinum resistance thermometer (Rosemount Engineering Co., Model 104-T), the resistance of which was measured with a Mueller bridge (Honeywell, Model 1551). The calibration accuracy of the platinum thermometer is stated by the manufacturer to be ± 0.028 , 0.056, and 0.076° at 0, 100, and 260°, respectively. The thermocouple calibration data was fitted to a fifth-degree polynomial by which later experimental emf's were converted to temperatures. The estimated total uncertainty in our measured temperatures is within $\pm 0.25^\circ$.

Preparation of Solutions. Water to be used for stock and experimental solutions was drawn by vacuum from a tin still into a Pyrex reservoir, degassed under reduced pressure for several hours, and stored under purified nitrogen. Water from the reservoir flowed into a silica glass boiling flask where it was distilled, under nitrogen, through a silica combustion tube heated to about 800° to ignite organic matter to CO₂. The effluent was condensed in a vertical section of silica tubing in a counter-current flow of nitrogen which swept volatile species through a pressure-con-

trolling water trap. This condensate then fed a final two-stage silica glass still (Heraeus, Model B-3) whose effluent was piped through silica tubing to a nitrogen-filled leucite glove box, where it was collected in a silica glass flask. At no stage in the process was the distillate in contact with anything but silica glass and purified nitrogen. The water produced had, at 25°, a specific conductance of about $2.5 \times 10^{-7} \text{ ohm}^{-1} \text{ cm}^{-1}$.

The solutions of acetic acid and ammonium acetate used in this work were prepared from ultrapure glacial acetic acid and concentrated aqueous ammonia (E. Merck AG Suprapur, Items No. 55 and 5428).

The stock of 10% HOAc was analyzed by potentiometric titration with aqueous NaOH, previously standardized against 99.98% potassium hydrogen phthalate. A 2% aqueous ammonia stock solution was analyzed by first neutralizing a weighed quantity with excess standard HCl (standardized gravimetrically as AgCl and by potentiometric titration against standard NaOH), followed by potentiometric titration of the excess HCl with standard NaOH. The standard error of the means of the NaOH, HCl, HOAc, and NH₃ analyses were, respectively, 0.04, 0.007, 0.02, and 0.1%.

A solution to be used in an experimental run was prepared within the inert-atmosphere glove box by diluting a known weight of stock solution(s) with a known weight of conductivity water. The solution was transferred to a separatory funnel fitted with a vacuum stopcock for later loading into the pressure vessel.

To load a solution into the vessel, the stoppered separatory funnel containing solution was connected to the external end of the vessel filling tube of Figure 1. The entire system was then evacuated, from the vessel interior to the base of the funnel stopcock. At about 100 μ , the valve to the pump was closed, the funnel stopcock opened, and the solution drawn into the vessel and discharged into the silica flask.

Conductance Measurements. At the beginning of each experimental run, the solution conductance was measured at 1 and 10 kHz to test the continuing effectiveness of the platinization in reducing the dependence of conductance on frequency. If the frequency dependence was greater than 0.5% of the conductance, the cell was replatinized.

Conductance-temperature data were normally obtained at several temperatures about 25°; the vessel and its contents were then heated successively to 100, 150, 200, 250, 300, and 350°. In the vicinity of each temperature, conductance-temperature data were taken at three points bracketing the temperature of interest and covering an interval of about 10°. This procedure allowed the conductance at the temperature of interest to be obtained by interpolation.

(8) J. E. Lind, J. J. Zwolenik, and R. M. Fuoss, *J. Amer. Chem. Soc.*, **81**, 1557 (1959).

On heating the solutions from 25 to 350°, their volumes nearly doubled, causing them to overflow the silica flask into the base of the vessel. Contraction on cooling from 350° lowered the solution level in the flask and decreased the depth of immersion of the electrodes to such an extent as to make useful measurements impossible after cooling through a decrease in volume of 30%, approximately the change between 350 and 200°. In addition, minimum duration of runs was desirable, particularly at the higher temperatures, due to the possibility of leaching contaminants from the flask or electrodes, or of catalytic decomposition of the solute at the platinum black surface of the electrodes. Consequently, only data taken on the heating portion of a run were used in subsequent calculations.

Results and Discussion

In the Appendix, an outline is given of the method used to calculate K_w^0 from conductance measurements on solutions of the conjugate salt of a weak acid and base and on mixed salt-acid solutions. This method requires data first on the temperature variation of the limiting equivalent conductivities (Λ^0) of acetic acid, ammonia, and ammonium acetate and of the molar ionization constants of acetic acid and ammonia.

Limiting Equivalent Conductivities. The necessary Λ^0 's as functions of temperature were calculated from literature data^{3,9} on the Λ^0 's of HCl, NaOAc, NaCl, NH_4Cl , and NaOH using

$$\Lambda^0(\text{HOAc}) = \Lambda^0(\text{HCl}) + \Lambda^0(\text{NaOAc}) - \Lambda^0(\text{NaCl}) \quad (1a)$$

$$\Lambda^0(\text{NH}_4\text{OH}) = \Lambda^0(\text{NH}_4\text{Cl}) + \Lambda^0(\text{NaOH}) - \Lambda^0(\text{NaCl}) \quad (1b)$$

$$\Lambda^0(\text{NH}_4\text{OAc}) = \Lambda^0(\text{NH}_4\text{Cl}) + \Lambda^0(\text{NaOAc}) - \Lambda^0(\text{NaCl}) \quad (1c)$$

Noyes' data were recalculated using Shedlovsky's¹⁰ equations and the Fuoss-Onsager¹¹ equation; the resulting Λ^0 's are averaged with those from similar calculations by Wright, Lindsay, and Druga.¹² The best values are in good agreement with those reported by Wright, *et al.*; serious disagreement with Noyes' old values exists only above 218°.

For calculation of Λ^0 's at temperatures of interest, polynomials in $\log \eta_{\text{H}_2\text{O}}$ were fitted by least squares to $\log \Lambda^0$. Using the viscosity of water, $\eta_{\text{H}_2\text{O}}$, at the appropriate temperatures,¹³ best fitting polynomials were determined by analysis of variance

$$\text{HCl: } \log \Lambda^0 = 0.79831219 - 1.1343866 \log \eta + 0.11776594 \log^2 \eta$$

$$\text{NaOAc: } \log \Lambda^0 = -0.07117134 - 0.98542553 \log \eta$$

$$\text{NaCl: } \log \Lambda^0 = 0.2404355 - 0.90786961 \log \eta$$

$$\text{NH}_4\text{Cl: } \log \Lambda^0 = 0.39116439 - 0.87074107 \log \eta$$

$$\text{NaOH: } \log \Lambda^0 = 0.53554921 -$$

$$1.0301125 \log \eta + 0.0597795 \log^2 \eta$$

and are shown in Figure 3.

Ionization Constants of HOAc and NH_4OH . The ionization constant of acetic acid from 25 to 350° was calculated from our conductance data for nine different concentrations.¹³ To be certain that solute volatility had no important effect on HOAc molality in high-temperature runs, the data of Othmer, Silvis, and Spiel¹⁴ on liquid-vapor equilibria in the HOAc- H_2O system were used to calculate the reduction of acid concentration due to its volatility. The maximum reduction found was 0.005% and so was neglected.

The equivalent conductivity at the selected temperatures was calculated in a series of steps. For each run, the conductance-thermocouple emf data were fitted by polynomials up to the sixth degree and then a single, best fitting function was selected by analysis of variance. From these, conductances were calculated for the emf's corresponding to selected temperatures. The resulting conductances (G) were converted to equivalent conductivities (Λ) using the relation $\Lambda = 1000kG/c$ where k is the cell constant and c the molar concentration.

The paired c , Λ data at each temperature, together with the fitted Λ^0 's, were used as input to a program which calculated the ionization constant, K , at each concentration using Shedlovsky's equation. Values of $\log K$ showed a slight linear dependence on the square root of ionic strength; this dependence was most pronounced at low temperatures, being hidden in scatter at high temperatures. At those temperatures where the dependence was clear, from a straight line fit of $\log K$ against $\sqrt{\mu}$, the intercept was taken as the final K^0 . At 300 and 350°, where scatter obscured the relation, K^0 was taken to be the average of the clustered K 's. Noyes' data were also reevaluated, using his c , Λ data and the recalculated limiting equivalent conductivities. Published constants are compared in Table I with our values and those we recalculated from Noyes' data. Standard errors roughly

(9) (a) B. B. Owen and F. H. Sweeton, *J. Amer. Chem. Soc.*, **63**, 2811 (1941), for HCl; (b) A. J. Ellis, *J. Chem. Soc. (London)*, 2299 (1963), for HCl; (c) D. P. Pearson, "The Electrical Conductance of Some Aqueous Electrolytes in the Vicinity of the Critical Temperature of Water," Ph.D. Dissertation, University of Southern California, 1960, for HCl and NaCl; (d) R. A. Robinson and R. H. Stokes, "Electrolyte Solutions," Butterworths, London, 1959, for NaOAc, NaCl, NH_4Cl , and NaOH; (e) K. N. Marsh and R. H. Stokes, *Aust. J. Chem.*, **17**, 740 (1964), for NaOH.

(10) T. Shedlovsky, *J. Amer. Chem. Soc.*, **54**, 1405 (1932); *J. Franklin Inst.*, **225**, 739 (1938).

(11) R. L. Kay, *ibid.*, **82**, 2099 (1960).

(12) J. M. Wright, W. T. Lindsay, Jr., and T. R. Druga, WAPD-TM-204, 1961.

(13) J. R. Fisher, "The Ion-Product Constant of Water to 350°C.," Ph.D. Dissertation, The Pennsylvania State University, University Microfilms, Ann Arbor, Mich., No. 70-7206, 1969.

(14) D. F. Othmer, S. J. Silvis, and A. Spiel, *Ind. Eng. Chem.*, **44**, 1864 (1952).

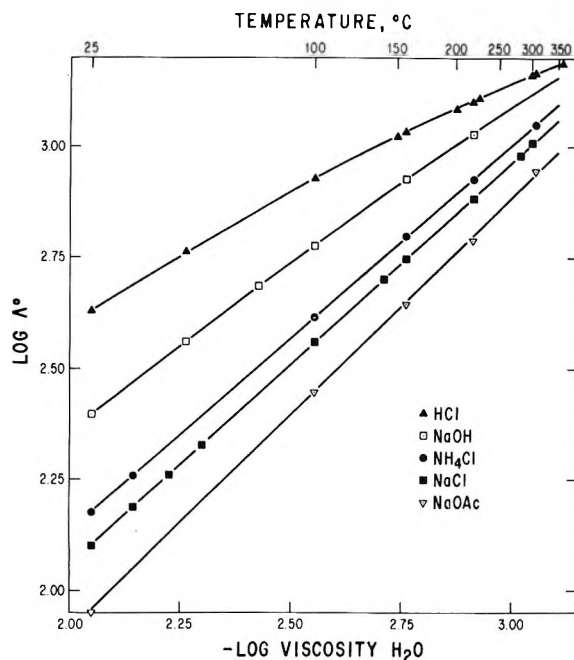


Figure 3. Limiting equivalent conductivity of several electrolytes vs. viscosity of water.

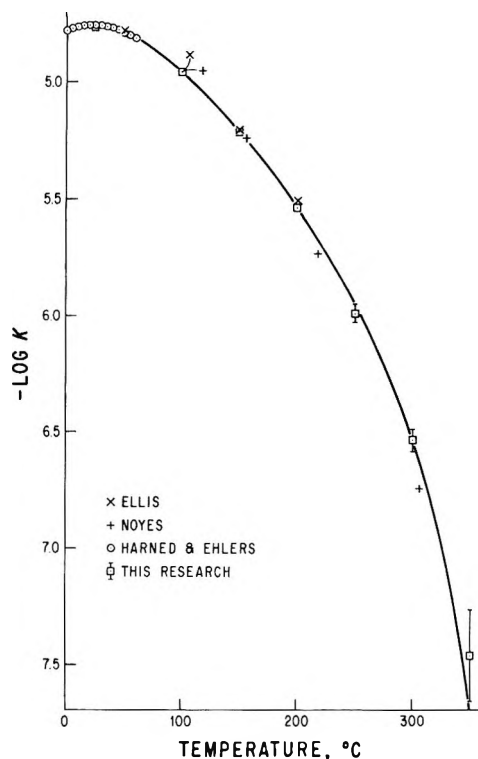


Figure 4. Temperature variation of the molal ionization constant of acetic acid along the liquid-vapor curve. Three data points at 100° are coincident; two have been displaced for clarity. The solid line represents the fit of Helgeson's equation to the data.

Published ionization constants for ammonia used in this work are summarized in Table II. Noyes' constants at 100, 156, 218, and 306° were recalculated

Table II: Ionization Constants of Ammonia

Lit. data		Best values	
$t, ^\circ\text{C}$		$t, ^\circ\text{C}$	$\text{p}K_m^\circ, M$
0	4.862 ± 0.001^a	25	4.752
5	4.830 ± 0.001	50	4.726
10	4.804 ± 0.001	75	4.76
15	4.782 ± 0.001	100	4.84
20	4.7664 ± 0.0007	125	4.96
25	4.752 ± 0.001	150	5.11
30	4.740 ± 0.001	200	5.47
35	4.734 ± 0.001	218	5.69
40	4.730 ± 0.001	225	5.68
45	4.726 ± 0.001	250	5.91
50	4.723 ± 0.001	275	6.17
71.1	4.74 ± 0.05^{12}	300	6.47
93.3	4.81 ± 0.05	306	6.70
115.6	4.92 ± 0.05	325	6.83
137.8	5.01 ± 0.05	350	7.30
160.0	5.15 ± 0.05		
182.2	5.31 ± 0.05		
204.4	5.48 ± 0.05		
226.7	5.68 ± 0.05		
248.9	5.93 ± 0.05		
271.1	6.10 ± 0.05		
293.3	6.48 ± 0.05		
100	4.87 ± 0.05^b		
156	5.18 ± 0.05		
218	5.66 ± 0.05		
112	4.86 ± 0.05^c		
167	5.21 ± 0.05		
212	5.67 ± 0.10		
249.5	5.87 ± 0.08		
280	6.13 ± 0.10		
306	6.54 ± 0.10		
326	6.85 ± 0.08		
343	7.10 ± 0.08		

^a R. G. Bates and G. D. Pinching, *J. Res. Nat. Bur. Stand.*, **42**, 419 (1949). ^b Noyes,³ recalculated. ^c A. S. Quist and W. L. Marshall, *J. Phys. Chem.*, **72**, 3122 (1968).

as for acetic acid, using his c, Λ data and Λ^0 of Table II. The data of Quist and Marshall were extrapolated to the L - V curve. Straight lines in $\log K^0$ vs. $1/T$ were fitted to linear portions of each isochore and extrapolated to intersect the L - V curve.

The parameters of Helgeson's equation were fitted to all available data (recalculated to molal units where necessary), excepting the outlying points of Wright, *et al.*, at 48.9° and Noyes at 306°. The resulting fitted parameters are

ΔH_r° (cal mol ⁻¹)	ΔS_r° (cal mol ⁻¹ K ⁻¹)	$\Delta S_{e,r}^\circ$ (cal mol ⁻¹ K ⁻¹)	a	$b \times 10^3$
1022.31	-18.3185	-3.48314	-43.3382	5.67177

and the fitted curve appears in Figure 5.

"Best" values for $\text{p}K^0$ of ammonia are given at 25-deg intervals from 25 to 350° in Table II.

Ion-Product Constants of Water. Conductance measurements were made between 25 and 350° on five

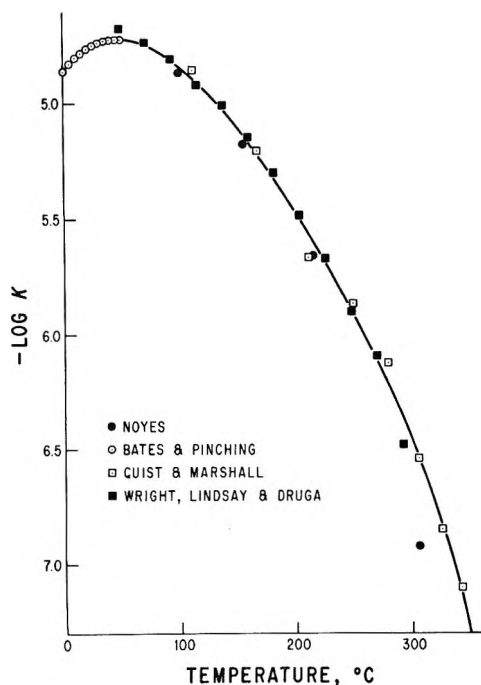


Figure 5. Temperature variation of the molal ionization constant of ammonia along the liquid-vapor curve. Data are from literature sources. The solid line represents the fit of Helgeson's equation to the data.

solutions of ammonium acetate and three salt-acid solutions; their concentrations and the conductance-emf data were recorded by Fisher¹³ and are shown in Figures 6 and 7, where the emf axis has been transformed to temperature.

During the experimental runs on the NH_4OAc -HOAc solutions of Figure 6, run AA-3 and Figure 7, considerable difficulty was encountered in obtaining stable and consistent conductance measurements at 100–200°. These unreliable data are reflected in the scatter and unlikely trend of the points in this region. For this reason, conductances for the NH_4OAc -HOAc runs in the 100–200° region were taken from the interpolated dashed portion of the curve in Figure 7. In Figure 6, curve AA-3 was located on the basis of best fit to both the data points at this concentration and isothermal plots of conductance vs. concentration.

With the above exception, the conductances of these solutions at the selected temperatures were taken from large-scale graphs of conductance against thermocouple emf. The observed background conductance of pure water was subtracted before calculating the specific conductance. The concentration variables C_B and C_A of the Appendix are, respectively, the ammonium acetate concentration and the sum of the concentrations of ammonium acetate plus acetic acid. The reduced data are given by Fisher.¹³ The sequence of calculations described in detail in the Appendix was carried out for all solutions at each temperature of interest. The resulting molar pK^0 's at each temper-

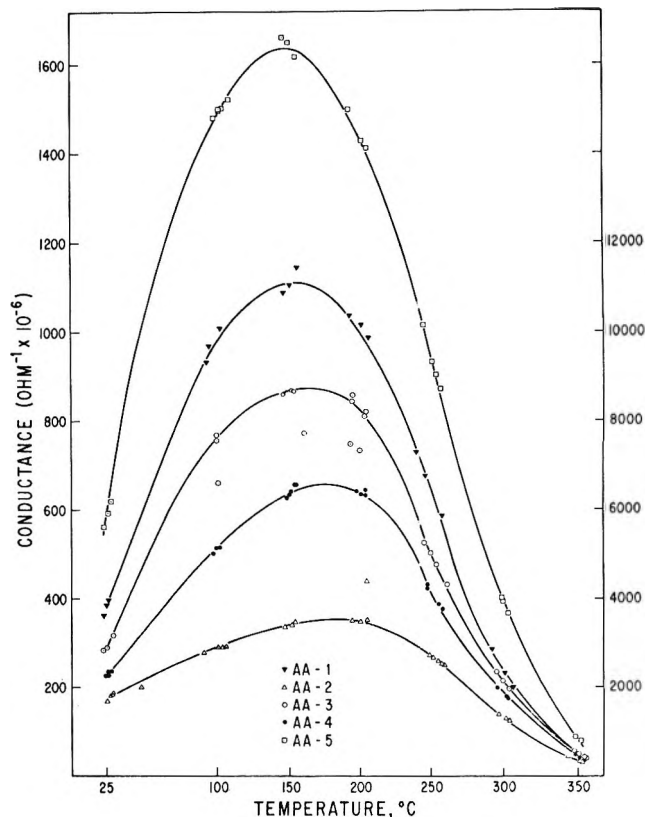


Figure 6. Conductance vs. temperature for experimental ammonium acetate runs. Conductance is shown on the right-hand ordinate for run AA-1 and on the left-hand ordinate for the other runs. The run compositions (molal) are

Run no.	HOAc	NH_4OAc
AA-1	1.248×10^{-4}	2.991×10^{-3}
AA-2	4.482×10^{-6}	1.600×10^{-4}
AA-3	1.0×10^{-7}	2.355×10^{-4}
AA-4	4.2×10^{-7}	2.091×10^{-4}
AA-5	3.8×10^{-7}	4.503×10^{-4}

ature are given in Table III. A plot of these values against temperature shows those at 150 and 200° to be high and inconsistent with all other values. Because this is the temperature region where experimental problems caused excessive scatter (Figures 6 and 7), these values are considered to be unreliable.

As with acetic acid and ammonia, the parameters of Helgeson's equation were fitted to 28 values of K_w^0 (molal) from Harned and Robinson⁵ (0–60°), Ackermann⁶ (10–120°), Noyes³ original data (converted to molal units) at 100, 156, and 218°, his point at 306° recalculated using our method, and the results of the present work at 100, 250, 300, and 350°. The agreement between our value of pK_w^0 at 300° (11.05) and that recalculated from the data of Noyes at 306° (11.04) is good; its variance from that originally given by Noyes (11.46) is most likely due to the improved values now available for the ionization constants of acetic acid and ammonia. A plot of the data used and the resulting fitted curve is given in Figure 8. The fitted parameters are

ΔH_r° (cal mol ⁻¹)	ΔS_r° (cal mol ⁻¹ K ⁻¹)	$\Delta S_{e,r}^\circ$ (cal mol ⁻¹ K ⁻¹)	a	b
13537.3	-18.633	-4.84256	-116.484	0.230895

Final values of pK_w^0 and the thermodynamic functions for the ionization reaction at 25-deg intervals from 25 to 350° are given in Table III. The values of pK_w^0 at 25 and 50° are taken from the compilation of Harned and Robinson; those at and above 75° were obtained from evaluation of Helgeson's equation using the parameters given above. The thermodynamic functions at all temperatures were calculated using the relations given by Helgeson.¹⁵

The agreement between experimental points of this study and those of Ackermann and Noyes is of interest. Our experimental pK_w^0 's at 100° and those of Ackermann and of Noyes are, respectively, 12.19, 12.259, and 12.28. The final (fitted) value is 12.25. The agreement between our result and the "accepted" value is adequate, considering the previously discussed experimental problems between 100 and 200°, and the fact that the basic sensitivity of the method is lowest at 100°, depending, as it does, on the extent of hydrolysis of NH_4OAc .

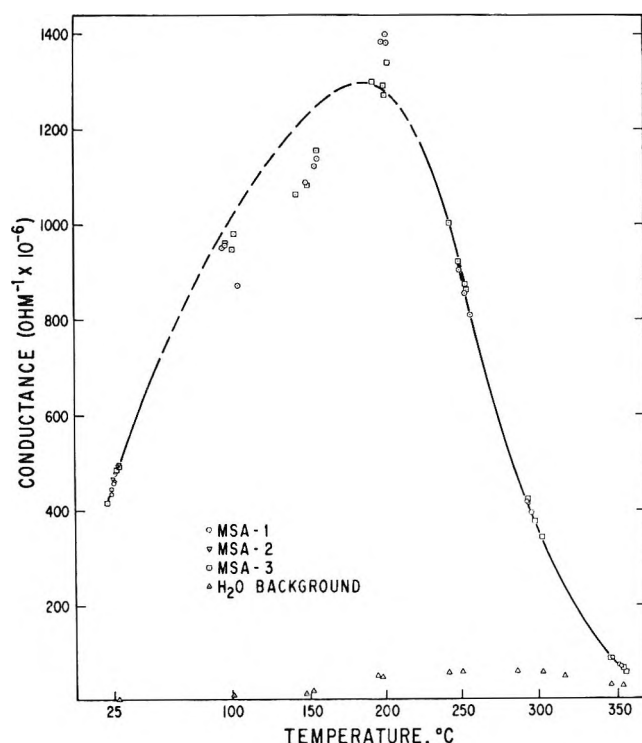


Figure 7. Conductance vs. temperature for experimental ammonium acetate-acetic acid runs. The measured background conductance of pure water is shown at the bottom of the figure. The run compositions (molal) are

Run no.	HOAc	NH_4OAc
MSA-1	3.0965×10^{-4}	3.031×10^{-4}
MSA-2	3.0653×10^{-4}	3.072×10^{-4}
MSA-3	3.0117×10^{-4}	3.024×10^{-4}

Table III: Equilibrium Constants and Free Energy Change for the Ionization of Water

t, °C	pK_w^0 , M ^a	pK_w^0 , m	ΔG° , kcal mol ⁻¹
25		13.997	19.09
50		13.262	19.61
75		12.697	20.22
100	12.23	12.26	20.92
125		11.91	21.70
150	11.22	11.64	22.53
175		11.42	23.42
200	11.20	11.26	24.37
225		11.14	25.38
250	11.23	11.05	26.45
275		11.01	27.62
300	11.33	11.04	28.94
325		11.15	30.51
350	11.90	11.42	32.57

^a Unsmoothed experimental values of this research.

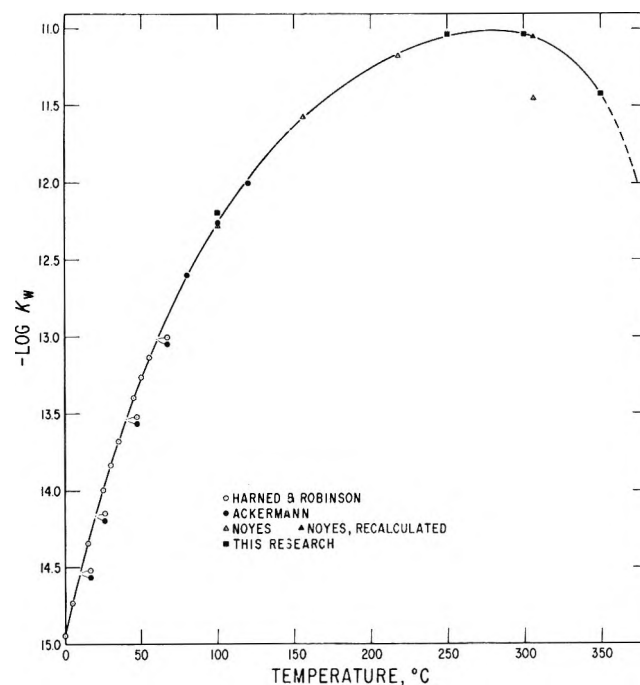


Figure 8. Experimentally determined values of the molal ion product of water. Four pairs of data points are coincident and have been displaced from the curve for clarity. The solid line represents the fit of Helgeson's equation to the data; the dashed portion represents extrapolation to the critical point.

From electrical conductance measurements on solutions in the system $HBr-NH_4Br-NH_4OH$, Quist¹⁷ has recently derived values for the ion product of water in the region 300–800°, 500–4000 bars using a similar technique but a less rigorous method of calculation (due to the lack of necessary data on the dielectric constant and viscosity of water and the limiting equivalent conductivities). Taking his stated uncertainties

(17) A. S. Quist, *J. Phys. Chem.*, **74**, 3396 (1970).

into account, extrapolation of his summary equation to the L - V curve gives pK_w^0 values which agree with ours except at our upper limit (350°) and near his lower limit (300°).

Dobson and Thirsk¹⁸ have also recently measured pK_w^0 at 100 to 200° using cmf measurements. Their values at 100, 125, 150, 175, and 200° are 12.17, 11.98, 11.72, 11.43, and 11.27, respectively, the differences from our's being -0.09 , $+0.08$, $+0.08$, $+0.01$, and $+0.01$. The agreement is within the combined uncertainties in these data and is excellent at the higher temperatures.

Appendix

Method of Calculation of K_w^0 from Conductance Data

The ion product of water, K_w^0 , may be determined from analysis of electrical conductance measurements on aqueous solutions of the conjugate salt (BA) of a weak acid (HA) and a weak base (BOH), and on mixed solutions of the salt and acid (or base).

In any salt or mixed salt-acid solution, these aqueous species will be present: H^+ , OH^- , B^+ , A^- , HA, and BOH. The following expressions formulate the equilibrium relations among the species

$$(H^+)(OH^-) = K_w^0/(\gamma_{\pm}^w)^2 = K_w \quad (A1)$$

$$(H^+)(A^-)/(HA) = K_A^0/(\gamma_{\pm}^A)^2 = K_A \quad (A2)$$

$$(B^+)(OH^-)/(BOH) = K_B^0/(\gamma_{\pm}^B)^2 = K_B \quad (A3)$$

Parentheses indicate molar concentrations. The effect of ion-pair formation between B^+ and A^- could be included using

$$(B^+)(A^-)/(BA) = K_S^0/(\gamma_{\pm}^S)^2 = K_S \quad (A4)$$

However, in the dilute solutions required, association should be negligible. The following calculations were largely developed from a similar treatment by Pearson.⁹

Mass balances on A and B provide two additional relations

$$C_A \equiv C_{HA} + C_{BA} = (A^-) + (HA) \quad (A5)$$

$$C_B \equiv C_{BA} + C_{BOH} = (B^+) + (BOH) \quad (A6)$$

where C_{HA} , C_{BOH} , and C_{BA} represent analytical concentrations of acid, base, and salt. Electrical neutrality provides

$$(H^+) + (B^+) = (A^-) + (OH^-) \quad (A7)$$

Equation A8, derived below, relates the conductivity (specific conductance) of a solution to the concentrations and equivalent conductivities of the ions present

$$L^* = (H^+)\Lambda_{acid}^i + (OH^-)\Lambda_{base}^i + [(B^+) - (OH^-)]\Lambda_{salt}^i \quad (A8)$$

For the purpose of the derivation of eq A8, each ion in solution may be conceptually "labeled" as belonging to either acid, base, or salt, whatever its actual origin.

Therefore, imagine all H^+ and an equal amount of A^- to "belong to" the acid, all OH^- and an equal amount of B^+ to the base, and all remaining B^+ and A^- to the salt. As the solution is electrically neutral, these last two concentrations must be equal. The conductivity of the solution may then be represented as

$$L_s = L_{acid}^i + L_{base}^i + L_{salt}^i \quad (A9)$$

where L_X^i represents the conductivity of the ions of substance X. Because the individual paired-ion conductivities (L_X^i) are not directly observable, they must be replaced by quantities which are, or which can be calculated from, observable quantities. This replacement is made using the general relation

$$L_X^* = 1000L_X = c_X^i\Lambda_X^i$$

where c_X^i and Λ_X^i are the molar concentration and equivalent conductivity of the ions of substance X. Equation A1 may now be rewritten

$$L_s^* = (c^i\Lambda^i)_{acid} + (c^i\Lambda^i)_{base} + (c^i\Lambda^i)_{salt} \quad (A10)$$

The concentration factors in eq A10 are replaced by appropriate ion concentrations, according to the "labeling" and "pairing" performed above

$$c_{acid}^i = (H^+)$$

$$c_{base}^i = (OH^-)$$

$$c_{salt}^i = (B^+) - (OH^-)$$

Equation A10 then becomes

$$L^* = (H^+)\Lambda_{acid}^i + (OH^-)\Lambda_{base}^i + [(B^+) - (OH^-)]\Lambda_{salt}^i \quad (A8)$$

Equations A1 to A3 and A5 to A7 may be combined and solved to yield a fourth-degree equation in (H^+) , ionization constants, and concentration variables

$$\begin{aligned} (H^+)^4K_B + (H^+)^3(K_w + K_B C_B + K_A K_B) + \\ (H^+)^2(K_w[K_A - K_B] + K_A K_B[C_B - C_A]) - \\ (H^+)(K_w K_A[C_A + K_B] + K_w^2) - K_A K_w^2 = 0 \end{aligned} \quad (A11)$$

Similarly, eq A8 may be reduced to

$$L^* = (H^+)\Lambda_{acid}^i + \frac{K_w\Lambda_{base}^i}{(H^+)} + \left[\frac{K_A C_A}{(H^+) + K_A} - (H^+) \right] \Lambda_{salt}^i \quad (A12)$$

Of the quantities appearing in eq A11 and A12, C_A , C_B , and L^* are calculated from the composition and conductance of each solution, Λ_{acid}^i , Λ_{base}^i , and Λ_{salt}^i are calculated from the known limiting equivalent conductivities and ionic strength using Shedlovsky's equation¹⁰

(18) J. V. Dobson and H. R. Thirsk, *Electrochim. Acta*, **16**, 315 (1971).

$$\Lambda^i_X = (\Lambda^0_X)^2 / [\Lambda^0_X + (\alpha\Lambda^0_X + \beta)\sqrt{\mu}] \quad (\text{A13})$$

where μ is ionic strength and α and β are parameters calculated at each temperature from the physical properties of water. The concentration "constants" K_A and K_B are calculated from the known thermodynamic constants K_A^0 and K_B^0 and activity coefficients obtained using the extended Debye-Hückel equation with an ion-size parameter of 3.5 Å.

At each temperature, a trial value of K_w^0 is assumed and, for each solution, the ionic strength approximated by the salt concentration. The Debye-Hückel equation is used to calculate the activity coefficients necessary to derive K_A , K_B , and K_w , after which (H^+) for each solution is obtained from eq A11 by Newton-Raphson iteration. An improved estimate of the ionic strength is then calculated from eq A1-A3 and A5-A7 and the current (H^+) and K_w . The above

process is repeated until successive calculated values of μ converge. The ionic equivalent conductivities are next calculated for each solution from eq A13 and finally a value of L^* for each obtained from eq A12. K_w^0 is then systematically varied, repeating the above steps, in such a way as to minimize (in a least-squares sense) the deviations between observed and calculated L^* 's. That value of K_w^0 which produces the lowest sum of squared residuals is taken as the value of K_w^0 for the temperature in question.

Acknowledgments. We wish to thank Professor C. W. Burnham, The Pennsylvania State University, for his invaluable advice and assistance throughout the investigation; to a major extent, he is responsible for the design and construction of the electrode assembly and seal.

A Thermodynamic Study of Solutions with Liquid Crystal Solvents

by Gas-Liquid Partition Chromatography^{1a,b}

by David G. Willey*^{1c} and Glenn H. Brown

Liquid Crystal Institute and Department of Chemistry, Kent State University, Kent, Ohio 44242 (Received April 15, 1971)

Publication costs assisted by the Air Force Office of Scientific Research

Thermodynamic parameters have been determined by gas-liquid partition chromatography for a variety of organic solutes at infinite dilution in the liquid crystalline and isotropic phases of 4,4'-di-*n*-heptyloxyazobenzene and *p*-(*p*-ethoxyphenylazo)phenyl undecylenate. Solute activity coefficients and partial molar enthalpies of solution are interpreted in terms of solvent-solute potential energies of interaction and changes in solute internal motion. An increase in solute excess enthalpies on going to a less ordered mesophase (smectic to nematic) is explained by an increase in solvent-solute intermolecular distances.

Introduction

Some organic compounds are known to behave as ordered fluids in a temperature region between the crystalline solid and isotropic liquid. These ordered fluids, referred to as liquid crystals, have the mobility of liquids and the optical properties of crystalline solids. The interested reader may learn more about liquid crystals by consulting general references by Brown,² Gray,³ Saupe,⁴ and Ferguson.⁵

The ordered arrangement of molecules in liquid crystals give them interesting solvent properties. Use has been made of the orienting effect of liquid crystalline solvents on solutes. These studies include electronic,⁶ infrared,⁷ nuclear magnetic resonance,⁸ and electron

spin resonance spectroscopy.⁹ Kinetics and mechanisms of selected reactions have been studied in liquid crystalline solvents.¹⁰

(1) (a) Abstracted from a dissertation presented by D. G. Willey in partial fulfillment of requirements for the doctorate at Kent State University. (b) Research supported in part by Contract F44620-69-C-0021 from the Air Force Office of Scientific Research. (c) Present address: Department of Chemistry, Georgetown University, Washington, D. C. 20007.

(2) (a) G. H. Brown and W. G. Shaw, *Chem. Rev.*, **57**, 1049 (1957); (b) G. H. Brown, *Anal. Chem.*, **41**, 26A (1969).

(3) G. W. Gray, "Molecular Structure and the Properties of Liquid Crystals," Academic Press, New York, N. Y., 1962.

(4) A. Saupe, *Angew. Chem. Int. Ed.*, **7**, 97 (1968).

(5) J. L. Ferguson, *Sci. Amer.*, **221**, 77 (1964).

(6) G. P. Ceasar and H. B. Gray, *J. Amer. Chem. Soc.*, **91**, 191 (1969).

Gas-liquid partition chromatography (glpc) offers an attractive method for investigating both the solute and liquid crystalline solvent in which it is dissolved. The effect of the solute on the liquid crystalline order of the solvent should be negligible in the very dilute solutions studied by glpc. This is in contrast to nmr studies, for example, where the solute concentrations are fairly high and the liquid crystalline order may be significantly disturbed.

The pioneering research on the use of liquid crystals as stationary phases in glpc was done by Kelker and coworkers¹¹⁻¹⁶ and Dewar and coworkers.¹⁷⁻¹⁹ Martire and coworkers²⁰⁻²³ have used glpc to investigate the thermodynamic aspects of dilute solutions involving liquid crystalline solvents. The adjustment of glpc experimental conditions to give accurate thermodynamic information has been discussed.²⁴ Infinite dilution activity coefficients have been determined by glpc that are nearly equal to those determined by static methods under well-defined equilibrium conditions.^{25,26}

Experimental Section

Instrumentation. The glpc apparatus used was a Hewlett-Packard-F & M Scientific series 5750 model. The temperatures of the injection port and thermal conductivity detector were maintained at 200 and 250°, respectively. Column temperatures were determined by chromel-alumel thermocouples referenced to a 0° ice bath and monitored potentiometrically. The maximum temperature difference along a coiled column was less than 0.3°. The fluctuation of the temperature at a given point on the column under isothermal conditions in the oven air bath was $\pm 0.1^\circ$. The current in the thermal conductivity detector was maintained at 140 mA. A Sargent Model SR recorder was used to trace the sample elution.

Helium was used as the carrier gas. It passed in succession through a pressure regulator, molecular sieve (Type 5A) moisture trap, differential flow controller, injection port, column, detector, and soap film flowmeter. Flow rate measurements using the flowmeter and stopwatch were very reproducible with an uncertainty of ± 0.002 ml sec⁻¹.

The pressure at the column inlet was monitored by an open-end mercury manometer. The pressure at the outlet was assumed to be atmospheric and was measured by a mercury barometer. The uncertainty of the manometer measurements was ± 0.7 mm; for the barometric measurements, it was ± 0.1 mm.

The Solvents. The two liquid crystalline compounds chosen for this study were *p*-(*p*-ethoxyphenylazo)phenyl undecylenate (EPAPU) and 4,4'-di-*n*-heptyloxyazoxybenzene (PHAB). Both were obtained from Eastman Organic Chemicals. EPAPU and PHAB were recrystallized twice from absolute methanol and chloroform, respectively. A differential thermal analysis (DTA) of each of these recrystallized compounds

using a DuPont 900 DTA unit showed sharp phase transitions. The mesomorphic ranges of EPAPU (nematic, 62–109°) and PHAB (smectic, 74–93°; nematic, 93–123°) were determined from the DTA thermograms. A literature value²⁷ for the nematic range of EPAPU is 62–106°. Arnold²⁸ observed the smectic range of PHAB to be 74–95° and the nematic range to be 95–124°.

Differential thermal analysis of the packing materials established that, although the transition temperatures of EPAPU and PHAB were slightly depressed (see Table I), they possessed well-defined liquid crystalline phases. Thermal analysis of the column packings after completion of a chromatographic experiment showed that there was no change in the transition temperatures of the liquid crystalline materials.

The Solutes. The solutes studied were *o*-, *m*-, and *p*-xylene, the *n*-alkanes from hexane to nonane inclusive, cyclohexane, and benzene. They were chosen because (a) they were easy to obtain in pure form, (b) vapor pressure and critical constant data were available, and (c) they seemed to be the simplest compounds available which could, under the imposed experimental conditions, demonstrate the role of the molecular geometry of the solute and solvent.

- (7) G. P. Ceasar, R. A. Levenson, and H. B. Gray, *J. Amer. Chem. Soc.*, **91**, 772 (1969).
- (8) J. C. Rowell, W. D. Phillips, L. R. Meloy, and M. Panar, *J. Chem. Phys.*, **43**, 3442 (1965).
- (9) D. H. Chen, P. G. James, and G. R. Luckhurst, *Mol. Cryst., Liquid Cryst.*, **8**, 71 (1969).
- (10) W. E. Bacon and G. H. Brown, *ibid.*, **6**, 155 (1969).
- (11) H. Kelker, *Ber. Bunsenges. Phys. Chem.*, **67**, 698 (1963).
- (12) H. Kelker, *Z. Anal. Chem.*, **198**, 254 (1963).
- (13) H. Kelker, "Gas Chromatographie 1965," H. G. Struppe, Ed., Akademie-Verlag, West Berlin, 1966, p B49.
- (14) H. Kelker and H. Winterscheidt, *Z. Anal. Chem.*, **220**, 1 (1966).
- (15) H. Kelker, B. Scheurle, and H. Winterscheidt, *Anal. Chim. Acta*, **38**, 17 (1967).
- (16) H. Kelker and E. von Schivizhoffen, "Advances in Chromatography," Vol. 6, J. C. Giddings and R. A. Keller, Ed., Marcel Dekker, New York, N. Y., 1968, p 247.
- (17) M. J. S. Dewar and J. P. Schroeder, *J. Amer. Chem. Soc.*, **86**, 5235 (1964).
- (18) M. J. S. Dewar and J. P. Schroeder, *J. Org. Chem.*, **30**, 3485 (1965).
- (19) M. J. S. Dewar, J. P. Schroeder, and D. C. Schroeder, *ibid.*, **32**, 1692 (1967).
- (20) D. E. Martire, P. A. Blasco, P. F. Carone, L. C. Chow, and H. Vicini, *J. Phys. Chem.*, **72**, 3489 (1968).
- (21) L. C. Chow and D. E. Martire, *ibid.*, **73**, 1127 (1969).
- (22) L. C. Chow and D. E. Martire, *Mol. Cryst., Liquid Cryst.*, in press.
- (23) L. C. Chow and D. E. Martire, *J. Phys. Chem.*, **75**, 2005 (1971).
- (24) D. E. Martire and L. Z. Pollara, "Advances in Chromatography," Vol. 1, J. C. Giddings and R. A. Keller, Ed., Marcel Dekker, New York, N. Y., 1966, p 335.
- (25) D. H. Everett and C. T. H. Stoddart, *Trans. Faraday Soc.*, **57**, 746 (1961).
- (26) D. E. Martire, R. L. Pecsok, and J. H. Purnell, *ibid.*, **61**, 2496 (1965).
- (27) D. Vorlander, *Z. Phys. Chem. (Leipzig)*, **126**, 449 (1927).
- (28) H. Arnold, *ibid.*, **226**, 146 (1964).

Table I: Transition Temperatures^a Determined by DTA for the Solvents in Bulk Form and When Coated on the Support

Solvent	Solid-smectic transition temperature, °C		Smectic-nematic transition temperature, °C		Nematic-isotropic transition temperature, °C	
	Bulk	Coated	Bulk	Coated	Bulk	Coated
EPAPU	62	62	109	108
PHAB	74	73	93	92	123	122

^a The transition temperatures were determined to the nearest degree Centigrade at the minima of the DTA endotherms.

The *n*-alkanes were obtained from Aldrich Organic Chemicals, and the other solutes were obtained from Matheson Coleman and Bell. They were reported to have purities greater than 99 mol % (spectroquality and chromatography). Since the chromatograms of the solutes showed at most only trace impurities, they were used without further purification.

Preparation of Columns. Six-foot sections of 0.25-in. (o.d.) copper tubing were used for the columns. The packings were prepared by coating 60/80 mesh acid-washed Chromosorb W (Johns-Manville) with the solvent compounds. This coating was accomplished by use of a Rinco rotating evaporator (Model VE-1000-B) with benzene as the solvent. The coated material was resifted to 60/80 mesh specifications to assure that the uniformity of the particle size was not destroyed in the coating process.

The difference in weight before and after the packing addition was a measure of the amount of packing in the column. The amount of liquid crystal in the packing was determined gravimetrically by burning off the organic coating in a crucible. Loading determinations were made before and after the column use. The latter was made to determine the effects (if any) of column contamination, degradation, or bleeding. Each loading determination was the average result of three samples. On the basis of all determinations, the uncertainty of the loading was estimated to be $\pm 0.10\%$.

Measurement of Retention Times. Solute samples were so small that the retention times were independent of sample size and the systems followed Henry's law. Each retention time used in the thermodynamic calculations was the average result of at least three determinations.

A few retention times were obtained from the average result of ten stopwatch determinations to permit the calculation of standard deviations with some justification. These retention times had standard deviations of ± 0.1 sec. Approximating the experimental uncertainty at twice the standard deviation gives an uncertainty of ± 0.2 sec. This good reproduction was enhanced by fairly sharp and symmetrical elution traces.

Distance measurements generally resulted in retention time uncertainties of ± 1.0 sec.

Results

Specific retention volumes (V_g°) were calculated from the expression²⁹

$$V_g^\circ = 273.15(P_o = P_w)t_r F_o j / P_o T_a g_1 \quad (1)$$

where P_o (mm) is the column outlet pressure, P_w (mm) is the vapor pressure of water at the ambient temperature T_a ($^\circ\text{K}$), t_r (sec) is the retention time, F_o (ml sec^{-1}) is the outlet flow rate, g_1 (g) is the mass of stationary liquid, and j is a compressibility factor. An error analysis gave an uncertainty of $\pm 1.0\%$ for V_g° values. This was supported by the experimental reproducibility of V_g° at given temperatures to within 1%. This kind of reproducibility held even over a period of several months as demonstrated with the EPAPU column.

Solute V_g° values at the same temperature were found to be independent (within experimental error) of the amount of PHAB on Chromosorb W in the smectic, nematic, and isotropic phases. This indicated the absence of surface effects at the gas-liquid interfaces.²¹ If only bulk solution behavior prevails, V_g° is independent of all operational variables except temperature. However, an adsorption contribution to V_g° will act to increase it as the loading percentage is decreased and the surface-to-volume ratio is increased. No significant upward trends of V_g° were seen with a decrease in PHAB solvent loading. This result and experimental evidence for *p*-azoxyanisole and 4,4'-di-*n*-hexoxyazoxybenzene²¹ suggest that bulk solution information was also provided in EPAPU because the loading was high enough (15.13%) to give a surface-to-volume ratio where surface effects at the gas-liquid crystal interface are usually negligible.

Uncorrected activity coefficients at infinite dilution (γ_p) were calculated using the expression²⁴

$$\gamma_p = 1.704 \times 10^7 / M_1 p_2^\circ V_g^\circ \quad (2)$$

where M_1 is the solvent molecular weight and p_2° (mm) is the vapor pressure of the pure solute. Vapor pressures were calculated using the Antoine equation and available constants.³⁰ The convention was used whereby solute activity coefficients greater than unity indicate positive deviations from Raoult's law and those less than unity indicate negative deviations from Raoult's law.

Activity coefficients corrected for vapor phase non-ideality (γ_f) were determined from the expression²⁰

$$\ln \gamma_f = \ln \gamma_p - p_2^\circ B_{22} / RT \quad (3)$$

(29) D. H. Desty and W. T. Swanton, *J. Phys. Chem.*, **65**, 766 (1961).

(30) R. R. Dreisbach, *Advan. Chem. Ser.*, **No. 15**, (1955); **No. 22**, (1959); **No. 29**, (1961).

where B_{22} is the second virial coefficient of the pure solute vapor at the absolute column temperature T . Second virial coefficients were calculated from the corresponding states equation of McGlashan and Potter^{31,32}

$$B_{22}/V_c = 0.430 - 0.886(T_c/T) - 0.694(T_c/T)^2 - 0.0375(n_c - 1)(T_c/T)^{4.5} \quad (4)$$

where T_c and V_c are the solute critical temperature ($^{\circ}\text{K}$) and volume (ml mol^{-1}), and n_c is the effective carbon number. Critical constants were obtained from a compilation by Kobe and Lynn.³³

A comparison with some previously determined B_{22} values³¹ indicates that the B_{22} values computed in this study are accurate to within $\pm 3\%$. From the deviations of B_{22} and V_g° , the uncertainty in the γ_f values was estimated to be $\pm 1.1\%$. This result compares favorably with the observation of Desty and Swanton²⁹ and Langer and Purnell.³⁴ Their independent glpc measurements using benzoquinoline as a stationary liquid gave activity coefficients which agree to within 1% or better. Chow and Martire²³ reported an activity coefficient probable error of $\pm 1.5\%$.

The solute partial molar excess enthalpies (\bar{H}_2^E) and excess entropies (\bar{S}_2^E) at infinite dilution were determined from the slopes and intercepts of least-squares linear fits for $\ln \gamma_f$ vs. $1/T(^{\circ}\text{K})$ sets of data according to the relationship²⁰

$$\ln \gamma_f = \bar{H}_2^E/RT - \bar{S}_2^E/R \quad (5)$$

Figure 1 shows $\ln \gamma_f$ vs. $1/T(^{\circ}\text{K})$ plots for a series of n -alkanes in the nematic and isotropic phases of EPAPU.

Using the reference state of the solute at infinite dilution in an ideal gaseous mixture,²⁰ the solute partial molar enthalpies ($\Delta\bar{H}_2^{\text{soln}}$) and entropies ($\Delta\bar{S}_2^{\text{soln}}$) of solution were determined from the equations

$$\Delta\bar{H}_2^{\text{soln}} = -\Delta\bar{H}_2^{\text{vap}} + \bar{H}_2^E \quad (6)$$

and

$$\Delta\bar{S}_2^{\text{soln}} = -\Delta\bar{H}_2^{\text{vap}}/T + \bar{S}_2^E \quad (7)$$

where $\Delta\bar{H}_2^{\text{vap}}$ is the solute molar heat of vaporization. Also, $\Delta\bar{H}_2^{\text{soln}}$ may be determined from the slope of a plot of $\log V_g^{\circ}$ vs. $1/T(^{\circ}\text{K})$. Such plots are shown in Figure 2.

From slope and intercept standard deviations about the best line for quantities determined by least-squares linear fits, the standard deviations of $\Delta\bar{H}_2^{\text{soln}}$, \bar{H}_2^E and \bar{S}_2^E values were typically about ± 0.2 kcal mol^{-1} , ± 0.2 kcal mol^{-1} , and ± 0.5 cal $^{\circ}\text{K}^{-1}$ mol^{-1} , respectively. The average \bar{H}_2^E (kcal mol^{-1}) values are approximately 2.9 (nematic EPAPU), 1.5 (isotropic EPAPU), 2.3 (smectic PHAB), 3.7 (nematic PHAB), and 2.3 (isotropic PHAB). The average \bar{S}_2^E (cal $^{\circ}\text{K}^{-1}$ mol^{-1}) values are approximately 6.0 (nematic EPAPU), 2.9 (isotropic EPAPU), 3.9 (smectic PHAB), 8.1 (nematic PHAB), and 5.0 (isotropic PHAB).

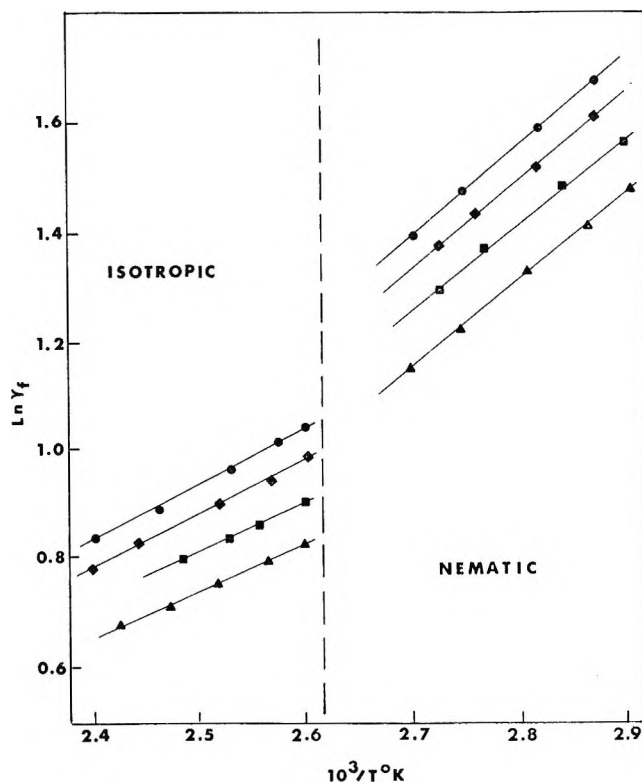


Figure 1. Natural logarithm of solute activity coefficients at infinite dilution ($\ln \gamma_f$) in EPAPU vs. $1/T(^{\circ}\text{K})$. Solutes: \blacktriangle , n -hexane; \blacksquare , n -heptane; \blacklozenge , n -octane; \bullet , n -nonane. The vertical dashed line separates the nematic and isotropic temperature regions.

For the n -alkanes from hexane to nonane inclusive, linear equations were determined by least-squares fits to give $\Delta\bar{H}_2^{\text{soln}}$, $\Delta\bar{S}_2^{\text{soln}}$, and γ_f values as functions of carbon number. The slopes and intercepts of these equations are reported in Table II. The average value of the linear correlation coefficient is 0.998, indicating good linear fits. The $\Delta\bar{H}_2^{\text{soln}}$, $\Delta\bar{S}_2^{\text{soln}}$, and γ_f values for the other solutes in EPAPU and PHAB are given in Tables III and IV.

Discussion

Interpretation of Thermodynamic Quantities. The thermodynamic process under consideration is taking a given solute at infinite dilution in an ideal gaseous mixture (vaporized solute and helium carrier gas) to infinite dilution in a real liquid mixture (condensed solute and glpc stationary solvent). Recent work by Chow and Martire²³ makes possible the interpretation of activity coefficients using the equation

$$\gamma_f = (1/Z)(q^E/q^S)_{\text{int}}e^{-1} \quad (8)$$

(31) M. L. McGlashan and D. J. B. Potter, *Proc. Roy. Soc., Ser. A*, **267**, 478 (1962).

(32) E. A. Guggenheim and C. J. Wormald, *J. Chem. Phys.*, **42**, 3775 (1965).

(33) K. A. Kobe and R. E. Lynn, *Chem. Rev.*, **52**, 117 (1953).

(34) S. H. Langer and J. H. Purnell, *J. Phys. Chem.*, **67**, 263 (1963).

Table II: Slopes and Intercepts^a from Least-Squares Linear Fits for Determining Thermodynamic Quantities (Y) as Functions of the Number of Solute Carbon Atoms (n) According to Equation, $Y = An + B$, for the n -Alkanes from Hexane to Nonane

Solvent	Phase	A	B
$Y = \Delta\bar{H}_2^{\text{soln}}$ (kcal mol ⁻¹)			
EPAPU	Nematic (85°)	-1.02 ± 0.04	2.27 ± 0.31
EPAPU	Isotropic (121°)	-0.91 ± 0.03	0.72 ± 0.24
PHAB	Smectic (80°)	-0.74 ± 0.03	-0.49 ± 0.20
PHAB	Nematic (100°)	-0.85 ± 0.05	1.81 ± 0.36
PHAB	Isotropic (131.8°)	-0.98 ± 0.02	2.19 ± 0.16
$Y = \Delta\bar{S}_2^{\text{soln}}$ (cal °K ⁻¹ mol ⁻¹)			
EPAPU	Nematic (85°)	-3.33 ± 0.10	7.45 ± 0.77
EPAPU	Isotropic (121°)	-2.69 ± 0.09	3.60 ± 0.71
PHAB	Smectic (80°)	-2.40 ± 0.06	-2.40 ± 0.48
PHAB	Nematic (100°)	-2.44 ± 0.13	3.55 ± 0.97
PHAB	Isotropic (131.8°)	-2.53 ± 0.07	4.65 ± 0.50
$Y = \gamma_f$			
EPAPU	Nematic (85°)	0.34 ± 0.01	1.63 ± 0.11
EPAPU	Isotropic (121°)	0.17 ± 0.01	1.17 ± 0.05
PHAB	Smectic (80°)	0.70 ± 0.03	-0.08 ± 0.22
PHAB	Nematic (100°)	0.29 ± 0.01	1.41 ± 0.05
PHAB	Isotropic (131.8°)	0.13 ± 0.00	1.19 ± 0.02

^a Slope and intercept standard deviations are given.

Table III: Solute Thermodynamic Quantities of the Xylenes at Infinite Dilution in EPAPU

Solute	Nematic (85°)	Isotropic (121°)
$\Delta\bar{H}_2^{\text{soln}}$, kcal mol ⁻¹		
<i>p</i> -Xylene	-7.17	-8.02
<i>m</i> -Xylene	-6.80	-7.83
<i>o</i> -Xylene	-6.96	-7.98
$\Delta\bar{S}_2^{\text{soln}}$, cal °K ⁻¹ mol ⁻¹		
<i>p</i> -Xylene	-20.8	-20.3
<i>m</i> -Xylene	-20.0	-19.9
<i>o</i> -Xylene	-20.3	-20.2
γ_f		
<i>p</i> -Xylene	1.54	1.02
<i>m</i> -Xylene	1.68	1.04
<i>o</i> -Xylene	1.60	0.99

In (8) Z represents the potential energy of interaction in the real liquid mixture and $(q^g/q^s)_{\text{int}}$ is the ratio of the solute internal energy partition function in the ideal gaseous mixture to that in the real liquid mixture. The internal energy of a molecule (referring to the energy associated with its internal coordinates) includes internal rotational and vibrational energies. The translational energy change that a solute experiences in the solution process is assumed to be entirely due to the potential energy of interaction in the real liquid mixture.²³ Thus, a greater change in internal energy

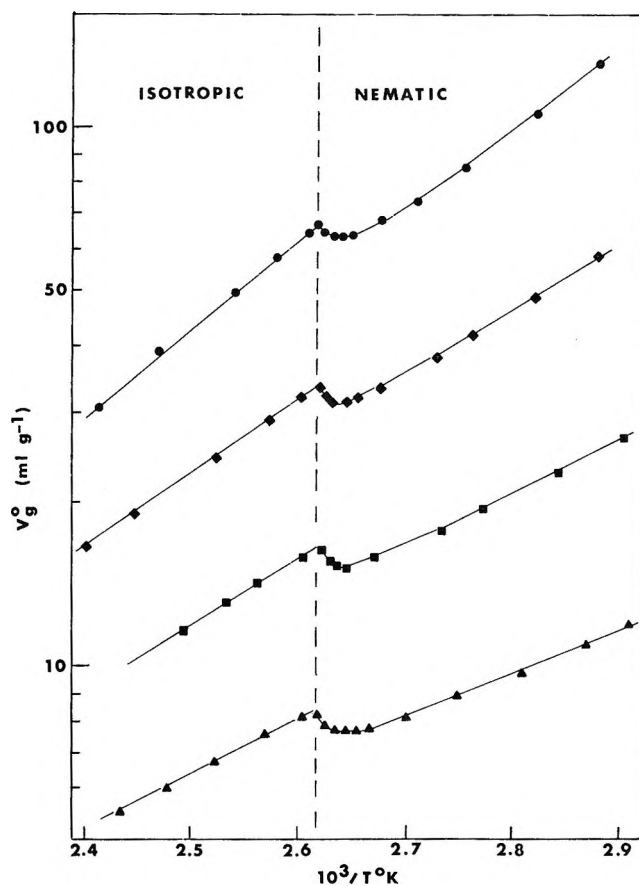


Figure 2. Solute specific retention volumes (V_g°) vs. $1/T$ (°K) in EPAPU. Solutes: ▲, *n*-hexane; ■, *n*-heptane; ◆, *n*-octane; ●, *n*-nonane. The V_g° values are plotted on a logarithmic scale. The vertical dashed line separates the nematic and isotropic temperature regions.

Table IV: Solute Thermodynamic Quantities for the Xylenes, Benzene, and Cyclohexane at Infinite Dilution in PHAB

Solute	Smectic (80°)	Nematic (100°)	Isotropic (131.8°)
$\Delta\bar{H}_2^{\text{soln}}$, kcal mol ⁻¹			
<i>p</i> -Xylene	-6.99	-5.37	-6.65
<i>m</i> -Xylene	-7.19	-5.24	-6.29
<i>o</i> -Xylene	-7.24	-5.30	-6.89
Cyclohexane	-5.62	-3.72	-4.05
Benzene	-5.22	-3.28	-4.48
$\Delta\bar{S}_2^{\text{soln}}$, cal °K ⁻¹ mol ⁻¹			
<i>p</i> -Xylene	-21.7	-15.5	-16.5
<i>m</i> -Xylene	-22.4	-15.3	-15.7
<i>o</i> -Xylene	-22.5	-15.4	-17.1
Cyclohexane	-18.1	-11.6	-10.7
Benzene	-16.3	-9.6	-10.9
γ_f			
<i>p</i> -Xylene	2.66	1.73	1.05
<i>m</i> -Xylene	2.82	1.85	1.07
<i>o</i> -Xylene	2.76	1.79	1.03
Cyclohexane	2.94	2.26	1.40
Benzene	2.14	1.50	0.91

acts to increase γ_f and disfavor solution; a greater change in translational energy acts to decrease γ_f and favor solution.

Furthermore, from the development of Chow and Martire²³ we may write

$$\Delta\bar{H}_2^{\text{soln}} = \Delta E_{\text{int}} + \Delta E_{\text{ext}} - RT \quad (9)$$

where ΔE_{int} corresponds to the internal energy change of a solute going into solution and ΔE_{ext} corresponds to the external (or translational) energy change. The ΔE_{int} and ΔE_{ext} values, like the observed $\Delta\bar{H}_2^{\text{soln}}$ values are negative. Therefore, while a greater ΔE_{int} makes the solution process more exothermic, it also increases γ_f . A greater ΔE_{ext} makes the solution process more exothermic and also decreases γ_f . Throughout this discussion, greater $\Delta\bar{H}_2^{\text{soln}}$, ΔE_{int} , and ΔE_{ext} values will mean that they are more negative.

1. *A General Smectic-Nematic-Isotropic Comparison.* For a given solute the excess enthalpy, excess entropy, and excess Gibbs free energy (equal to $RT \ln \gamma_f$) are all more positive in the nematic than in the isotropic phase of the same solvent. This reflects the increased difficulty of dissolving a solute in a more ordered solvent. The more positive \bar{S}_2^{E} values in the nematic phase are more favorable for solution but are dominated by the enthalpic effects. The larger γ_f values in the nematic phase indicate greater deviations from the ideality expressed by Raoult's law when the activity coefficient is unity. All solutes in the nematic phase exhibit positive deviations from Raoult's law. Most deviations from Raoult's law are also positive in the isotropic phases, but a few are negative.

The \bar{H}_2^{E} values are more positive in the nematic phase of PHAB than in its smectic phase. Because of the smaller molar volume (or greater density) of the smectic phase compared to the nematic phase, shorter solvent-solute intermolecular distances should result in the smectic phase. It is known that the forces of attraction between uncharged molecules decrease rapidly with the distance of separation. Therefore, the solvent-solute interaction energy may be more favorable in the smectic phase and account for the less positive \bar{H}_2^{E} values.

The magnitudes of the solvent-solvent interaction energies probably have little effect on the relative \bar{H}_2^{E} values in the mesomorphic and isotropic phases of the same solvent. Evidence for this has been provided by calorimetric studies which indicate that the average molecular interactions of the smectic, nematic, and isotropic phases differ by small amounts of energy. Mesophase-mesophase and mesophase-isotropic transition energies are usually small. In particular, the smectic-nematic and nematic-isotropic heats of transition of PHAB²⁸ are, respectively, 0.381 and 0.243 kcal mol⁻¹. Therefore, one may consider the magnitudes of the solvent-solute interactions as the dominating influence on the relative \bar{H}_2^{E} values in the phases

of the same solvent compound. The experimental \bar{H}_2^{E} values suggest that the solvent-solute interactions in the nematic phase are weaker than those in either the smectic or isotropic phases. This also suggests that the ΔE_{ext} values follow the order: smectic > nematic < isotropic. Assuming that a more ordered solvent will impose more restrictions to the internal molecular motion of a solute, the ΔE_{int} values should follow the order: smectic > nematic > isotropic.

2. *n-Alkane Thermodynamic Quantities.* In the nematic phases of EPAPU and PHAB, the $\Delta\bar{H}_2^{\text{soln}}$ values followed the trend: *n*-nonane > *n*-octane > *n*-heptane > *n*-hexane. This is explained by (a) a greater ΔE_{int} of the longer and more flexible molecules and (b) a greater ΔE_{ext} of the longer molecules which have a greater polarizability and a stronger interaction with the solvent through dispersion forces. Since the γ_f values of these alkanes increase with increasing chain length, it is evident that the effect of ΔE_{ext} (which decreases γ_f) is overpowered by the effect of ΔE_{int} (which increases γ_f). A greater loss of entropy with increasing chain length is observed. This partially reflects the greater sacrifice in internal motion for a longer and more flexible molecule to go into solution.

In all isotropic phases and in the smectic phase of PHAB, the trends in the $\Delta\bar{H}_2^{\text{soln}}$ and γ_f values for the *n*-alkane series are the same as in the nematic phases—and probably for the same reasons. However, the ΔE_{int} effect should be greater in the smectic phase and less in the isotropic phase than in the nematic phase. It is the large ΔE_{int} effect in the smectic phase of PHAB which increases the γ_f values to the extent that they are greater than in the nematic phase even though previous considerations indicate greater solvent-solute interactions in the smectic phase.

A linear relationship is observed between the $\Delta\bar{H}_2^{\text{soln}}$ and $\Delta\bar{S}_2^{\text{soln}}$ values of the *n*-alkanes in the different solvent phases. An example of this behavior is shown in Figure 3 where $\Delta\bar{H}_2^{\text{soln}}$ and $\Delta\bar{S}_2^{\text{soln}}$ values for the *n*-alkane series (and also for the xylene series) in nematic PHAB are plotted. Correlations such as those in Figure 3 have been previously observed.^{20,35-37} This study fits into one of Bell's³⁵ general classifications where the solute molecules are small compared to those of the solvent and the same type of intermolecular forces operate for a solute series. Two separate correlations are evident from Figure 3 for the *n*-alkane and xylene series.

3. *Xylene Thermodynamic Quantities.* In the nematic phases of EPAPU and PHAB, the $\Delta\bar{H}_2^{\text{soln}}$ values followed the trend: *p*-xylene > *o*-xylene > *m*-xylene. The solute entropy losses followed the same trend and the trend in γ_f values was the reverse of that for $\Delta\bar{H}_2^{\text{soln}}$.

(35) R. P. Bell, *Trans. Faraday Soc.*, **33**, 496 (1937).

(36) I. M. Barclay and J. A. V. Butler, *ibid.*, **34**, 1445 (1938).

(37) O. K. Rice, *J. Chem. Phys.*, **15**, 875 (1947).

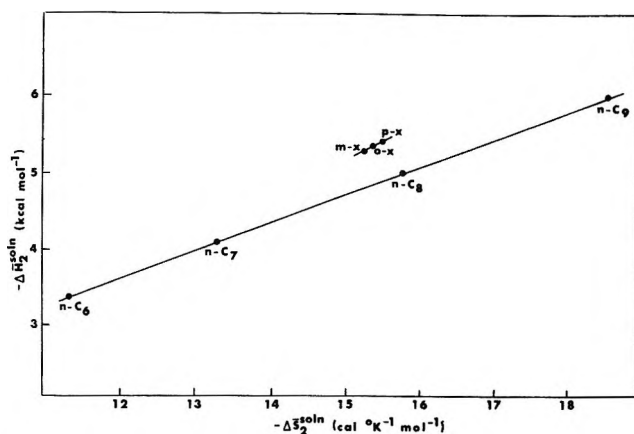


Figure 3. Solute partial molar enthalpies of solution ($\Delta\bar{H}_2^{\text{soln}}$) vs. solute partial molar entropies of solution ($\Delta\bar{S}_2^{\text{soln}}$) in the nematic phase of PHAB. Solutes: *n*-hexane (n-C₆); *n*-heptane (n-C₇); *n*-octane (n-C₈); *n*-nonane (n-C₉); *p*-xylene (p-x); *m*-xylene (m-x); *o*-xylene (o-x).

This indicates a nematic solvent behavior based on solute shape. The most linear isomer, *p*-xylene, appears to fit better in the ordered nematic structure.

Assuming that the longest isomers lose the greatest amounts of internal energy, the ΔE_{int} values should follow the order: *p*-xylene > *m*-xylene > *o*-xylene. The translational energy changes stemming from solute interactions with the solvent is more difficult to interpret. Since *o*-xylene is the most polar of the three isomers, it would be expected to have the strongest dipolar interactions with the solvent. However, a more favorable spatial orientation might be expected with the most rodlike isomer, *p*-xylene, which would give it the best interaction.

In all isotropic phases, the γ_t values followed the trend: *m*-xylene > *p*-xylene > *o*-xylene. A trend based on solute polarities would reverse the relative

positions of *m*- and *p*-xylene. However, short-range order in the isotropic phases may carry over a portion of the linear aspect of *p*-xylene that was so important in the nematic phases.

In the smectic phase of PHAB, the $\Delta\bar{H}_2^{\text{soln}}$ values followed the trend: *o*-xylene > *m*-xylene > *p*-xylene. This trend is surprising since it does not follow the solute linearity sequence as seen in the nematic phases. But instead, a sequence based on solute polarities is followed. The trend in γ_t values is the same in the smectic phase of PHAB as in the nematic phase. These trends suggest that although the ΔE_{ext} values follow the same sequence in both phases, the ΔE_{int} effect for *m*- and *o*-xylene is greater than that for *p*-xylene in smectic PHAB. Greater entropy losses are also apparent for *m*- and *o*-xylene. Further investigation is necessary to explain this contrast in the solvent behavior of smectic and nematic PHAB.

4. *Benzene and Cyclohexane Thermodynamic Quantities.* Benzene and cyclohexane were studied only in PHAB. In the smectic and nematic phases, the $\Delta\bar{H}_2^{\text{soln}}$ values followed the order: cyclohexane > benzene; the reverse of this order was found in the isotropic phase. In all phases, the order of the γ_t values was cyclohexane > benzene. Since the benzene molecule is much more rigid than the cyclohexane molecule, the ΔE_{int} associated with benzene going into solution should be less than that for cyclohexane. However, the ΔE_{ext} associated with the solution process should be greater for benzene since it is more polarizable than cyclohexane. Therefore, the ΔE_{int} effect apparently dominates in the mesophases while the ΔE_{ext} effect dominates in the isotropic phase. The relative $\Delta\bar{S}_2^{\text{soln}}$ values for benzene and cyclohexane in the mesophases of PHAB show a greater entropy loss for cyclohexane going into solution. This supports our claim of a greater ΔE_{int} for cyclohexane.

Thermochemistry of the Diels–Alder Reaction. II. Heat of Addition of Several Dienes to Tetracyanoethylene

by F. E. Rogers

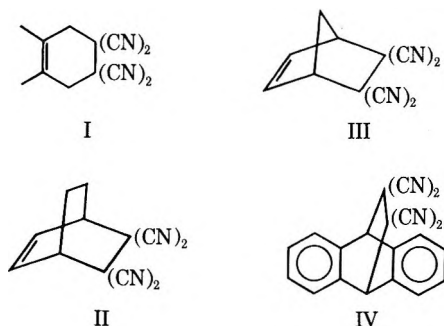
Department of Chemistry, University of Dayton, Dayton, Ohio 45409 (Received June 30, 1971)

Publication costs assisted by The University of Dayton

The heat for the Diels–Alder addition of tetracyanoethylene to 2,3-dimethyl-1,3-butadiene, 1,3-cyclohexadiene, cyclopentadiene, and anthracene has been determined by solution calorimetry. Corrections for heats of solution and vaporization gave the heat of the gas phase reaction at 25°. Comparison is made with the analogous ethylene reactions.

Introduction

We have been interested in the thermochemical aspects of the Diels–Alder (D–A) reaction and recently reported on the heat of addition of tetracyanoethylene (TCNE) to isoprene.¹ The heat of addition was determined for the solution, standard state, and gas phase reaction, and comparison was made with the analogous ethylene reaction. This initial work suggested that the heat of any D–A reaction of TCNE will approximate the value for the corresponding ethylene reaction. This conclusion has been investigated further, and we now wish to report the heat of addition of TCNE to 2,3-dimethyl-1,3-butadiene, 1,3-cyclohexadiene, cyclopentadiene, and anthracene to form the following adducts.



Corrections for the heats of solution and vaporization gave the heat of the Diels–Alder reaction in the solution, standard state, and gas phase. The heats of formation of the adducts were calculated and examined in terms of strain energy.

Experimental Section

The TCNE (Aldrich Chemical Co.) was sublimed and stored in amber bottles under nitrogen. It was sublimed again immediately before using. Anthracene (Aldrich Chemical Co., puriss, 99.9%) was used without further purification. Cyclohexadiene (Aldrich Chemical Co.) showed only one component on glpc analysis suitable for detecting 0.1% impurity. 2,3-

Dimethyl-1,3-butadiene (K and K Laboratories) showed two impurities on glpc analysis which were removed by slow distillation through a 16 theoretical plate fractionation column.

The adducts were prepared according to the previously reported procedure.² Except for the anthracene adduct, each was further purified by two sublimations. The anthracene product was recrystallized twice from dichloromethane. The melting point, nmr spectrum, and elemental analysis of the adducts are as follows. *1,2-Dimethyl-4,4,5,5-tetracyanocyclohexene*, mp 124.5° (lit.² mp 136–137°), nmr: CH₃, s, 1.75δ, 6H; CH₂, s, 3.00δ, 4H. *Anal.* Calcd for C₁₂H₁₀N₄: C, 68.55; H, 4.79; N, 26.65. Found: C, 68.71; H, 4.89; N, 26.60. *2,2,3,3-Tetracyanobicyclo[2.2.1]heptene*, mp 215–217° dec (lit.² mp 223°), nmr: CH₂, s, 2.16δ, 2H; CH, t, 4.27δ, 2H; =CH, t, 6.78δ, 2H. *Anal.* Calcd for C₁₁H₆N₄: C, 68.03; H, 3.11; N, 28.86. Found: C, 68.09; H, 3.14; N, 28.77. *2,2,3,3-Tetracyanobicyclo[2.2.2]octene*, mp 264.5–266° (lit.² mp above 300°), nmr: CH₂, m, 1.33δ, 4H; CH, m, 3.43δ, 2H; =CH, m, 6.22δ, 2H. *Anal.* Calcd for C₁₂H₈N₄: C, 69.21; H, 3.87; N, 26.91. Found: C, 69.22; H, 3.93; N, 26.78.

9,10-Dihydro-9,10-tetracyanoethanoanthracene, mp 266° dec (lit.² mp 268–270°), nmr: CH, s, 5.95δ, 2H; =CH, m, 7.65δ, 8H. *Anal.* Calcd for C₂₀H₁₀N₄: C, 78.41; H, 3.29; N, 18.29. Found: C, 78.42, H, 3.29; N, 18.30. These compounds were used in the heat of solution determinations.

The addition reactions were run at 25.0 ± 0.5° in a solution calorimeter by previously described techniques.¹ The reactions are quantitative and complete in less than 10 min when an excess of one component is used. To compensate for the slow dimerization reaction of cyclopentadiene both reference and reaction

(1) F. E. Rogers, *J. Phys. Chem.*, **75**, 1734 (1971).

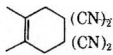
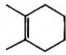
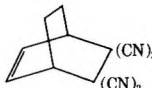
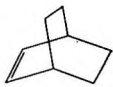
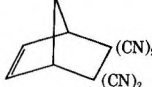

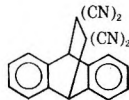
(2) W. J. Middleton, P. E. Heckert, E. L. Little, and C. G. Krespan, *J. Amer. Chem. Soc.*, **80**, 2783 (1958).

Table I: Heats of Solution, Vaporization, and Reaction (kcal/mol)

	$\Delta H_{\text{soln}} (25.0 \pm 0.5^\circ)$		$\Delta H_v (T, ^\circ\text{C})$		$\Delta H_r(\text{exptl})^f$
	Addenda	Adduct	Addenda	Adduct	
TCNE	5.60 ± 0.13 (0.13225) ^a		19.4 ± 1.0^b		
2,3-Dimethyl-1,3-butadiene	0.25 (0.450) ^a	3.21 ± 0.04 (0.07209) ^a	7.4 ^c	25.8 ± 1.0^e (105)	$-41.96 \pm 0.27[\text{D}]$
Cyclopentadiene	0.1 (0.080) ^a	4.28 ± 0.15 (0.11003) ^a	6.9 ^c	28.0 ± 1.3^e (135)	$-21.28 \pm 0.55[\text{T}]$
1,3-Cyclohexadiene	0.1 (0.080) ^a	3.58 ± 0.18 (0.10046) ^a	7.9 ^d	26.7 ± 1.3^e (160)	$-30.8 \pm 0.46[\text{D}]$
Anthracene	5.99 ± 0.25 (0.1724) ^a	2.76 ± 0.15 (0.10250) ^a			$-12.92 \pm 0.10[\text{T}]$

^a Average amount of component (grams) injected into 200 ml of dichloromethane. ^b R. H. Boyd, *J. Chem. Phys.*, **38**, 2529 (1963).
^c D. R. Stull, E. F. Westrum, Jr., and G. C. Sinke, "The Chemical Thermodynamics of Organic Compounds," Wiley, New York, N. Y., 1969. ^d Estimated from Trouton's rule using 22.47 as constant. ^e Estimated uncertainty. These values were used without correction to 25°. ^f Heat of reaction when bracketed component is added to dichloromethane solution of other component: [T] = TCNE, [D] = diene.

Table II: Heats of Diels-Alder Reaction and Heat of Formation of Adducts (kcal/mol)

Adduct formed	$\Delta H_r^\circ(\text{soln})$	ΔH_r°	$\Delta H_f^\circ(\text{g})$	$\Delta H_f^\circ(\text{g})$		Strain energy
				Exptl	Est.	
I. 	-42	-39.57 ± 0.44	-40.57 ± 2.4	138.7	127.1	11.6
Ia. 			-39.65	-16.4	-19.9	3.5
II. 	-31	-28.90 ± 0.77	-29.5 ± 3.1	164.3	139.4	25.0
IIa. 			-32.9	4.88 ^a	-7.66	12.5
III. 	-26.88 ± 0.68	-25.56 ± 0.70	-23.8 ± 3.0	176.6	144.5	32.1
IIIa. 		-22.6	-23.8	20.6	-2.53	23.1
IV. 	-18.52 ± 0.23	-9.69 ± 0.50	(-10)			

^a S. S. Wong and E. F. Westrum Jr., *J. Amer. Chem. Soc.*, **93**, 5317 (1971).

calorimeter contained the same amount of the diene. The reactions were initiated by the injection of about 0.5 mmol of one component into 200 ml of dichloromethane containing a five- to tenfold excess of the other component. The results in Table I are the average of at least two runs.

With the exception of the anthracene adduct which decomposes, the vapor pressures were determined by the McLeod gauge method previously described.¹

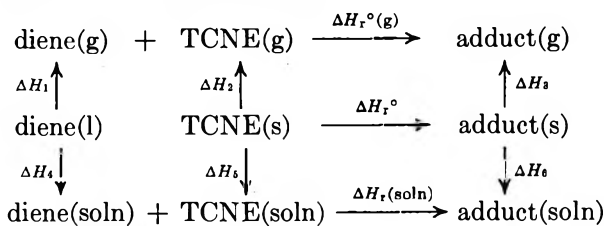
The vapor pressures (vp) were measured over a 20–30° temperature range at 4 or 5° intervals. For low vp measurements, 30–100 μ , an inert gas pressure of 200–250 μ was used; for vp's above 100 μ the inert gas pressure was increased to ca. 500–600 μ . The heat of sublimation was calculated in the usual manner from the least-squares slope of a plot of log (vp) against 1/T. The results appear in Table I.

The heat of solution was determined by the injection

of three successive portions of the diene, dienophile, or adduct into 200 ml of dichloromethane at $25.0 \pm 0.5^\circ$. Each injection represents the approximate amount involved in the Diels-Alder reaction. The three runs were averaged and reported in Table II.

Discussion

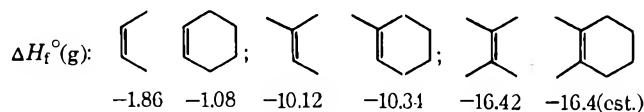
The heat of the Diels-Alder reaction in the solution, standard state, and vapor phases, was calculated according to the following cycle.



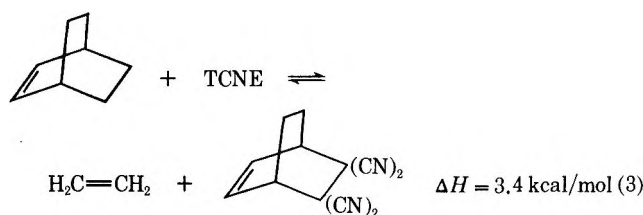
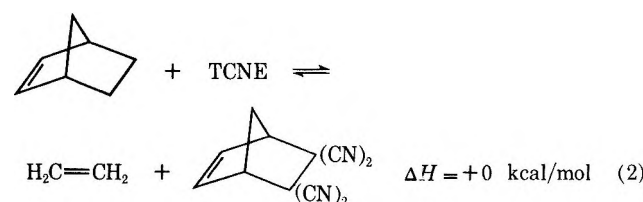
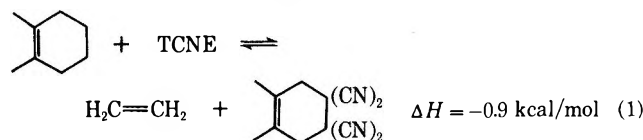
When TCNE was added to the reaction solution $\Delta H_r(\text{exptl}) = \Delta H_r^\circ(\text{soln}) + \Delta H_5$; when the diene was injected $\Delta H_r(\text{exptl}) = \Delta H_r(\text{soln}) + \Delta H_4$. In the former case the $\Delta H_r^\circ = \Delta H_r(\text{exptl}) - \Delta H_6 + \Delta H_4$ and $\Delta H_r^\circ(\text{g}) = \Delta H_r^\circ + \Delta H_3 - \Delta H_1 - \Delta H_2$. Similar expressions can be derived for the case when the diene is injected to initiate the reaction. These results are shown with the analogous D-A reaction of ethylene in Table II. The instability of the anthracene made it impossible to determine the heat of sublimation but the closeness of the gas and standard state heats of addition for the other three reactions suggest a value of -10 kcal/mol. In comparison to the "normal" D-A reaction which forms a monocyclic product, the decrease in $\Delta H_r^\circ(\text{g})$ on going down the table parallels the increase in strain energy in the products. In addition to ring strain the anthracene adduct forms at a cost of 11.3 kcal/mol resonance energy in anthracene,³ combining to make this reaction the least exothermic of the group. How closely the reaction heat [$\Delta H_r^\circ(\text{g})$] follows the increase in ring strain can be seen by comparing the increase in ring strain of the analogous hydrocarbons (last column, Table II) with the difference in $\Delta H_r^\circ(\text{g})$.

$\Delta(\text{strain energy})$	$\Delta[\Delta H_r^\circ(\text{g})]$
-9.0 (Ia-IIa)	-11.1 (I-II)
-19.6 (Ia-IIIa)	-16.8 (I-III)
	ca. -30.6 (I-IV)

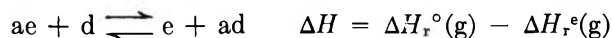
The heats of addition for the reference reactions of ethylene were calculated from the heat of formation data of Cox and Pilcher.⁴ It was necessary, however, to estimate the heats of formation of dimethylcyclohexene (Ia) and norbornene (IIIa). Benson's group increment scheme⁵ gives -16.5 kcal/mol for the former, and the structural relationship below also indicates the same value.



Combining a recent value for the gas phase heat of formation of norbornane, -12.42 kcal/mol,⁶ and the heat of hydrogenation of norbornene, -33.0 kcal/mol gives 20.6 kcal/mol for the heat of formation of norbornene. The reported value of 24.7 kcal/mol⁷ for this compound was based on a high estimate for the heat of sublimation which has since been measured. Comparison of the TCNE and ethylene reaction with the same diene is equivalent to subtracting one reaction from another. The resulting equations are



These disproportionation reactions may be represented as



where e = ethylene, d = any other dienophile, ae and ad the corresponding adducts, and $\Delta H_r^\circ(\text{g})$ the heat of addition for the analogous ethylene reaction. When d is an acyclic dienophile, the number of rings in ae equals the number in ad. For cyclic dienophiles the number in ad is larger than in ae by the number of rings in d. In the usual type of rings formed in the D-A reaction we may assume to a first approximation that ring strain is additive. Therefore the difference $\Delta H_r^\circ - \Delta H_r^\circ(\text{e})$ will be largely determined by the relative behavior of the dienophiles e and d in losing a double bond. The similarity between the D-A reaction and hydrogenation

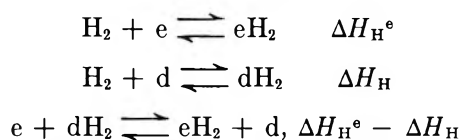
(3) Taken as the difference in the heat of hydrogenation of anthracene to 9,10-dihydroanthracene (-17.1 kcal/mol) and cyclohexene to cyclohexane (-28.4 kcal/mol). Heat of formation data from ref 4.

(4) J. D. Cox and G. Pilcher, "Thermochemistry of Organic and Organometallic Compounds," Academic Press, New York, N. Y., 1970.

(5) S. W. Benson, "Thermochemical Kinetics," Wiley, New York, N. Y., 1968.

(6) P. v. R. Schleyer, J. E. Williams, and K. R. Blanchard, *J. Amer. Chem. Soc.*, **92**, 2377 (1970).

(7) R. B. Turner, P. Goebel, B. J. Mallon, W. von E. Doering, J. F. Coburn, Jr., and M. Pomerantz, *ibid.*, **90**, 4315 (1968).



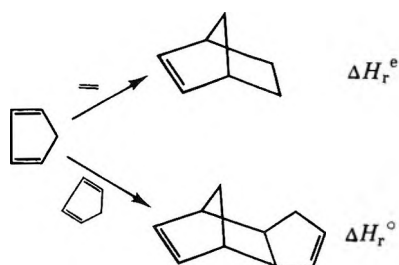
allows the useful approximation that

$$\Delta H_{\text{r}}^e(\text{g}) - \Delta H_{\text{r}}^{\circ}(\text{g}) \simeq \Delta H_{\text{H}}^e - \Delta H_{\text{H}} \simeq -32.8 - \Delta H_{\text{H}}$$

and

$$\Delta H_{\text{r}}^{\circ}(\text{g}) = \Delta H_{\text{r}}^e(\text{g}) + \Delta H_{\text{H}} + 32.8$$

the equation which fits reactions 1, 2, and 3 (above) is $\Delta H_{\text{r}}^{\circ}(\text{g}) = \Delta H_{\text{r}}^e(\text{g}) + 1.3 \pm 2.2$. This equation suggests a small difference in the heat of hydrogenation of ethylene and TCNE. This equation can be applied to the D-A reaction of cyclopentadiene with itself and ethylene.



From Table II, $\Delta H_{\text{r}}^e = -23.8$ kcal/mol and the heat of hydrogenation of cyclopentadiene to cyclopentene (ΔH_{H}) calculated from the heats of formation is -23.7 kcal/mol.⁴ Substitution gives $\Delta H_{\text{r}}^{\circ}(\text{g}) = -15$ com-

pared with a literature value of -17.0 ± 1.1 .⁸ If as Table II suggests, $\Delta H_{\text{r}}^e - \Delta H_{\text{r}}^{\circ}$ is essentially constant for a series of D-A reactions then the estimation possibilities are broadened considerably. Further work in this area is underway. The heats of formation of the TCNE adducts were calculated from the heats of formation of the reactants and $\Delta H_{\text{r}}^{\circ}(\text{g})$ are shown in Table II. The strain energy in a molecule is generally assigned as the difference between this experimental value and the heat of formation predicted on the basis of some empirical scheme. We have adopted the olefinic increment values of Benson⁵ and the "single conformation" values of the saturated CH_3 , CH_2 , CH , C groups from Schleyer.⁶ The predicted heats of formation and the strain energy are given in Table II. Since the value for the $\text{C}(\text{CN})_2$ group (68.4 kcal/mol)⁹ was calculated from malononitrile, it contains the nonbonded interaction energy of two geminal cyano groups. Tetracyanodimethylcyclohexene (I), tetracyanobicyclooctene (II), and tetracyanobicycloheptene (III) are more strained than the parent hydrocarbon by 8, 12.5, and 9 kcal/mol, respectively. This strain is assigned to the repulsive interaction of two adjacent $\text{C}(\text{CN})_2$ groups and agrees closely with the predicted value of 10 kcal/mol.¹

(8) A. Wasserman, "Diels-Alder Reaction," Elsevier, Amsterdam, 1965.

(9) Calculated by the formula $\Delta H[>\text{C}(\text{CN})_2] = \Delta H_{\text{f}}[\text{CH}_2(\text{CN})_2] - \Delta H[\text{C}-(\text{H})_2(\text{C})_2]$, where $\Delta H_{\text{f}}[\text{CH}_2(\text{CN})_2]$ is 63.5 and $\Delta H[\text{C}-(\text{H})_2(\text{C})_2]$ is -4.95 kcal/mol.

A Study of the Nature of Active Sites on Zeolites by the Measurement of Heat of Immersion. II. Effects of Silica/Alumina Ratio to Electrostatic-Field Strength of Calcium-Exchanged Zeolites

by Kazuo Tsutsumi* and Hiroshi Takahashi

Institute of Industrial Science, The University of Tokyo, Roppongi, Minato-ku, Tokyo, Japan (Received May 21, 1970)

Publication costs borne completely by The Journal of Physical Chemistry

The electrostatic-field strengths of Na- and Ca-exchanged zeolites were determined by measurements of the heats of immersion into various organic liquids. The correlation between the silica/alumina ratio and the electrostatic-field strength of zeolites was studied. The electrostatic-field strength of Na-form zeolites is not much affected by the silica/alumina ratio. In the case of Ca-exchanged zeolites, however, the more the silica/alumina ratio increases, the stronger the electrostatic field becomes. It was noted that the cumene cracking activity of Ca-form zeolites follows in magnitude the change in the electrostatic-field strength. The electrostatic-field strength of decationated zeolite was also investigated.

Introduction

Crystalline zeolites show a very characteristic adsorption behavior with a molecular sieve character. Our fundamental knowledge of the structure, properties, and synthesis of several zeolites is due largely to Barrer, *et al.*¹ Ever since Barrer first reported the results of the measurement of the peculiar adsorptive character of zeolites, various practical methods of utilization have been developed; certain species have, for example, been used for the drying, separation, and purification of solvents. Besides, their ion-exchange property is also widely helpful in water softening.

In 1960, Rabo, *et al.*,² and Weisz and Frilette³ found a high catalytic activity of X and Y zeolites for the cracking of paraffins, olefins, and alkyl aromatics and for isomerization, etc. Thereafter, the application of zeolites as catalysts was rapidly developed, and the zeolite catalyst became the subject of intensive investigation. Though the catalytic character has been discussed in connection with various kinds of zeolites, in order for zeolite to be of practical use, its pore size must be large enough to adsorb reactants. Therefore, interest is focused on faujasite-type synthetic zeolites, X and Y, and mordenite.

It is considered that the activity of zeolite catalysts stems from one of the following three factors: (1) the molecular sieve character, (2) solid acid, as observed in the case of the silica-alumina catalyst, and (3) the electrostatic-field strength on the surface, which may promote carboniogenic reaction. The solid acids mentioned in 2 including both Brønsted and Lewis acid sites have been investigated by amine titration,⁴⁻⁶ electron spin resonance spectroscopy,⁷⁻¹⁰ infrared spectroscopy,¹¹⁻¹⁷ etc. The effect of electrostatic field

was discussed by Rabo, *et al.*,^{2,18,19} and by Boudart, *et al.*²⁰ The electrostatic-field strength was calculated on the model of the ionic crystal.

- (1) For example, R. M. Barrer, *Proc. Roy. Soc., Ser. A*, **167**, 392 (1938); R. M. Barrer, *J. Soc. Chem. Ind.*, **44**, 130 (1945); R. M. Barrer and L. Belchetz, *ibid.*, **44**, 131 (1945); R. M. Barrer, *Trans. Faraday Soc.*, **45**, 358 (1949); R. M. Barrer and A. B. Robins, *ibid.*, **49**, 807, 929 (1953); R. M. Barrer and B. E. F. Fender, *J. Phys. Chem. Solids*, **21**, 1, 12 (1961); R. M. Barrer, *Endeavour*, **23**, No. 90, 122 (1964).
- (2) J. A. Rabo, P. E. Pickert, D. N. Stamires, and J. E. Boyle, *Actes 2nd Congr. Int. Catalyse, Paris*, Sec. II, No. 104 (1960).
- (3) P. B. Weisz and V. J. Frilette, *J. Phys. Chem.*, **64**, 382 (1960).
- (4) A. E. Hirschler, *J. Catal.*, **2**, 428 (1963).
- (5) M. Ikemoto, K. Tsutsumi, and H. Takahashi, *Seisan Kenkyu*, **21**, 453 (1969).
- (6) H. Otouma, Y. Arai, and H. Ukihashi, *Bull. Chem. Soc. Jap.*, **42**, 2449 (1969).
- (7) D. N. Stamires and J. Turkevich, *J. Amer. Chem. Soc.*, **86**, 749 (1964).
- (8) J. T. Richardson, *J. Catal.*, **9**, 172 (1967).
- (9) F. R. Dollish and W. K. Hall, *J. Phys. Chem.*, **71**, 1005 (1967).
- (10) W. K. Hall and F. R. Dollish, *J. Colloid Interface Sci.*, **26**, 261 (1968).
- (11) J. B. Uytterhoeven, L. G. Christner, and W. K. Hall, *J. Phys. Chem.*, **69**, 2117 (1965).
- (12) T. R. Hughes and H. M. White, *ibid.*, **71**, 2192 (1967).
- (13) J. W. Ward, *J. Catal.*, **9**, 225, 396 (1967); **10**, 34 (1968); **11**, 238, 251 (1968); **13**, 321 (1969).
- (14) P. E. Eberly, Jr., *J. Phys. Chem.*, **72**, 1042 (1968).
- (15) F. R. Cannings, *ibid.*, **72**, 4691 (1968).
- (16) J. A. Rabo, C. L. Angell, and V. Schomaker, *Proc. 4th Int. Congr. Catalysis, Moscow*, No. 54 (1968).
- (17) J. B. Uytterhoeven and R. Schoonheydt, *J. Catal.*, **13**, 425 (1969).
- (18) P. E. Pickert, J. A. Rabo, E. Dempsey, and V. Schomaker, *Proc. 3rd Int. Congr. Catalysis, Amsterdam*, 714 (1964).
- (19) J. A. Rabo, C. L. Angell, P. H. Kasai, and V. Schomaker, *Discuss. Faraday Soc.*, **41**, 328 (1966).
- (20) Y.-Y. Huang, J. E. Benson, and M. Boudart, *Ind. Eng. Chem., Fundam.*, **8**, 346 (1969).

In a previous paper,²¹ we measured the heat of the immersion of cation-exchanged zeolites using an organic adsorbate and established quantitatively that, when Na of Na-Y zeolite is replaced with Ca, the electrostatic-field strength increases. When the Ca exchange is low, Ca ions mainly occupy the S_I site, which is linked to the large cavity through pores about 2 Å in diameter. As the pore is not large enough for the organic liquid to pass through, the cation exchange does not influence the heat of immersion. With increasing exchange, the Ca ions saturate the S_I site and then occupy sites in the large cavity. With Ca ions at the later sites, the electrostatic-field strength, as calculated from the heat of immersion, increases remarkably.

This paper will report a study on the effect of changing silica/alumina ratio on the electrostatic-field strength, using five different faujasite-type zeolites. The correlation of the silica/alumina ratio with the catalytic activity for cumene cracking will also be discussed.

Experimental Section

The zeolites used for the experiment were Na-X_{2.5}, Na-Y_{5.0}, Na-Y_{3.25}, Na-Y_{3.85}, and Na-Y_{4.6}; the first two are Linde molecular sieve 13X and SK-40, respectively, while the last three were synthesized from silica-alumina gel and caustic soda. The silica/alumina ratio was obtained by chemical analysis and by evaluating the unit-cell dimensions from the X-ray diffraction pattern. The diffraction pattern and water sorption capacity were similar to those of binder-free Linde 13X. The Ca form was prepared by the cation exchange of Na-form zeolite with an aqueous solution of the CaCl₂. The exchange was performed at about 90° while stirring; the same treatment was then repeated to increase the degree of exchange. Finally, the exchanged material was washed until AgNO₃ treatment confirmed the presence of no Cl⁻, and then it was dried.

The cation exchange was determined by chemical analysis and by flame photometry. It was represented as mole per cent of Na exchanged.

The heat of immersion was measured by a method reported previously.²¹ Some 0.2–0.3 g of zeolite was placed in a glass ampoule and then activated by heat treatment for 10 hr at the chosen temperature at 10⁻⁵ mm and then sealed. The heat of immersion at 25° was measured on a twin-conduction-type microcalorimeter (Applied Electric Laboratory Co.). The adsorbates used for the measurement were commercial reagents which were purified by conventional methods and then dehydrated by molecular sieve 4A.

The BET specific surface area was obtained from the amount of nitrogen adsorption and was calculated from the finite-layer adsorption isotherm by means of the BET equation for narrow capillaries. The pretreatment of the zeolite sample was the same as that described in the measurement of the heat of immersion.

The catalytic activity for cumene cracking was measured by means of a pulse reactor. Sixty milligrams of 28–60 mesh activated zeolite was packed in a reaction tube with an inside diameter of 4 mm and was then treated for 2 hr at 450° by using helium as carrier gas (at a flow rate of 60 cc/min). After the pretreatment, cumene pulses were injected into the helium stream to the catalyst. The pulse volume was 8 μl. The products were analyzed by means of a gas chromatograph. The flow rate of helium during the reaction was 60 cc/min.

Results

The heats of immersion of zeolite in various organic solvents are listed in Table I. The Na- and Ca-form zeolites here were pretreated at 450°, while the H form was obtained by heating NH₄-exchanged zeolite at 400°. With *n*-hexane, whose dipole moment μ is zero, neither the cation type nor the silica/alumina ratio affects the heat of immersion and the amount of the heat is almost fixed, whereas with 1-nitropropane, which has a dipole moment of 3.57 D, some effects are observed. In the case of the Na form, the difference in silica/alumina ratio does not affect the heat of immersion; however, with the Ca form the effect of the

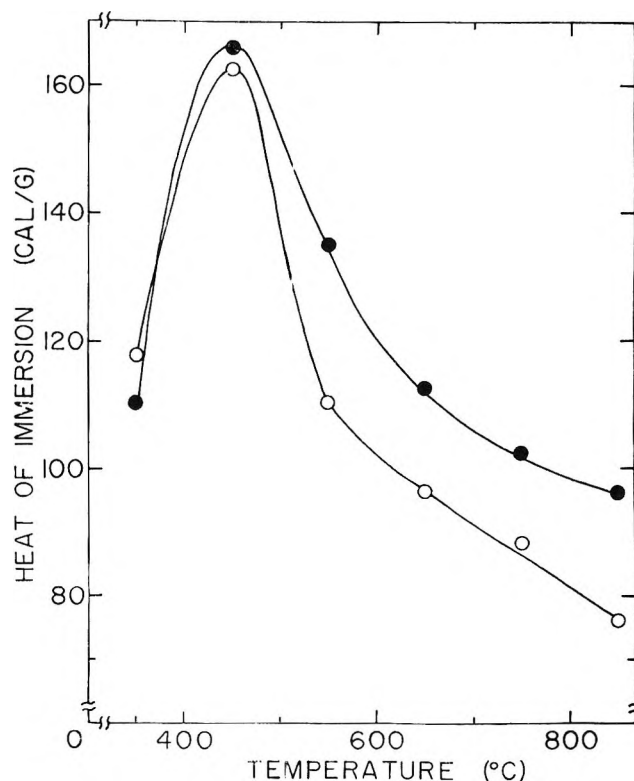


Figure 1. Dependence of heats of immersion of Ca-exchanged zeolites in 1-nitropropane on pretreatment temperature: open symbol, Ca-X_{2.5} (Ca²⁺, 98.9%); closed symbol, Ca-Y_{5.0} (Ca²⁺, 84.6%).

(21) K. Tsutsumi and H. Takahashi, *J. Phys. Chem.*, **74**, 2710 (1970).

Table I: Heats of Immersion of Zeolites^a in Organic Liquids at 25°

Silica/ alumina ratio	Cation	Degree of exchange, mol %	Heats of immersion, cal/g ^b		Heats of immersion, ergs/cm ²	
			<i>n</i> -Hexane (0) ^c	1-Nitro- propane (3.57 D)	<i>n</i> -Hexane	1-Nitro- propane
2.5	Na	98.9	32.4	73.5	161	369
	Ca		29.1	102.7	136	759
3.25	Na	95.7	28.0	67.4	144	346
	Ca		31.4	198.8	159	1007
3.85	Na	89.5	28.8	65.7	143	325
	Ca		29.7	216.2	136	989
4.6	Na	89.8	27.5	57.2	129	269
	Ca		28.0	213.8	131	997
5.0	Na	84.6	24.3	53.2	121	264
	Ca		24.7	166.0	110	733
	H ^d		19.7	59.4	92	277

^a Evacuated at 450°. ^b The weight of zeolite was represented by that of dehydrated species. ^c Dipole moment. ^d Evacuated at 400°.

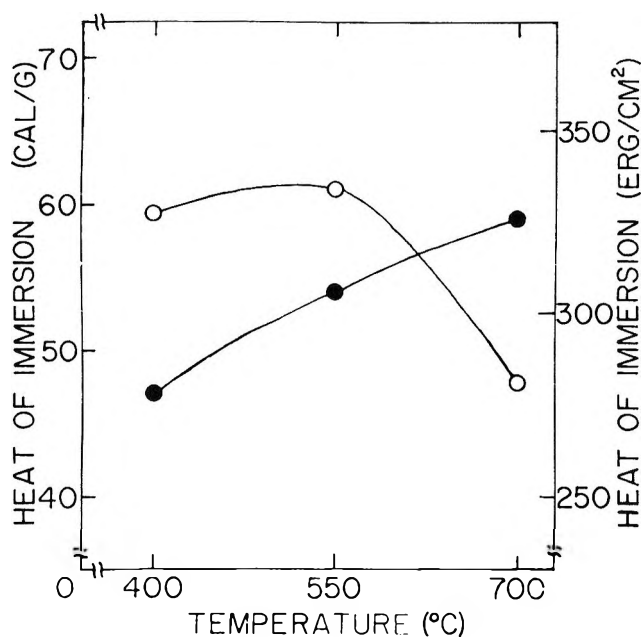


Figure 2. Dependence of heats of immersion of decationated zeolites in 1-nitropropane on pretreatment temperature: open symbol, cal/g; closed symbol, ergs/cm².

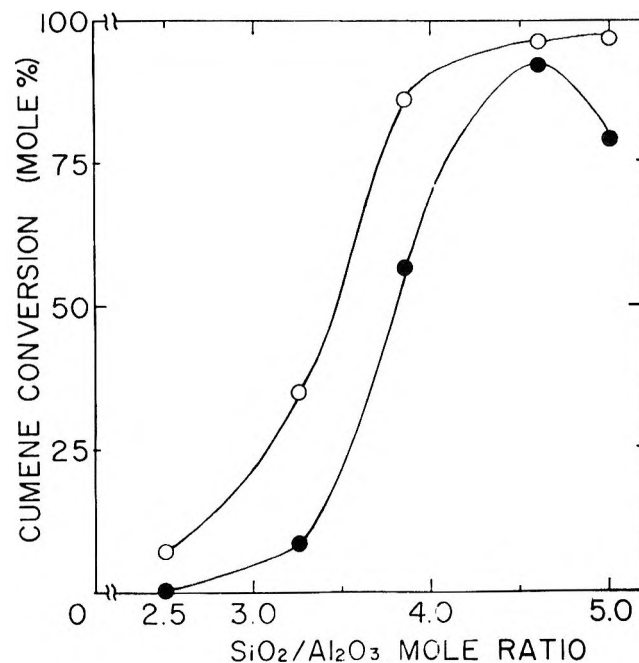


Figure 3. Correlation between cumene cracking activity and silica/alumina ratio of Ca-exchanged zeolites: open symbol, reaction at 450°; closed symbol, reaction at 400°.

silica/alumina ratio becomes large and, moreover, the heat increases remarkably. According to Zettlemoyer, *et al.*,²² the heats of immersion in 1-nitropropane for titanium dioxide (rutile) and calcium fluoride, which are both highly ionic and which have many electric-charge sites on the surface, are 665 and 570 ergs/cm², respectively. Here it must be noted that the heat of immersion of Ca-form zeolite is almost equal to the above values. The heat of immersion with the H-form zeolite, however, remains smaller, almost identical with that of the Na form.

Figures 1 and 2 show the changes in the heat of immersion in 1-nitropropane when the preparation temperature is varied. All the samples reach a maximum when

pretreated at 450°, while when pretreated at a higher temperature they show, rather, a decrease.

Figure 3 illustrates the change in the catalytic activity for cumene cracking on Ca-form zeolite pretreated at 450°. The main products of cumene cracking are benzene and propylene; the other products are negligible. The Na-form zeolite is inactive at any silica/alumina ratio, whereas the Ca form shows a high catalytic activity with an increase in the silica/alumina ratio, and Ca-Y_{4.6} gives the highest.

(22) A. C. Zettlemoyer, J. J. Chessick, and C. M. Hollabaugh, *ibid.*, 62, 489 (1958).

Discussion

The heat of immersion is a change in energy following the disappearance of a solid surface and the formation of a new solid-liquid interface when a solid is immersed in a liquid. Assuming that the intermolecular force is additive, the energy generated by the interaction between solid molecules and liquid molecules can be expressed, as was shown in a previous report,²¹ by the sum of the dispersion force (h_i^d), the polarization force (h_i^p), and the force due to the interaction of a permanent dipole with the electrostatic field of the solid (h_i^u). If the polarizability, surface enthalpy, and cross-sectional area of the *n*-hexane and 1-nitropropane used in the experiment are assumed to be equal, the h_i^u ($= -n\mu F$) value mentioned above is equivalent to the difference between the heat of the immersion of 1-nitropropane and that of *n*-hexane. If the cross-sectional area per molecule is assumed to be 25 \AA^2 , the electrostatic-field strength on the zeolite surface, F , is as given in Table II. On the zeolite surface, as the

tion of a strong electrostatic field is apparent. Furthermore, it becomes larger with an increase in the silica/alumina ratio.

Faujasite-type zeolite has several cation sites. The S_I site (16 per unit cell) is situated at the center of a hexagonal prism and is linked to sodalite cages by six puckered oxygen rings about 2 \AA in diameter. The S_{II} site (32 per unit cell) is located inside the large cavity and cations at this position are exposed to adsorbed molecules. Besides, as has been reported previously,²¹ since the S_I site does not interact directly with adsorbed molecules, the most important point concerning the sites is the change in the electrostatic field caused by the cations located on the S_{II} site inside the large cavity. The cations at the S_{II} site, having a three-fold oxygen-ion coordination all at one side with no electrostatic shielding on the other side, induce a large electrostatic field in the large zeolite cavity.

The effect of the silica/alumina ratio is considered to be as follows. In the case of univalent cations like Na^+ , since the number of the cation and the number of the site that form the electrostatic field decrease with an increase in the silica/alumina ratio, the net electrostatic-field strength becomes smaller. On the other hand, in the case of bivalent cations like Ca^{2+} , parts of cation sites in the large cavity become to be positively charged and others to be negatively charged with an increase in the silica/alumina ratio.¹⁹ The polarization thus occurs, and a strong electrostatic field is formed. This tendency seems remarkable when the silica/alumina ratio is high. However, it is necessary to consider that the net electrostatic-field strength is calculated by multiplying the strength by the number of each site.

The Ca-form zeolite used in the experiment does not have a 100% Ca exchange, but contains residual Na ions. When the degree of exchange is low, the electrostatic-field strength and the catalytic activity of the Ca form is almost the same as those of the Na form.^{21,23} These facts suggest that the S_I site, which is prevented from interacting with adsorbed molecules, has priority for bivalent cations. The number of the S_I site is 16 per unit cell. Accordingly, if Ca ions in addition to the 16 Ca ions at S_I site contribute to the increase in the electrostatic-field strength, the field strength, F_0 , of the Ca-type zeolite fully exchanged can be calculated using the observed strength of the Ca-Na-type zeolite. The values of F_0 were calculated at various silica/alumina ratios; the results are listed in Table II. Apparently, F_0 increases remarkably with an increase in the silica/alumina ratio, and besides, the difference in F_0 between the Na- and Ca forms becomes large. However, F_0 decreases with Ca-Y_{5.0}. This is because the electrostatic-field strength obtained from the heat measurement is a product of the number and the strength of each electrostatic-field site. The increase in the silica/alumina ratio brings about a decrease in the

Table II: Electrostatic-Field Strength of Zeolites

Silica/ alumina ratio	Cation	Degree of exchange, mol %	Field strength	
			$F \times 10^{-6}$, esu/cm ²	$F_0 \times 10^{-6}$, esu/cm ²
2.5	Na		1.4	
	Ca	98.9	4.4	
3.25	Ca	100		4.4
	Na		1.4	
	Ca	95.7	5.9	
3.85	Ca	100		6.3
	Na		1.3	
	Ca	89.5	6.0	
4.6	Ca	100		7.2
	Na		1.0	
	Ca	89.8	6.1	
5.0	Ca	100		7.6
	Na		1.0	
	Ca	84.6	4.4	
	Ca	100		6.3
	H ^a	90.5	1.3	

^a Evacuated at 400°.

exposed cations represent points of very high charge, whereas other points of the area may even bear the opposite charge, a uniform charge distribution cannot be attained. Furthermore, a fraction of the organic molecules must be adsorbed at locations which cannot contribute to the interaction between the electrostatic field and the dipole of the molecule. These facts show that the F value obtained in this way must be considered to be the average electrostatic-field strength within the accessible cavities in the zeolite crystal.

F of the Na form decreases with an increase in the silica/alumina ratio. F of the Ca form, on the other hand, is larger than that of the Na form, and the forma-

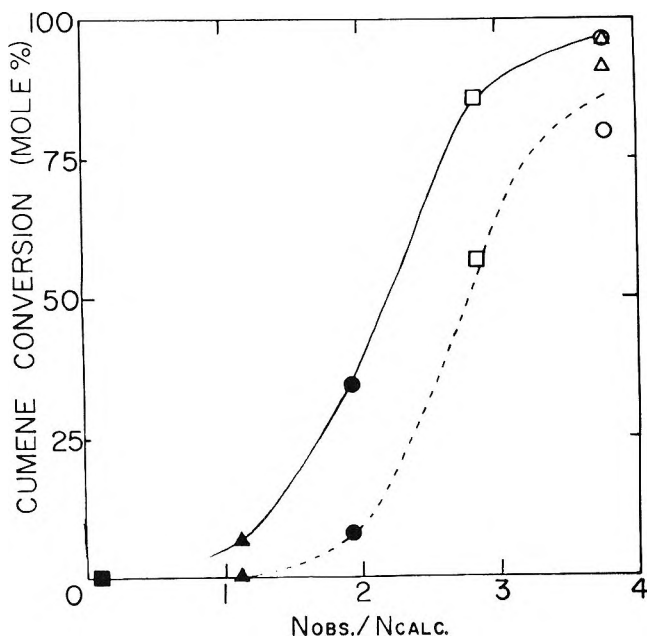


Figure 4. Correlation between cumene cracking activity and value of $N_{\text{obsd}}/N_{\text{calcd}}$ of Ca-exchanged zeolites: solid line, reaction at 450°; broken line, reaction at 400°; ○, Ca-Y_{5.0}; △, Ca-Y_{4.6}; □, Ca-Y_{3.85}; ●, Ca-Y_{3.25}; ▲, Ca-X_{2.5}; ■, Na-Y_{5.0}.

number of the site. The field strengths of Ca-form zeolites can be recalculated using the F_0 values of 1.32, 1.89, 2.16, 2.28, and 1.89 V/Å for zeolites with silica/alumina ratios of 2.5, 3.25, 3.85, 4.6, and 5.0, respectively. These values are considered to be the field strengths at the distance of 2.8 Å (the radius of a molecule with the 25 Å² area).

According to the Gauss theorem, the observed charge density of the Ca-form zeolite, N_{obsd} , can be calculated from the value of F_0 , as in a previous paper.²¹ The results are shown in Table III. Also the number of Ca ions located in the large cavity, N_{calcd} , which are calculated from the value of the surface area, are listed in Table III. The most important thing to notice here

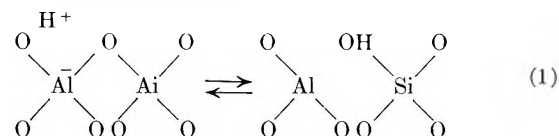
Table III: The Values of N_{obsd} , N_{calcd} , and $N_{\text{obsd}}/N_{\text{calcd}}$ of Ca-Form Zeolites

Silica/ alumina ratio	$N_{\text{obsd}} \times 10^{-14}/$ cm ²	$N_{\text{calcd}} \times 10^{-14}/$ cm ²	$N_{\text{obsd}}/$ N_{calcd}
2.5	1.5	1.3	1.1
3.25	2.1	1.1	1.9
3.85	2.4	0.8	2.8
4.6	2.5	0.7	3.8
5.0	2.1	0.6	3.8

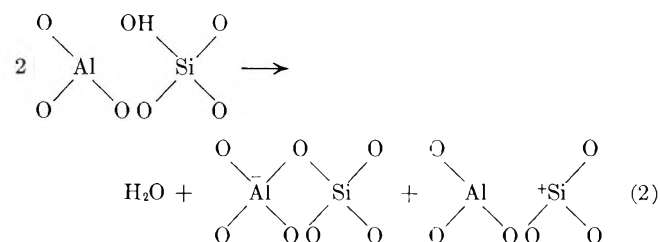
is that the value of $N_{\text{obsd}}/N_{\text{calcd}}$ shows the proportion of the point charge effective for the formation of the electrostatic field among cation-anion sites inside the zeolite; that is, it represents the relative field strength of

each site. The effect of the silica/alumina ratio on $N_{\text{obsd}}/N_{\text{calcd}}$ is obvious.

The F value calculated for H-form zeolite with a silica/alumina ratio of 5.0 is shown in Table II. It resembles that of the Na form, for the proton, corresponding to the anion in a ratio of 1:1, does not particularly contribute to the formation of a strong electrostatic field. Furthermore, protons easily form hydroxyl groups at low temperatures by reacting with lattice oxygens.¹¹ The heat of immersion per unit of the weight of



H-form zeolite in 1-nitropropane reaches a maximum at the pretreatment temperature of 550°, as is illustrated by the open symbols in Figure 2; however, the heat per unit of surface area increases with a rise in the preparation temperature. The heat of immersion in *n*-hexane, on the other hand, is constant within the limits of experimental error. It is considered that, since with H-form zeolite the hydroxyls can be removed by forming water upon heat treatment, sites have the possibility of being divided into positive and negative charge sites²⁴ according to eq 2 and that this division will probably have a positive effect on the electrostatic-field strength.

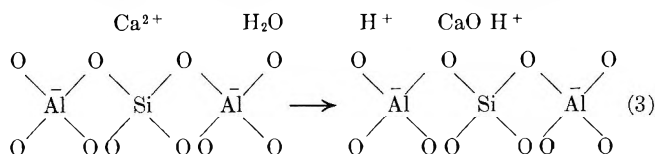


The heat of the immersion of Ca-form zeolite in 1-nitropropane is plotted against the pretreatment temperature in Figure 1. The maximum value is attained with 450° pretreatment; later, it decreases. The surface area of Ca-form zeolite is almost constant on pretreatment below around 750°. It shows especially strong thermal stability when the silica/alumina ratio is high. Therefore, the amount of the heat of immersion in 1-nitropropane corresponds directly to the electrostatic-field strength. With pretreatment at a low temperature, if there are free water molecules inside the main cavity, the electrostatic field formed on the surface is shielded by the high dielectric constant of water. The electrostatic field does not become effective for the adsorption of molecules until the water molecules are removed to some extent. It is supposed that Ca-form

(23) K. Tsutsumi and H. Takahashi, *J. Catal.*, in press.

(24) It is known that this positive site, together with aluminum with threefold oxygen coordination, acts as Lewis acid site.

zeolite changes according to eq 3 when treated at a high temperature. It is very likely that, if the change follows



the above equation completely, the Ca-form zeolite takes the form of the H-form zeolite, into which CaO is then dispersed and its electrostatic-field strength comes to correspond to the strength of the H-form zeolite. Thus, it is possible to interpret the above experimental data by saying that the heat of immersion, though it reaches a maximum with 450° pretreatment, afterwards decreases remarkably; following the complete dehydration, the electrostatic-field strength is reduced by the formation of a Lewis acid site similar to that of the H-form zeolite.

The catalytic activity of the Ca-form zeolite for cumene cracking is plotted against $N_{\text{obsd}}/N_{\text{calcd}}$ in Figure 4. The higher the $N_{\text{obsd}}/N_{\text{calcd}}$ ratio, the larger the activity becomes. What is notable here is that, while the $N_{\text{obsd}}/N_{\text{calcd}}$ ratio is the same in both Ca-Y_{4.6} and Ca-Y_{5.0}, the catalytic activity is higher with Ca-Y_{4.6}. The catalytic activity depends on the strength and

the number of the sites of high electrostatic field. This is the same phenomenon as when the activity is determined by the acid strength and acidity of solid acid.²⁵ In the case of cumene cracking, since the $N_{\text{obsd}}/N_{\text{calcd}}$ ratio and activity show a linear relationship, it is clear that a stronger field generates a higher activity. Hence, the reason for the reversion of activity between Ca-Y_{4.6} and Ca-Y_{5.0} when the $N_{\text{obsd}}/N_{\text{calcd}}$ ratio is the same is the difference in the number of Ca ions on the S_{II} site which are effective on the reaction, that is, 10 and 5 per unit cell with Ca-Y_{4.6} (Ca²⁺, 89.8%) and Ca-Y_{5.0} (Ca²⁺, 84.6%), respectively, which were used for the reaction.

While the electrostatic-field strength of H-Y_{5.0} keeps a value similar to that of the Na form, its catalytic activity for cumene cracking is extremely high; it reaches 100% at a reaction temperature of 400°. ²³ Here the process of cumene cracking must be considered. It is known that the cracking proceeds in the form of a carbonium-ion intermediate; in this case, the effective active site is a Brønsted acid. The high activity of H-Y_{5.0} is derived from this high Brønsted acidity.^{5,6}

(25) M. Misono, Y. Saito, and Y. Yoneda, *Proc. 3rd Int. Congr., Catalysis, Amsterdam*, 408 (1964).

Studies of Transition Phenomena of Some Organic Solids by Electrical

Conductivity Measurement at Low Temperature

by Hajime Kadoi, Yoneho Tabata,* and Keichi Oshima

*Department of Nuclear Engineering, Faculty of Engineering, University of Tokyo, Tokyo, Japan
(Received February 19, 1971)*

Publication costs borne completely by The Journal of Physical Chemistry

The electrical conductivities of vinyl acetate (VA) and acrylonitrile (AN) monomers were measured during temperature elevation between -196° and the melting points. This method is useful for the observation of transition phenomena. The glass transition and crystallization temperature of VA were observed at -151 and -132°, respectively. The transition points of AN were found to be at -160, -142, -131, and -112°. The results are in good agreement with those obtained by thermal and X-ray analyses. The transition of AN at -160° is not a crystallization, but a glass transition. The amorphous part in crystalline AN is difficult to crystallize.

Introduction

Chemical reactions in organic solids at low temperature are expected to be influenced by phase. In particular, the effects of different phases of solid on radiation-induced polymerization and radiolysis at low tem-

peratures have a marked influence on reaction characteristics and have been studied by a few groups recently.¹⁻⁵ In most cases, phase transition measurements are made by calorimetry. However, electrical conductivity measurements, which have been to study

the behavior of active species captured in irradiated organic solids,⁶⁻¹⁰ have also been found to be a simple and sensitive means for the detection of transition temperature.^{8,10} The authors have reported some measurements of transitions of solid monomers by the electrical conductivity technique.¹⁰ In the present paper, further detailed study of phase transitions of vinyl acetate (VA) and acrylonitrile (AN) is described.

Seki, *et al.*, studied VA by detailed thermal analysis and found the glass transition and crystallization temperatures of the solid at -148 and -125° , respectively, and concluded that the monomer is in a supercooled liquid state in the region between -148 and -125° .¹¹ The results of this study suggest that the glass transition temperature at -129° reported by Goldanskii, *et al.*,^{12,13} might have to be assigned as a crystallization. On the other hand, the transition at -151° observed by the authors in their previous conductivity measurements¹⁰ should be assigned to glass transition according to Seki, *et al.*¹¹

As for AN, the transition points are observed at -160 , -145 , -130 , and -110° by thermal measurements,^{1,14-16} X-ray,¹⁷ and conductivity measurement.¹⁰ The transitions at -145 , -130 , and -110° have been assigned to crystal-crystal transitions. The transition at -160° was assigned to be a glass-crystal transition by Kargin, *et al.*, with some ambiguity.¹ In the present work, transitions of these solid monomers were studied by conductivity measurement to obtain further informations.

Experimental Section

Sample preparation procedures and the apparatus used for the conductivity measurements were identical with those described previously.¹⁰ A pair of aluminum electrodes of 1 cm^2 were set parallel with a separation of about 0.5 mm . A guard electrode was not employed, because the surface current on the sample was negligible. Purified samples were introduced into the vessel by distillation *in vacuo* below 10^{-4} Torr and cooled to liquid nitrogen temperature. The current measurements were performed during temperature elevation from -196° with the heating rate of about $1^\circ/\text{min}$.

It has been suggested in previous papers^{6,8,10} that the so-called intrinsic current, due to the motion of electrons or holes, was undetectable and only polarization (positive) and depolarization (negative) currents, due to the rotation of permanent dipoles, would be detected in the low-temperature region.

In order to make this point clear, the measurements of conductivity were performed in the following three processes: (1) cooling down to -196° without an applied field and hence warming up with the applied field, "OFF-ON"; (2) both cooling down to -196° and warming up with an applied field, "ON-ON"; (3) cooling down to -196° with an applied field and

hence warming up without the applied field, "ON-OFF."

These processes are the same as applied by Willard, *et al.*, for studying 2-methyltetrahydrofuran and methylcyclohexane.⁸

Results and Discussion

Vinyl Acetate. Noncrystalline VA was prepared by rapid cooling from liquid state. Currents as a function of temperature are shown in Figures 1A, B, and C, for the three processes mentioned above, respectively.

When the external field was applied to the sample which was cooled down rapidly to -196° without an applied field, a transient current due to the initial polarization, as explained by Willard, *et al.*, was detected.^{6,10}

After this transition current faded away, no detectable current was observed at -196° . Then, when the temperature of the sample was elevated from -196° under the applied electric field, a positive peak appeared at -151° which was followed immediately by a negative peak, and a large positive peak appeared again at -132° , and hence the current increased monotonously with the increase of temperature up to the melting point at -94° . The results for this "OFF-ON" process are shown in Figure 1A.

The sample which was cooled down to -196° under the applied field had no positive peak at -151° during the elevation of temperature. The negative peak,

- (1) V. A. Kargin, V. A. Kabanov, I. M. Papisov, and B. P. Zubov, *Dokl. Akad. Nauk SSSR*, **141**, 389 (1961); *J. Polymer Sci. Part C*, **4**, 767 (1964).
- (2) I. M. Barkalov, V. I. Goldanskii, N. S. Enikolopyan, S. F. Terekhova, and G. M. Trofimova, *J. Polymer Sci. Part C*, **4**, 897 (1964).
- (3) I. M. Barkalov, V. I. Goldanskii, N. S. Enikolopyan, S. F. Terekhova, and G. M. Trofimova, *J. Polymer Sci. Part C*, **4**, 909 (1964).
- (4) T. Miyazaki, T. Wakayama, K. Fueki, and Z. Kuri, *Bull. Chem. Soc. Jap.*, **42**, 2086 (1969).
- (5) T. Wakayama, T. Miyazaki, K. Fueki, and Z. Kuri, *J. Phys. Chem.*, **74**, 3584 (1970).
- (6) B. Wiseall and J. E. Willard, *J. Chem. Phys.*, **46**, 4387 (1967).
- (7) I. Kosa-Somogyi and J. Balog, *Advan. Chem. Ser.*, **No. 82**, 291 (1962).
- (8) A. C. Ling and J. E. Willard, *J. Phys. Chem.*, **73**, 2408 (1969).
- (9) I. Kosa-Somogyi, *Proc. Jap. Conf. Radioisotop. 9th*, 588 (1969).
- (10) H. Kadoi, Y. Tabata, and K. Oshima, *J. Phys. Chem.*, **74**, 3262 (1970).
- (11) K. Nakatsuka, K. Adachi, H. Suga, and S. Seki, *J. Polymer Sci. Part B*, **6**, 779 (1968).
- (12) I. M. Barkalov, V. I. Goldanskii, N. S. Enikolopyan, S. F. Terekhova, and G. M. Trofimova, *Dokl. Akad. Nauk SSSR*, **147**, 395 (1962).
- (13) I. M. Barkalov, V. I. Goldanskii, and V. B. Rapoport, *Dokl. Akad. Nauk SSSR*, **161**, 1368 (1965).
- (14) R. Bensasson and A. Dwarin, *C. R. Acad. Sci.*, **256**, 4903 (1963).
- (15) R. Bensasson, A. Dwarin, and R. Marx, *J. Polymer Sci. Part C*, **4**, 881 (1964).
- (16) B. V. Lebedev, I. B. Rabinovich, and L. Ya. Martynenko, *Vysokomol. Soedin. Ser. A*, **9**, 1640 (1967).
- (17) K. Ishigure, Theses, University of Tokyo, 1966.

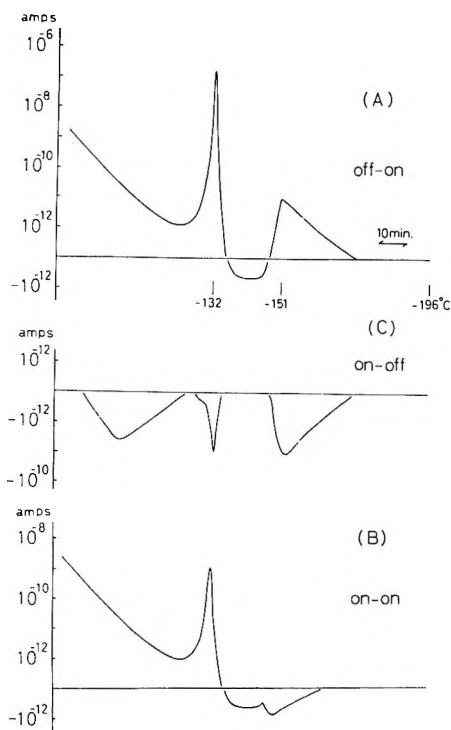


Figure 1. Current vs. temperature during warming up from -196° for VA glass; applied voltage, 300 V; initial transient currents at -196° were omitted in each curve; (A), OFF-ON; (B), ON-ON; (C), ON-OFF.

however, was still observed, though the peak has shifted to lower temperature than in the case of the "OFF-ON" process. Moreover, intensity of the positive peak at -132° was reduced by two orders of magnitude as compared with that in the "OFF-ON" process. After this point, the current has increased gradually with increase of temperature, coinciding with the curve of the "OFF-ON" process near the melting point. The results for the "ON-ON" process are shown in Figure 1B.

When the applied field was removed from the sample cooled to -196° under electric field, a negative transient current, due to the initial depolarization as explained by Willard, *et al.*,⁶ in the case of 3-methylpentane, was observed. However, since these currents due to initial depolarization in the "ON-OFF" process and the initial polarization in the "OFF-ON" process are also observed even without existence of the sample in the cell, it can be concluded that these initial transient currents are mainly due to the polarization and the depolarization of materials other than the sample such as the insulators of wires and terminals. When the sample was warmed up from -196° after the initial depolarization current faded away, only negative peaks were observed at -151° , -132° , and -105° and hence the current decreased gradually. The results for the "ON-OFF" process are shown in Figure 1C. The negative peak at -151° has about the same shape and intensity as that of the "OFF-ON" process, but the peak at -132° is lower in intensity than that of the "OFF-ON" process.

The peaks observed at -151° and -132° correspond well with the glass transition and crystallization temperatures reported by Seki, *et al.*¹¹ Although the permanent dipoles of the molecules should be randomly frozen in the "OFF-ON" process, the molecules can not move freely below the glass transition temperature, and the polarization phenomenon does not occur at -196° on application of external field, except for the initial polarization as already explained above. If the molecules are warmed up under this condition, they become rotatable into the direction of the applied field at the glass transition temperature, producing the orientational polarization current. In the case of the "ON-ON" process, however, the dipoles should already be frozen into the direction of the applied field in the initial stage. The positive peak thus does not appear but a negative peak more intensified than in the case of the "OFF-ON" process is observed, due to thermal randomization of oriented dipoles (orientational depolarization). In the case of the "ON-OFF" process, only the negative peak due to thermal randomization is observed at -151° . The same phenomena have been observed by Willard, *et al.*, for 2-methyltetrahydrofuran and methylcyclohexane.⁸ They explained it in terms of the competition between the processes of polarization by the applied field and of depolarization by thermal agitation in the vicinity of the glass transition point in the case of the "OFF-ON" process.

With all these processes, a peak at -151° is reproducible with the recycle of cooling and warming, if the sample is not warmed to the temperature region above -132° . At the crystallization temperature of -132° , a large positive peak reaching a value of up to 10^{-4} A was observed in the "OFF-ON" process. This suggests an occurrence of a large rotational orientation into the direction of the applied field, when the molecules crystallize at -132° . In comparison to this large orientation at the crystallization temperature, it can be concluded that the orientation at the glass transition temperature of -151° is a much slighter one. The appearance of a negative peak in the "ON-OFF" process at -132° also suggests that the orientation of dipoles cannot be completely removed by thermal agitation in the supercooled liquid state between -151° and -132° . This indicates that the supercooled VA is in a considerably restricted state in which only a slight rotation of the molecules is possible. Above the crystallization temperature, the current in the "ON-ON" process is less than that in the "OFF-ON" process. This "ON-ON" current can be regarded as due to the intrinsic conductivity of VA. The "OFF-ON" current, however, is the sum of the intrinsic current and the polarization current. The broad peak at -105° can be attributed to the depolarization of residual polarization because no corresponding peak is observed in either of the "OFF-ON" and "ON-ON" processes.

When the sample was warmed up to near the melting

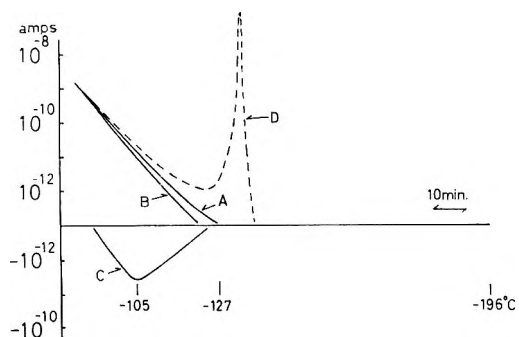


Figure 2. Current vs. temperature during warming up from -196° for VA crystal; applied voltage, 300 V; initial transient currents at -196° were omitted in each curve; curve A, OFF-ON; B, ON-ON; C, ON-OFF; and D, crystallization peak in OFF-ON process of VA glass.

point for completion of crystallization and recooled to -196° and then warmed up again by any of the processes, no current was observed below -127° except for the initial polarization and depolarization currents, although the current increased with increasing the temperature above -127° in accordance with the curve observed with glassy samples near the melting point. The results are shown in Figure 2 with the crystallization curve for VA glass in "OFF-ON" process for comparison. This fact supports the assignment that the peak at -132° corresponds to the crystallization temperature.

Acrylonitrile. The same measurements were carried out with AN solid. Crystalline AN is obtained by rapid cooling of the liquid phase, but small amounts of amorphous monomer are contained. The currents as a function of temperature are shown in Figures 3A, B, and C, for the three different processes, respectively.

In the "OFF-ON" process, a positive peak at -160° , followed by a negative peak, was observed corresponding to the peak of VA at -151° . In the "ON-ON" process, however, both the positive and negative peaks were also observed in the vicinity of -160° as in the case of the "OFF-ON" process. This is different from the case of VA. When, however, the sample was warmed up after keeping it for at least 10 hr at -196° under the applied field in the "ON-ON" process, a positive peak disappeared and only a negative peak was observed as in the case of VA (Figure 3B). In the "ON-OFF" process, no current was observed in this region. However, when the applied field was removed after keeping the sample for an extended period at -196° under the applied field, a negative peak due to depolarization was observed at -160° during warming up of the sample as in the case of VA (Figure 3C). The peak at -160° was always observed repeatedly by either of the three processes (in cooling and warming) in the temperature region below the melting point at -83° . This transition point (at -160°) was found by Kargin, *et al.*, from thermal analysis and it was as-

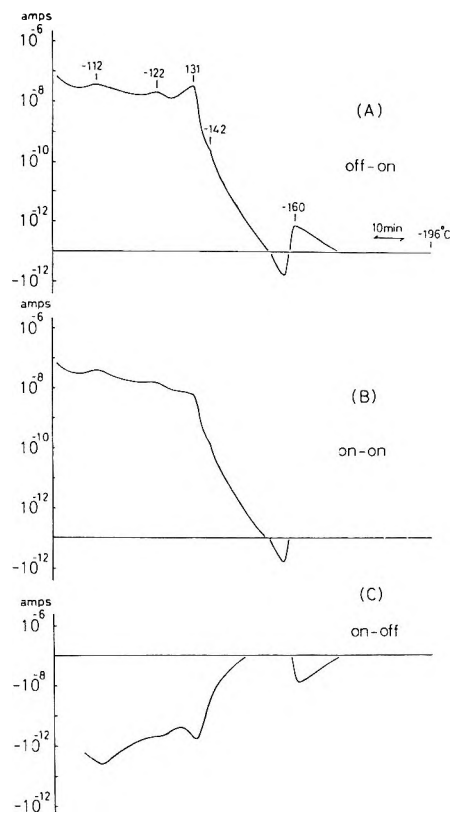


Figure 3. Current vs. temperature during warming up from -196° for AN; applied voltage, 300 V; initial transient currents at -196° were omitted in each curve; (A), OFF-ON; (B), ON-ON; (C), ON-OFF.

signed to be the glass-crystal transition point, based on the results of polymerization of monomers condensed on a metal surface with Mg vapor.¹ Crystallization phenomenon in a glass is an irreversible process; therefore, the peak should not be expected to be observed repeatedly, and only once with the new glassy AN sample produced by rapid cooling from the liquid phase. The peak at -160° was observed repeatedly in recycled processes of cooling and warming of the sample below the melting point. This result means that this peak is not due to crystallization, but rather to a glass transition of the amorphous part of AN coexisting with the crystal.

The experimental results described show that the dipoles of AN cannot be orientated to the field immediately, when the monomers are cooled down to -196° in either the "ON-ON" or "ON-OFF" processes. Orientation can, however, be achieved by keeping the sample for a long period at -196° under the applied field. Under such conditions the result is very similar to the case of VA. In contrast to VA, solid AN is crystalline; X-ray studies indicate that the amorphous content of AN is very low.^{17,18} The results show that the crystallization of this remaining amorphous part in AN is difficult. In the case of the

(18) Y. Tabata, *Advan. Macromol. Chem.*, **1**, 283 (1968).

“OFF-ON” process (Figure 3A), the current increased rapidly with increasing temperature, and a large peak appears at -131° , accompanied by a small shoulder at -142° . Then other positive peaks appear at -122° and -112° and hence the current increases up to the melting point. In the case of the “ON-ON” process (Figure 3B), positive peaks are also observed at -142° , -131° , -122° , and -112° as in the case of the “OFF-ON” process. The current then increases with increasing temperature, coinciding with that of the “OFF-ON” process near the melting point. In the case of the “ON-OFF” process (Figure 3C), only negative peaks are observed at -160° , -131° , -122° , and -112° . The peaks at -131° and -112° are in corre-

spondence to the crystal-crystal transition points which have been identified by thermal^{1,14-16} and X-ray analysis.^{17,18} The transition points at -131° and -112° correspond to the transformations from the unstable phase to stable phase, namely α to β at -131° in a lower temperature region and β to α at -112° in a higher temperature region, respectively, as was reported earlier.^{10,17,18} A transition at -142° was also reported earlier;^{17,18} in the present study this peak was irreproducible and depended significantly on the purification process of AN. The peak at -122° was irreproducible in both the appearance temperature and the intensity. The present study cannot tell whether this peak results from a transition phenomenon or not.

Reactions of Coordination Compounds in the Solid State.

The Racemization of (+)-[Co(en)₃]X₃·nH₂O^{1a,b}

by Charles Kutal and John C. Bailar, Jr.*

Department of Chemistry and Chemical Engineering, University of Illinois, Urbana, Illinois 61801
(Received August 2, 1971)

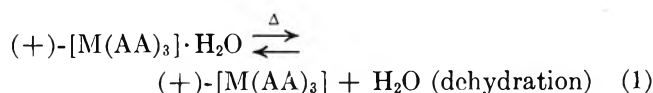
Publication costs assisted by The Advanced Research Projects Agency

The solid-state racemization of (+)-[Co(en)₃]X₃·nH₂O (where X = Cl⁻, Br⁻, I⁻, NCS⁻ and n = 0, 1) has been investigated. The hydrated iodide and bromide complexes were found to racemize considerably faster than their anhydrous analogs. This rate enhancement results from the physical modification of the lattice during dehydration rather than a displacement of one end of an ethylenediamine ligand by a water molecule (aquation). The actual mechanism of racemization is attributed to a twist process, an assignment which is consistent with the observed sequence for the racemization rates of the anhydrous complexes, X = I⁻ > Br⁻ > NCS⁻ > Cl⁻. Taken together with previously published studies, the present results suggest that lattice water can play a dual role in the solid-state reactions of metal complexes.

Introduction

The earliest reports²⁻⁴ of the racemization of coordination compounds in the solid state concerned salts of the complex ion [M(C₂O₄)₃]³⁻ (M = (Co(III) or Cr(III))). It was noted that lattice water in a sample enhanced the loss of optical rotation upon heating; a more recent study⁵ of K₃(+)-[Cr(C₂O₄)₃]·2H₂O has confirmed this result. A similar effect is found during the racemization of (+)-[Cr(en)₂Cl₂]Cl·H₂O⁶ and isomerization of *trans*-[Co(NH₃)₄Cl₂]IO₃·2H₂O,⁷ suggesting that lattice water generally plays an important role in the solid state reactions of metal complexes.

One explanation of this effect is provided by the mechanism below (shown for the racemization of a trischelate complex).⁸



(1) (a) Based on the doctoral dissertation of C. Kutal, University of Illinois, 1970; (b) en = ethylenediamine.

(2) C. H. Johnson and A. Mead, *Trans. Faraday Soc.*, **29**, 626 (1933).

(3) C. H. Johnson, *ibid.*, **31**, 612 (1935).

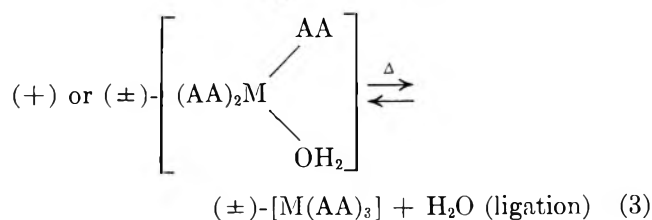
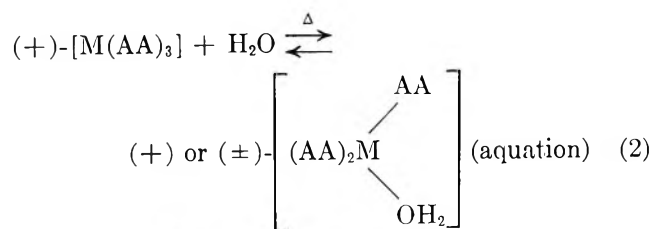
(4) C. H. Johnson and A. Mead, *ibid.*, **31**, 1621 (1935).

(5) D. M. Chowdhury and C. M. Harris, *J. Phys. Chem.*, **73**, 3366 (1969). Under extreme pressure, however, the presence of lattice water retards racemization. Cf. C. D. Schmulbach, J. Brady, and F. Dacheille, *Inorg. Chem.*, **7**, 287 (1968).

(6) H. E. LeMay, Jr., and J. C. Bailar, Jr., *J. Amer. Chem. Soc.*, **90**, 1729 (1968).

(7) H. E. LeMay, Jr., and J. C. Bailar, Jr., *ibid.*, **89**, 5577 (1967).

(8) A similar mechanism is applicable to [M(AA)X₂] complexes; in this case, however, water displaces a monodentate ligand (X) in eq 2.



According to this mechanism, racemization occurs *via* eq 2 and/or eq 3, with lattice water assuming the role of a reactive species capable of coordinating to the metal atom.

Since reactions like those shown in eq 2 and 3 are also thought to cause the racemization of $(+)-[Cr(C_2O_4)_3]^{3-9}$ and $(+)-[Cr(en)_2Cl_2]^+$ ¹⁰ in solution, it appears that for these complexes the same mechanism is operative in two phases. This situation undoubtedly does not exist in all cases, however. The mechanism shown above, for example, becomes less likely in the solid state relative to solution as the charge on the complex increases, since the absence of solvation in the transition state should inhibit the breaking of the metal-ligand bond (eq 2). For this reason a twist mechanism¹¹ might be favored. To explore this possibility, the solid-state racemization of several $(+)-[Co(en)_3]X_3$ complexes has been studied. Both anhydrous and hydrated samples were examined to note the effect of lattice water on the observed kinetics.

Experimental Section

Preparation of Complexes. *a.* $(+)-[Co(en)_3]I_3$ and $(+)-[Co(en)_3]I_3 \cdot H_2O$. Racemic $[Co(en)_3]Cl_3$ was prepared by the procedure of Work¹² and resolved as the chloro tartrate by the method of Busch.¹³ The optically active material was converted into the iodide salt by metathesis with sodium iodide. Recrystallization from an aqueous solution yielded crystals of the monohydrate, which could be dehydrated by heating *in vacuo* at 55° for 2 hr.¹⁴ A sample of the anhydrous complex was doped with Co^{2+} by being placed between pieces of filter paper moistened with a 0.1 *M* aqueous solution of $CoCl_2$.

b. $(+)-[Co(en)_3]Br_3$ and $(+)-[Co(en)_3]Br_3 \cdot H_2O$. The resolved chloro tartrate complex was dissolved in a dilute hydrobromic acid solution and precipitated with absolute ethanol, and the resulting solid was recrystallized from an approximately 6 *M* HBr solution. An aqueous solution of the solid was slowly evaporated in a vacuum desiccator, resulting in crystals of the monohydrate complex. A portion of this sample was dehydrated by heating at 80° for 2 hr *in vacuo*.¹⁴

c. $(+)-[Co(en)_3]Cl_3$ and $(+)-[Co(en)_3]Cl_3 \cdot H_2O$. The resolved chloro tartrate complex was dissolved in hot concentrated hydrochloric acid and reprecipitated with absolute ethanol. A portion of this material was dissolved in water and left to crystallize in a vacuum desiccator. Although the compound has been formulated with 2 mol of water of crystallization,¹⁵ the present method of preparation yielded a complex containing only one.

The remainder of the material precipitated from the hydrochloric acid solution was dehydrated by heating at 80° for 24 hr in a vacuum oven.¹⁴

d. $(+)-[Co(en)_3](NCS)_3$. This compound was prepared by the method of LeMay.¹⁶ The various samples of the optically active complexes are listed in Table I; also included are the particle size and specific rotation. The 20–40 mesh sample was prepared by gently breaking larger crystals with a pestle, passing these through a 20 mesh screen, and catching the suitably sized particles on a 40 mesh screen. Samples denoted as 200–325 mesh were passed through a 200 mesh screen with the aid of a pestle and caught on a 325 mesh screen. The general effect of the pestle was to crush the crystals. The <325 mesh samples were first ground to a fine powder and then passed through a 325 mesh screen. The particle sizes quoted are only approximate. In the absence of distribution studies, it can only be stated that the average particle sizes of the three types of sample lie in the order (20–40 mesh) > (200–325 mesh) > (<325 mesh).

e. $(\pm)-[Co(en)_3]X_3 \cdot nH_2O$. The racemic chloride complex was prepared as the 2.5 hydrate by the method of Work.¹² The corresponding iodide and bromide complexes were prepared from it by metathesis and crystallized from solution as monohydrates. The anhydrous complexes were formed upon heating the hydrated material at approximately 110° for 2 hr *in vacuo*.

Physical Measurements. Weight loss measurements were obtained using both isothermal and thermogravimetric analysis (tga) methods. Samples (0.15–0.25 g) studied isothermally were contained in a weighing bottle which was heated in a constant temperature ($\pm 2^\circ$)

(9) C. A. Bunton, J. H. Carter, D. R. Llewellyn, C. O'Connor, A. L. Odell, and S. Y. Yih, *J. Chem. Soc.*, 4615 (1964). In this case, it appears that a water molecule does not occupy the position vacated by one end of an oxalate ligand.

(10) J. Selbin and J. C. Bailar, Jr., *J. Amer. Chem. Soc.*, 79, 4285 (1957).

(11) P. C. Ráy and N. K. Dutt, *J. Indian Chem. Soc.*, 20, 81 (1943); J. C. Bailar, Jr., *J. Inorg. Nucl. Chem.*, 8, 165 (1958); C. S. Springer and R. E. Sievers, *Inorg. Chem.*, 6, 852 (1967); J. E. Brady, *ibid.*, 8, 1208 (1969).

(12) J. B. Work in "Inorganic Syntheses," Vol. 2, W. C. Fernelius, Ed., McGraw-Hill, New York, N. Y., 1946, p 221.

(13) D. H. Busch, *J. Amer. Chem. Soc.*, 77, 2747 (1955).

(14) Racemization is negligible at this temperature.

(15) W. W. Wendlandt, T. D. George, and K. V. Kirshnamurty, *J. Inorg. Nucl. Chem.*, 21, 69 (1961).

(16) H. E. LeMay, Jr., Ph.D. Thesis, University of Illinois, 1966, p 102.

Table I: Various Samples of (+)-[Co(en)₃]X₃·nH₂O Used in the Racemization Rate Studies^a

X	Batch no. ^b	Particle size	[α] _D , ^c deg	Water content
I ⁻	I	Small crystals	+100.0	Monohydrate
	I	200-325	+100.6	Anhydrous
	I	<325	+100.4	Anhydrous
	V	20-40	+100.8	Anhydrous
	V	200-325	+102.3	Anhydrous
	V	<325	+100.5	Anhydrous
Br ⁻	VII	Small crystals	+127.0	Monohydrate
	VII	Small crystals	+131.2	Anhydrous
Cl ⁻	...	200-325	+174.5	Anhydrous
NCS ⁻	...	200-325	+134.4	Anhydrous

^a The elemental analysis for each sample was satisfactory.

^b The batches are numbered the same as in ref 1; a batch corresponds to a separate preparation of the complex. ^c Specific rotation measured at the sodium D line.

oven. Tga measurements were obtained with a thermobalance arrangement recently described by Hertzberg.¹⁷ A heating rate of 2°/min and either a static air or flowing nitrogen atmosphere (130 ml/min) were employed in each run. Generally, 100-110-mg samples were used.

Visual observations on single crystals were made using a Reichert hot-stage microscope with a magnification of 100X.

An electron microscope examination of the iodide complex was made with a Cambridge Mark IIA Stereo-scan scanning electron microscope at 10 or 20 kV, using a 50- or 100-μ final aperture.

Infrared spectra were obtained using a Perkin-Elmer 521 spectrophotometer with sodium chloride optics. Both Nujol mulls and KBr disks were employed.

Measurements of optical rotation were made using a ETL-NPL Bendix automatic polarimeter (Type 143A) and a Pyrex cell of 1-cm path length. Within experimental uncertainty, the specific rotations of aqueous solutions of the complexes were independent of concentration and temperature. Generally the solutions contained 0.35-0.8% of the complex and the temperature was 26 ± 5°. Two independent readings were made on each solution, with the results usually agreeing to within ± 2%.

X-Ray powder patterns were obtained using a 114.6-mm diameter camera and nickel-filtered Cu Kα radiation. The exposure time for all samples was 20 hr.

Rate Studies. The solid samples (0.03-0.06 g) were placed in nmr tubes (4 mm o.d.). Tubes containing anhydrous complex were covered with thin pieces of Teflon sheet and plastic caps to prevent the entry of oil vapor from the surrounding bath. Heating control samples in uncovered tubes verified that this procedure did not affect the rate of racemization. Hydrated samples

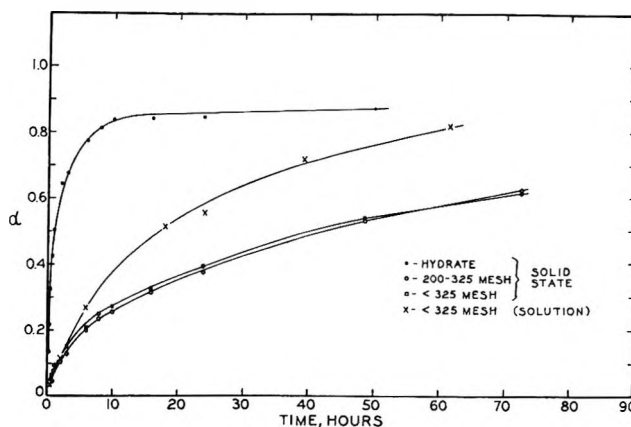


Figure 1. The racemization at 127° of samples of (+)-[Co(en)₃]I₃ from batch I.

were heated in tubes covered with plastic caps, which contained a pinhole to permit ready escape of water vapor. Finally, some samples were contained in tubes which were sealed off with a torch.

The sample tubes were placed in a constant-temperature oil bath maintained to within ± 0.05° by a Sargent Thermonitor. Approximately 1 min was needed for the sample to reach bath temperature. Elemental analyses, infrared spectra, and X-ray power photographs confirmed the absence of decomposition upon heating, even for samples which had undergone a considerable loss of optical rotation.

Results

Racemization Studies. The loss of optical rotation for various samples of (+)-[Co(en)₃]I₃·H₂O from batch I is illustrated in Figure 1; the data are plotted as α (per cent racemization) vs. time. In general, the same characteristics are exhibited by each curve. The rate of racemization is deceleratory throughout, with no evidence of an induction period down to the shortest time interval studied (15 min). One obvious result is the extremely rapid initial rate of racemization of the hydrated complex in the solid state; α = 0.6 after 2 hr. At the end of this period, the rate falls to a value more characteristic of the anhydrous complex, while beyond 10 hr the loss of rotation is very slow. In contrast, the anhydrous complex exhibits a smoothly decreasing rate of racemization up to the longest time studied. Even after 136 hr, however, it is not as extensively racemized as the hydrated complex after 6 hr.

For comparison, aqueous solutions of the <325 mesh sample of batch I were heated in sealed tubes at 127°. Sufficient water was added initially to ensure that the complex was always in solution. From the α,t curve obtained, it is evident that the huge excess of water is ineffective in increasing the overall rate of racemization.

(17) E. P. Hertzberg, Ph.D. Thesis, University of Illinois, 1969; E. P. Hertzberg and J. C. Bailar, Jr. *Inorg. Chem.*, **10**, 2371 (1971).

In fact, the curve lies below that of the solid hydrated complex up to at least 60 hr.

Some additional evidence concerning the effect of water can be mentioned. Anhydrous samples heated in a sealed tube containing water vapor showed no increase in the rate of racemization. Likewise, the hydrated complex exhibited no additional rate enhancement when heated in a sealed tube.

As seen in Figure 1, the 200–325 and <325 mesh samples racemize at slightly different rates. Initially, the <325 mesh sample has the higher rate, but at $\alpha = 0.56$, the α, t cross and the situation is reversed. A similar effect of particle size was found for the 200–325 and <325 mesh samples from batch V. Interestingly, there was little difference between the 20–40 and 200–325 mesh samples.

The α, t curves for a given sample of the anhydrous iodide complex are highly reproducible. One batch showed no significant change in its rate of racemization when tested over a period of 13 months.¹⁸ Samples which have the same mesh size but came from different batches, however, generally racemized at different rates. Raising the temperature increased the rate of racemization without changing the general shape of the α, t curves. Doping a sample of the anhydrous iodide complex with Co^{2+} , on the other hand, caused a rate decrease.

As seen in Figure 2, both (+)- $[\text{Co}(\text{en})_3]\text{Br}_3 \cdot \text{H}_2\text{O}$ and its anhydrous analog racemize at 127°. Although only a few experimental points were determined, it is evident that the presence of lattice water enhances the rate of racemization in the solid state. More extensive studies on the anhydrous material yielded results similar to those found for the iodide complex. Reducing the particle size from 200–325 to <325 mesh caused a decrease in the rate of racemization. The reproducibility of the α, t curves for a given sample was moderately good; however, samples which had the same particle size but came from different batches generally racemized at different rates.

Anhydrous (+)- $[\text{Co}(\text{en})_3]\text{Cl}_3$ lost none of its optical activity at 127° even after 85 hr. No studies of the hydrated complex were made.

Figure 3 contains the α, t curve for the racemization of (+)- $[\text{Co}(\text{en})_3](\text{NCS})_3$ at 127°. The shape of the curve is similar to those obtained for the anhydrous bromide and iodide complexes, although the scatter of experimental points (about a smooth curve) is largest for the thiocyanate complex. Included in Figure 3, for the sake of comparison, are the α, t curves for 200–325 mesh samples of the other (+)- $[\text{Co}(\text{en})_3]\text{X}_3$ complexes. The rate of racemization is seen to decrease in the order $\text{X} = \text{I}^- > \text{Br}^- > \text{NCS}^- > \text{Cl}^-$.

A first-order expression adequately describes the loss of rotation of aqueous solutions of the <325 mesh sample from batch I. The values of the specific rate constant, as determined by a least-squares analysis of plots

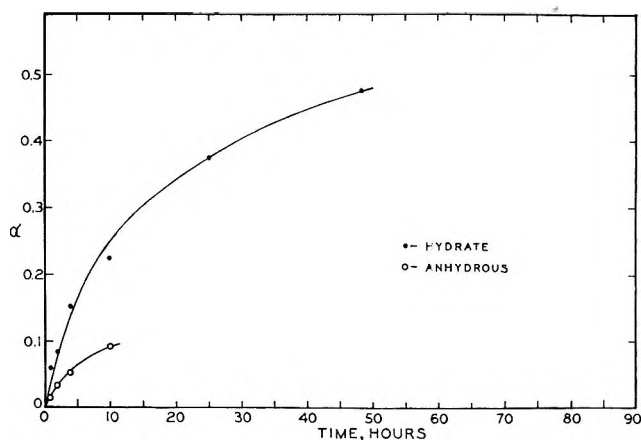


Figure 2. The racemization at 127° of samples of (+)- $[\text{Co}(\text{en})_3]\text{Br}_3$ from batch VII.

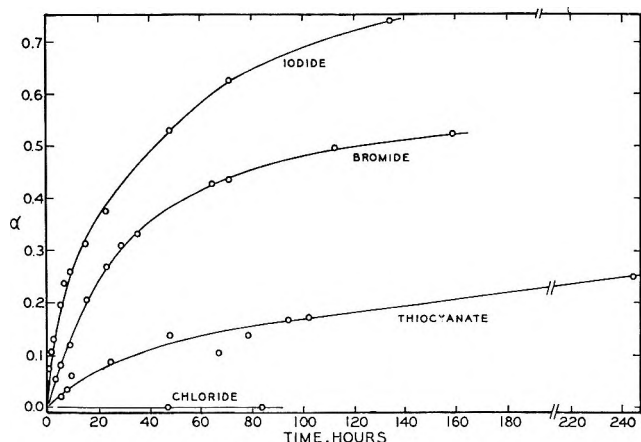


Figure 3. The racemization at 127° of 200–325 mesh samples of (+)- $[\text{Co}(\text{en})_3]\text{X}_3$.

of $\log(1 - \alpha)$ vs. t , are $9 \pm 1 \times 10^{-6} \text{ sec}^{-1}$ at 127.0°, $9 \pm 1 \times 10^{-5} \text{ sec}^{-1}$ at 135.3°, and $4 \pm 0.5 \times 10^{-4} \text{ sec}^{-1}$ at 146.3°, where the uncertainties are estimated using the method of Benson.¹⁹ The corresponding Arrhenius plot yields an activation energy of $61 \pm 10 \text{ kcal/mol}$. The large uncertainties in the values of the kinetic parameters are probably due to the high complex concentrations ($>0.5 \text{ M}$), where specific ionic interactions can affect the rate of racemization.²⁰

Dehydration Studies. The results described in the previous section indicate that lattice water markedly affects the rate of racemization of certain (+)- $\text{Co}(\text{en})_3\text{X}_3 \cdot n\text{H}_2\text{O}$ complexes in the solid state. Because of this, information about the corresponding dehydration reactions is of interest.

A tga run on (+)- $[\text{Co}(\text{en})_3]\text{I}_3 \cdot \text{H}_2\text{O}$ in static air shows that dehydration occurs in a single step. De-

(18) The value of the specific rotation before heating decreased slightly during this time, however, indicating that racemization occurs very slowly in the solid state at room temperature.

(19) S. W. Benson, "The Foundations of Chemical Kinetics," McGraw-Hill, New York, N. Y., 1960, pp 86–94.

(20) H. E. Swift and B. E. Douglas, *J. Inorg. Nucl. Chem.*, **26**, 601 (1964).

pending upon the batch studied, water loss commences at 60–73° and is almost complete at 100°. The remaining water (<5%) is then evolved more slowly, with the anhydrous weight level being attained between 113 and 133°. The difficulty in obtaining reproducible results for different batches was particularly noticeable for this complex. Upon standing in sealed bottles for several weeks, for example, some preparations were found to lose water. A tga run on the aged material showed that dehydration began as early as 38°. Crushing a sample of the hydrate with a mortar and pestle resulted in water loss, as did blowing a stream of dry nitrogen gas over the powdered sample.

The dehydration of (+)-[Co(en)₃]I₃·H₂O was also studied under the conditions employed in the racemization rate studies. Again the results depended on the batch of complex employed. Generally, dehydration was nearly complete (>90%) after 1 hr at 127°, although one sample retained 42% of its lattice water after this time and an additional hour of heating was required to completely remove it.

A tga run on (+)-[Co(en)₃]Br₃·H₂O in static air revealed that dehydration occurs in a single step. For a sample of batch VII (gently broken single crystals), dehydration begins at 90° and is complete at 125°. For a <200 mesh sample of (+)-[Co(en)₃]Cl₃·H₂O run in a flowing nitrogen atmosphere, dehydration occurs in a single step commencing at 101° and reaches the anhydrous weight level at 123°.

Visual Observations. Single crystals of (+)-[Co(en)₃]I₃·H₂O appear as lustrous, orange-colored rods under a microscope. When heated in air, they undergo marked visual changes resulting from the loss of lattice water. Typically, at the onset of dehydration, a few cracks develop parallel to the needle axis of the crystal. For most runs, this occurs at approximately 60°. Further cracking then occurs perpendicular to this direction; at 70–75° these cracks penetrate to some depth within the crystal and frequently cause it to fracture into a number of smaller fragments. Each fragment continues to crack until it no longer transmits light, beyond which point (80–85°) no further changes are evident. A crystal dehydrated at room temperature in a vacuum is similar in appearance to one heated in air, and subsequent heating causes little additional change.

When (+)-[Co(en)₃]Br₃·H₂O is heated to 80° in air, tiny cracks appear and rapidly spread over the entire surface. At about 90° the crystal becomes opaque, making further observation difficult. No large cracks are visible, however, and the external morphology of the crystal remains intact.

Heating a crystal of (+)-[Co(en)₃]Cl₃·H₂O to 100–110° produces compact nuclei of the anhydrous product. The dehydration interface is clearly visible and little, if any, cracking occurs. As the temperature is raised, the crystal loses its transparency and no further changes are evident.

Each of the temperatures reported above is the average of several runs; they depend both on the batch of complex studied and the heating rate. In general, however, they correspond quite well to the temperatures at which weight loss occurs on the thermobalance. The present results clearly indicate that the visual changes undergone by a crystal hydrate parallel its dehydration process.

Electron Microscope Studies. Figure 4 is a scanning electron micrograph (SEM) of a small crystal of (+)-[Co(en)₃]I₃·H₂O. Though formulated as the monohydrate, the actual water content of the complex is unknown, since some dehydration undoubtedly occurred

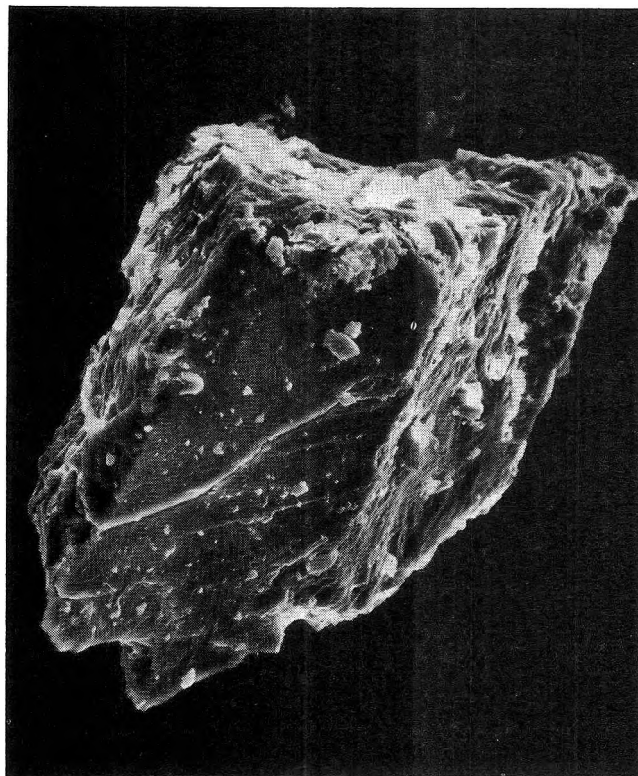


Figure 4. A scanning electron micrograph of a small crystal of (+)-[Co(en)₃]I₃·H₂O (magnified 1000×).

while mounting the specimen. The surface contains a few cracks, resulting from either dehydration or physical treatment (cleavage from a larger crystal). In contrast, a 200–325 mesh sample which was dehydrated at 55° in a vacuum showed extensive cracking, as seen in Figure 5. Additional heating at higher temperatures in air caused even more pronounced physical changes. Figure 6 reveals what appear to be small needle crystals growing from a larger particle of the anhydrous complex. Further discussion of this effect will be postponed until the X-ray results on the complex have been presented.

X-Ray Studies. Table II lists the main reflections from the X-ray powder photographs of samples of the optically active and the partially racemized iodide com-

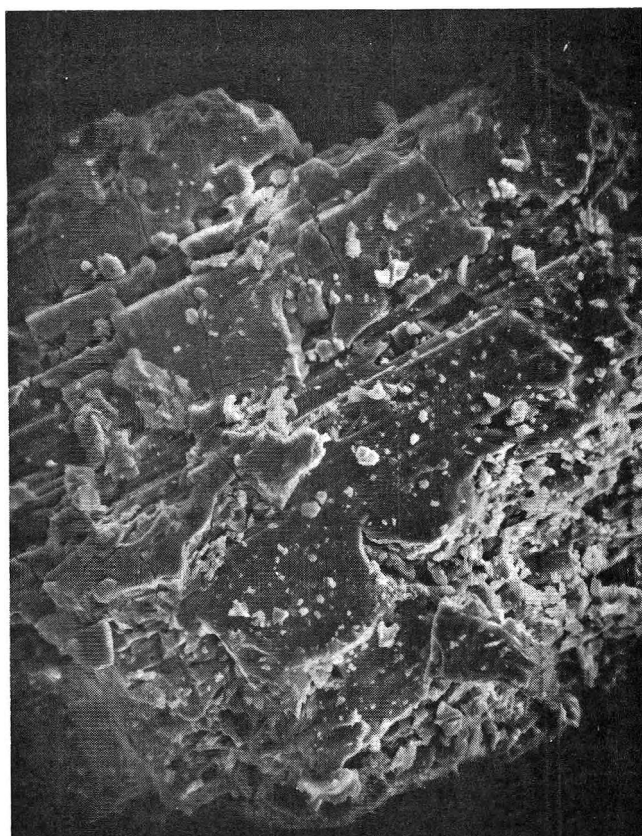


Figure 5. A scanning electron micrograph of a 200-325 mesh sample of (+)-[Co(en)₃]I₃ after dehydration *in vacuo* at 55° (magnified 2000×).

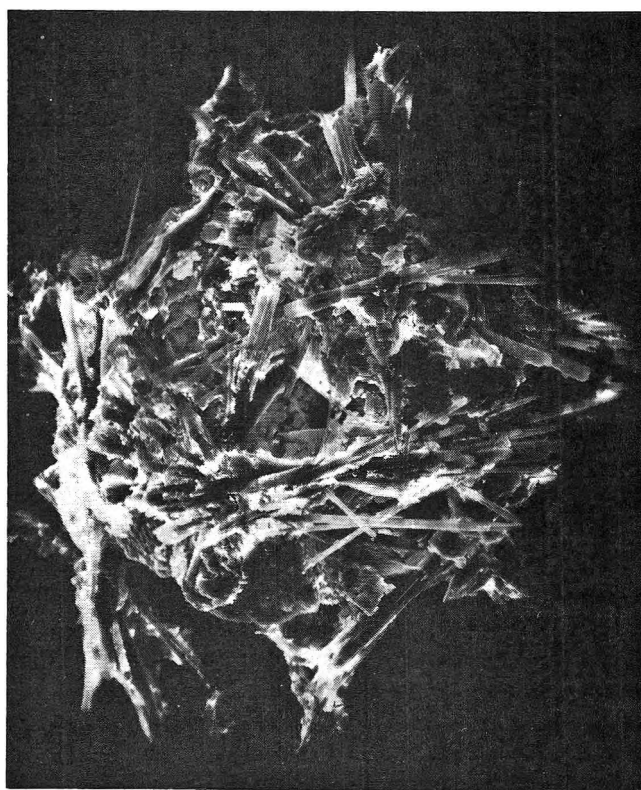


Figure 6. A scanning electron micrograph of a sample of (+)-[Co(en)₃]I₃ after heating at 127° for several hours (magnified 1000×).

plex. The corresponding data for the bromide complex are found in Table III.

Table II: The Prominent Lines in the X-Ray Powder Photographs of Optically Active [Co(en)₃]I₃·nH₂O

$$(+)-[\text{Co}(\text{en})_3]\text{I}_3 \cdot \text{H}_2\text{O} \xrightarrow[2 \text{ hr}]{55^\circ \text{ vac}} (+)-[\text{Co}(\text{en})_3]\text{I}_3 \xrightarrow[121 \text{ hr}]{127^\circ} \text{rac}-[\text{Co}(\text{en})_3]\text{I}_3^{\text{a}}$$

<i>d</i> , Å	<i>d</i> , Å	<i>d</i> , Å
9.44 (w) ^b	6.95 (m)	6.95 (w)
7.27 (m)	5.95 (vw)	5.79 (vw)
5.49 (m)	5.68 (vw)	5.31 (vw)
4.21 (s)	5.36 (vw)	4.97 (w)
3.76 (s)	4.98 (w)	4.66 (w)
3.58 (vw)	4.64 (w)	4.48 (w)
3.44 (s)	4.51 (m)	4.29 (s)
3.36 (s)	4.29 (s)	4.12 (w)
3.30 (s)	4.14 (w)	3.94 (vw)
3.16 (vw)	3.91 (vw)	3.72 (w)
3.02 (w)	3.75 (w)	3.55 (w)
2.94 (w)	3.67 (w)	3.45 (m)
2.78 (w)	3.56 (w)	3.30 (vw)
2.73 (w)	3.45 (m)	3.10 (w)
2.69 (vw)	3.30 (vw)	2.78 (w)
2.62 (w)	3.14 (m)	2.68 (w)
2.55 (w)	3.05 (w)	2.55 (w)
2.47 (vw)	2.77 (w)	2.44 (w)
2.42 (m)	2.68 (w)	2.28 (w)
2.33 (w)	2.55 (vw)	2.14 (w)
2.22 (w)	2.44 (vw)	
2.11 (vw)	2.35 (vw)	
1.90 (s)	2.28 (w)	
1.65 (m)	2.14 (w)	
	1.90 (s)	
	1.65 (m)	

^a Sample >50% racemized. ^b Intensities estimated visually: s = strong, m = medium, w = weak, vw = very weak.

The powder patterns taken before and after the dehydration (*in vacuo* at 55°) of (+)-[Co(en)₃]I₃·H₂O are not identical, indicating the crystal structure has undergone a change. Subsequent heating of the anhydrous complex in air for 121 hr at 127° had no effect on its powder pattern, other than to broaden the lines slightly. During the same period, however, the sample lost 50-70% of its optical activity. Thus, changes in the crystal structure parallel dehydration rather than racemization, in contrast to some recent results on *cis*-[Cr(en)₂Cl₂]Cl·H₂O.⁶ Similar behavior is observed for (+)-[Co(en)₃]Br₃·H₂O; the powder patterns taken before and after dehydration are different, while heating the anhydrous complex at 127° resulted in >40% racemization but no change in its powder pattern. When (+)-[Co(en)₃]Cl₃·H₂O was dehydrated, its powder pattern remained unchanged, suggesting that the presence of hydrate water was not a major factor in stabilizing the crystal lattice. Heating (+)-[Co-

Table III: The Prominent Lines in the X-Ray Powder Photographs of Optically Active $[\text{Co}(\text{en})_3]\text{Br}_3 \cdot n\text{H}_2\text{O}$

$(+)-[\text{Co}(\text{en})_3]\text{Br} \cdot \text{H}_2\text{O} \xrightarrow[1 \text{ hr}]{95^\circ \text{ vac}}$		
$(+)-[\text{Co}(\text{en})_3]\text{Br}_3 \xrightarrow[121 \text{ hr}]{127^\circ} \text{rac}-[\text{Co}(\text{en})_3]\text{Br}_3^a$		
$d, \text{Å}$	$d, \text{Å}$	$d, \text{Å}$
7.06 (m) ^b	6.76 (s)	6.76 (s)
6.78 (vw)	6.49 (w)	5.98 (w)
6.43 (m)	5.97 (w)	5.03 (w)
5.37 (w)	5.02 (vw)	4.36 (w)
4.97 (m)	4.37 (m)	4.11 (s)
4.77 (m)	4.10 (s)	3.99 (w)
4.31 (w)	3.98 (w)	3.66 (w)
4.17 (s)	3.64 (w)	3.53 (w)
3.71 (w)	3.51 (w)	3.38 (m)
3.44 (w)	3.36 (m)	3.28 (m)
3.24 (s)	3.26 (m)	2.99 (m)
3.15 (w)	2.98 (m)	2.61 (w)
3.09 (w)	2.60 (w)	2.34 (vw)
2.96 (w)	2.33 (vw)	2.25 (vw)
2.75 (w)	2.25 (vw)	
2.68 (w)		
2.51 (m)		
2.46 (w)		
2.35 (vw)		
2.18 (w)		
2.12 (vw)		

^a Sample >40% racemized. ^b Intensities estimated visually: s = strong, m = medium, w = weak, vw = very weak.

$(\text{en})_3](\text{NCS})_3$ at 146.3° for 11 hr caused no change in its powder pattern other than a slight line broadening, even though the sample lost 60% of its optical activity. Finally, the powder patterns taken before and after the dehydration of $(\pm)-[\text{Co}(\text{en})_3]\text{X}_3 \cdot \text{H}_2\text{O}$ (X = I⁻ and Br⁻) are different, while those of $(\pm)-[\text{Co}(\text{en})_3]\text{Cl}_3 \cdot 2.5\text{H}_2\text{O}$ show no change.

There is little correspondence between the powder patterns of analogous racemic and optically active complexes. This result is expected, since a racemate generally possesses the higher crystal symmetry. More significantly, the powder pattern of a sample of the anhydrous iodide or bromide complex which has lost >40% of its optical activity by heating contains no new lines characteristic of the corresponding racemic complex. This indicates a difference in crystal structure between a racemic sample crystallized from solution and one formed from the optically active complex by heating in the solid state.

Discussion

The marked effect of lattice water on the rates of racemization of $(+)-[\text{Co}(\text{en})_3]\text{I}_3 \cdot \text{H}_2\text{O}$ (Figure 1) and $(+)-[\text{Co}(\text{en})_3]\text{Br}_3 \cdot \text{H}_2\text{O}$ (Figure 2) has several possible explanations. If the aquation-ligation mechanism (eq 1-3) mentioned earlier were responsible, increasing the concentration of water in the system should accel-

erate the loss of rotation. No effect was observed, however, when a sample of the iodide salt was heated with excess water vapor in a sealed tube. In fact, an aqueous solution of the complex had a lower rate of racemization at 127° than the corresponding crystal hydrate. This is exactly opposite to the behavior observed for complexes reported to exhibit an aquation-ligation mechanism.²¹ For example, $(+)-[\text{Cr}(\text{en})_2\text{Cl}_2]^+$ racemizes in aqueous solution at 25° with a half-life of approximately 1 hr,¹⁰ whereas in the solid state only a few per cent racemization occurs at 140° during the same interval.⁶ Likewise, solid $\text{K}_3(+)-[\text{Cr}(\text{C}_2\text{O}_4)_3] \cdot 2\text{H}_2\text{O}$ must be heated at 236°⁵ before racemizing at a rate comparable to that of an aqueous solution of the complex at 50°.²² The results for the iodide complex are therefore not readily explainable in terms of a mechanism involving metal-ligand bond rupture.

Some similarities exist between the present results and those reported for the solid-state exchange of cobalt(III) complexes doped with radioactive Co^{2+} .²³ The plots of per cent exchange vs. time resemble the curves shown in Figures 1 and 2; in addition, lattice water accelerates the rate of exchange. It was suggested that free electrons in the crystal are captured by Co^{2+} to form excited Co^+ (or Co_0), which instantaneously reacts with a neighboring complex resulting in exchange. The higher dielectric constant of the hydrated crystal presumably lowers the energy gap between the forbidden and conduction bands in the crystal and thus increases the supply of free electrons at a given temperature. It is conceivable that exchange of a catalytic amount of Co^{2+} could lead to steric rearrangement²⁴ and thus be responsible for the racemization observed in the present case. In the absence of labeling studies, however, two pieces of evidence can be cited against this mechanism. First, crushing a sample, which is known to produce electrons in a solid,²³ decreased the rate of racemization. Second, doping Co^{2+} into a sample did not enhance the loss of rotation (in fact, the rate decreased).

The most probable mechanism for the solid state racemization of the iodide, bromide, and thiocyanate complexes is an intramolecular twist.¹¹ The high charge on the cation, the large ligand field stabilization energy (LFSE) possessed by cobalt(III), and the lack of solvation energy make this a particularly favorable

(21) Although care must be exercised when comparing rates between two phases, the preference for a bond rupture mechanism in aqueous solution appears reasonable. The mole ratio of water molecules to complex ions is considerably higher in solution than in the crystal lattice, thus leading to a higher probability of reaction. Also, in solution the possibility exists for solvation of the incipient charge separation in the transition state caused by the breaking of the metal-ligand bond.

(22) E. Bushra and C. H. Johnson, *J. Chem. Soc.*, 1937 (1939).

(23) A. Nath, S. Khorana, P. K. Mathur, and S. Sarup, *Indian J. Chem.*, **4**, 51 (1966).

(24) N. Saito, H. Sano, T. Tominaga, F. Ambe, and T. Fujino, *Bull. Chem. Soc. Jap.*, **35**, 744 (1962).

pathway.²⁵ The lower rate of racemization in solution may mean either that a different mechanism (presumably bond rupture) is occurring, or the twisting motion is inherently slower than in the solid. There is insufficient evidence to decide which is more likely, but the former explanation receives some support from the recently reported isolation of a monodentate ethylenediamine-cobalt(III) complex.²⁶

Three factors contribute to the activation energy of the twisting motion in the solid state: (a) changes in LFSE, (b) changes in ligand-ligand repulsion, and (c) changes in the interaction between $[\text{Co}(\text{en})_3]^{3+}$ and the lattice anions. If a and b are considered essentially constant within the present series of complexes, differences in the rates of racemization must arise from c. To understand fully the nature of the interactions between the ions in the lattice, an accurate crystal structure is needed for each of the hydrated and anhydrous complexes. Except for $(+)\text{-Co}(\text{en})_3\text{Br}_3 \cdot \text{H}_2\text{O}$,^{27,28} however, this information is lacking. Nevertheless, it is interesting to note that the observed sequence for the rates of racemization, $\text{X} = \text{I}^- > \text{Br}^- > \text{NCS}^- > \text{Cl}^-$, lies in the order expected for decreased hydrogen bonding between the protons on the nitrogen atoms and the anions in the lattice²⁹ (assuming $\text{N-H} \dots \text{N}$ bonding for thiocyanate). As the strength of the hydrogen bonds which must be broken decreases, the energy of activation for a twist process will similarly decrease. The importance of hydrogen bonding in determining the conformations of metal-chelate rings in a crystal has recently been discussed.³⁰

Since the influence of lattice water on the rate of racemization does not result from chemical combination with the complex (aquation), it must instead involve the physical modification of the crystal lattice during dehydration. Visual observations on single crystals of $(+)\text{-[Co}(\text{en})_3\text{]I}_3 \cdot \text{H}_2\text{O}$ and $(+)\text{-Cl}(\text{en})_3\text{Br}_3 \cdot \text{H}_2\text{O}$ reveal that the loss of lattice water is accompanied by extensive cracking, indicating the introduction of a large number of defects into the solid. Since the complex ions near a defect are known to experience enhanced reactivity,³¹ their inversion is expected to be rapid. The rate accelerating effect continues until the cessation of dehydration, at which point the rapid production of defects also ends. Further racemization is then effected at a lower rate by the remaining optically active ions. This latter process would be expected to obey a first-order rate expression if the ions had an equal probability of inversion. Such behavior has been reported for the racemization of $\text{K}_3(+)\text{-[Cr}(\text{C}_2\text{O}_4)_3\text{]}$ beyond $\alpha = 0.3$.⁵ In the present case, however, the experimentally observed rotations are invariably larger than the calculated first-order values, suggesting that some factor may be slowing the racemization process. One possible explanation is provided by the effect of heating on a sample of $(+)\text{-[Co}(\text{en})_3\text{]I}_3$. A scanning electron micrograph (SEM) reveals the existence of small needle-

like crystals protruding from the larger particles (Figure 6). The solid appears to be recrystallizing, although an X-ray powder pattern reveals the same crystal structure. It is not unreasonable to describe this behavior as a form of annealing, in that the disrupted lattice formed upon dehydration becomes more ordered. This process would decrease the number of lattice defects with a consequent reduction in the rate of racemization. The similarity in the α, t curves of the anhydrous iodide, bromide, and thiocyanate complexes suggests that this explanation might be extended to include the latter two complexes.

The lower rates of racemization of the optically pure anhydrous complexes (relative to their hydrated analogs) suggest the production of fewer defects during their preparation. The anhydrous iodide complex, for example, is formed upon heating the hydrate for 2 hr at 55° . Either this procedure inherently produces fewer defects than are formed by dehydration at 127° , or considerable annealing occurs at 55° . On the basis of a SEM study of a 200-325 mesh sample of $(+)\text{-[Co}(\text{en})_3\text{]}^{3+}$ (Figure 5), the latter explanation seems less likely. Treating a sample of the anhydrous iodide complex with a solution of cobalt(II) chloride results in the dissolution of ions on the extensively cracked surfaces of the solid. The general effect is to smooth the surfaces and decrease the number of defects, resulting in the observed decrease in the rate of racemization.

An alternative explanation of the effect of lattice water is suggested from the X-ray data. The fact that the powder patterns of $(+)\text{-[Co}(\text{en})_3\text{]I}_3 \cdot \text{H}_2\text{O}$ and $(+)\text{-[Co}(\text{en})_3\text{]Br}_3 \cdot \text{H}_2\text{O}$ are different from those of their anhydrous analogs indicates that dehydration has caused a change in the crystal lattice. If, for example, the dimensions of the unit cell shrink upon water loss, the closer packing would inhibit the twisting motion and result in a decreased rate of racemization. Such a situation exists for ammonium perchlorate, whereby a phase transformation markedly affects the energetics of decomposition.³²

Attempts were made to fit the racemization data to

(25) R. C. Fay and T. S. Piper, *Inorg. Chem.*, **3**, 348 (1964).

(26) M. D. Alexander and C. A. Spillert, *ibid.*, **9**, 2344 (1970).

(27) K. Nakatsu, *Bull. Chem. Soc. Jap.*, **35**, 832 (1962).

(28) A preliminary study in this laboratory has shown that single crystals of $(+)\text{-[Co}(\text{en})_3\text{]I}_3 \cdot \text{H}_2\text{O}$ belong to the orthorhombic system with unit cell dimensions $a = 8.44 \text{ \AA}$, $b = 18.95 \text{ \AA}$, and $c = 11.28 \text{ \AA}$. The space group is $P2_12_12_1$, an assignment which is consistent with the optical activity of the complex. Assuming four $[\text{Co}(\text{en})_3\text{]I}_3 \cdot \text{H}_2\text{O}$ aggregates per unit cell, the calculated density is 2.35 g/ml , in good agreement with the experimental value of 2.32 g/ml . It proved impossible to obtain single crystal photographs of the anhydrous complex, due to extensive cracking upon dehydration.

(29) J. Fujita, K. Nakamoto, and M. Kobayashi, *J. Amer. Chem. Soc.*, **78**, 3295 (1956).

(30) K. N. Raymond, P. W. R. Corfield, and J. A. Ibers, *Inorg. Chem.*, **7**, 842 (1968).

(31) J. M. Thomas, *Chem. Britain*, **6**, 60 (1970).

(32) L. L. Bircumshaw and B. H. Newman, *Proc. Roy. Soc., Ser. A*, **227**, 228 (1954).

various topochemical rate laws common to solid-state reactions.^{33,34} Although some expressions were consistent with the kinetics of the racemization of the anhydrous iodide and bromide complexes over various portions of the α, t curve, such agreement is not in itself sufficient proof that a given kinetic model is applicable. The prerequisites can be utilized, however, to test for a topochemical process.³⁵ First, some evidence of an acceleratory period must exist in the α, t plot. In the present study the plots were invariably deceleratory throughout the course of the racemization. Secondly, there should be evidence of nucleus formation and growth with the presence of a sharp interface. If such an interface does exist during the racemization under consideration, it would seemingly be impossible to detect. The effect of a twist mechanism on the lattice is not expected to be large, since the anions effectively shield the complex ions from each other. The powder patterns of the optically pure iodide, bromide, and thiocyanate complexes, for example, are identical with those of samples which are >40% racemized by heating. Since no definite basis for assigning a topochemical process exists, any fit to such kinetic expressions must be regarded as empirical. Although it might be tempting to use a rate law in this manner, it has been pointed out that rate constants and activation energies can only be clearly defined when a suitable hypothesis exists for the mechanism of the reaction.³⁶

Concluding Remarks

It appears that lattice water can play a dual role in

the solid-state reactions of metal complexes. The present study has shown that dehydration can affect the rate of racemization of (+)-[Co(en)₃]I₃·H₂O and (+)-[Co(en)₃]Br₃·H₂O by physical modification of the crystal lattice. For K₃-(+)[Cr(C₂O₄)₃]·2H₂O and (+)-[Cr(en)₂Cl₂]Cl·H₂O, on the other hand, lattice water is thought to react chemically *via* aquation of the complex. Undoubtedly, several factors combine to determine which behavior prevails; the charge on the complex, LFSE of the metal, and ease of replacement of the coordinated ligands are some of the more apparent ones.

The two explanations (lattice defect and change in crystal structure) offered for the effect of dehydration in the present study are not meant to be mutually exclusive. In fact, both may contribute to the enhanced rate of racemization. Further studies are needed to resolve this point.

Acknowledgments. The authors gratefully acknowledge the financial assistance of the Advanced Research Projects Agency (Contract HC 15-67-C-0221), a fellowship which was granted to Charles Kutal by the Monsanto Company, and the help of Mrs. Judith Murphy, who made the photomicrographs.

(33) P. W. M. Jacobs and F. C. Tompkins in "Chemistry of the Solid State," W. E. Garner, Ed., Academic Press, New York, N. Y., 1955, Chapter 7.

(34) D. A. Young, "Decomposition of Solids," Pergamon Press, Oxford, 1966, pp 72-107.

(35) D. A. Young, private communication, 1969.

(36) W. Gomes, *Nature*, **192**, 865 (1961).

The Intrinsic Viscosities of Bovine Serum Albumin in *n*-Propyl Alcohol–Water Mixtures

by S. F. Sun

Department of Chemistry, St. John's University, Jamaica, New York 11432 (Received September 25, 1971)

Publication costs borne completely by The Journal of Physical Chemistry

Measurements have been made of the intrinsic viscosities of bovine serum albumin in water–*n*-propyl alcohol mixtures at the isoionic point, ionic strength 0.03, and temperature 25°. It was found that the intrinsic viscosity does not increase until the concentration of *n*-propyl alcohol increases to 25% by volume. In 25% *n*-propyl alcohol–75% water the intrinsic viscosity, 0.085 dl g⁻¹, is unexpectedly high. In order to clarify the nature of this sudden increase, two additional experiments were carried out: ultracentrifuge sedimentation and difference spectra. All the results seem to indicate a conformational change which occurs not only in the secondary and tertiary structures, but also possibly in the quaternary structure of the protein.

In a previous communication,¹ we reported on the intrinsic viscosity of bovine serum albumin (BSA) in 25% dioxane–75% water (v/v) at the isoionic point (pH 5.63), ionic strength *I* (0.03), and 25°, whose value was unexpectedly low, *i.e.*, 0.019 dl g⁻¹, in comparison with the range 0.033–0.040 dl g⁻¹ for most globular proteins in aqueous solutions under the same conditions. Herein, we report a case in which the intrinsic viscosity is unexpectedly high. For BSA in 25% *n*-propyl alcohol–75% water the value is 0.085 dl g⁻¹.

Measurements were taken on BSA in various water–*n*-propyl alcohol mixtures, the data being shown in Figure 1. The ionic strength was kept constant at 0.03 in all cases. The pH of each solution is presumably the isoionic point of the protein. It varies a little from solvent to solvent (0% *n*-propyl alcohol, 5.30; 10%, 5.57; 15%, 5.73; 20%, 5.88; 25%, 5.89). Since the reduced viscosity is not sensitive in that pH region,^{2,3} no attempt was made to adjust the pH's to a common value. The temperature was 25.00 ± 0.01°.

Figure 2 shows the dependence of intrinsic viscosity on the concentration of *n*-propyl alcohol in the solvent medium. From 0% to 15% *n*-propyl alcohol, the intrinsic viscosity remains very nearly constant, but from 15% on, it increases rapidly. The value at 25% is double that at 0%. This observation is consistent with that observed before,⁴ *i.e.*, η_{sp}/C for BSA in a 25% *n*-propyl alcohol–75% water mixture is much higher than that in some other solvent media. The sudden change of intrinsic viscosity near 25% *n*-propyl alcohol would suggest that the viscosity behavior of BSA in *n*-propyl alcohol–water mixture is "cooperative," if the curve levels off after the concentration passes 25%. Unfortunately, no data are available for the concentration of *n*-propyl alcohol above 25% at the isoionic point, ionic strength 0.03 and 25°. The BSA solution is no more stable when the concentration of *n*-propyl alcohol is above 25%.

The interpretation of the high value for BSA in 25% *n*-propyl alcohol–75% water is even more difficult than that of the low value for BSA in 25% dioxane–75% water. We are reasonably sure that the low value of intrinsic viscosity is due to the change of the asymmetry of the molecule.¹ At the isoionic point, there appeared to be no change in the effective volume of BSA in a 25% dioxane–75% water mixture, but there was a decrease in the axial ratio *a/b* (where *a* refers to the semimajor axis and *b* the semiminor axis). The molecule approximated the form of a sphere.

The *n*-propyl alcohol is known to have properties favoring the formation of helical content and the stabilization of proteins in aqueous solutions.⁵ These properties, however, are not observed in BSA. The results obtained from optical rotatory dispersion measurements with a Cary 60 spectropolarimeter showed that there was no increase in helical content of BSA in aqueous solutions when *n*-propyl alcohol was added. The Cotton effect in the far ultraviolet region was virtually the same in water as in 25% *n*-propyl alcohol–75% water mixture.

To search for some information toward the understanding of the behavior of BSA in 25% *n*-propyl alcohol–75% water, we performed two more experiments: the ultracentrifuge sedimentation and difference spectra.

A Spinco Model E analytical ultracentrifuge was used for sedimentation velocity study. The speed was set up at 56,000 rpm and the temperature at 25°. A small amount of the more rapidly sedimenting component which has been frequently reported in serum albu-

- (1) S. F. Sun and N. O. del Rosario, *Chem. Commun.*, 669 (1971).
- (2) C. Tanford and J. G. Buzzell, *J. Phys. Chem.*, **60**, 225 (1956).
- (3) S. F. Sun, *Arch. Biochem. Biophys.*, **129**, 411 (1969).
- (4) S. F. Sun, *Biochim. Biophys. Acta*, **181**, 473 (1969).
- (5) B. Jurgensons, *J. Biol. Chem.*, **242**, 912 (1967).

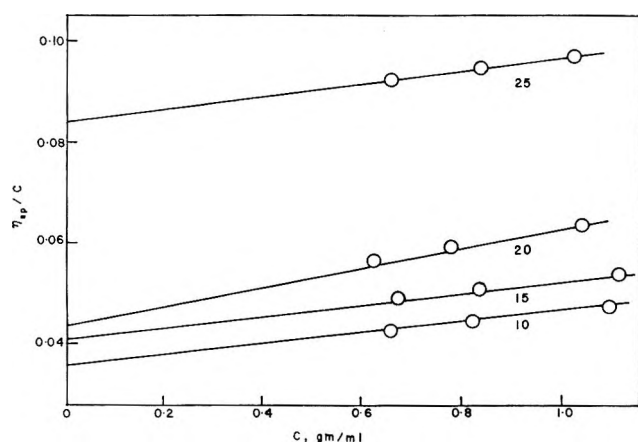


Figure 1. Determination of intrinsic viscosities of BSA in *n*-propyl alcohol-water mixtures at isoionic point, ionic strength 0.03, and 25°. The percentage of *n*-propyl alcohol is indicated by the number below each line.

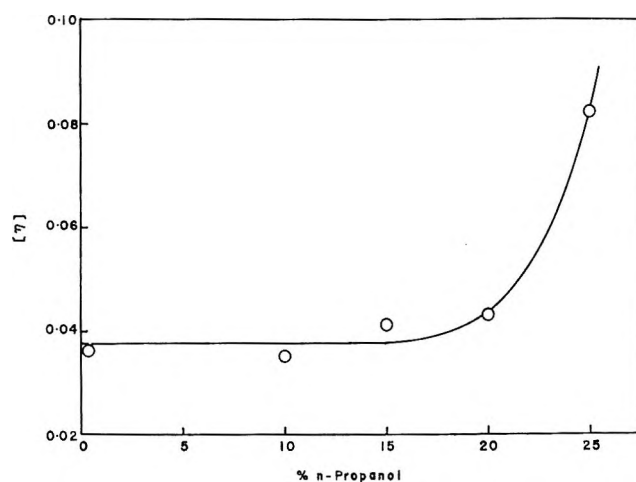


Figure 2. Dependence of the intrinsic viscosity of BSA on the concentration of *n*-propyl alcohol in *n*-propyl alcohol-water mixtures at isoionic point, ionic strength 0.03, and 25°.

min was observed.⁶ This more rapidly sedimenting component is supposed to be a dimer. In the first hour after full speed was reached the boundary for BSA in 25% *n*-propyl alcohol-75% water was nearly identical with that for BSA in water alone (0.03 *M* KCl), an almost symmetrical, sharp boundary. In the second hour a peculiar phenomenon was observed. A shoulder developed on the trailing side of the boundary. Near the end of the first two hours, the shoulder was better resolved. This suggests a possibility of association-dissociation of subunits of BSA and is consistent with the model of BSA molecule proposed in the last decade.^{7,8} Work is in progress for detailed sedimentation studies

on BSA in *n*-propyl alcohol-water mixtures. If it is true that an association-dissociation occurs when BSA dissolves in the 25% *n*-propyl alcohol-75% water, the high value of the intrinsic viscosity becomes understandable; but at the same time the conformational study of BSA in 25% *n*-propyl alcohol-75% water becomes more interesting and gets more complicated.

A differential absorption spectrum was obtained for BSA in 25% *n*-propyl alcohol-75% water using the protein in water alone as reference under the same conditions: isoionic and $I = 0.03$. Measurements were carried out on a Cary 14 spectrophotometer at 25°. The differential absorption spectrum shows three bands: 275, 285, and 293 $m\mu$ (in comparison with one band for differential spectrum of BSA in 25% dioxane-75% water, 282 $m\mu$, and in 25% EtOH-75% water, 285 $m\mu$, respectively). The first two bands 275 and 285 $m\mu$ are clearly due to the tyrosine residues, with the third one at 293 $m\mu$ due to the tryptophan residues. In the case of tyrosine residues there is a shift of the absorption peak to 275 from 278 $m\mu$ as usually observed in the difference absorption spectrum of proteins. The three bands observed indicate two things: (1) BSA is unfolded as sufficient *n*-propyl alcohol is present in the aqueous solution, so that the tyrosine residues are now exposed to the solvent or, more possibly, are located on the surface of the molecule; (2) there may be a transfer of the tyrosine groups from a hydrophobic to an aqueous environment, so that a blue shift occurred at the 278 $m\mu$ band.

Therefore, we conclude that in 25% *n*-propyl alcohol-75% water the BSA molecule undergoes conformational change. The change occurs not only in the secondary and tertiary structure, but also possibly in the quaternary structure of the protein. The high value of intrinsic viscosity may be attributed to the change of the structure of the molecule.

At the pH range between 4.3 and 10.5, BSA is known to exist in a compact, but not rigid, form in aqueous solutions.^{1,9} As the concentration of *n*-propyl alcohol increases, the BSA molecule becomes less rigid and more obscure in its boundaries. This conclusion is in accord with what we deduced before, *i.e.*, the protein molecule approximated the form of a sphere in the isoionic dioxane-water mixture,¹ and greatly elongated in the acidic dioxane-water mixture.¹³

(6) K. E. Van Holde and S. F. Sun, *J. Amer. Chem. Soc.*, **84**, 66 (1962).

(7) J. F. Foster in "The Plasma Proteins," F. W. Putnam, Ed., Vol. I, Academic Press, New York, N. Y., 1960, p 221.

(8) G. Weber and L. B. Young, *J. Biol. Chem.*, **239**, 1415, 1424 (1964).

(9) W. Kauzmann and R. E. Simpson, *J. Amer. Chem. Soc.*, **75**, 5154 (1953).

(10) S. F. Sun and N. O. del Rosario, *ibid.*, **92**, 1837 (1970).

NOTES

Proton Magnetic Resonance in Concentrated Aqueous Solutions of Tetraalkylammonium Bromides and Inorganic Halides at 25 and 65°

by Antonio LoSurdo and Henry E. Wirth*

Department of Chemistry, Syracuse University,
Syracuse, New York 13210 (Received February 27, 1970)

Publication costs assisted by Syracuse University

Aqueous solutions of tetraalkylammonium halides have been investigated by a variety of techniques (*i.e.*, density, viscosity, thermodynamic measurements, near-infrared, ultrasonic, nmr spectroscopy and dielectric relaxation).¹⁻¹⁰ These studies have indicated that quaternary ammonium salts increase the water structure around the hydrophobic surfaces of the ions^{1,2,6} forming clathratelike⁴ arrangements of water molecules around the tetraalkylammonium salts. Recent studies have also suggested an overall structure breaking¹¹ effect and micelle formation^{12,13} in concentrated aqueous solutions of the larger tetraalkylammonium halides. However, there is no general agreement on the exact nature of the ion-solvent and ion-ion interactions. To obtain further understanding of these interactions we have obtained the proton magnetic resonance (pmr) spectra of concentrated aqueous solutions of quaternary ammonium bromides, cetyltrimethylammonium bromide, and some inorganic halides.

Experimental Section

Materials. Recrystallized tetramethylammonium bromide, tetraethylammonium bromide, tetra-*n*-propylammonium bromide, and tetra-*n*-butylammonium bromide (Eastman) and cetyltrimethylammonium bromide (Pfaltz and Bauer) were used. Ammonium bromide (Fisher analytical reagent grade), MgCl₂, and LiBr (Fisher purified) were used without further purification. Solutions of known molality were prepared by weight.

Procedure. The relative shifts, δ , of proton resonance in water were determined for several concentrations of salt solutions using a Varian A-60 spectrometer with the samples at 25 and 65°. All proton shifts were measured in parts per million relative to sodium 2,2-dimethyl-2-silapentane-5-sulfonate (DDS) as the internal standard and are reported in ppm relative to pure water, *i.e.*

$$\delta = (\delta_{\text{solution}})_{\text{H}_2\text{O}} = (\delta_{\text{solution}})_{\text{DDS}} - (\delta_{\text{H}_2\text{O}})_{\text{DDS}}$$

Results and Discussion

The relative shifts, δ , of the proton resonances for the various electrolyte solutions are plotted in Figures 1 to 3. The shift δ is defined¹⁴ as

$$\delta = \left[\frac{10^6(H_{\text{H}_2\text{O}} - H_{\text{solution}})}{H_{\text{H}_2\text{O}}} \right]_t = \left[\frac{10^6(\nu_{\text{H}_2\text{O}} - \nu_{\text{solution}})}{60 \times 10^6} \right]_t \quad (1)$$

These shifts correspond to the displacement of proton peaks from that of pure water at 25 and at 65°.

Positive δ 's are observed for MgCl₂, and negative δ 's for the tetraalkylammonium bromides, cetyltrimethylammonium bromide, and LiBr at 25 and 65° (Figures 1 to 3). For ammonium bromide δ is negative at 25° and positive at 65° (Figure 1). It should be noted that regardless of the sign of δ the δ 's become more positive with increase in temperature.

The results at 25° (Figures 1 and 2) are consistent with those of Shoolery and Alder¹⁵ for LiBr and MgCl₂ and Kay¹⁶ for (*n*-Bu)₄NBr. In general, the observed absolute values of δ are lower for MgCl₂ and higher for LiBr when compared with the results of Shoolery and Alder.¹⁵ This difference may be due to the fact that the δ 's in the present investigation were determined relative to an internal standard (DDS), while the published data were determined relative to an external standard. However, the right order in the sign of the δ 's is observed.

Shoolery and Alder¹⁵ consider water molecules as polarizable charge distributions, and attribute positive

- (1) H. S. Frank and W. Y. Wen, *Discuss. Faraday Soc.*, **24**, 133 (1957).
- (2) H. S. Frank, *Proc. Roy. Soc., Ser. A*, **247**, 481 (1958).
- (3) E. R. Nightingale, Jr., *J. Phys. Chem.*, **66**, 894 (1962).
- (4) W. Y. Wen and S. Saito, *ibid.*, **68**, 2639 (1964).
- (5) R. L. Kay, *et al.*, *ibid.*, **70**, 2325, 2336 (1966).
- (6) H. S. Frank and M. W. Evans, *J. Chem. Phys.*, **13**, 507 (1945).
- (7) K. W. Bunzl, *J. Phys. Chem.*, **71**, 1358 (1967).
- (8) S. Schiavo, B. Scrosati, and A. Tommasini, *Ric. Sci.*, **37**, 219 (1967).
- (9) J. B. Haggis, J. B. Hasted, and T. J. Buchanan, *J. Chem. Phys.*, **20**, 1452 (1952).
- (10) H. G. Hertz and M. D. Zeidler, *Ber. Bunsenges. Phys. Chem.*, **68**, 821, 907 (1964).
- (11) K. A. Hartman, Jr., *J. Phys. Chem.*, **70**, 270 (1966).
- (12) H. E. Wirth, *ibid.*, **71**, 2922 (1967).
- (13) H. E. Wirth and A. LoSurdo, *ibid.*, **72**, 751 (1968).
- (14) J. W. Emsley, J. Feeney, and L. H. Sutcliffe, "High Resolution Nuclear Magnetic Resonance Spectroscopy," Vol. 1, Pergamon Press, Elmsford, N. Y., 1965, pp 5, 512.
- (15) J. N. Shoolery and B. M. Alder, *J. Chem. Phys.*, **23**, 805 (1954).
- (16) R. L. Kay, *Advan. Chem. Ser.*, No. 73, 14 (1968).

and negative δ shifts to polarization, electrostrictive, and structure-breaking effects of the ions. A negative δ , *i.e.*, an upfield shift of water peaks in the electrolyte solution relative to pure water, is attributed to structure-breaking effects of the ions. Similarly, a positive δ , *i.e.*, a downfield shift of water peaks in the electrolyte solutions relative to pure water, is attributed to electrostrictive structure making.

The results plotted in Figures 1-3 may be qualitatively described by cation-solvent or coulombic-hydrophobic cation-cation interactions. If the Shooley-Alder criterion is accepted at 25°, the tetraalkylam-

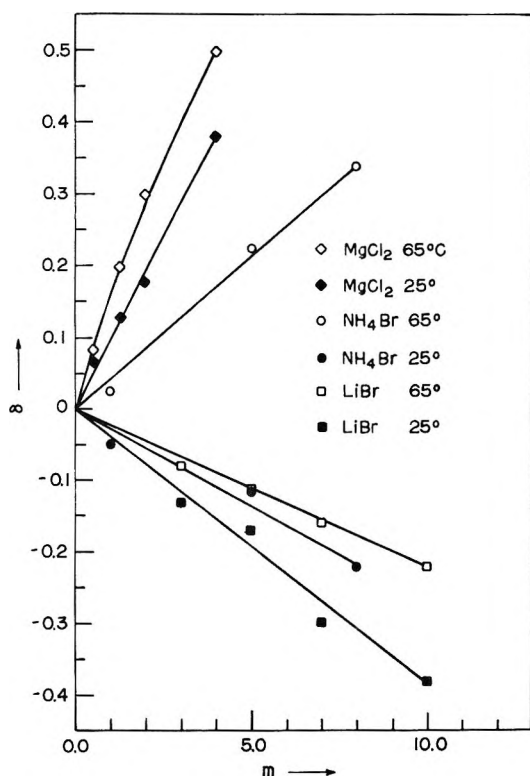


Figure 1. Proton shifts in aqueous electrolyte solutions of NH_4Br , LiBr , and MgCl_2 vs. the molal concentration at 25 and 65°.

monium bromides, cetyltrimethylammonium bromide, LiBr , and NH_4Br are structure breakers and MgCl_2 is a structure maker. The behavior of NH_4Br , $(n\text{-Bu})_4\text{NBr}$, and R_4NX as structure breakers is consistent with the results of Wirth,¹⁷ the nmr data of Kay,¹⁶ and the ir and pmr data of Hartman,¹¹ respectively.

The temperature effect on δ may be explained in terms of a two environment model for water in an aqueous solution.¹⁸ The assumption is that the observed δ is an average of the relative shifts due to the protons in the normal hydrogen-bonded and ion-polarized environments. Both hydrogen-bond formation¹⁹ and polarization¹⁵ interactions with cations or anions cause downfield shifts (positive change in δ). An increase in temperature will cause an upfield shift

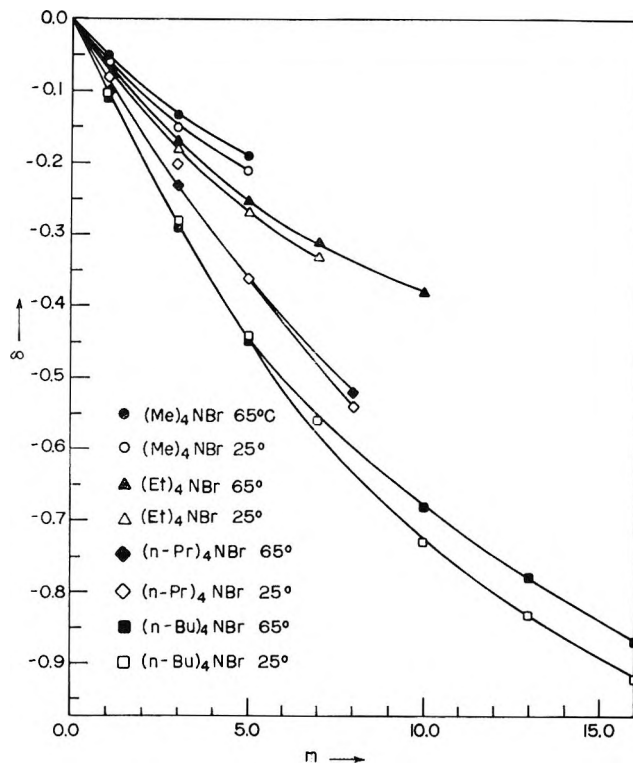


Figure 2. Proton shifts in aqueous electrolyte solutions of tetraalkylammonium bromides vs. the molal concentration at 25 and 65°.

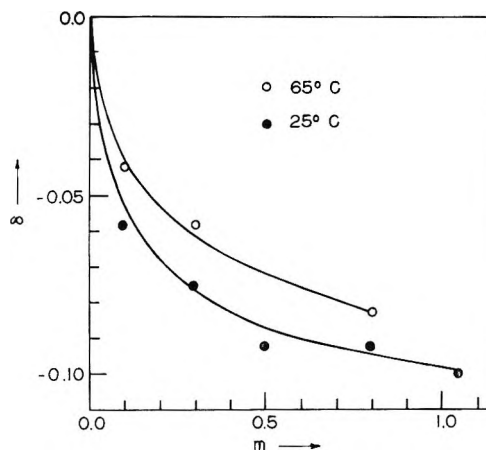


Figure 3. Proton shifts in aqueous electrolyte solutions of cetyltrimethylammonium bromide vs. the molal concentration at 25 and 65°.

(negative change in δ) due to some hydrogen-bond breaking²⁰ and a decrease in the ion-solvent interactions (*i.e.*, a decrease in the polarization effect).

(17) H. E. Wirth and F. N. Collier, Jr., *J. Amer. Chem. Soc.*, **72**, 5292 (1950).

(18) Referee, private communication.

(19) D. Eisenberg and W. Kauzmann, "The Structure and Properties of Water," Oxford, 1969, pp 195, 196.

(20) J. D. Bernal and R. H. Fowler, *J. Chem. Phys.*, **1**, 515 (1933); G. Némethy and H. A. Scheraga, *ibid.*, **36**, 3382 (1962).

A semiquantitative description for the positive change in δ with temperature observed for MgCl_2 , LiBr , NH_4Br , cetyltrimethylammonium bromide, and tetraalkylammonium bromides is given as follows. Let the observed relative δ shifts at 25 and 65° be given by¹⁸

$$\delta_{\text{obsd}}^{25} = f_{\text{H}}^{25}\delta_{\text{H}}^{25} + f_{\text{P}}^{25}\delta_{\text{P}}^{25} \quad (2)$$

and

$$\delta_{\text{obsd}}^{65} = f_{\text{H}}^{65}\delta_{\text{H}}^{65} + f_{\text{P}}^{65}\delta_{\text{P}}^{65} \quad (3)$$

where the superscripts denote the temperature in degrees centigrade, and f_{H} and f_{P} are the fraction of water molecules in the hydrogen-bonded and ion-polarized environments, respectively. As the temperature increases from 25 to 65° it is expected that $\delta_{\text{H}}^{25} \approx \delta_{\text{H}}^{65}$ but $\delta_{\text{P}}^{25} > \delta_{\text{P}}^{65}$. If we assume that $f_{\text{H}}^{25} > f_{\text{H}}^{65}$ and $f_{\text{P}}^{25} < f_{\text{P}}^{65}$, and that δ_{P}^{65} is not too much smaller than δ_{P}^{25} while $f_{\text{P}}^{25} \ll f_{\text{P}}^{65}$, it may be possible for $\delta_{\text{obsd}}^{25} < \delta_{\text{obsd}}^{65}$ in agreement with the experimental results.

Alternatively, the increase in the relative shift δ with temperature, *i.e.*

$$\delta = (\delta_{\text{obsd}}^{65} - \delta_{\text{obsd}}^{25})_m \quad (4)$$

where the subscript m is the molal concentration of the solution, may be considered as a measure of the strength of the ion-solvent interactions. The large positive change in δ with temperature found for NH_4Br , LiBr , and MgCl_2 , respectively, may be described in terms of electrostrictive hydration of the ions or the interaction of cations²¹ with the water of hydration layers. Since the relative order of the charges divided by ionic radius is $\text{NH}_4^+ \ll \text{Li}^+ < \text{Mg}^{2+}$, the ion-solvent interactions would be expected to follow the same relative order, however, would be much weaker at 65°. Thus, the observed order and magnitude for the positive change in δ , *i.e.*, $\text{NH}_4\text{Br} \gg \text{LiBr} > \text{MgCl}_2$, is as expected.

The increase in δ with temperature observed for the quaternary ammonium bromides (Figure 2) and cetyltrimethylammonium bromide (Figure 3) is also probably due to some type of ion-solvent interaction. Solvation^{22,23} and structure-breaking⁵ tendencies of $(\text{Me})_4\text{N}^+$ and $(\text{Et})_4\text{N}^+$ ions have been reported. However, due to large size and small effective charge not much water of hydration is expected for these ions. At higher temperatures the interactions of $(\text{Me})_4\text{N}^+$ and $(\text{Et})_4\text{N}^+$ with water will be reduced and the observed small positive change in δ is as expected for these cations.

The larger tetraalkylammonium bromides, *i.e.*, $(n\text{-Bu})_4\text{NBr}$ and $(n\text{-Pr})_4\text{NBr}$, seem to have no water of

hydration at lower concentrations when compared with the smaller quaternary ammonium bromides, but become more hydrated as the concentration is increased beyond 5 *m*. The latter is evidenced from the large positive change of δ with temperature at higher concentrations (Figure 2). Cetyltrimethylammonium bromide also shows hydration effects with temperature (Figure 3). Evidence²⁴⁻²⁶ from light scattering, X-rays, and conductivity experiments indicate that there are spherical micelles present at low concentrations (0.05 *M*) of cetyltrimethylammonium bromide solutions. The above water of hydration effects appear to be a function of the size of the alkyl group in the symmetrical quaternary ammonium bromides²⁷ since the observed relative order of the increase in δ shift is $(n\text{-Bu})_4\text{NBr} > (n\text{-Pr})_4\text{NBr} \gg \text{cetyl}(\text{Me})_3\text{NBr}$.

The authors prefer an explanation for the observed behavior of the tetraalkylammonium bromides as being due to the formation of multiple charged aggregates.^{28,29} At higher concentrations the larger quaternary ammonium bromides show strong coulombic-hydrophobic cation-cation interactions which lead to aggregated species arranged in a three-dimensional quasicrystalline lattice. To reduce the repulsive coulombic interactions between the cations, hydrated Br^- ions may be trapped within the aggregates or on their surface. At 65° these interacting forces are reduced and the aggregates may disrupt giving more available water.

Acknowledgments. We wish to thank Drs. E. Enrione and J. Vriesenga for valuable discussions, and Mr. Richard B. Hammer for his assistance in taking the nmr measurements. This work was supported by the Office of Saline Water, Grant No. 14-01-0001-623.

(21) If we assume that the Cl^- ion produces the same effect as Br^- ion in the case of MgCl_2 , all the salts studied have common anions. Hence, the observed effects are due to different cations.

(22) E. R. Nightingale, Jr., *J. Phys. Chem.*, **63**, 1381 (1959).

(23) D. S. Allam and W. H. Lee, *J. Chem. Soc. A*, 426 (1966).

(24) G. S. Hartley, *et al.*, *Trans. Faraday Soc.*, **32**, 795 (1936); C. S. Sarnis and G. S. Hartley, *ibid.*, **34**, 1288 (1938).

(25) F. Reiss-Husson and V. Luzzati, *J. Phys. Chem.*, **68**, 3505 (1964).

(26) M. Czerniawski, *Roczniki Chem.*, **40**, 1935 (1966); **41**, 119 (1967).

(27) The spherical micelles present in aqueous solutions of cetyltrimethylammonium bromide are "soap-type" micelles. The hydrophobic interior of these micelles is not appreciably hydrated causing the hydration effect of cetyl $(\text{Me})_3\text{N}^+\text{Br}$ to be correspondingly much less than $(n\text{-Bu})_4\text{NBr}$ and $(n\text{-Pr})_4\text{NBr}$.

(28) Since this article was written, H. G. Hertz, B. Lindman, and V. Scipe, *Berichte Bunsenges. Phys. Chem.*, **73**, 542 (1969), have measured the proton and deuteron relaxation rates of $(\text{Me})_4\text{NCl}$ and $(\text{Et})_4\text{NCl}$ in concentrated aqueous solutions. These authors have found evidence of "cation-cation contact" with $(\text{Et})_4\text{N}^+$ ion. In the case of tetra-*n*-propyl- and tetra-*n*-butylammonium salts a greater cation association was predicted by these authors.

(29) A. LoSurdo and H. E. Wirth, to be published.

Irradiated Single Crystal Clathrate of Dianin's Compound and 1,2-Dibromo-1,1-difluoroethane: Electron Spin Resonance Observation of the Br_2^- Radical^{1a}

by Lowell D. Kispert* and Jane Pearson^{1b}

Department of Chemistry, University of Alabama, University, Alabama 35486 (Received June 7, 1971)

Publication costs assisted by the U. S. Atomic Energy Commission

During the past few years, several examples of irradiated single crystals of organic inclusion compounds have been reported.²⁻⁴ Examination of these examples indicates that a clathrate host lattice can serve as a convenient means of stabilizing a free radical derived from compounds of more than three carbons normally found in the liquid state, permitting the study of new radicals,⁴ potential barrier effects,^{2b} and orientation.^{2b,3}

We wish to report the use of the clathrate 4-*p*-hydroxyphenyl-2,2,4-trimethylchroman (Dianin's compound) in trapping and orienting the Br_2^- radical at 77°K. The Br_2^- radical is believed to have been formed from the reaction of included 1,2-dibromo-1,1-difluoroethane and ionizing radiation yielding 1,1-difluoroethene and the Br_2^- radical. The fact that the Br_2^- radical was found oriented in the Dianin's clathrate suggests the possibility that the anisotropic esr hyperfine parameters and *g* tensors of radicals composed of two or three atoms may be studied by choosing the appropriate radical precursors to be included in the Dianin's clathrate.

Flippen and his coworkers⁵ have shown that the cavity in Dianin's compound is formed by the hydrogen bonding of the OH groups from 6 different molecules. Since there is only one OH group available for bonding from each molecule, there are separate columns of independent cages. Each cage is 11 Å long, 6.2 Å wide at the point of maximum extension, and 4.2 Å wide where the methyl groups protrude into the cage to give its hourglass shape. The *Z* direction lies along the needle axis of the crystal, and the cage size can vary for shapes that differ from cylindrical symmetry. It has also been determined by crystallography that when ethanol is included in Dianin's compound, it lies across the hourglass cavity at its widest point, thus compounds with one or two carbons can be included.

The unsolvated Dianin's compound was prepared and carefully purified by methods of Baker, *et al.*⁶ Dianin's compound was found to be insoluble in 1,2-dibromo-1,1-difluoroethane; however, it was found soluble in a mixture of 1,2-dibromo-1,1-difluoroethane

and ethanol from which single crystals were grown.⁷ The resulting crystals were X-irradiated at 77°K, and mounted on quartz rods for electron spin resonance (esr) investigation at that temperature.

The esr spectrum of the 77°K irradiated crystals resulted in a spectrum (Figure 1) of 7 groups of lines spread over 2600 G at *g* = 1.9980 when the crystals were mounted with the magnetic field parallel to the *Z* hexagonal crystal axis, an axis coincident with the long direction of the hourglass cavity. On rotation towards the *X* crystal direction, a large anisotropy in *g* and *A* was noted. Comparison of the *g* value and the spectral width in the *Z* direction with that found for the ⁸¹Br₂⁻ radical in irradiated KBr,⁸ or in irradiated lithium halide glasses,⁹ indicated that the Br₂⁻ radical had been trapped in Dianin's compound. A calculation based on the *A* and *g* values given in Table I for ⁸¹Br₂⁻ trapped in Dianin's compound and the quadrupole coupling constant reported by Lücken and Mazeline¹⁰ for the (CH₃)₂SBr radical was carried out using the computer program MAGNSPEC.¹¹ The results indicated that the outside high- and low-field esr lines were due to ⁸¹Br₂⁻, the middle line of the outside group was due to ⁸¹Br⁷⁹Br⁻ and ⁷⁹Br⁸¹Br⁻, and the inside line of the outside group was due to ⁷⁹Br₂⁻. The other groups of lines showed large second-order effects as indicated by the theoretical stick diagram calculated from the MAGNSPEC program. The fact that the Br₂⁻ radical lies parallel to the long direction of the hourglass rather than across the hourglass cavity like included ethanol also explains the presence of only one radical site per unit cell. Upon

(1) (a) This research was partially supported by the U. S. Atomic Energy Commission under Contract No. At-(40-1)-4062 and this is AEC Document No. ORO-4062-2. (b) NSF Undergraduate Participant, 1969-1970.

(2) (a) O. H. Griffith and A. L. Kwiram, *J. Amer. Chem. Soc.*, **86**, 3937 (1964); T. Ichikawa, M. Iwasaki, and K. Kuwata, *J. Chem. Phys.*, **44**, 2979 (1966); O. H. Griffith, *Proc. Natl. Acad. Sci. U. S.*, **54**, 1296 (1965); C. Corvaya, *J. Chem. Phys.*, **44**, 1958 (1966); (b) O. H. Griffith, *J. Chem. Phys.*, **41**, 1093; **42**, 2651 (1965); O. H. Griffith and H. M. McConnell, *Proc. Natl. Acad. Sci. U. S.*, **48**, 1877 (1962).

(3) H. Ohigashi and Y. Kurita *J. Chem. Soc. Jap.*, **40**, 704 (1967).

(4) G. A. Helcke and R. F. Euratom, *Mol. Phys.*, **18**, 1 (1970); D. E. Wood and R. V. Lloyd, *J. Chem. Phys.*, **52**, 3840 (1970); D. E. Wood, R. V. Lloyd, and D. W. Pratt, *J. Amer. Chem. Soc.*, **92**, 4115 (1970).

(5) J. L. Flippen, J. Karle, and I. L. Karle, *ibid.*, **92**, 3750 (1970).

(6) W. Baker, A. J. Floyd, J. F. W. McOmie, G. Pope, A. S. Weaving, and J. H. Wild, *J. Chem. Soc.*, 2010 (1956).

(7) W. Baker and J. F. W. McOmie, *Chem. Ind. (London)*, 256 (1955).

(8) T. G. Castner and W. Kenzig, *J. Phys. Chem. Solids*, **3**, 178 (1957).

(9) E. B. Zvi, R. A. Beaudet, and W. K. Wilmarth, *J. Chem. Phys.*, **51**, 4166 (1969).

(10) E. A. C. Lücken and C. Mazeline, *ibid.*, **48**, 1942 (1968).

(11) M. Kapp and J. H. Mackey, *J. Comput. Phys.*, **3**, 539 (1969); J. H. Mackey, M. Kapp, and E. C. Tynan in "Electron Spin Resonance of Metal Complexes," T. F. Yen, Ed., Plenum, New York, N. Y., 1969. An expanded and revised version has been written for the Univac 1108 at the University of Alabama.

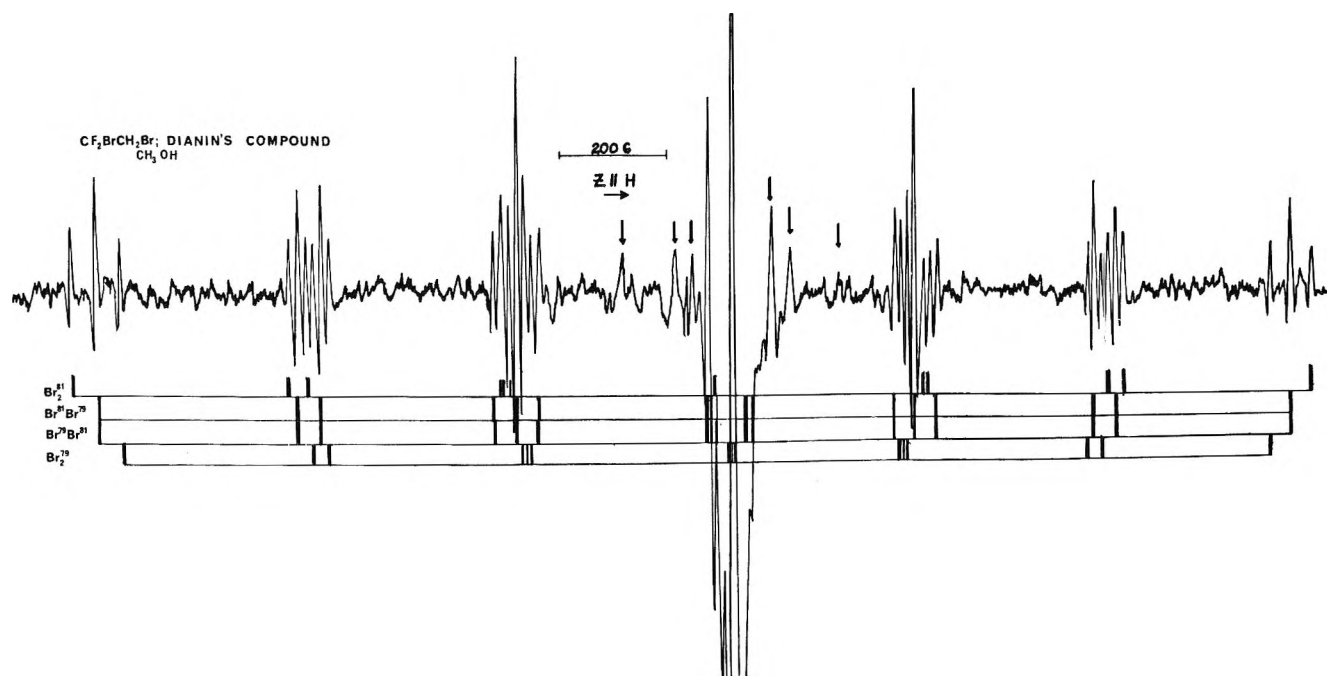


Figure 1. ESR spectrum of irradiated Dianin's compound with 1,2-dibromo-1,1-difluoroethane included. The hexagonal Z axis is parallel to the magnetic field. The theoretical stick diagram calculated for each Br_2^- isotope is reconstructed below the spectrum.

Table I: g and A Values Found for the $^{81}\text{Br}_2^-$ Radical

Radical	Matrix	Z		X		Y	
		g	A	g	A	g	A
Br_2^-	KBr	1.980	455	2.179	80	2.175	80
Br_2^-	$\text{CF}_2\text{BrCH}_2\text{Br}$ in Dianin's compound	1.998	450	2.151	90	2.16	90
Br_2^-	Lithium halide glasses	1.969	459	2.112	50-70	2.112	50-70

warming to 110°K the spectrum decays irreversibly, not unexpected from the large degree of motional freedom present.

Additional lines (indicated by arrows in Figure 1) spread over 500 G were also observed when the crystals was mounted with $Z||H$. The large spectral width suggested either the presence of a biradical or a fluorine containing radical; however, it appeared that these lines were dependent on the purity of the $\text{CF}_2\text{Br-CBrH}_2$ and, therefore, were ignored. The large central line (Figure 1) observed for all irradiated samples, including an irradiated powder sample of pure Dianin's compound, could be due to a radical with the odd electron centered on a nucleus of zero spin such as the substituted acetyl radical¹² or from a color center such as a trapped electron.

The possibility still exists that the Br_2^- radical was due to a trace of molecular bromine rather than the product of ionized $\text{CF}_2\text{BrCH}_2\text{Br}$. However, carefully purified $\text{CF}_2\text{BrCH}_2\text{Br}$ included in Dianin's compound

showed no change in the Br_2^- radical esr spectral intensity over that of a sample containing a slight trace of Br_2 . On the other hand, an irradiated frozen sample of very carefully purified $\text{CBrF}_2\text{CBrH}_2$ showed no Br_2^- radical. However, if the reasonably weak esr signals of Br_2^- found in the Dianin's clathrate were averaged over a powder spectrum, it is doubtful whether they would be observed.

Acknowledgment. The authors wish to acknowledge the University of Alabama's Research Committee, Project 600 for support of this work, an NSF departmental matching grant which provided for the Varian E-12 esr spectrometer, the Physics Department at the University of Alabama for use of their X-ray machine, and the University of Alabama computer center for providing a generous amount of computer time.

(12) R. C. McCalley and A. L. Kwiram, *J. Amer. Chem. Soc.*, **92**, 1441 (1970).

Free-Radical Intermediates in the Reaction of the Hydroxyl Radical with Dialkyl Sulfoxides¹

by Hitoshi Taniguchi,* Hideo Takagi,
and Hiroyuki Hatano

Department of Chemistry, Faculty of Science, Kyoto University,
Kyoto 606, Japan (Received June 7, 1971)

Publication costs borne completely by The Journal of
Physical Chemistry

The principal features in reactivities of the hydroxyl radical produced in a titanous (Ti^{3+}) chloride-hydrogen peroxide (H_2O_2) system are known to abstract the hydrogen atom from the C-H bond and add to the double bond of the organic substrates containing not only carbon, hydrogen, and oxygen atoms² but also nitrogen,³⁻²¹ phosphorus,²²⁻²⁴ fluorine,²⁵⁻²⁷ and chlorine^{3,26} atoms.

As to the organosulfur compounds with -C-S-H or -C-S-S-C- groups, sulfur free radicals were observed in the reaction of cysteine, cystine, homocystine, cysteamine, cystamine, and penicillamine with a Ti^{3+} - H_2O_2 system.^{10,28} Intermediate radicals from dimethyl sulfoxide and methionine in a Ti^{3+} - H_2O_2 system were also reported.^{3,29} However, the identification of radicals from methionine is considered to be ambiguous.

In this work, free radicals produced in the reaction of the hydroxyl radical with methionine and related sulfur compounds having dialkyl sulfoxide groups [CS(\rightarrow O)C] have been studied by electron spin resonance (esr) spectroscopy using a continuous flow method. The hydroxyl radical was generated chemically in a Ti^{3+} - H_2O_2 system. The reaction scheme between the hydroxyl radical and dialkyl sulfoxides is proposed to explain the yield of alkyl radicals. In this scheme, the cleavage of the C-S bond is introduced, which is a new aspect in a Ti^{3+} - H_2O_2 reaction system.

From the results of radiation-biochemical studies,³⁰⁻³³ it is found that the sulfur-containing amino acid, methionine, is very radiation sensitive among the biologically important amino acids in aqueous solution. Since the hydroxyl radical is one of the active species formed in the radiolysis of water and plays a positive role in the radiation damage to organic solutes,³⁴⁻³⁶ it is considered of interest to investigate the intermediate radicals in the reaction of the hydroxyl radical with methionine in order to elucidate the process of the decomposition of dialkylsulfur compounds induced by the irradiation in aqueous solution.

Experimental Section

The experimental arrangements and procedures for the observation of intermediate radicals in a Ti^{3+} -

H_2O_2 system were essentially the same as described previously.^{12,19,20} The mixing cell used in this experiment was made in our laboratory, consisting of double polyethylene tubes. The volume between the mixing point of the two streams and the center of the

- (1) This work was presented at the 23rd Annual Meeting of the Chemical Society of Japan, Tokyo, April 1970.
- (2) R. O. C. Norman and B. C. Gilbert, *Advan. Phys. Org. Chem.*, **5**, 53 (1967), and references therein.
- (3) W. T. Dixon, R. O. C. Norman, and A. L. Buley, *J. Chem. Soc.*, 3625 (1964).
- (4) J. T. Pearson, P. Smith, and T. C. Smith, *Can. J. Chem.*, **42**, 2022 (1964).
- (5) H. Fischer, *Z. Naturforsch. A*, **19**, 267 (1964).
- (6) C. Corvaja, H. Fischer, and G. Giacometti, *Z. Phys. Chem. (Frankfurt am Main)*, **45**, 1 (1965).
- (7) M. G. Ormerod and B. B. Singh, *Int. J. Radiat. Biol.*, **10**, 533 (1966).
- (8) T. Shiga, A. Boukhors, and P. Douzou, *J. Phys. Chem.*, **71**, 4264 (1967).
- (9) J. Q. Adams, *J. Amer. Chem. Soc.*, **89**, 6022 (1967).
- (10) W. A. Armstrong and W. G. Humphreys, *Can. J. Chem.*, **45**, 2589 (1967).
- (11) R. E. Florin, F. Sicilio, and L. A. Wall, *J. Res. Nat. Bur. Stand., Sect. A*, **72**, 49 (1968).
- (12) H. Taniguchi, K. Fukui, S. Ohnishi, H. Hatano, H. Hasegawa, and T. Maruyama, *J. Phys. Chem.*, **72**, 1926 (1968).
- (13) T. Yonezawa, I. Noda, and T. Kawamura, *Bull. Chem. Soc. Jap.*, **42**, 650 (1969), and references therein.
- (14) C. Nicolau, M. McMillan, and R. O. C. Norman, *Biochim. Biophys. Acta*, **174**, 413 (1969).
- (15) P. Smith and W. M. Fox, *Can. J. Chem.*, **47**, 2227 (1969).
- (16) P. Smith, W. M. Fox, D. J. McGinty, and R. D. Stevens, *ibid.*, **48**, 480 (1970).
- (17) H. Paul and H. Fischer, *Ber. Bunsenges. Phys. Chem.*, **73**, 972 (1969).
- (18) R. Poupko, A. Loewenstein, and B. L. Silver, *J. Amer. Chem. Soc.*, **93**, 580 (1971).
- (19) H. Taniguchi, H. Hatano, H. Hasegawa, and T. Maruyama, *J. Phys. Chem.*, **74**, 3063 (1970).
- (20) H. Taniguchi, *ibid.*, **74**, 3143 (1970).
- (21) J. Hüttermann, J. F. Ward, and L. S. Myers, Jr., *ibid.*, **74**, 4022 (1970).
- (22) E. A. C. Lucken, *J. Chem. Soc. A*, 1354 (1966).
- (23) E. A. C. Lucken, *ibid.*, **A**, 1357 (1966).
- (24) A. R. Metcalfe and W. A. Waters, *ibid.*, **B**, 340 (1967).
- (25) P. Smith, J. T. Pearson, and R. V. Tsina, *Can. J. Chem.*, **44**, 753 (1966).
- (26) W. E. Griffiths, G. F. Longster, J. Myatt, and P. F. Todd, *J. Chem. Soc. B*, 530 (1967).
- (27) C. R. E. Jefcoate and R. O. C. Norman, *ibid.*, **B**, 48 (1968).
- (28) C. Nicolau and H. Dertinger, *Radiat. Res.*, **42**, 62 (1970). Sulfur free radicals were also observed by the oxidation of cysteine and related thiols with ceric ion: W. Wolf, J. C. Kertesz, and W. C. Landgraf, *J. Magn. Resonance*, **1**, 618 (1969).
- (29) G. K. Bürk and G. Schoffa, *Int. J. Protein Res.*, **1**, 113 (1969).
- (30) L. Duran and A. L. Tappel, *Radiat. Res.*, **9**, 498 (1958).
- (31) H. Hatano, S. Ganno, and A. Ohara, *Bull. Inst. Chem. Res. Kyoto Univ.*, **41**, 61 (1963).
- (32) F. Shimazu and A. L. Tappel, *Radiat. Res.*, **23**, 203 (1964).
- (33) A. Ohara, *J. Radiat. Res. (Tokyo)*, **6**, 130 (1965).
- (34) Z. M. Bacq and P. Alexander, Ed., "Fundamentals of Radio-biology," 2nd ed, Pergamon Press, New York, N. Y., 1961.
- (35) A. M. Kuzin, "Radiation Biochemistry," Israel Program for Scientific Translations, Jerusalem, 1964, Chapter 4.
- (36) J. K. Thomas, "Advances in Radiation Chemistry," Vol. 1, M. Burton and J. L. Magee, Ed., Wiley, New York, N. Y., 1969, p 103.

Table I: Structures, g Values, and Hyperfine Coupling Constants of the Intermediate Radicals^a

Substrate	Radical	g Value	Coupling constant, G ^b	
			C ₁ -H	C ₂ -H
Methionine	$\left\{ \begin{array}{l} \dot{\text{C}}\text{H}_2\text{-CH}_2\text{-CH(N}^+\text{H}_3\text{)COOH} \\ \text{CH}_3 \end{array} \right\}$	2.0026	22.3	25.7
Methionine sulfoxide		2.0024	22.8	
Dimethyl sulfoxide	$\dot{\text{C}}\text{H}_3$	2.0024	22.8	
Thiodiglycolic acid	$\dot{\text{C}}\text{H}_2\text{-S-CH}_2\text{COOH}$...	(16.7)	(2.0) ^d
Sulfoxide of thiodiglycolic acid	$\dot{\text{C}}\text{H}_2\text{COOH}$	2.0032	21.3	

^a See text and ref 41 for the notations in column 4. ^b The values in parentheses were obtained by Kurita.³⁹ ^c g Value was not measured. ^d Coupling constant due to two protons in the methylene group adjacent to carboxyl group.

esr cavity is about 0.015 ml. The esr spectra of intermediate radicals were recorded on an X-band spectrometer (JEOL, Model PIOS) at room temperature within 5 to 30 msec after mixing two reactants. The hyperfine (hf) coupling constants and g values were calibrated by comparison with a sample of potassium peroxyaminodisulfonate in aqueous sodium carbonate solution (nitrogen hf splitting, 13.0 ± 0.1 G; $g = 2.00550 \pm 0.00005$).³⁷

All materials were obtained commercially except the sulfoxides of methionine and thiodiglycolic acid, which were prepared by the oxidation of them with hydrogen peroxide in an 0.5 *N* hydrochloric acid solution.³⁸ The purity of methionine sulfoxide was checked by an amino acid analyzer (Hitachi, Model KLA-3). The concentrations of titanous chloride and hydrogen peroxide were 0.015 and 0.3 *M*, respectively. The organosulfur substrates were added only to H₂O₂ reactant unless specially mentioned, in 0.3 to 1.0 *M* concentration according to their reactivity and solubility. Both reactant solutions were acidified to about pH 1.5 with dilute hydrochloric acid and deoxygenated by bubbling nitrogen gas. When dilute sulfuric acid was used to acidify reactant solutions, there were no differences essentially in the esr spectra of substrate radicals.

Results and Discussion

1. *Identification of the Intermediate Radicals.* ESR spectra with sufficient signal-to-noise ratios were obtained from methionine, methionine sulfoxide, dimethyl sulfoxide (DMSO), and the sulfoxide of thiodiglycolic acid. The structures of the intermediate radicals deduced from the analysis of the spectra and the estimated g values and hf coupling constants are summarized in Table I; hf coupling data of the thiodiglycolic acid radical obtained by Kurita³⁹ are also shown in parentheses.

An esr spectrum of the intermediate radicals from methionine sulfoxide is reproduced in Figure 1, in which two peaks designated by S₁ ($g = 2.0135$) and S₂ ($g = 2.0120$) are due to the titanium peroxy radical species according to the assignment of Fischer.⁴⁰ When methionine was a substrate of a Ti³⁺-H₂O₂

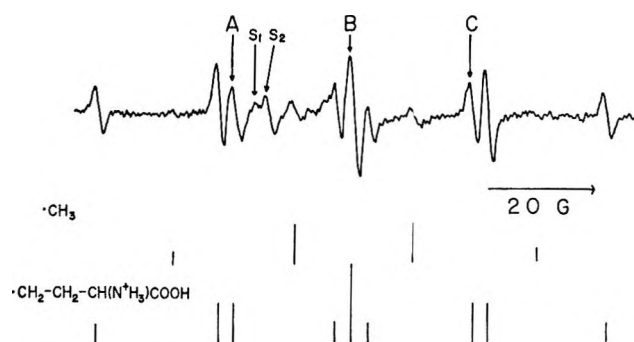


Figure 1. Electron spin resonance spectrum of the intermediate radicals from 0.3 *M* methionine sulfoxide with reconstruction.

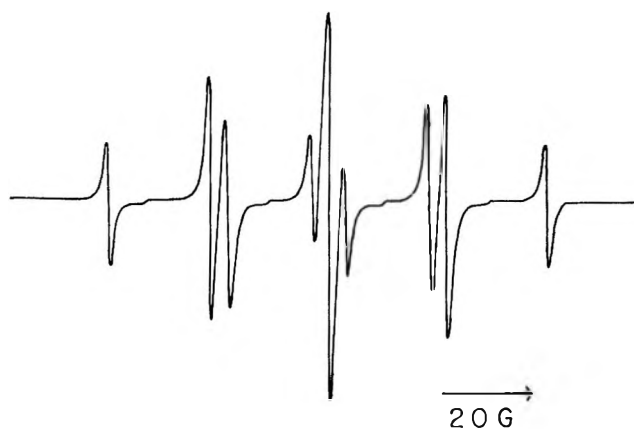


Figure 2. Simulated spectrum of the ethyl-type radical based on coupling constants given in the text. The line shape is considered to be Lorentzian, and the line width is taken to be 1.25 G.

system, the same intermediate radicals were obtained as in the case of methionine sulfoxide.

The ethyl-type radical ($\dot{\text{C}}\text{H}_2\text{CH}_2\text{-}$) was assigned as a predominant one for methionine and its sulfoxide. Hyperfine coupling constants due to the C₁-H and

(37) J. S. Hyde, unpublished result quoted by J. Q. Adams, S. W. Nicksic, and J. R. Thomas, *J. Chem. Phys.*, **45**, 654 (1966).

(38) J. P. Greenstein and M. Winitz, "Chemistry of the Amino Acids," Vol. 3, Wiley, New York, N. Y., 1961, p 2145.

(39) Y. Kurita, private communication (1965).

(40) H. Fischer, *Ber. Bunsenges. Phys. Chem.*, **71**, 685 (1967).

C_2 -H protons⁴¹ presented in Table I are comparable to those of the structurally similar radical; *i.e.*, $a_{C_1-H} = 22.3$ and $a_{C_2-H} = 26.7$ G for the *n*-propylamine radical, $\dot{C}H_2CH_2CH_2N^+H_3$.¹² In an esr spectrum of the ethyl-type radical, it is strange that line widths of three spectrum components designated by A, B, and C in Figure 1 are broader than the other six components. This is presumably because of small inequivalency of the hf interaction between the unpaired electron and two C_2H protons as is the case in the propagating radical of methacrylic acid formed in a $Ti^{3+}-H_2O_2$ system.⁴² A computer-simulated spectrum of the ethyl-type radical is shown in Figure 2 and agrees well with the observed one. Hyperfine coupling constants obtained from reasonably fit computer simulations are 22.30 G for a_{C_1-H} and 25.65 and 26.39 G for a_{C_2-H} .

Recently, Bürk and Schoffa²⁹ observed a similar esr spectrum of the methionine radical formed in a $Ti^{3+}-H_2O_2$ system. They reported a $\dot{C}H_2CH(N^+H_3)-COOH$ radical (I) with a large C_2H coupling constant, 52 G and without nitrogen splitting, as one of the intermediate radicals from methionine. The large value of a_{C_2-H} indicates that the structure of radical I is so restricted that the internal rotation of the C_2H bond around the C_1-C_2 axis is much hindered.⁴³ However, this is improbable; the internal rotation in radical I would be expected to occur freely in aqueous solution. Besides, from α -alanine in a $Ti^{3+}-H_2O_2$ system, the same radical structure as I had been identified with the following hf coupling constants: $a_{C_2-H} = 26.6$ and $a_N = 3.6$ G.¹² Therefore, we cannot follow their assignment.

In the esr spectra from methionine and its sulfoxide, the methyl radical was also assigned in addition to the ethyl-type radical, although its spectrum was poor in signal-to-noise ratio. The *g* value and C_1H proton coupling constant of the methyl radical presented in Table I are in good agreement with those of the methyl radicals formed in the reaction of DMSO and acetic acid with a $Ti^{3+}-H_2O_2$ system.^{3,44} From methionine and DMSO we could not observe the $\dot{O}SCH_3$ radical detected by Bürk and Schoffa,²⁹ probably because of different conditions for observation.

The 1:2:1 triplet spectrum from the sulfoxide of thiodiglycolic acid gives the same *g* value and C_1H proton coupling constant as the acetic acid radical produced as a result of the hydrogen abstraction from a methyl group,¹¹ leading to the assignment to the structure CH_2COOH .

2. *Reaction Scheme between the Hydroxyl Radical and Dialkyl Sulfoxides.* Results in Table I suggest that the cleavage of CS bonds occurs and alkyl radicals are formed after the hydroxyl radical reacts with dialkyl sulfoxides. However, the esr spectra of counterpart sulfur free radicals were not observed from dialkyl sulfoxides $[CS(\rightarrow O)C]$, while those with *g*

values near 2.01 were obtained from sulfur compounds with CSH or CSSC groups.^{10,28} It can be considered that there are different reactivities peculiar to dialkyl sulfoxides, and the formation of alkyl radicals is not ascribed to the simple scission of CS bonds. Alkyl radicals arise probably from the addition of the hydroxyl radical to dialkyl sulfoxides and not from the hydrogen abstraction, since the esr spectra of other resultant organic radicals were not observed.

Although the esr spectra of the intermediate radicals generated from methionine and its sulfoxide are identical in a $Ti^{3+}-H_2O_2$ system, esr spectra from methionine were not observed without the substrate in H_2O_2 solution. The yield of the ethyl-type radical from methionine is dependent on the time between the preparation of the H_2O_2 reactant solutions and the observation of esr spectra. The signal intensity of the ethyl-type radical increases gradually with the time.⁴⁵ It is well known that methionine is readily oxidized in H_2O_2 solution.³⁸ Consequently, the ethyl-type radical observed from methionine in H_2O_2 solution is considered to form in the reaction between the hydroxyl radical and methionine sulfoxide obtained by the oxidation of methionine itself with hydrogen peroxide.

When methionine (0.3 *M*) was initially dissolved in Ti^{3+} (0.015 *M*) solution, the esr spectra due to substrate radicals were not observed, while methionine sulfoxide (0.3 *M*) added in Ti^{3+} (0.015 *M*) solution gave a 23% concentration of the ethyl-type radical from methionine sulfoxide (0.3 *M*) in H_2O_2 (0.3 *M*) solution. This is probably because methionine forms a characteristic complex with titanium ion preventing the substrate from reacting with the hydroxyl radical and/or the oxidation of methionine to the corresponding sulfoxide remains incomplete.

In the case of thiodiglycolic acid, if the substrate was reacted with the hydroxyl radical before it was oxidized completely, another radical was assigned by Kurita³⁹ as shown in Table I. In our work, the sulfoxide of thiodiglycolic acid was added into H_2O_2 solution in place of thiodiglycolic acid.

The reaction scheme between the hydroxyl radical and methionine is proposed tentatively as described below, and it might be common to the cases of methionine, methionine sulfoxide, DMSO, thiodiglycolic acid, and the sulfoxide of thiodiglycolic acid.

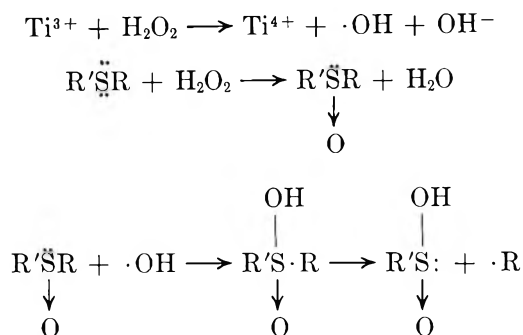
(41) The designations C_1 and C_2 refer to the position relative to the carbon atom which bears the unpaired electron.

(42) H. Fischer, *Z. Naturforsch. A*, **19**, 866 (1964).

(43) C. Heller and H. M. McConnell, *J. Chem. Phys.*, **32**, 1535 (1960).

(44) R. O. C. Norman and R. J. Pritchett, *Chem. Ind. (London)*, 2040 (1965).

(45) For example, methionine (0.3 *M*) standing about 15 min in H_2O_2 (0.3 *M*) solution gave a fourth concentration of the ethyl-type radical obtained from methionine sulfoxide (0.3 *M*) in H_2O_2 (0.3 *M*) solution. ESR spectra could not be recorded within 10 min after the addition of methionine into H_2O_2 solution.



The hydroxyl radical adds to the substrate of dialkyl sulfoxide form and simultaneously the SR bond becomes unstable, leaving an alkyl group after the cleavage of the bond.

In the case of methionine, the cleavage of the CS bond occurs at both sides of methylene and methyl groups after methionine has been oxidized to its sulfoxide. The ethyl-type radical, however, exists mainly, showing that the cleavage occurs more easily at the methylene site. This is probably because the structure of the ethyl-type radical containing two methylene groups has a larger conjugated system than the methyl radical, and it becomes more stable.

Dixon, *et al.*,³ supposed that the methyl radical of DMSO may arise from the addition of the hydroxyl radical to the sulfoxide group and subsequent cleavage of a CS bond. However, the SO bond in sulfoxide is considered to be a semipolar bond rather than a double bond,⁴⁶ and the addition of the hydroxyl radical is not so likely to occur to the sulfoxide group as it occurs to the double bond.

The reaction scheme proposed in this work is a new mechanism of the addition of the hydroxyl radical generated in a Ti^{3+} - H_2O_2 reaction system, although the possibility cannot be completely neglected that alkyl radicals could be formed through different consecutive reactions of other radicals such as chlorine atom and primary substrate radicals resulting from hydrogen abstraction.

In a γ -irradiated aqueous solution of methionine, it has been known that methionine is first oxidized to methionine sulfoxide and further to methionine sulfone.⁴⁷ A cleavage of the CS bond of methionine appears to occur mainly after these oxidation of the sulfur atom.⁴⁷ The reaction scheme proposed in this work is consistent with the above process and presents important information about an elementary process of the radiolysis of methionine in aqueous solution.

Acknowledgment. The authors are very grateful to Mr. Hideo Hasegawa of Japan Electron Optics Laboratory Co. for his considerable assistance with the spectrum simulation.

(46) C. C. Price and S. Oae, "Sulfur Bonding," Ronald Press, New York, N. Y., 1962, Chapters 3 and 4.

(47) A. Ohara, *J. Radiat. Res. (Tokyo)*, **7**, 18 (1966).

Ethylene as an Actinometer in the Wavelength Region 147–185 Nanometers

by L. C. Glasgow* and P. Potzinger

Max-Planck-Institut für Kohlenforschung, Abteilung Strahlenchemie, Mülheim/Ruhr, Germany (Received August 30, 1971)

Publication costs assisted by Max-Planck-Institut für Kohlenforschung, Abteilung Strahlenchemie

Among the many actinometers for the vacuum uv region reported in the literature, only a few fulfill the criteria of a good actinometer.¹ Although in many respects N_2O serves as an acceptable actinometer in the region 147–185 nm, it suffers from two distinct disadvantages: the extinction coefficient is rather small in the 150–170-nm region (below $30 \text{ l. mol}^{-1} \text{ cm}^{-1}$), and a mixture of the gases N_2 , O_2 , and NO results from photolysis of N_2O thus requiring an analytical separation. It has been shown by Greiner² that the N_2O actinometer can be used without analytical separation by measurement of the pressure increase, but this method necessitates an extremely precise pressure determination. Recently, the photolysis of hexafluoroacetone has been suggested³ as a simple actinometer at 147 nm. At 185 nm the H_2 yields from C_2H_4 ^{4,5} and HBr ¹⁰ have been proposed as an actinometer.

We have investigated the photolysis of C_2H_4 at 147, 163, and 185 nm⁶ and wish to report here our results for the quantum yield of H_2 formation ($\phi[\text{H}_2]$). The data indicate that C_2H_4 is well suited as an actinometer in this wavelength region. Although the photolysis of C_2H_4 has been investigated in several laboratories,^{7–9} quantum yields have been reported only at 185 nm.^{4,5}

Experimental Section

Phillips Research grade C_2H_4 was used without further purification. N_2O from Hoechst and HBr from Matheson were further purified by trap-to-trap distillation *in vacuo*. All gases were shown to be better than 99.99% pure *via* gas chromatography. A new Hg-free vacuum system fitted with greaseless stop-

(1) J. G. Calverts and J. N. Pitts, Jr., "Photochemistry," Wiley, New York, N. Y., 1966, p 780.

(2) N. R. Greiner, *J. Chem. Phys.*, **47**, 4373 (1967).

(3) J. J. Magenheim and R. B. Timmons, *ibid.*, **52**, 2790 (1970).

(4) H. D. Beckey, W. Groth, H. Okabe, and H. J. Rommel, *Z. Naturforsch. A*, **19**, 1511 (1964).

(5) (a) P. Borrell, P. Cashmore, and A. E. Platt, *J. Chem. Soc. A*, 3063 (1968); (b) P. Borrell, A. Cervenka, and J. W. Turner, *ibid.*, to be published.

(6) L. C. Glasgow and P. Potzinger, *Z. Naturforsch.*, to be submitted.

(7) M. C. Sauer, Jr., and L. M. Dorfman, *J. Chem. Phys.*, **35**, 497 (1961).

(8) H. Okabe and J. R. McNesby, *ibid.*, **36**, 601 (1961).

(9) R. A. Back and D. W. L. Griffiths, *ibid.*, **46**, 4839 (1967).

cocks was employed. The absence of Hg was systematically checked throughout the course of this work by photolysis of N_2O or C_2H_4 at 254 nm.

The 185-nm source was a flat spiral low pressure Hg lamp (Quarzlampengesellschaft Hanau) of diameter 5 cm. The Hg lamp was positioned *ca.* 2 cm in front of a 10-cm long cylindrical cell of diameter 5 cm. The 163-nm radiation was produced with a bromine lamp constructed from a 200-ml round flask fitted with a Suprasil window and a cold finger and filled with *ca.* 1 Torr of argon and several Torr of Br_2 vapor. The excess Br_2 was frozen out in the cold finger at -63° (chloroform slush). Emissions shorter than 160 nm were eliminated by the Suprasil window. A Xe resonance lamp with a sapphire window was used for the 147-nm irradiations. Spectral purity of the lamps and absorption coefficients of the gases used were determined with a McPherson Model 235 vacuum uv spectrograph. The photolyses at 147 and 163 nm were performed in a 150-cm³ chamber connected directly to the microwave lamp.

N_2O was used as primary actinometer for all wavelengths. At 185 nm, HBr was also employed with H_2 as well as Br_2 being determined. Assuming $\phi[N_2] = 1.44$ from N_2O , and $\phi[H_2] = \phi[Br_2] = 1.00^{10}$ from HBr, agreement to within 10% was obtained with the two actinometers. Every photolysis was preceded and followed by an actinometric run. The optical density of the actinometer was always chosen to be the same as that of the sample.

The pressure gauge used for measuring H_2 yields was a membrane manometer from Datametries capable of measuring absolute pressure in the range 10^{-4} to 1 Torr to better than 0.5% accuracy. It should be noted that a normal thermal conductivity pressure gauge (Heraeus Autovac) could be calibrated to measure small amounts of H_2 . We found it convenient to calibrate the conductivity gauge without the use of a McLeod gauge by using HBr photolyses. The amount of Br_2 produced can be accurately measured spectrophotometrically and then set equal to the H_2 yield.

At long irradiation times small amounts of polymer were observed in the irradiation cells, especially at 185 nm. The polymer was removed from quartz cells by washing with dilute HF solution. Cells having water sensitive windows could be cleaned by reaction with O_2 induced thermally or by electrical discharge.

Results and Discussion

We investigated $\phi[H_2]$ as a function of wavelength, temperature, and pressure. Because of the polymer formation and larger extinction coefficients of the higher olefin products^{6,7,9} relative to that of C_2H_4 at 185 nm, $\phi[H_2]$ was also investigated as a function of per cent conversion at 185 nm. Figure 1 shows that $\phi[H_2]$ decreases with increasing per cent conversion

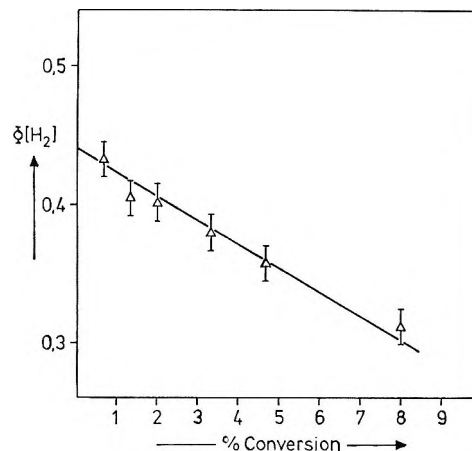


Figure 1. Effect of per cent conversion on $\phi[H_2]$ at 185 nm.

(based on HBr as well as N_2O actinometry). The effect is largely due to polymer formation on the windows. Our extrapolated value of 0.44 is considerably smaller than the values of 0.8⁴ and 0.62;⁵ however, a value of 35 ± 3 l. mol⁻¹ cm⁻¹ was assumed for the extinction coefficient of C_2H_4 . This is much lower than our value measured using a combination of low pressure Hg light source and spectrograph. As shown in Table I, our value is in substantial agreement with

Table I: Extinction Coefficients of N_2O and C_2H_4 at 185 nm

	ϵ , l. mol ⁻¹ cm ⁻¹
C_2H_4	87.5 ^a
	80 ^b
	90 ^c
	35 ^d
N_2O	36 ^e
	40 ^c
	30.9 ^d

^a P. G. Wilkinson and R. S. Mulliken, *J. Chem. Phys.*, **23**, 1895 (1955). ^b K. Watanabe, *ibid.*, **40**, 558 (1964). ^c This work. ^d Reference 5. ^e M. Zelikoff, K. Watanabe, and E. C. Y. Inn, *J. Chem. Phys.*, **21**, 1643 (1953).

previous measurements. The choice of an extinction coefficient for ethylene a factor of 2 too small would contribute to the higher quantum yield previously observed.⁵

As can be seen from Table II, $\phi[H_2]$ is independent of pressure over the range 0.1 to 100 Torr and independent of energy of the photolyzing radiation at the three wavelengths tested. Table III shows that $\phi[H_2]$ is also temperature independent in the range 22 to 175°.

(10) R. M. Martin and J. E. Willard, *J. Chem. Phys.*, **40**, 2999 (1964).

Table II: Quantum Yield of H₂ as a Function of Ethylene Pressure and Photolyzing Wavelength

C ₂ H ₄ , Torr	λ, nm	φ[H ₂]
0.12	185	0.43 ± 0.03
0.24		0.40
5.0		0.43
20.0		0.44
38.1		0.43
52.3		0.43
100		0.41
20	163	0.46 ± 0.05
5	147	0.37 ± 0.05
10		0.40
50		0.40
70		0.35

The values shown in Table II represent average values from several measurements. The lower error limits on the values for 185 nm reflect the better stability of the mercury lamp as opposed to the microwave powered lamps. The average value of φ[H₂] for all experiments is 0.42 ± 0.05.

It is concluded that the determination of the hydrogen yield from C₂H₄ photolysis offers the following advantages as an actinometer. (1) φ[H₂] is independent of temperature, pressure, and wavelength. (2) φ[H₂]

Table III: Quantum Yield of H₂ as a Function of Temperature from the 185-nm Photolysis of 20 Torr of C₂H₄

T, °C	φ[H ₂]
22	0.43
50	0.45
100	0.46
150	0.40
175	0.43

may be determined by a simple pressure measurement since H₂ is the only product not condensable at 77°K. (3) C₂H₄ photolysis is not sensitive to small amounts of impurities and degree of conversion (at wavelengths shorter than 180 nm).^{6,7} (4) C₂H₄ is a readily available, easy to handle gas. (5) C₂H₄ absorbs strongly over the entire vacuum uv region.

In using the C₂H₄ actinometer, care must be exercised at λ > 180 nm because of the sensitivity to per cent conversion. Also, polymer formation on the windows must be considered. Neither disadvantage presents serious difficulties.

Acknowledgment. We are especially grateful to Dr. von Büнау for pointing out ref 5 and for helpful suggestions regarding the manuscript. The assistance of Mrs. C. Neumann in performing the spectrographic measurements is gratefully acknowledged.

COMMUNICATIONS TO THE EDITOR

Electron Spin Resonance Detection of Sn^{3+} and Pb^{3+} Complexes in γ -Irradiated Stannous, Plumbous, and Plumbic Salts

Publication costs borne completely by The Journal of Physical Chemistry

Sir: Exposure of tin and lead salts or their aqueous solutions to ^{60}Co γ -rays at 77°K gave centers whose esr spectra were characterized by features in the $g = 2$ region (~ 3200 G) together with features in the 5000 G region assignable to the high-field hyperfine components of the doublets from ^{117}Sn , ^{119}Sn , and ^{207}Pb . These are assigned to Sn^{3+} and Pb^{3+} centers having A_{iso} in the region 8550 G (Sn^{3+}) and 12000 G (Pb^{3+}).

hyperfine components were so well resolved that even the low abundant $^{115}\text{Sn}^{3+}$ ions could be detected (Figure 1).

Two factors distinguish these centers from those previously described:^{1,2} one is that the magnitudes of the hyperfine coupling constants are definitely dependent upon environment, and the other is the fact that pure salts give good yields of ions that can, formally, be described as ns^1 species.

The former result, although to be expected, was not found for other ions of this class, even though it was sought. For example, thallos and thallic ions gave Tl^{2+} having identical properties.² The problem is complicated by the fact that several centers show a marked anisotropy in the high-field components, such

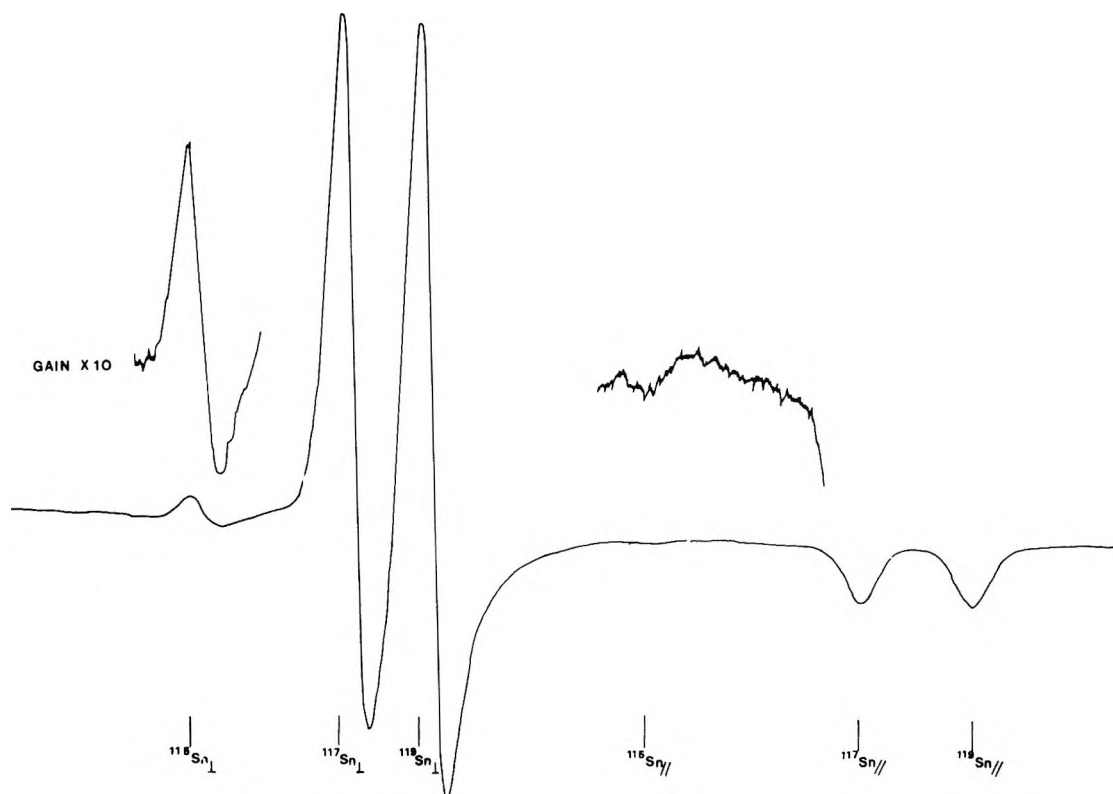


Figure 1. High-field hyperfine components in the esr spectrum of γ -irradiated SnSO_4 .

In the light of our success in preparing and detecting by esr ns^1 cations such as Cd^+ , Hg^+ , and Tl^{2+} ,^{1,2} we have investigated various stannous, plumbous and plumbic salts and their aqueous solutions, and find that in most cases species having the properties expected for Sn^{3+} and Pb^{3+} ions are formed (Table I). In the particular case of stannous sulfate, the high-field

as that for the magnetic tin isotopes in Figure 1. If this is interpreted as a hyperfine anisotropy, as has been done in Table I, and as one would normally do in such cases, the resulting anisotropy is, apparently,

- (1) R. S. Eachus and M. C. R. Symons, *J. Chem. Soc. A*, 3080 (1970).
- (2) M. C. R. Symons and J. K. Yandell, *ibid.*, A, 760 (1971).

Table I: ESR parameters of Sn^{3+} and Pb^{3+}

Material	Species	Field value for high-field lines, G		A value, G		g value	
$\text{Pb}(\text{NO}_3)_2$ in frozen 2.5 M aq HNO_3	$^{207}\text{Pb}^{3+}$	5500 (isotropic)		14,052		2.00	
Solid PbCO_3	$^{207}\text{Pb}^{3+}$	5348 (isotropic)		12,400		2.00	
Pb^{2+} doped into CdS	$^{207}\text{Pb}^{3+}$	5393 (isotropic)		13,150		2.006	
			⊥		⊥		⊥
Solid SnSO_4	$^{119}\text{Sn}^{3+}$	5007	5231	10,480	8,677	1.993	2.029
	$^{117}\text{Sn}^{3+}$	4976	5186	9,883	8,338		
	$^{116}\text{Sn}^{3+}$	4916	5098	8,830	7,722		
Solid SnCl_2	Sn^{3+} (separate components not resolved)	4780 (isotropic)		6,251		2.00	
Solid SnI_2	$^{119}\text{Sn}^{3+}$	5255 (isotropic)		10,246		2.00	
	$^{117}\text{Sn}^{3+}$	5215		9,733			
	$^{116}\text{Sn}^{3+}$ not resolved)						

far too large for any reasonable admixture of an outer p-orbital, induced, for example, by ligand bonding. We are not yet clear why this should be, and the factors governing the form and magnitude of these large hyperfine couplings are presently being assessed.

The latter result is unexpected, as was stressed previously.³ Thus one might have expected Sn^{3+} , for example, to be just a crude representation of an electron in the conduction band or a hole in the valence band, or at least that it would be highly mobile. This

indicates that there is a considerable modification of the environment around the M^{3+} units so that a relatively deep trapping center results. Thus these two factors are probably closely linked.

(3) R. S. Eachus and M. C. R. Symons, *Chem. Commun.*, 70 (1970).

DEPARTMENT OF CHEMISTRY
THE UNIVERSITY
LEICESTER, LE1 7RH, ENGLAND

R. J. BOOTH
H. C. STARKIE
M. C. R. SYMONS*

RECEIVED AUGUST 6, 1971

American Chemical Society

"Primary Publications on Microfilm"

Your Key to—

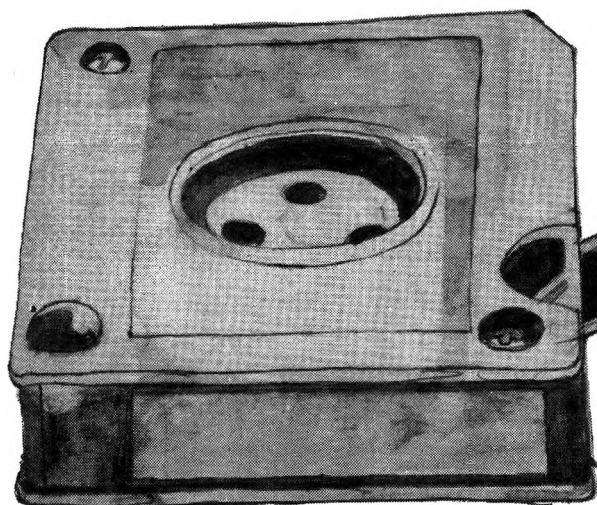
■ Dramatic savings in archival space and dollars . . . over **1,000,000** pages of chemical literature contained in a carousel measuring only 17" x 17" x 39".

■ Faster access to needed data. Slash costly search and retrieval time required of your scientists and librarians.

■ Unlimited distribution of copyrighted scientific data. "ACS Primary Publications on Microfilm" are available under a unique licensing agreement permitting you to make as many enlarged photocopies per page as desired . . . for distribution throughout your company.

American Chemical Society Primary Publications included in this microfilm program:

JOURNAL OF THE AMERICAN CHEMICAL SOCIETY
INDUSTRIAL & ENGINEERING CHEMISTRY
CHEMICAL TECHNOLOGY
CHEMICAL & ENGINEERING NEWS
CHEMICAL & ENGINEERING NEWS ANNUAL INDEXES
ANALYTICAL CHEMISTRY
JOURNAL OF PHYSICAL CHEMISTRY
JOURNAL OF AGRICULTURAL AND FOOD CHEMISTRY
JOURNAL OF ORGANIC CHEMISTRY
JOURNAL OF CHEMICAL AND ENGINEERING DATA
CHEMICAL REVIEWS
JOURNAL OF CHEMICAL DOCUMENTATION
I&EC FUNDAMENTALS
I&EC PROCESS DESIGN AND DEVELOPMENT
I&EC PRODUCT RESEARCH AND DEVELOPMENT
BIOCHEMISTRY
INORGANIC CHEMISTRY
JOURNAL OF MEDICINAL CHEMISTRY
CHEMISTRY
ENVIRONMENTAL SCIENCE & TECHNOLOGY
ACCOUNTS OF CHEMICAL RESEARCH
MACROMOLECULES



For information on "ACS Primary Publications on Microfilm", write or call:
Mr. George Virvan
Special Issues Sales
American Chemical Society
1155 16th Street, N.W.
Washington, D.C. 20036
(202-737-3337)

BROADEN

Your Chemical Information Base

Enter your low-cost charter subscription now to the American Chemical Society's exciting new "SINGLE ARTICLE ANNOUNCEMENT SERVICE" and select relevant current material from fifteen major ACS primary journals.

Starting in January 1971, you can vastly increase your available range of chemical data . . . in a fraction of your current reading time . . . and at a minimum of cost.

Beginning that month, the ACS "SINGLE ARTICLE ANNOUNCEMENT SERVICE" will bring subscribers twice-monthly announcements containing reproductions of contents pages from fifteen major ACS primary journals . . . as well as I & EC's "Research Results Service."

By scanning the tables of contents, you can decide which articles are pertinent to your needs. Then, using an order form included with the announcement, you can check the desired articles and return it to us. Your reprints will be sent to you via first class mail . . . within twenty-four hours of receipt.

Publications included in this service are: ANALYTICAL CHEMISTRY . . . BIOCHEMISTRY . . . ENVIRONMENTAL SCIENCE & TECHNOLOGY . . . I&EC-FUNDAMENTALS . . . I&EC-PROCESS DESIGN & DEVELOPMENT . . . I&EC-PRODUCT RESEARCH & DEVELOPMENT . . . INORGANIC CHEMISTRY . . . JOURNAL OF AGRICULTURAL AND FOOD CHEMISTRY . . . JOURNAL OF THE AMERICAN CHEMICAL SOCIETY . . . JOURNAL OF CHEMICAL DOCUMENTATION . . . JOURNAL OF CHEMICAL AND ENGINEERING DATA . . . JOURNAL OF MEDICINAL CHEMISTRY . . . JOURNAL OF ORGANIC CHEMISTRY . . . JOURNAL OF PHYSICAL CHEMISTRY . . . MACROMOLECULES . . . plus the "Research Results Service" (which provides titles and short summaries of all manuscripts being considered for future publication in the three I&EC Quarterlies).

Cost for the reprints is quite low: \$1 *or the first individual reprint and \$.60 for each additional reprint order entered in the same request. Papers from the "Research Results Service" are available in manuscript form, at a nominal cost per page.

Enter your charter subscription now to the exciting "SINGLE ARTICLE ANNOUNCEMENT SERVICE" . . . and save 20% as a charter subscriber.

Single Article Announcement Service

American Chemical Society, 1155 16th Street, N.W., Washington, D.C. 20036

Yes—I wish to receive the ACS SINGLE ARTICLE ANNOUNCEMENT SERVICE at the one-year rate checked below.

ACS Member <i>Personal Use</i> Charter One-Year Rate	<input type="checkbox"/> U.S. \$8.00	<input type="checkbox"/> Canada, PUAS \$11.00	<input type="checkbox"/> Other Nations \$11.50	
Nonmember Charter One-Year Rate	<input type="checkbox"/> \$16.00	<input type="checkbox"/> \$19.00	<input type="checkbox"/> \$19.50	
<input type="checkbox"/> Payment enclosed	<input type="checkbox"/> Bill me	<input type="checkbox"/> Bill company	<input type="checkbox"/> I am an ACS member	<input type="checkbox"/> I am not an ACS member

Name _____ Position _____
Address Home _____ (Specific title please)
 Business _____

City _____ State/Country _____ Zip _____

Your employer _____

Nature of your employer's business: Manufacturing or Processing _____
(Please Indicate)

If manufacturer, type of products produced _____

N- LN-O